2015-02-02

Quantifying Temporal Changes in Knee Joint Laxity and Dynamic Knee Stability for Healthy and Acute ACL Injured Individuals

Bishop, Emily Lynn

UNIVERSITY OF CALGARY

Quantifying Temporal Changes in Knee Joint Laxity and Dynamic Knee Stability for Healthy and Acute ACL Injured Individuals

by

Emily Lynn Bishop

A THESIS

SUBMITTED TO THE FACULTY OF GRADUATE STUDIES

IN PARTIAL FULFILMENT OF THE REQUIREMENTS FOR THE

DEGREE OF DOCTOR OF PHILOSPHY

GRADUATE PROGRAM IN BIOMEDICAL ENGINEERING

CALGARY, ALBERTA

JANUARY, 2015

Abstract

ACL rupture causes altered joint dynamics and leads to greater risk of joint degeneration and development of knee OA. The current study investigated relations amongst passive knee laxity and dynamic knee stability in healthy and ACLD individuals over time to understand adaptations following ACL rupture during a sub-acute stage post-injury. An in vivo MR based measure of passive knee laxity was obtained using a novel knee loading apparatus to image the knee joint under various loading conditions. Dynamic knee stability was evaluated during two dynamic tasks using the finite helical axis (FHA) approach to quantify kinematics, combined with wavelet analysis of muscle activity.

The healthy group demonstrated side-to-side differences in FHA measures not present in the ACLD group. This revealed asymmetrical movement in the healthy group and enabled appropriate interpretation of side-to-side differences due to ACL rupture. Passive knee laxity was larger in the ACLD injured limb compared to the healthy dominant limb at six weeks post-injury, and did not significantly change in the injured limb between six and twelve weeks post-injury. FHA measures in the ACLD injured limb were not significantly different from healthy at six weeks post-injury. However, the ACLD group demonstrated changes in both limbs in FHA measures and muscle power between six and twelve weeks post-injury suggesting bilateral adaptations to ACL rupture. These changes resulted in increased limb symmetry during the swing task, and decreased limb symmetry during the squat task. At twelve weeks post-injury, ACLD individuals revealed significant correlations between passive knee laxity and FHA measures not present in the contralateral limb or the healthy group. ACLD individuals with increased passive knee laxity demonstrated more constrained movement during the swing, and less constrained movement during the squat. Relationships amongst passive knee laxity and

dynamic knee stability in the ACLD group provided an understanding of the influence of structural joint laxity on dynamic movement patterns. Early adaptations in the ACLD knee joint are speculated to contribute to the initiation of degenerative changes in the knee joint, which may be modifiable with targeted rehabilitation protocols aimed at minimizing or slowing the progression of OA.

Acknowledgements

I would like to extend my sincerest gratitude to the following people:

Dr. Janet Ronsky for her continual support and encouragement throughout this journey, for pushing me to set my goals high, and for believing that I could achieve them.

Dr. Richard Frayne for his support during the many stages of MR data collection, and for serving on my supervisory committee and providing valuable feedback throughout my research program.

Dr. Cy Frank for serving on my supervisory committee and providing an invaluable clinical perspective. His enthusiasm towards OA research is contagious.

Dr. Nick Mohtadi for taking interest in my research and allowing me into the AKIC; and Niko Lagumen, Meryl Wheeler, and Tori Thome for their assistance with ACLD recruitment.

Fran, Elrie and Wendy at the Seaman Family MR Centre for their assistance with MR scheduling and lengthy scanning sessions.

Peter Byrne and Dan Fantini for their assistance with manufacturing projects, for providing valuable suggestions and for teaching me about design for manufacturability.

Dr. Jacob Jaremko for providing his radiology expertise for clinical MR image assessment.

Dr. Jackie Whittaker for her assistance with the development of biomechanical assessment forms for study participants, and for providing physiotherapy expertise for data interpretation.

Dr. Peter Faris for taking the time to understand my research study design and providing his expertise in biostatistics.

All of my study participants for their patience, interest, and for making the process enjoyable.

The research group for providing a comfortable environment for learning, and for asking the tough questions first, especially Steve, Jess, Payam, Greg, and Jill.

Terri and Swathi, for the many enjoyable coffee breaks, the occasional TGIF, and the constant support, understanding and encouragement.

Juno and Kogan for their companionship over the years.

Table of Contents

List of Tables

List of Figures and Illustrations

List of Symbols, Abbreviations and Nomenclature

Symbol	Definition
3D	Three dimensional
ACL	Anterior cruciate ligament
ACLD	Anterior cruciate ligament deficient
ACLR	Anterior cruciate ligament reconstructed
AP	Anterior/posterior
ATT	Anterior tibial translation
BF	Biceps femoris
CNS	Central nervous system
EMG	Electromyography
FHA	Finite helical axis
GCS	Global coordinate system
ICS	Image coordinate system
KLA	Knee loading apparatus
LCS	Local coordinate system
LG	Lateral gastrocnemius
MA	Motion analysis
MDD	Minimal detectable difference
MR	Magnetic resonance
MUAP	Motor unit action potential
MVC	Maximum voluntary contraction
OA	Osteoarthritis
PD	Proximal/distal
ROI	Range of interest
SEM	Semitendinosus
SVD	Singular value decomposition
TA	Tibialis anterior
VL	Vastus lateralis
VM	Vastus medialis

Variability is the law of life, and as no two faces are the same, so no two bodies are alike, and no two individuals react alike and behave alike under abnormal conditions which we know as disease

William Osler (1903)

Chapter One: **Introduction**

1.1 Background

The anterior cruciate ligament (ACL) is the most commonly injured ligament of the knee, with approximately 200,000 ACL ruptures annually in the United States, and 100,000 ligament reconstructions performed each year (AAOS, 2009). The risk of developing osteoarthritis (OA), a very painful degenerative joint disease, is greatly increased following ACL injury. Studies have shown that more than 50% of individuals will already have radiographic OA in their injured knee twelve years after ACL injury (Lohmander et al., 2004). Even with ACL reconstruction, the progression of OA cannot be significantly prevented (Lohmander et al., 2004). OA currently affects one in eight Canadians, and that number is expected to rise to one in four in the next thirty years (Arthritis Alliance of Canada, 2011). The economic burden of OA in Canada is high and is expected to rise to $405.1 billion by 2020 (Arthritis Alliance of Canada, 2011). Therefore, a growing body of research is dedicated to understanding why OA develops in ACL deficient (ACLD) individuals, and how we can slow the progression of this debilitating disease or prevent it completely.

The knee is one of the largest and most complex joints of the human body (Figure 1-1). The knee consists of four bones: the femur (thigh bone), the tibia (shin bone), the patella (kneecap), and the fibula (outer shin bone). The knee joint capsule is a dense connective tissue structure surrounding the knee joint that is lined with synovium, which in turn provides nourishment and lubrication to the joint surfaces, as well as adding some strength and stability to the otherwise unstable joint. The meniscus is a c-shaped fibrocartilaginous structure that increases joint congruency, transmits compressive joint forces, and provides additional stability to the knee. The

articulating surfaces of the bones are covered in articular cartilage, which creates a smooth surface to allow for low friction movement between bones during motion. Four major ligaments in the knee control bone positions during joint motion: the anterior and posterior cruciate ligaments control movement in the anterior/posterior direction, while the medial and lateral collateral ligaments control medial/lateral movement. The primary function of the ACL is to prevent anterior translation of the tibia with respect to the femur, and its secondary function is to prevent excessive internal rotation of the tibia.

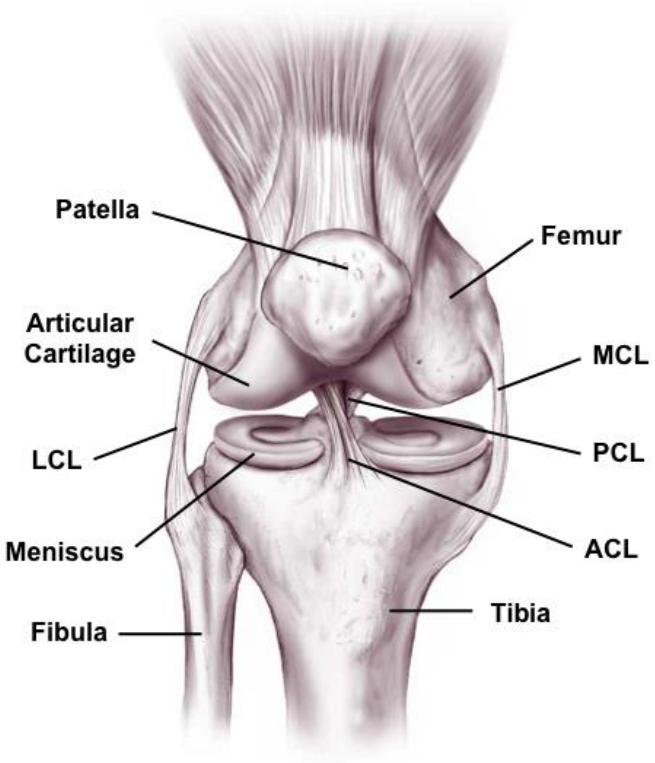

Figure 1-1: Labelled diagram of the knee joint structures including the femur, tibia, fibula and patella bones; articular cartilage, meniscus, and the LCL (lateral collateral ligament), MCL (medial collateral ligament), PCL (posterior cruciate ligament), and ACL (anterior cruciate ligament). Adapted from Media Partners Inc.

The ACL is the primary restraint to anterior tibial translation (ATT), hence anterior tibiofemoral laxity is the most predictable impairment resulting from an ACL tear (Snyder-Mackler et al., 1997). In a study by Daniel et al. (1985), ACLD individuals had an average of 11.4 ± 2.9 mm of anterior tibial displacement in the injured limb compared to 7.2 ± 1.9 mm in healthy individuals, with a twenty pound force applied anteriorly to the proximal tibia. Within a group of individuals there was a large range of values for anterior tibial displacement, thus it was concluded that a side to side difference in anterior tibial displacement greater than 3 mm was indicative of ACL rupture (Daniel et al., 1985). Increased laxity is thought to lead to functional knee instability and dysfunction, causing an increased risk for OA development (Snyder-Mackler et al., 1997). Several devices have been developed to quantify knee laxity, one of the most common being the KT-2000 arthrometer (MedMetric, San Diego CA, USA). However, the majority of laxity measurement devices are limited to measure uniaxial (tibial) displacement in the assumed anterior/posterior direction. Any out of plane motion, such as internal/external tibial rotation, which will affect the resultant laxity measure, is not accounted for (Logan, 2004b). The current study uses a custom built magnetic resonance (MR) imaging based knee loading apparatus (KLA) to obtain a three dimensional measure of passive knee laxity (Küpper et al., 2013). This device has been used previously to quantify laxity in healthy individuals, and showed a decrease in variability of anterior tibial displacement across days compared to the KT-2000 (Kupper, 2008). The current study uses the KLA to quantify passive knee laxity in ACLD individuals over time following injury.

Altered joint dynamics are speculated to contribute to the development of OA (Andriacchi et al., 2004). Several studies have investigated the kinematics of the ACLD knee in an effort to identify a specific change in knee mechanics. Increased ATT and internal tibial rotation in ACLD

subjects are consistently reported (Andriacchi and Dyrby, 2005; Dennis et al., 2005; Georgoulis et al., 2003; Logan, 2004a; Scarvell et al., 2004). However findings relating to varus/valgus angles remain inconsistent. These discrepancies may be attributed to differences in measurement techniques or specific tasks being investigated. Additionally, resulting joint motion is highly dependent on the definition of the local coordinate system (LCS), making it difficult to compare results between studies.

The finite helical axis (FHA) provides an alternative approach to describe knee joint motion through the definition of a single axis that moves as the joint articulates. This method is independent of the LCS definition as well as the order in which translation and rotation occur (Blankevoort et al., 1990). When applied to the knee joint, tibial motion can be expressed as a translation along and rotation about a helical axis embedded in the femur (Bull and Amis, 1998). Using the FHA approach, knee joint motion is not constrained to three pre-defined planes of motion as it is with a joint coordinate system approach. Rather, the FHA is defined in three-dimensional space based on the relative movement of the femur and tibia throughout a dynamic movement. Therefore, it is believed that the FHA may provide a truer representation of knee joint motion, especially in an ACLD joint where the axes of motion may be altered relative to a healthy knee joint.

The FHA approach has been used previously to examine the effect of ACL rupture on knee joint motion (Dennis et al., 2005; Jonsson and Kärrholm, 1994; Mannel et al., 2004). However, FHA error is sensitive to small rotation angles (Woltring et al., 1985), which is often solved by using a larger step size between data points. Furthermore, there is a lack of consistent variables to quantify the FHA. Fjeld (2007) developed a set of variables to quantitatively describe the FHA within the knee to address the small rotation error, and evaluated these FHA variables in a

healthy and an ACLD population during a seated leg swing and a single leg squat task. The FHA of the ACLD knee was located more anterior and proximal within the femur compared to the healthy knee during both tasks. Further, the angle of the FHA with the mediolateral axis of the knee, and the dispersion of this angle throughout the tasks were both decreased in the ACLD knee. Translation of the tibia along the FHA was reduced in the ACLD group during the squat, and increased in the ACLD group during the swing, compared to healthy. Overall, these results demonstrated that the healthy group had increased movement of the FHA during these tasks, while the ACLD group had less overall movement of the FHA. These findings were unexpected, and were interpreted as a compensation strategy in the ACLD group to reduce movement in the injured joint.

One limitation associated with the work of Fjeld (2007) is that data was only collected on the injured limb of the ACLD group and the dominant limb of the healthy group. This required the assumption of limb symmetry in the healthy group. Many studies assume limb symmetry in healthy individuals to simplify data collection and analysis, and/or to justify pooling data from left and right limbs. However, a comprehensive review by Sadeghi and colleagues (2000) provided ample evidence of differences between left and right limbs during gait using kinematic variables, suggesting that human able-bodied gait is asymmetrical. In order to compare the injured limb to the contralateral limb of an ACLD group, a comparison of dominant and contralateral limbs in a healthy group is required. Therefore, in the current study outcome variables are quantified in both limbs of the healthy and ACLD groups to enable appropriate interpretation of side to side differences in an ACLD group.

The contribution of the quadriceps and hamstrings to knee joint stability is altered following ACL rupture. There is general consensus that decreased quadriceps activation occurs in ACLD

individuals (Chmielewski et al., 2004; Snyder-Mackler et al., 1994; Swanik et al., 1999; Urbach et al., 1999). The hamstrings also play an important role in maintaining joint stability and preventing excessive ACL strain by preventing or decreasing anterior and rotary displacement of the tibia on the femur (Boerboom et al., 2001; Isaac et al., 2005; Liu and Maitland, 2000; MacWilliams et al., 1999). There is growing evidence to suggest that neuromuscular adaptation occurs bilaterally after ACL rupture (Konishi et al., 2003; Urbach et al., 1999). Urbach et al. (1999) used a combination of maximal voluntary contraction and supermaximal electrical stimulation (twitch interpolation technique), to demonstrate that the ability to fully activate the quadriceps muscle was significantly decreased in both the ACLD injured and contralateral limbs compared to a healthy control group. Therefore, it is thought that there are central mechanisms responsible for changes in muscle activation following unilateral ACL rupture. These are speculated to cause bilateral changes in muscular control and affect movement patterns in both the injured and contralateral limbs.

These neuromuscular adaptations in the ACLD knee can be investigated through the use of electromyography (EMG), which is the study of motor unit action potentials through the recording of a myoelectric signal. EMG signal amplitude is typically analysed with respect to time, often using root mean squared values or a rectified signal (Basmajian and De Luca, 1985; De Luca, 1997; Farina and Merletti, 2000). However, the EMG signal also contains valuable information about the frequency content of the signal, relating to slow and fast muscle fibres and muscle force requirements (J. Wakeling et al., 2002a). Therefore, information regarding EMG signal frequency may be helpful in relating muscle patterns to specific functions aimed at providing dynamic knee joint stability. The wavelet transform technique developed by von Tscharner (2000) allows the EMG signal to be analyzed simultaneously in both the time and

frequency domains. This provides an advantage over the traditional techniques that primarily limit analysis to the time domain. Using the wavelet analysis approach the intensity for each muscle is calculated, representing the power of the EMG signal within the frequency band at each time point. In the current study, muscle intensity and power are used to describe the myoelectric signal in terms of muscle activation over time.

The current study defines "dynamic joint stability" as the state of minimum deviation from healthy movement and muscle activity patterns during a given dynamic task and for a desired range of motion. Using this definition, dynamic joint stability is assessed using kinematics and muscle activity patterns. It would be expected that increased passive joint laxity in ACLD individuals would translate into increased movement in the joint during dynamic tasks. However, the work of Fjeld (2007) actually suggested tighter dynamic movement control in ACLD individuals. Therefore, we believe that ACLD individuals adapt to extra degrees of freedom in the knee joint due to ACL rupture by constraining knee movement. This decrease in dynamic stability would be characterized by a decrease in FHA translation and dispersion in the ACLD group relative to healthy, and an increased contribution from the hamstrings to compensate for the loss of the ACL. Furthermore, we expect ACLD individuals to have an altered joint position due to the loss of the ACL, resulting in a more anterior location of the FHA (tibia translated anteriorly relative to the femur) and an increased orientation angle (tibia internally rotated).

Single leg squat and seated leg swing tasks are used in the current study to investigate differences in dynamic joint stability between healthy and ACLD groups. The single legged squat is a loaded, closed-chain task, expected to introduce a component of stability, therefore requiring muscle co-contraction. Closed-chain weight-bearing exercises are known to produce increased co-contraction of the quadriceps, hamstrings and gastrocnemius muscle groups, which

is thought to reduce the strain on the ACL (Kozánek et al., 2011). In contrast, the seated leg swing is an unloaded, open-chain task with movement primarily in the sagittal plane controlled via quadriceps contraction. Open-chain exercises are believed to produce increased anterior shear force on the knee (Kozánek et al., 2011). Therefore, it is expected that the closed-chain squat task would highlight changes in muscular control patterns due to ACL rupture, while the open-chain swing task would highlight changes in joint movement patterns, both resulting in altered dynamic knee joint stability.

The severity of joint laxity is commonly assumed to be directly related to the degree of instability in the knee. However, the relationships amongst knee laxity, instability, and functional outcome in the ACLD population remain unclear (Shultz et al, 2004). Studies attempting to relate passive joint laxity to functional outcome following an ACL tear have not found significant relationships, suggesting that the degree of passive joint laxity is not indicative of functional outcome in ACLD individuals (Eastlack et al., 1999; Snyder-Mackler et al., 1997). However, recent studies investigating relationships amongst static and dynamic measures of knee laxity have shown significant correlations between passive knee laxity and kinematic measures in ACLD and ACL reconstructed individuals (Boeth et al., 2013; Sato et al., 2013). For example, Boeth et al. (2013) found that ACLD individuals with increased passive laxity demonstrated an increased range of anterior/posterior tibial translation during walking. It is believed that our novel approach to obtain a more precise measure of joint laxity using imaging techniques combined with the FHA approach for describing ACLD kinematics will reveal correlations between passive joint laxity and movement patterns.

While there is an abundance of literature addressing differences in kinematics, muscle activity, and joint structure between healthy and ACLD individuals, the information regarding changes

over time in the ACLD joint is limited. There is however evidence of adaptation in joint structures following ACL rupture. It is thought that the secondary joint stabilizing structures, including ligaments, joint capsule, and meniscus of the knee adapt to the loss of the ACL to provide additional joint stability. Several animal model studies show that ATT during dynamic movement reduces over time after ACL rupture, and suggest remodelling of the meniscus and joint capsule (Jackson et al., 1999; Lopez et al., 2003; Maitland et al., 1998). Furthermore, Atarod et al. (2013) found altered loading in the collateral and posterior cruciate ligaments after ACL transection in an ovine model, supporting the role of these ligaments as secondary stabilizers to ATT in an ACLD joint. Daniel et al. (1994) provided evidence of decreased ATT over time in ACLD humans (average 64 months post-injury). However the time course in human studies is generally long-term and does not capture acute changes in the joint. Therefore, a need for studies addressing acute (0-3 months post-injury) changes in the knee joint following ACL rupture has been identified.

There are very few human studies quantifying kinematic changes over time immediately following ACL rupture. This is likely due to challenges recruiting participants at an acute stage post-injury, difficulty controlling confounding variables, and because a large percentage of ACLD individuals undergo surgical repair at an early time point (Lohmander et al., 2004). Therefore, the majority of studies quantifying serial kinematic changes following ACL rupture use an animal model. Tashman et al. (2004b) used a canine model, and Tapper et al. (2008) used an ovine model to show that anterior tibial position during the swing phase of gait was not significantly different from intact immediately following ACL transection. However, over time the tibial position became significantly more anterior in the ACLD joint during the swing phase of gait. It was suggested that in these models secondary joint stabilizers (*i.e.*, meniscus) initially

provided AP knee stability after ACL rupture, but over time these structures became damaged from repeated loading and ATT increased in the ACLD knee.

Studies examining kinematic changes in ACLD individuals at an acute stage post injury are also limited. Furthermore, the definition of "acute" varies greatly between studies, ranging from 1 to 15 weeks (Chmielewski et al., 2001; Gardinier et al., 2012; Hurd and Snyder-Mackler, 2007). Results from acute studies have consistently shown decreased peak knee flexion angle, and a lower knee moment at peak knee extension during gait. Thus, the presence of kinematic adaptations at an "acute" stage following ACL rupture is evident. However studies are limited to walking, and the primary kinematic outcomes are in the sagittal plane only. Clearly, there is a need to quantify ACLD kinematics at a well-defined acute time point post injury, and to track kinematic changes over time to understand early adaptations in this population. Applying the FHA to quantify kinematics during open and closed chain tasks may provide a truer representation of ACLD knee joint motion, and is expected to reveal joint and neuromuscular adaptations due to ACL deficiency over time. These early adaptations in the ACLD knee joint may be linked to the initiation of degenerative changes in the knee joint, and could potentially be modified with targeted rehabilitation protocols aimed at minimizing, or slowing the progression of OA.

1.2 Specific Aims and Hypotheses

The overall long-term research goal is to better understand the relations between joint structure, joint function, and the development of degenerative changes associated with ligament injury. Towards this goal, the objective of this thesis research study is to investigate relations between structural joint laxity and dynamic joint stability in healthy and ACLD participants over time. To meet this objective the project is directed towards achieving the following specific aims (SA):

SA1: Determining dynamic joint stability relations in healthy knee joints and in joints with ACL deficiency, using the finite helical axis method and wavelet analysis of muscle patterns

SA2: Quantifying passive laxity in healthy and ACLD knee joints *in-vivo* using MR imaging combined with a novel joint loading device

The following hypotheses (H) will be tested in accordance with the above specific aims:

H1: Healthy participants will show significant differences in FHA measures and muscle power between the single leg squat task and the seated leg swing

H1a: The FHA will have a more anterior location in the tibiofemoral joint, and decreased translation and dispersion during the swing task relative to the squat task in healthy participants

H1b: The swing task will be quadriceps dominant indicated by an increased ratio of quadriceps to hamstring muscle power (QH ratio), while the squat task will exhibit co-contraction of the quadriceps and hamstring muscles in healthy participants

H2: ACLD participants will have increased passive knee laxity and decreased dynamic knee stability six weeks post injury relative to healthy participants

H2a: ACLD participants will have increased side-to-side differences in passive knee laxity, FHA measures, and muscle power at six weeks post injury relative to healthy participants

H2b: ACLD participants will have decreased dynamic stability relative to healthy participants at six weeks post injury indicated by:

a. A more anterior FHA location and increased orientation angle

b. Decreased FHA translation and dispersion

H2c: ACLD participants with increased ATT will exhibit decreased dynamic knee stability at six weeks post injury, indicated by correlations between passive knee laxity and FHA measures

H3: ACLD participants will not show a change in passive knee laxity between six and twelve weeks post-injury, but will show changes in dynamic knee stability during this period

H3a: ACLD participants will not show a significant change in passive knee laxity between six and twelve weeks post injury

H3b: ACLD participants will demonstrate changes between six and twelve weeks post injury in dynamic knee stability in both the injured and contralateral limbs, affecting limb symmetry

H3c: At twelve weeks post injury, ACLD participants will show altered correlations (compared to six weeks post injury) between passive knee laxity and FHA measures

1.3 Study Design

The study was designed in order to test the hypotheses listed above (Figure 1-2). Power calculations were carried out a priory to determine the required sample size for this study using a power of 80% and an alpha level of 0.05. For anterior tibial translation, a between group difference of 3 mm was assumed based on literature (Daniel et al., 1985), and a variance of 2.9 mm was used based on the work of Kupper (2008). A one-sided independent samples T-test specified a sample size of twelve. For FHA orientation angle, a between group difference of 6°, and a variance of 4.5° was used based on the work of Fjeld (2007). A one-sided independent samples T-test required a sample size of seven. Based on these power calculations, the study aimed to have twelve participants in both the healthy and ACLD groups.

Twelve healthy participants and nine ACLD participants were recruited into the study. Only nine ACLD participants were recruited into the study due to strict study inclusion criteria, the time commitment involved for participants and the study timeline and scope, which hindered recruitment of additional ACLD participants into the study. Testing was performed on the dominant and contralateral limbs of the healthy group, as well as the injured and contralateral limbs of the ACLD group. The healthy group was tested once, while the ACLD group was tested twice: at six and twelve weeks post-injury. Passive laxity was quantified using the knee loading apparatus to apply an anterior force to the tibia within the MR scanner. The resulting outcome measure was ATT for each participant at the desired level of tibial loading. Dynamic stability was assessed during two dynamic tasks. Motion analysis was used to measure kinematics for FHA determination. EMG was collected to assess muscle activity. The outcome measures for dynamic stability were FHA measures and muscle power from wavelet analysis of muscle

activity patterns. Relationships between passive knee laxity and dynamic knee stability were assessed using correlations between ATT and FHA measures for each participant group.

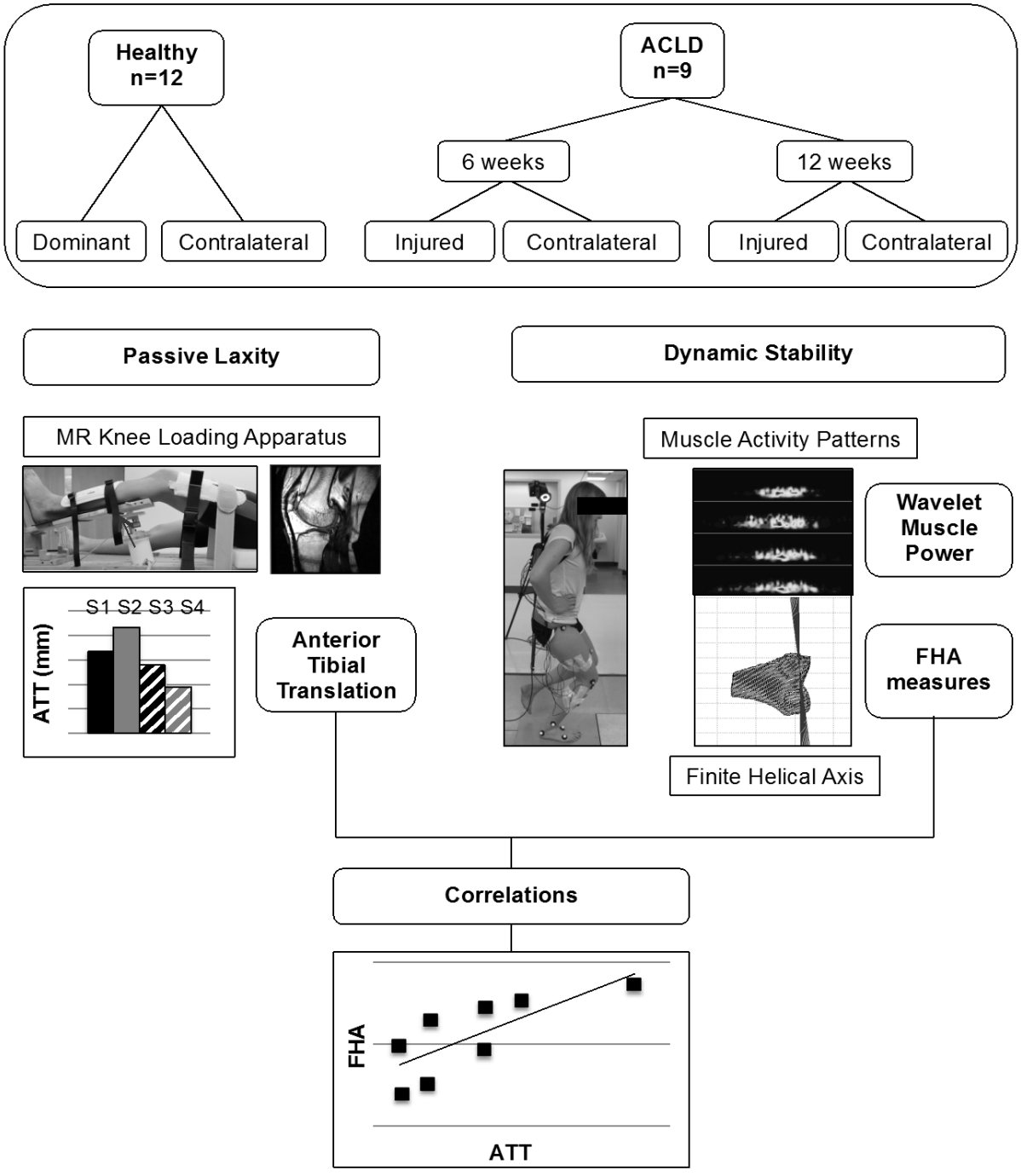

Figure 1-2: Research study design including study participants, and outcome measures for passive knee laxity, dynamic stability, and correlations.

1.4 History

This section acknowledges the history of work in the current research group that enabled the undertaking of this thesis research project.

The knee loading apparatus (KLA) was originally developed by Ms. Jessica Kupper to enable anterior loading of the tibia to assess knee joint laxity. The imaging parameters to enable imaging of bone, cartilage and ligaments in the knee joint were developed by experienced MR physicists and physicians including Dr. Richard Frayne, Dr. Mohammad Sabati, and Dr. Houman Mahallati. This KLA device was modified by Mr. Ion Robu to apply compressive forces to the patellofemoral joint during MR imaging. Ms. Nazanin Sinaei later developed a custom hydraulic system to accurately apply forces to cadaver knee joints during MR imaging to assess joint and ligament displacements under applied loading. The knee loading apparatus and custom hydraulic system were combined and refined for use in the current project to assess knee joint laxity in healthy and ACLD individuals. Validation of the surface registration technique for bone surface matching was completed by Ms. Rita Cheng. This surface registration technique was applied in the current study for accurate registration of low and high resolution MR images. Ms. Ingrid Fjeld developed and tested the main FHA approach used in the current study.

This research project would not have been possible without the contributions of these individuals.

1.5 Thesis Outline

This thesis is divided into seven chapters. Details of the pilot work completed to ensure confidence in the methods applied in this research, and to inform the study protocols are presented in Chapter 2. Chapters 3 to 5 each contain a literature review, methods, results and discussion section. Chapter 3 examines the dynamic squat and swing tasks using the FHA and muscle activity patterns in the healthy group to characterize these tasks in a healthy population, addressing hypothesis 1. Chapter 4 examines differences in passive knee laxity and dynamic knee stability between the healthy and ACLD group at six weeks post injury to address hypothesis 2. Chapter 5 identifies changes in passive knee laxity and dynamic knee stability over time in the ACLD group between six and twelve weeks post injury, addressing hypothesis 3. Chapter 6 highlights the key contributions of the study to the understanding of adaptations in the ACLD joint over time after injury, as well as the relationship to potential mechanisms of OA development. Chapter 6 also addresses study limitations. Lastly, Chapter 7 discusses suggested areas for future research to build on the contributions of the current study.

1.6 Previously Presented Work

Parts of this thesis have been presented at scientific conferences and appear in several conference proceedings:

Bishop, E L; Kuntze, G; Ronsky, J L. Finite Helical Axis and Muscle Power in the Squat and Swing. *World Congress of Biomechanics*. July 6-11, 2014, Boston, Massachusetts.

Bishop, E L; Kuntze, G; Frayne, R; Frank, C; Ronsky, J L. Quantifying differences in passive knee laxity and finite helical axis measures between healthy and anterior cruciate ligament deficient individuals. *OARSI World Congress*. April 24-27, 2014, Paris, France.

Bishop, E L; Kuntze, G; Frayne, R; Frank, C; Ronsky, J L. Relationships between passive knee laxity and finite helical axis measures in healthy individuals. *Orthopaedic Research Society 2014 Annual Meeting*. March 15-18, 2014, New Orleans, Louisiana.

Bishop, E L; Kuntze, G; Ronsky, J L. Comparison of MRI-based and Marker-based Coordinate Systems for FHA Calculation. *14th Alberta Biomedical Engineering Conference*. October 26-27, 2013, Banff, AB.

Bishop, E L; Kuntze, G; Ronsky, J L. Effects of ACL deficiency on lower limb muscle activation patterns. *International Workshop on the Biomedical Basis of Human Performance across the Lifespan*. June 5-6, 2013, Calgary, AB.

Bishop, E L; Kuntze, G; Ronsky, J L. Changes in the finite helical axis over time in two ACL deficient individuals. *13th Alberta Biomedical Engineering Conference*. October 20-21, 2012, Banff, AB.

Bishop, E L; Kukulski, D; Mathison, C; Enns-Bray, W; Frank, C; Ronsky, J L. Differences in Dynamic Joint Stability Between Dominant and Contralateral Knees in Healthy Individuals. *Orthopaedic Research Society 2012 Annual Meeting.* February 4-7, 2012, San Francisco, California.

Bishop, E L; Kukulski, D; Mathison, C; Enns-Bray, W; Ronsky, J L. Differences in Active Muscular Control Between Dominant and Contralateral Knees in Healthy Individuals. *12th Alberta Biomedical Engineering Conference*. October 22-23, 2011, Banff, AB.

Chapter Two: **Pilot Studies**

A series of pilot studies were conducted to quantitatively evaluate function of equipment used for data collection, and to finalize the study protocol design. Details of methodology, results of these studies and as well as discussion of important findings for the main study are presented in this section.

2.1 Knee Loading Apparatus Redesign and Calibration

Knee joint laxity, a key variable in the main study, is quantified with the knee loading apparatus (KLA, Küpper et al., 2013). The KLA system is composed of the positioning apparatus, the hydraulic system, and the software interface (Figure 2-1). The positioning apparatus provides a platform to support the participant in a supine position during magnetic resonance (MR) imaging, while the test leg is supported with the thigh support and the shank is secured to the tibial platform. The hydraulic system is used to apply an anterior force to the proximal tibia to produce anterior tibial translation (ATT), while the software interface records voltage from a pressure transducer (Omega Engineering, Quebec, Canada). Previous work quantifying laxity in healthy individuals found that the average variability of anterior tibial displacement across days was 0.58 mm for the KLA compared to 1.47 mm for the KT-2000 (Kupper, 2008).

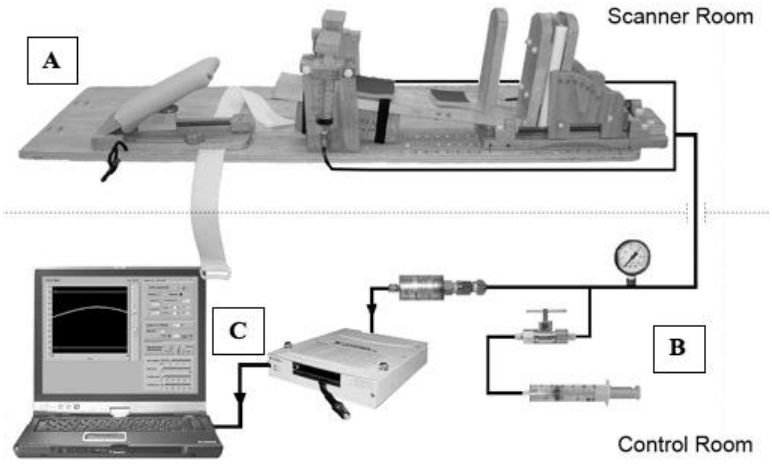

Figure 2-1: 'Knee Loading Apparatus System Components including a positioning apparatus [A], hydraulic system [B], and software interface [C]' with permission from Kupper (2008).

In the current study, the KLA is used to generate forces of 0 Newtons (N), 30 N, 50 N, 89 N, and 133 N at the knee joint. A calibration equation (described in Section 4.3.2.1) determines the required applied KLA force to achieve the desired resultant force at the knee (applied KLA force is larger than the resultant force at the knee). The device is used within a MR scanner to capture images of the knee joint under varying levels of applied load. Fluid pressure developed in the hydraulic system is measured in Volts (V) using a pressure transducer (General Purpose Pressure Sensor - PX303-015G5V, Omega Engineering, Quebec, Canada), and converted to force (N) based on a calibration relation. The pressure transducer had a voltage range of 0.5 to 5.5 V, and a pressure range of 0 to 15 pounds per square inch gage (Psig). The design requirements for the KLA included 1) an applied force range of 0-200 N to achieve anterior forces in the knee joint of up to 133 N; 2) load application to the tibia for up to 1.5 minutes to provide a set load for the entire duration of the MR imaging sequence; and 3) between day voltage variability of piston displacements within 2% (0.1 V) of the pressure transducer total voltage range (5 V). This series

of pilot studies was dedicated to the redesign of the hydraulic force system, calibration, and evaluation of the hydraulic component of the KLA.

2.1.1 Hydraulic Cylinder

A new design for the hydraulic system was required to address problems identified with friction and difficulty with operations. The original KLA design used plastic syringes to deliver the desired force to the knee (Küpper et al., 2013) (Figure 2-2). However, the rubber stoppers in the syringes were prone to degradation from the hydraulic fluid (70% isopropyl alcohol), causing increased friction in the system leading to erroneous pressure and force relations. Regular replacement of syringes was not desirable due to unknown timecourse of syringe degradation and change in friction as well as the substantial time requirements, making system operation potentially unreliable and cumbersome. To address these problems, a variety of materials and system designs were evaluated. A custom hydraulic cylinder, manufactured to apply a known force to cadaver knees (Sinaei, 2012), was evaluated. This cylinder was incorporated into the KLA design to provide a more robust hydraulic system (Figure 2-3). This design alteration allowed for the removal of the original vertical syringe supports thereby easily accommodating a wide range of leg sizes.

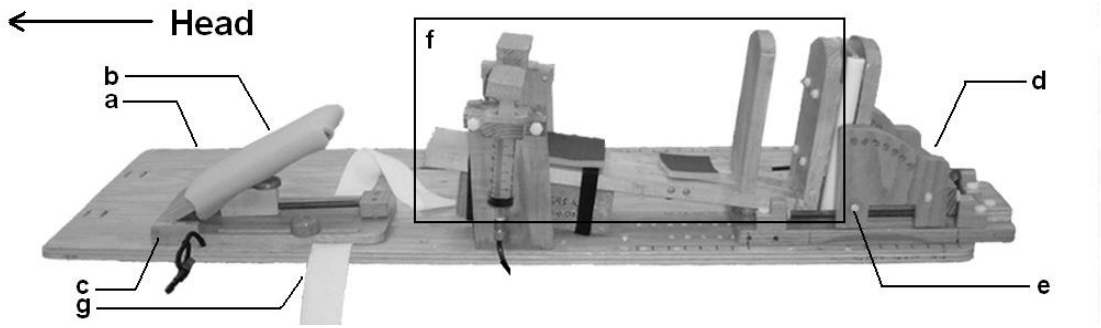

Figure 2-2: Original KLA design using plastic syringes for hydraulic cylinders: (a) base plate, (b) thigh support, (c) hinge, (d) foot plate, (e) hinge, (f) tibial platform (with permission from (Kupper, 2008)

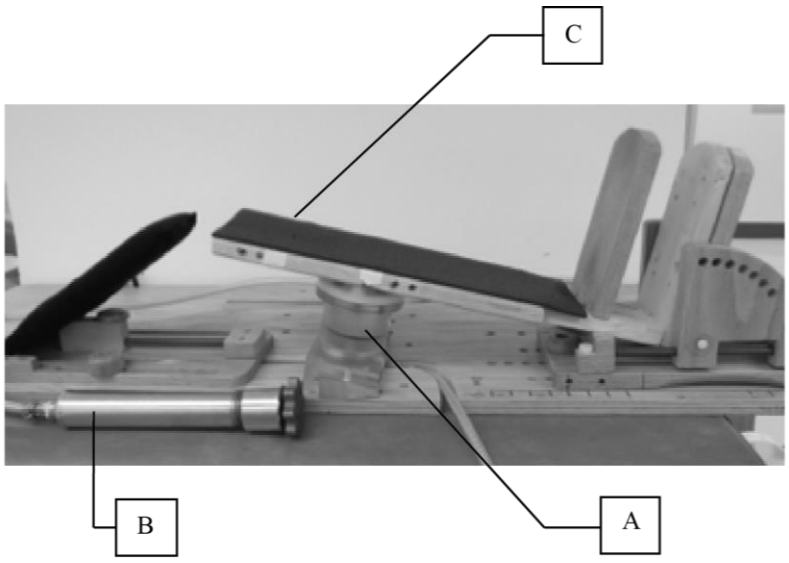

Figure 2-3: New KLA design using custom manufactured hydraulic cylinder (A) and hydraulic piston (B), with a wider tibial support (C).

Static loading tests of hydraulic system

The load response of the hydraulic cylinder (output, V) was evaluated throughout its range of movement (input) to verify uniform behaviour along the height of the cylinder walls. A 3 kg weight was stacked on top of the cylinder and the cylinder was moved through its range of movement (0 to 3 cm), holding each cylinder height for 30 seconds (s). These time durations corresponded to the times that would be held at each position during the MR scanning session with the KLA. Overall, the cylinder was raised from 0 to 230 s to the maximum displacement, and lowered between 230 and 380 s back to the initial position (Figure 2-4). To determine the potential influence of the hydraulic fluid on the cylinder position (output) as a function of time, tests were performed under two conditions: first with the hydraulic fluid in the system for less than 2 hours, and second with the hydraulic fluid in the system for 24 hours. The voltage trace from the cylinder after having 70% isopropyl alcohol in the system 24 hours (Figure 2-4)

indicates there is high variability both within a cylinder position (over time), displaying a maximum standard deviation of 1.45 V at a given cylinder position, and between cylinder positions, having a standard deviation of 0.35 V. The first spike in voltage at ~15 s shows initial "sticking" of the piston before it overcomes the static friction and begins to rise. The variability within and between cylinder positions exceeded the tolerated variability of 0.1 V, and was therefore considered unacceptable. Isopropyl alcohol was the optimum hydraulic fluid for MR scanner compatibility reasons. Consequently, it was decided to change the material of the cylinder.

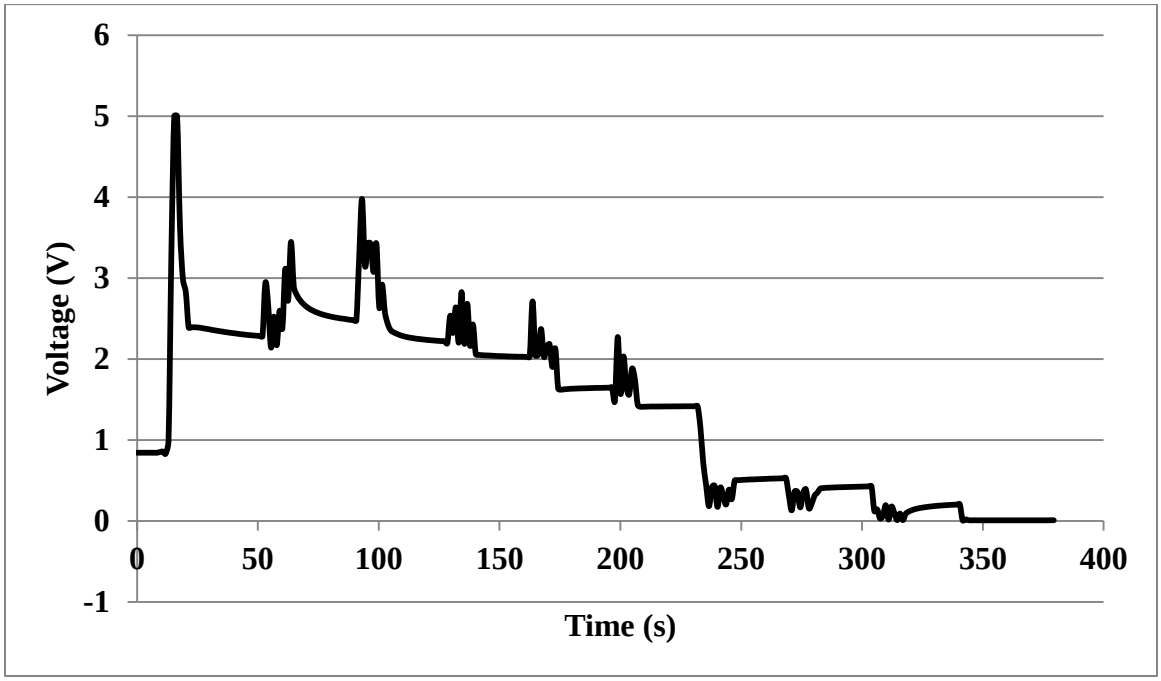

Figure 2-4: Voltage trace from the hydraulic cylinder as it is raised and lowered through its range of movement. The hydraulic fluid is 70% isopropyl alcohol, and the cylinder has a 3 kg weight applied on top.

Delrin® (DuPont, Canada), an acetal resin polymer, was researched and found to be compatible with isopropyl alcohol. A wedge of the material was soaked in isopropyl alcohol for one week.

There were no changes to its structure that were visible by eye or by touch. A new cylinder was manufactured from Delrin® and the fit between the fixed cylinder component and the moving piston was optimized to maintain a seal with the least amount of friction. The components of the hydraulic cylinder are shown in Figure 2-5.

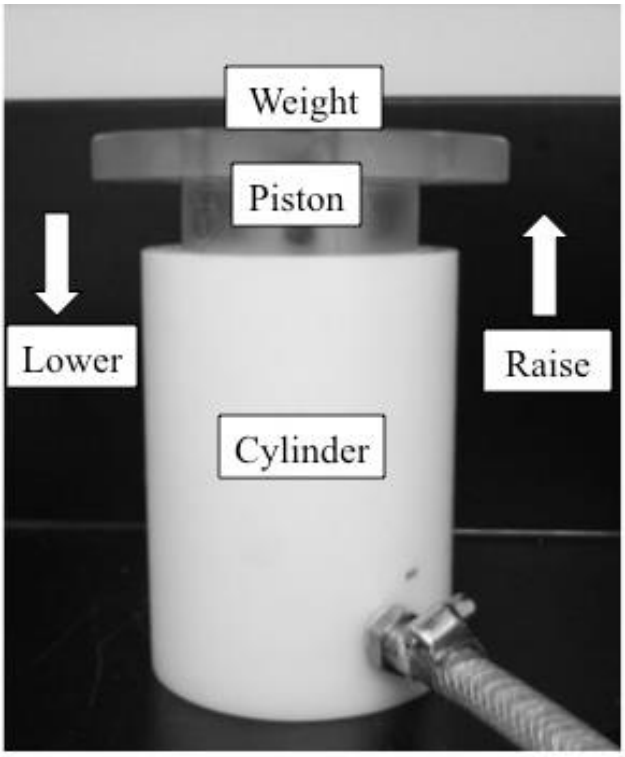

Figure 2-5: The new Delrin® hydraulic cylinder system which raises and lowers consisting of cylinder, piston and weight platform.

2.1.2 Development and Validation of Calibration Procedure

The accuracy and repeatability of force application for the new Delrin® hydraulic cylinder was unknown. Therefore, several tests were performed to determine the optimal calibration procedure for the system. Free weights of 3 kg, 5 kg, 10 kg, 15 kg and 20 kg were used for calibration to cover the desired range of applied forces from 0 to 200 N. The exact masses were measured using a calibrated force plate (AMTI type OR6-6, Advanced Mechanical Technology, Inc.,

Watertown, MA, USA) (Table 2-1). Corresponding forces were calculated using Equation 2-1. In the following sections, the weights used will be referred to by the calibration weight.

$$\boldsymbol{Force(N) = mass(kg) * 9.81 \frac{m}{s^2}} \quad \textbf{(Eqn. 2-1)}$$

Table 2-1: Exact mass and force for each calibration weight.

Calibration weight	Exact mass (kg)	Force (N)
3 kg	3.25	31.88
5 kg	5.38	52.78
10 kg	10.57	103.65
15 kg	16.13	158.20
20 kg	21.16	207.55

2.1.2.1 Dynamic Calibration

A test was performed to quantify the variability in fluid pressure (Volts) as the piston was moved through its full range of movement with a constant applied calibration weight (range 0 to 10 kg) to quantify variability in voltage across piston positions and across time points. The piston height was raised and lowered sequentially using six displacements measured from the bottom of the cylinder, encompassing the entire range of movement of the piston: 11.5 cm, 12.0 cm, 12.5 cm, 13.0 cm, 13.5 cm, and 14.0 cm. Voltage was continuously recorded while the system was allowed 20 s to relax at each height to simulate the KLA calibration protocol (Figure 2-6). This test was performed four times with weights of 0 kg, 3 kg, 5 kg and 10 kg stacked on top of the piston, and repeated at three separate time points (Day 1 am, Day 1 pm, and Day 2 am). These tests were performed with a single tester, in a temperature controlled room, and the order of loading and piston position remained constant for the three separate time points.

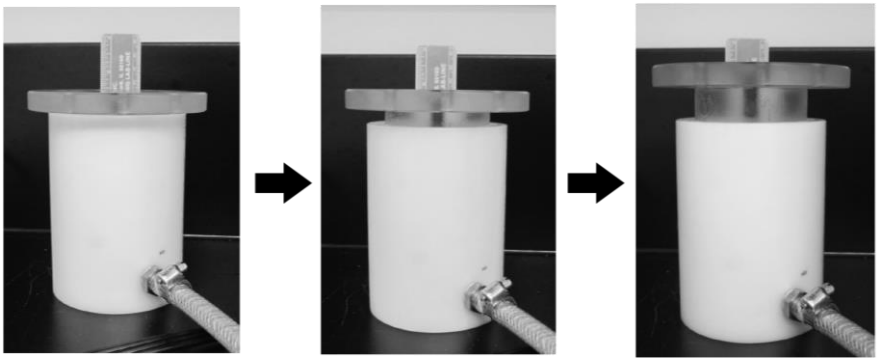

Figure 2-6: Hydraulic cylinder with piston at different heights to test variability of voltage values throughout the range of movement.

An exemplar plot of the raw voltage as a function of time for each piston height and weight for Day 2 am (Figure 2-7) reveals low variability both within piston positions over time (standard deviation = 0.08-0.14 V) and across piston positions (standard deviation = 0.09 V) for the 3 kg calibration weight during raising. Similar results were found for the two additional test times (Day 1 am, Day 1 pm). A 1.07 ± 0.10 V drop in voltage occurred consistently as the cylinder initiated the lowering phase. This is most likely attributed to the nature of the hydraulic piston, where an initial suction is required to begin lowering the piston. In consideration of this condition, the results of the experiment are separated into raising and lowering phases.

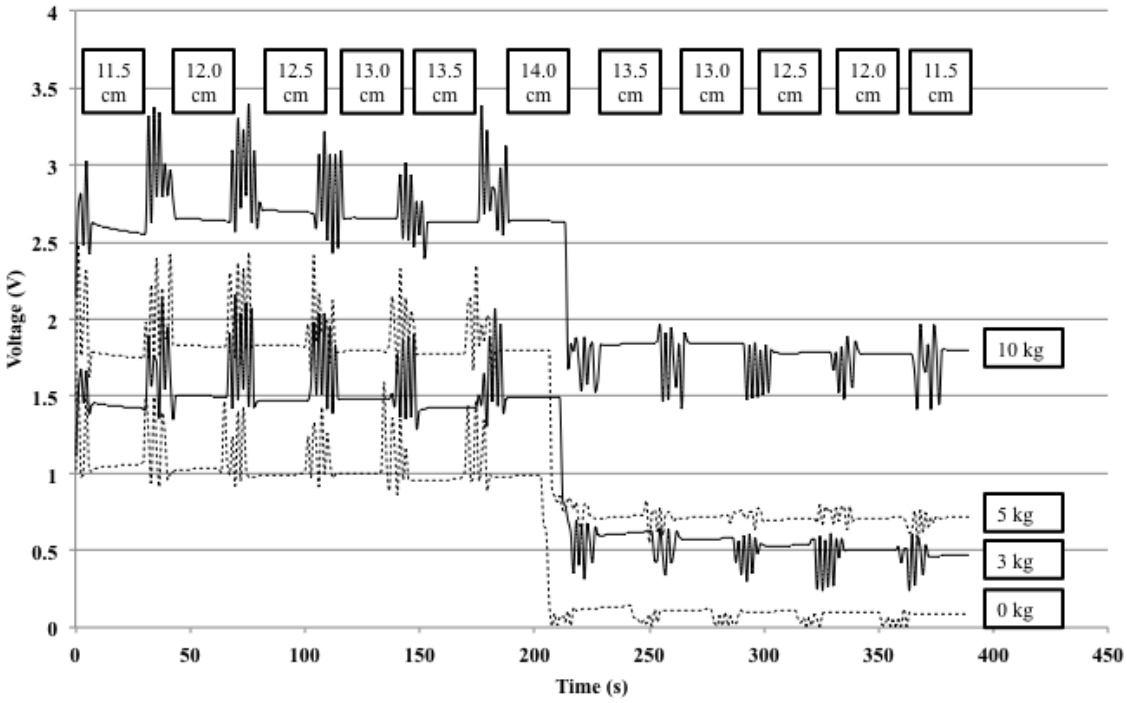

Figure 2-7: Exemplar plot of raw voltage versus time as the piston is raised and lowered throughout its range of movement (Day 2 am), for 0 kg, 3 kg, 5 kg, and 10 kg (represented by different lines) weight applied on top of the piston.

The mean and standard deviation of the voltage at each cylinder displacement was determined over the 20 s relaxation period. An average value (mean and standard deviation) for each weight was determined over all piston heights for each of the raising and lowering phases (Table 2-2) for each day. Variation between days was determined by averaging across days for each weight and displacement phase.

Table 2-2: Average voltages [mean (std)] across piston displacements for the raising and lowering phases. Values are shown for each weight (0, 3, 5 and 10 kg), and each day. Average voltage across days is shown in the bottom row.

Weight	0 kg		3 kg		5 kg		10 kg	
Phase	**Raise (V)**	**Lower (V)**	**Raise (V)**	**Lower (V)**	**Raise (V)**	**Lower (V)**	**Raise (V)**	**Lower (V)**
Day 1 (am)	0.79 (0.08)	0.28 (0.07)	1.25 (0.08)	0.87 (0.05)	1.58 (0.07)	1.31 (0.05)	2.44 (0.07)	1.91 (0.04)
Day 1 (pm)	0.98 (0.25)	0.21 (0.11)	1.28 (0.08)	0.88 (0.05)	1.58 (0.05)	1.21 (0.08)	2.45 (0.05)	1.78 (0.08)
Day 2 (am)	0.89 (0.20)	0.28 (0.06)	1.24 (0.09)	0.87 (0.05)	1.57 (0.05)	1.22 (0.05)	2.47 (0.06)	1.78 (0.08)
Average	0.89 (0.10)	0.26 (0.04)	1.26 (0.02)	0.87 (0.01)	1.58 (<0.01)	1.25 (0.06)	2.45 (0.01)	1.82 (0.08)

The standard deviations for each weight and phase represent the variability in voltage as the piston is raised and lowered. Within a given test, these values are less than 0.1 V (range = 0.01-0.08 V), except for raising and lowering on Day 1 (pm) with 0 kg of weight (0.25 V and 0.11 V, respectively), and raising on Day 2 (am) with 0 kg of weight (0.20 V). These results suggest that there is higher variability between positions when there is no weight on the piston. The standard deviations for the average voltages across days are less than or equal to 0.1 V (range = 0.01-0.10 V). However, most values are between 0.01 V and 0.06 V, so this is a very conservative estimate of the day-to-day variability in voltage. The variability in voltage between piston displacements is primarily due to changes in friction along the inside surface of the cylinder. It is speculated that with no weight on the piston, the force helping to counteract the frictional forces is absent, resulting in larger variability between piston displacements. The variability between piston displacements and across days was generally within the tolerated variability of 0.1 V, therefore the new hydraulic cylinder was considered acceptable for use with the KLA in the current study.

2.1.2.2 Static Calibration

A static calibration procedure was performed to determine the force-voltage relationship for the hydraulic cylinder. This experiment was also used to determine the effect of room temperature on calibration, since the MR scanner room is maintained at 18 °C, while the lab where the calibration is performed is maintained at 23 °C.

The position of the piston was held constant while calibration weights of 0 kg, 3 kg, 5 kg, 10 kg, 15 kg and 20 kg were applied sequentially to the top of the piston (one repetition). These six weights represented the desired range of applied forces from the hydraulic cylinder (0 to 200 N). The hydraulic cylinder was allowed 20 s to relax between weight applications, after which the pressure transducer voltage was recorded. Six trials consisting of three repetitions each were performed at 18 °C and the entire protocol was repeated at 23 °C. The voltage for each calibration weight was averaged across repetitions for each trial and plotted against force (Figure 2-8).

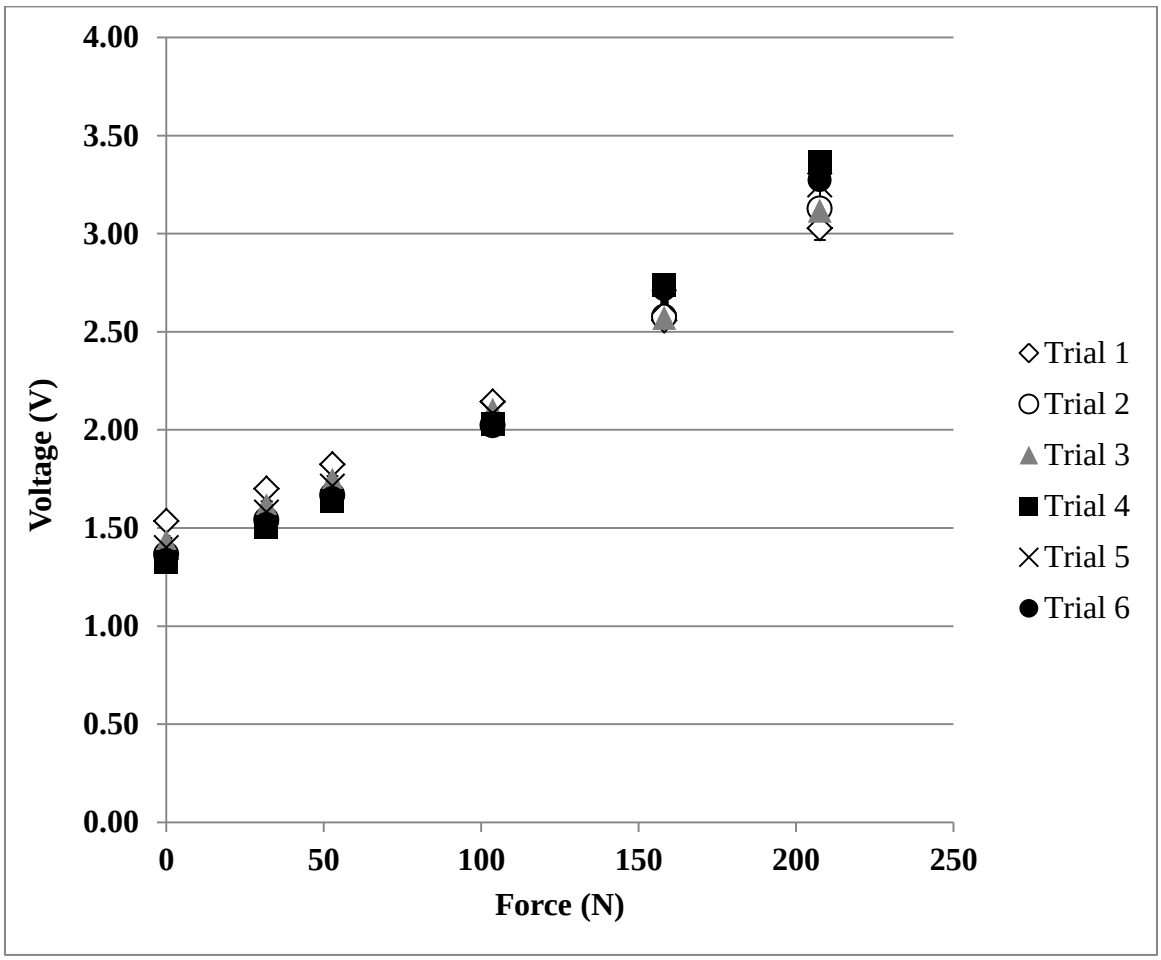

Figure 2-8: Pressure transducer voltage versus applied force with a fixed piston height at 18 °C. Each symbol represents one of 6 trials performed.

Linear regression was performed to obtain values for slope and intercept for each trial, and averaged across trials for each temperature. The slope and intercept of the force-voltage relationships for the hydraulic cylinder were statistically different between the two temperatures (α=0.05, Table 2-3). The slope of the force-voltage relationship was 0.08 ± 0.01 V/N at 18 °C, and 0.07 ± 0.01 V/N at 23 °C (p=0.005). The intercept was 1.30 ± 0.11 V at 18 °C, and 1.49 ± 0.07 V at 23 °C (p=0.006). The difference in intercept values exceeded the tolerated variability (0.1 V) for the hydraulic system. Therefore, the cylinder calibration was performed at 18 °C for

all future tests, and the hydraulic system was stored at 18 °C to ensure consistency between calibration in the lab and testing in the MR scanner.

Table 2-3: Average slope and intercept [mean(std)] for each temperature, obtained from linear regressions performed for each trial.

Temp (°C)	Slope (V/N)	Intercept (V)
18	0.08 (0.01)	1.30 (0.11)
23	0.07 (0.01)	1.49 (0.07)

To evaluate the effect of calibration variability on desired force output, the force-voltage equations for each of the six trials at 18 °C were used to calculate required voltage for 0 N, 30 N, 50 N, 89 N, and 133 N, which are the desired applied forces at the knee for the current research study. The voltages for each force level were averaged across trials ranging from 1.76 V for 0 N to 2.46 V for 133N (Figure 2-9). Paired t-tests (α=0.05) confirmed that all neighbouring force levels were significantly different from one another. These results indicated that it was reasonable to expect that the measured voltages for the chosen force levels were distinguishable, and therefore all force levels were used for testing.

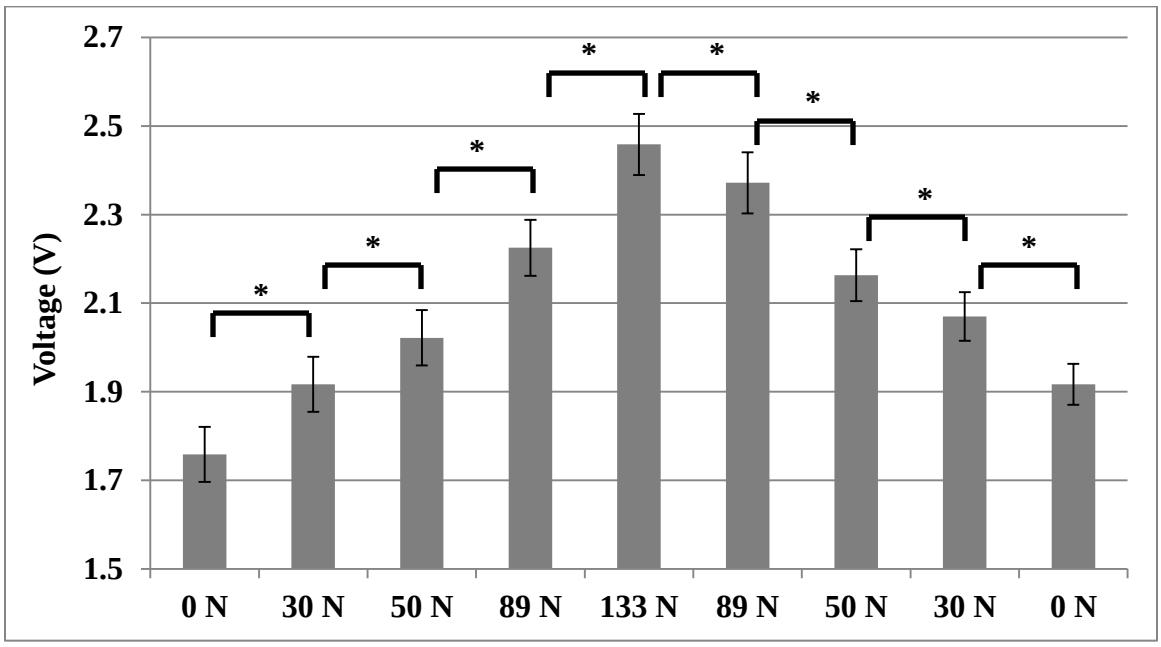

Figure 2-9: Average voltages (y-axis) and standard deviations (6 trials) required to produce desired force (x-axis) using hydraulic cylinder calibrations performed at 18 degrees Celsius. (* indicates significance at α=0.05).

2.1.2.3 Evaluation of Calibration Procedure

To independently verify the hydraulic cylinder calibration protocol, an S-type compression load cell (Model SSM-AJ-250, Interface, Scottsdale Arizona) was used in conjunction with the KLA. The approach consisted of two parts: 1) a static calibration of the compression load cell and hydraulic cylinder to verify force output from the hydraulic cylinder, and 2) a dynamic calibration procedure with a human participant to simulate the KLA testing protocol. The acceptance criterion for the hydraulic cylinder calibration was to provide a force measurement within 5% of the "true" value (measured with the compression load cell) for calibration weights ranging from 10 to 20 kg. The weight range was chosen to represent applied forces to the knee of 89 and 133 N, which are clinically relevant and provide the most reliable measures of passive knee laxity (Daniel et al., 1985; Stratford et al., 1991).

First, the hydraulic cylinder (Figure 2-10) and compression load cell (Figure 2-11) were calibrated separately to determine the force-voltage relationship using known weights (0 kg, 3 kg, 5 kg, 10 kg, 15 kg, and 20 kg).

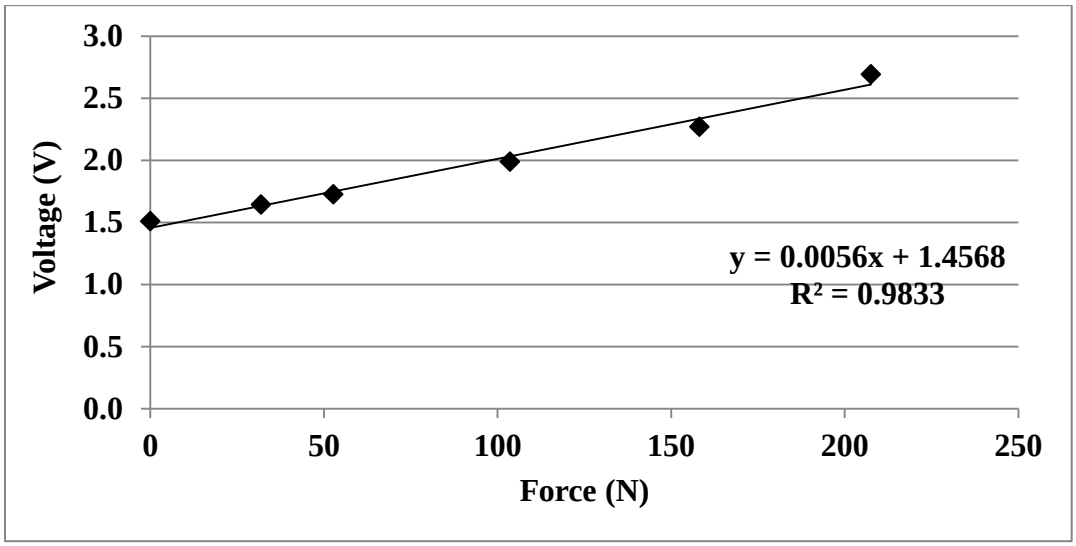

Figure 2-10: Force-voltage relationship for the hydraulic cylinder showing linear regression equation.

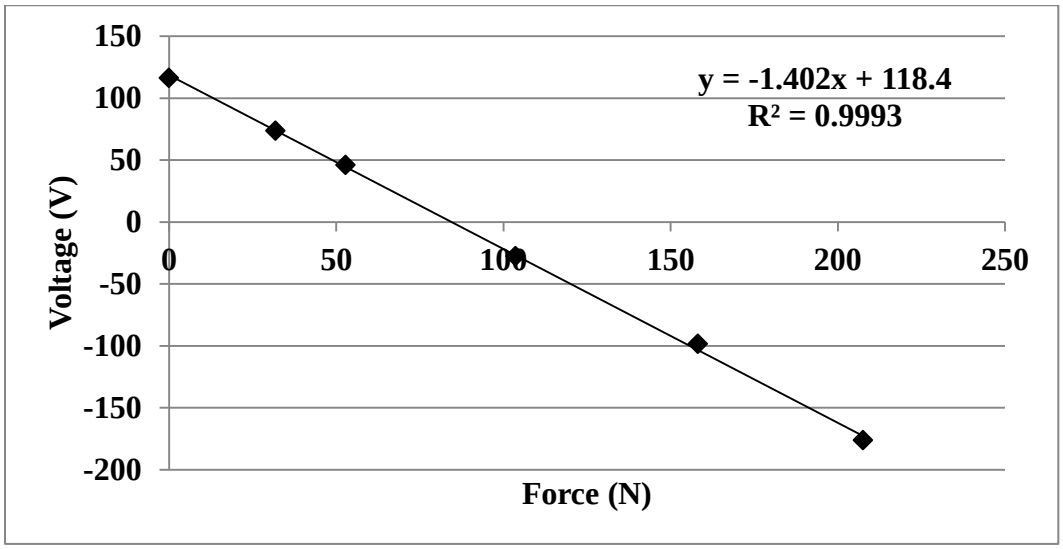

Figure 2-11: Force-voltage relationship for compression load cell showing linear regression equation.

The compression load cell was then mounted between the hydraulic cylinder and the KLA shank support (Figure 2-12). Calibration weights (0 kg, 3 kg, 5 kg, 10 kg, 15 kg, and 20 kg) were hung from the shank support at a known distance from the shank support hinge while voltages from the hydraulic cylinder and the compression load cell were recorded simultaneously. The force applied to the system was calculated using force and moment balance equations based on a free body diagram of the KLA (Section 4.3.2.1). The force for each of the compression load cell and hydraulic cylinder was calculated using the force-voltage relationship obtained during calibration. The force values for the calculated force (KLA) and the force measured from the hydraulic cylinder were within 5% of the force measured from the compression load cell ("true" value) for the specified weight range (10 to 20 kg, range 0.6-4.9%), except for 10 kg unloading for the hydraulic cylinder, which was 9.9% (Table 2-4). Therefore, the design criterion was satisfied for the KLA hydraulic cylinder static calibration.

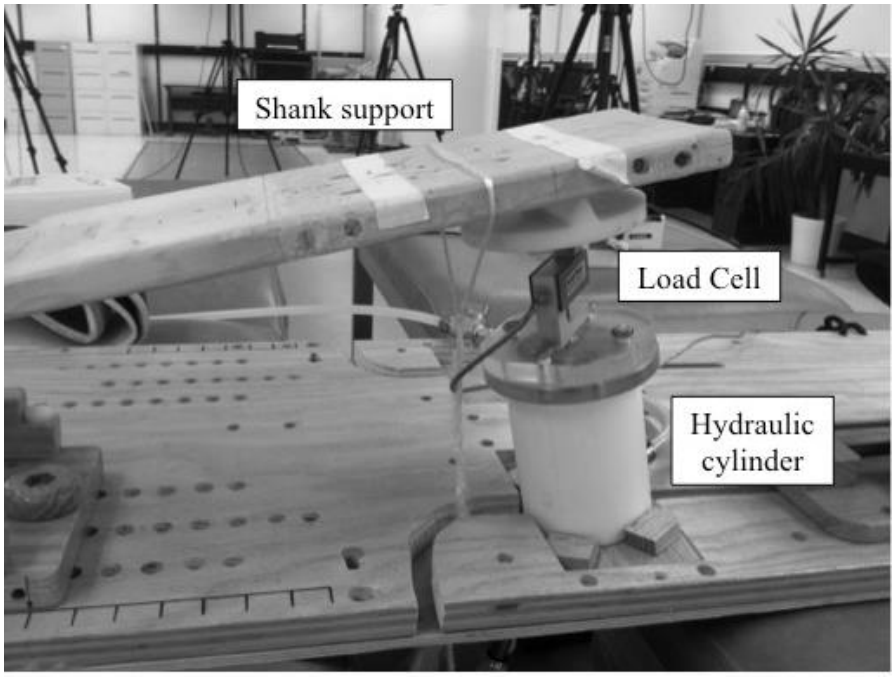

Figure 2-12: Compression load cell mounted between the hydraulic cylinder and shank support of the KLA.

Table 2-4: Comparison of force measured by compression load cell, calculated force applied (KLA), and force measured by hydraulic cylinder. Differences between the calculated force applied and the load cell, and the hydraulic cylinder and the load cell are shown.

Calibration Weight (kg)	Load cell (N)	Force Applied (N)	% Difference (Force Applied - Load Cell)	Hydraulic Cylinder (N)	% Difference (Hydraulic Cylinder - Load Cell)
0	10.60	13.55	27.8	24.77	133.6
3	36.91	41.36	12.1	46.11	24.9
5	54.26	59.78	10.2	61.15	12.7
10	100.55	104.33	3.8	102.40	1.8
15	145.15	147.55	1.7	143.67	-1.0
20	194.23	195.32	0.6	195.90	0.9
15	148.42	147.55	-0.6	155.76	4.9
10	102.62	104.33	1.7	112.82	9.9
5	55.93	59.78	6.9	68.93	23.2
3	37.73	41.36	9.6	51.03	35.3
0	10.69	13.55	26.8	24.01	124.6

The second phase of the validation involved verifying the hydraulic cylinder calibration protocol during a dynamic testing scenario. To accomplish this component, a human volunteer was positioned in place within the KLA with the compression load cell mounted in parallel with the hydraulic cylinder. The hydraulic piston was incrementally raised and lowered, with voltages simultaneously recorded from both the hydraulic cylinder and the load cell. The force-voltage relationship from the static calibration was applied to the hydraulic cylinder to calculate force (Figure 2-10). The percent difference in hydraulic cylinder force compared to compression load cell force ranged from 175% to 220% during raising, and 103% to 414% during lowering (Figure 2-13). Furthermore, the cylinder force jumped substantially (265 N) from the first to the second height of the piston. Similarly, the force dropped significantly (361 N) as the system switched from being raised to being lowered. Clearly, the design criterion (within 5%) for the hydraulic

cylinder was not met, and it was concluded that the static calibration does not apply to the hydraulic cylinder when it is used dynamically to apply force to a human leg.

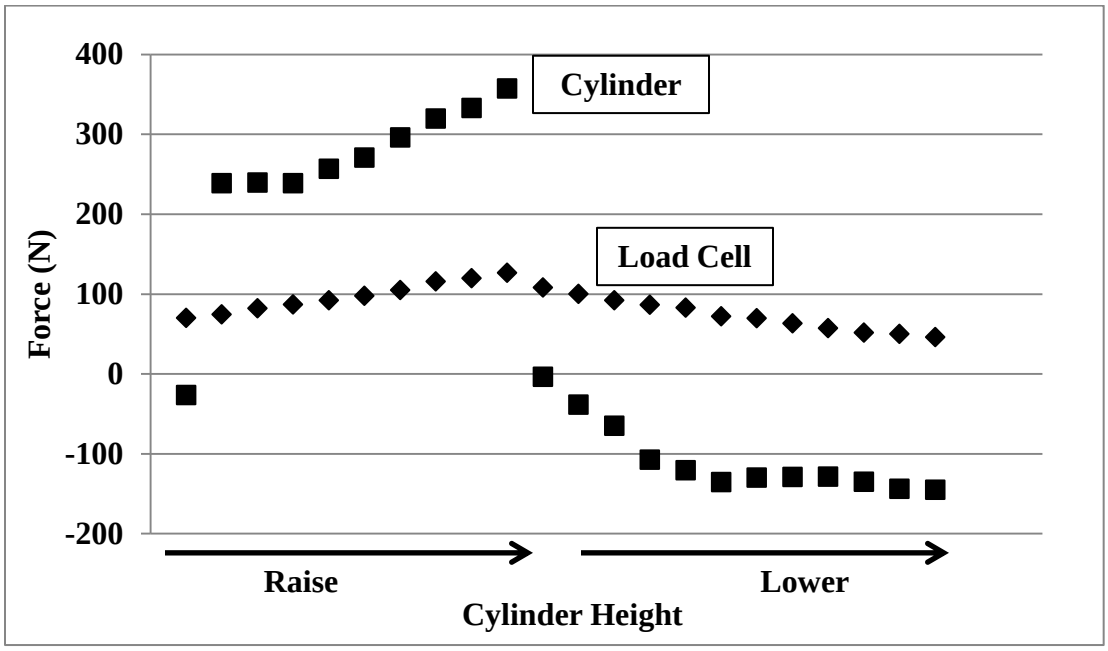

Figure 2-13: Force calculated from the hydraulic cylinder and compression load cell as the hydraulic piston is raised and lowered incrementally with a human volunteer in the KLA.

A second calibration approach was developed to replace the static calibration. A new force-voltage curve for the hydraulic cylinder was generated using the force values from the load cell (Figure 2-13) and the voltage values from the cylinder during the dynamic test described above. Linear regression produced an r-squared value >0.95 indicating an excellent fit (Figure 2-14).

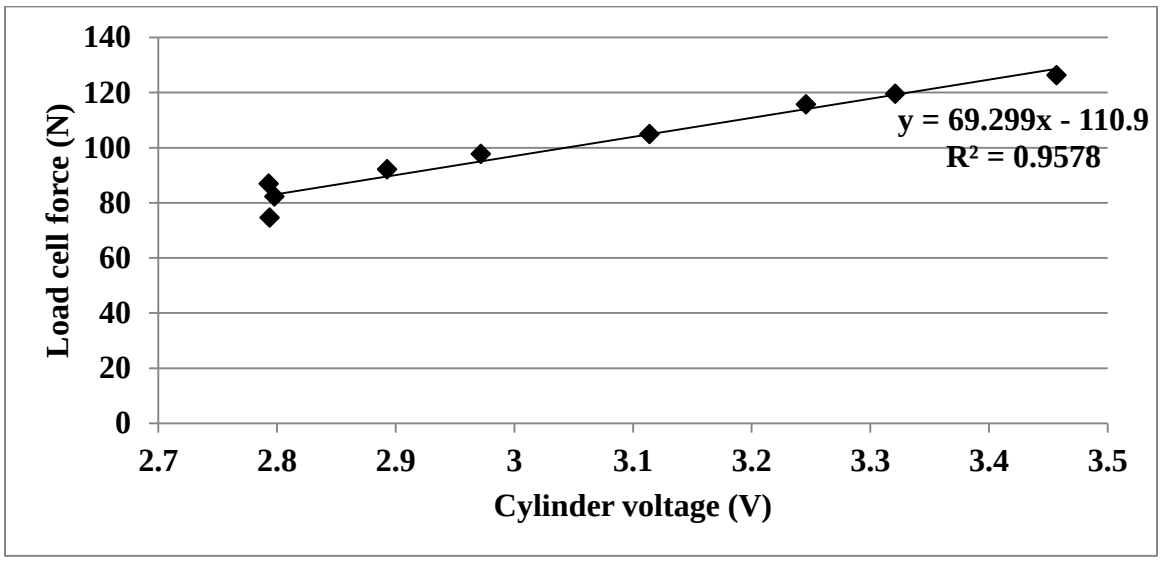

Figure 2-14: Force calculated from the compression load cell plotted against voltage measured from the hydraulic cylinder during a dynamic test with a human volunteer. The linear regression line is shown with the corresponding equation.

The dynamic experiment was repeated by raising and lowering the hydraulic piston with the human volunteer used previously strapped into the KLA. Using the linear regression equation from Figure 2-14, the force from the hydraulic cylinder was calculated and compared with the force from the compression load cell (Figure 2-15). The percent difference in hydraulic cylinder force compared to compression load cell force ranged from 2.3% to 8.9% in the 100 to 150 N range during raising, a marked improvement over the previous results using the static calibration equation (Figure 2-13). Although the acceptance criterion for the hydraulic cylinder was not achieved during the dynamic calibration, the hydraulic cylinder force was within 10% of the true value (compression load cell) and was deemed satisfactory for the current study.

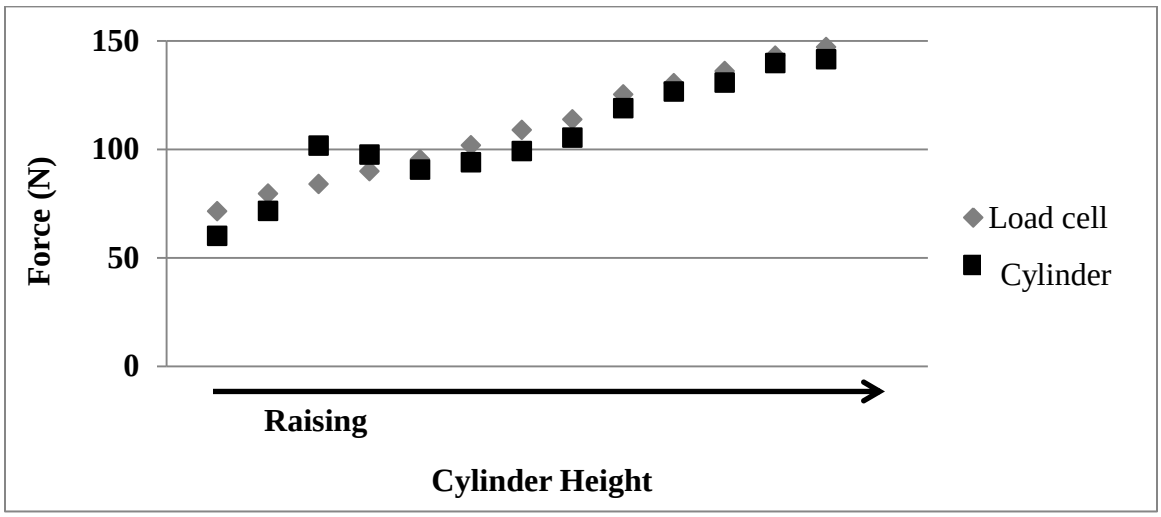

Figure 2-15: Force calculated from the hydraulic cylinder (using load cell calibration) and the compression load cell as the hydraulic piston is raised incrementally with a human volunteer in the KLA.

The repeatability of the new approach for calibrating the hydraulic cylinder (using the compression load cell) was assessed by repeating the entire calibration procedure three times. This method of calibration was highly repeatable, with the R^2 values for the linear regression for both raising (R^2 = 0.9497) and lowering the cylinder (R^2 = 0.9986) were >0.94 indicating an excellent fit (Figure 2-16).

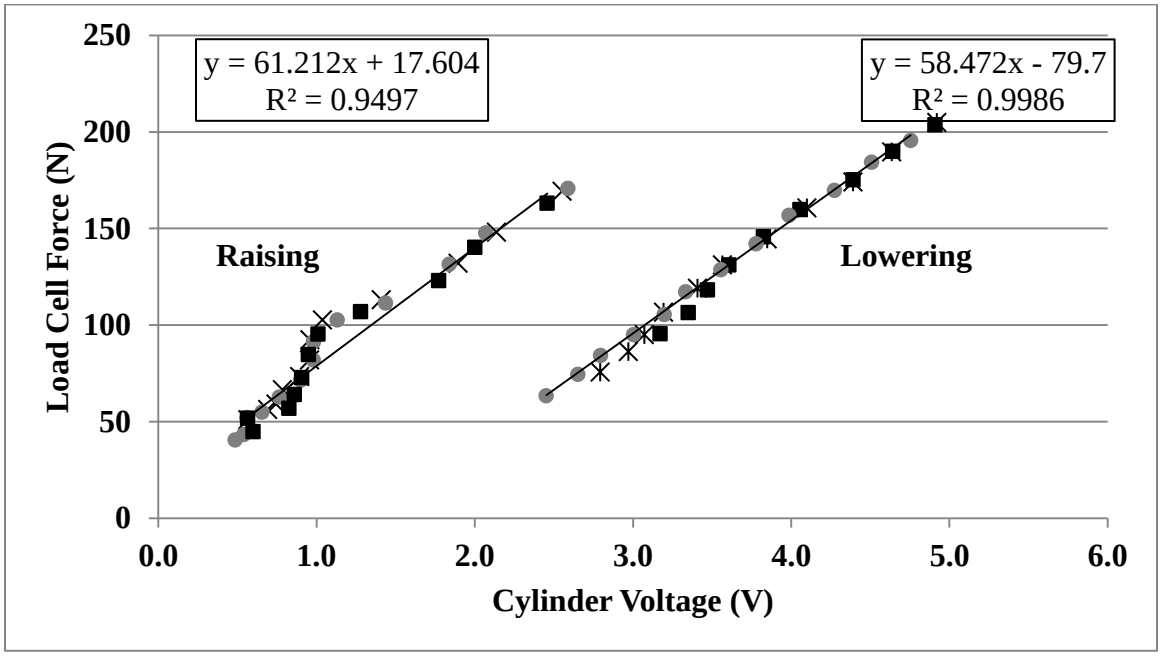

Figure 2-16: Force calculated from the compression load cell plotted against voltage measured from the hydraulic cylinder during 3 dynamic tests with a human volunteer. The linear regression line is shown with the corresponding regression equation.

From the tests above it was determined that a dynamic calibration was required for the hydraulic cylinder, using the compression load cell to generate a force-voltage relationship. Since the compression load cell was not MR safe, this calibration was performed for each participant in the motion analysis laboratory prior to load application in the MR scanner. The load cell was then removed from the KLA for MR imaging.

Numerous additional improvements were made to the KLA, during the course of this research. These improvements and corresponding outcomes are summarized as follows (Table 2-5).

Table 2-5: List of improvements made to KLA

Improvement	Outcome
Shank support widened	KLA can accommodate wider range of participants
Constant 18 V power source	Eliminates error associated with variable power output from batteries and eliminates need to change batteries
Replaced pressure transducer	Pressure transducer operating in optimal range
Replaced hydraulic tubing	Polyethylene tubing clear so that air bubbles and debris can be seen
Created quick disconnect for hydraulic cylinder	Ability to detach hydraulic cylinder for cleaning and re-lubrication without emptying entire system
New hydraulic cylinder material	Cylinder manufactured from Delrin® which is compatible with isopropyl alcohol and will not degrade
New o-rings and lubrication for hydraulic cylinder	O-ring size optimized for low friction movement, and silicone lubrication to provide smooth cylinder motion
Improved thigh straps	Elastic thigh straps replaced with rigid straps to limit movement of thigh during KLA force application
Cylinder temperature dependence controlled	Hydraulic system stored and used in constant temperature to reduce error associated with temperature difference between lab and MR scanner
Dynamic calibration	Cylinder calibrated dynamically using a compression load cell and participants

2.2 Coordinate Transformations

A key component of the current study is the linkage between passive laxity measures within the MR scanner and dynamic stability measures using motion analysis. This requires a common representation of the local coordinate system (LCS) used to identify joint orientations and translations between measurement systems. In the current study, the LCS is created using bone

geometry from MR images. The LCS and kinematic data are then described in the same coordinate system through the use of a transformation matrix for application to the finite helical axis (FHA). The coordinates of three markers on the femur are used to determine the transformation matrix between the two coordinate systems with the technique described by Soderkvist and Wedin (1993). This technique uses a least squares approach to minimize the error associated with the marker positions (Section 3.3.3.1). Results from previous research within our group suggested that there is a potential for high singular value decomposition (SVD) residuals from the transformation (~6 mm), which can cause inaccuracies in the FHA outcome measures (Fjeld, 2007). Therefore, this series of pilot studies aimed to reduce the error associated with the transformation between the motion analysis and MR scanner coordinate systems. Two key variables were investigated: positioning of the limb, and of the markers.

2.2.1 Limb Positioning

One identified source of error was the difference in body position between the motion analysis system (standing in full knee extension) and the MR scanner (supine in 30° knee flexion). To reduce error due to limb positioning, a supine neutral trial (30° knee flexion) was incorporated into the motion analysis data collection.

An experiment was performed to quantify the repeatability of positioning a participant in a supine position with 30° of knee flexion. Three markers were placed on a healthy volunteer's thigh (medial femoral epicondyle, lateral femoral epicondyle, and superior patella) and an additional marker was placed on the greater trochanter to create the LCS. Three additional markers were placed on the tibia (superior to the lateral malleolus, anterior tibia, and lateral proximal tibia) to transform the LCS for each trial. To determine the repeatability of positioning, the volunteer mounted a physiotherapy bench in the centre of the motion analysis capture volume

and the knee was positioned in 30° flexion with a support under the leg. An arthrometer was used to verify the knee flexion angle. A two second motion capture trial was taken, after which the volunteer dismounted the bench. This procedure was repeated fifteen times (markers were left on between trials).

To calculate the coordinate system, the flexion extension axis (z-axis) of the LCS was defined as the vector between the femoral epicondyle markers. The longitudinal axis (x-axis) was defined as the vector between the centre of the femoral epicondyle markers and the hip marker. The cross-product of the z and x axes was determined to obtain the third anterior-posterior axis (y-axis).

Marker coordinates were transformed into the LCS and averaged across trials (Figure 2-17). In the frontal plane, the mean position of the superior patella marker was -24.49 ± 1.60 mm in the proximal/distal direction, and -9.08 ± 2.11 mm in the medial/lateral direction. The mean position of the medial epicondyle marker was 0.87 ± 1.40 mm in the proximal/distal direction, and 64.13 ± 1.12 mm in the medial/lateral direction. The mean position of the lateral epicondyle marker was 0.93 ± 0.97 mm in the proximal/distal direction, and -64.68 ± 1.34 mm in the medial/lateral direction. The maximum standard deviation between trials due to repositioning was 2.11 mm for the medial/lateral position of the superior patella.

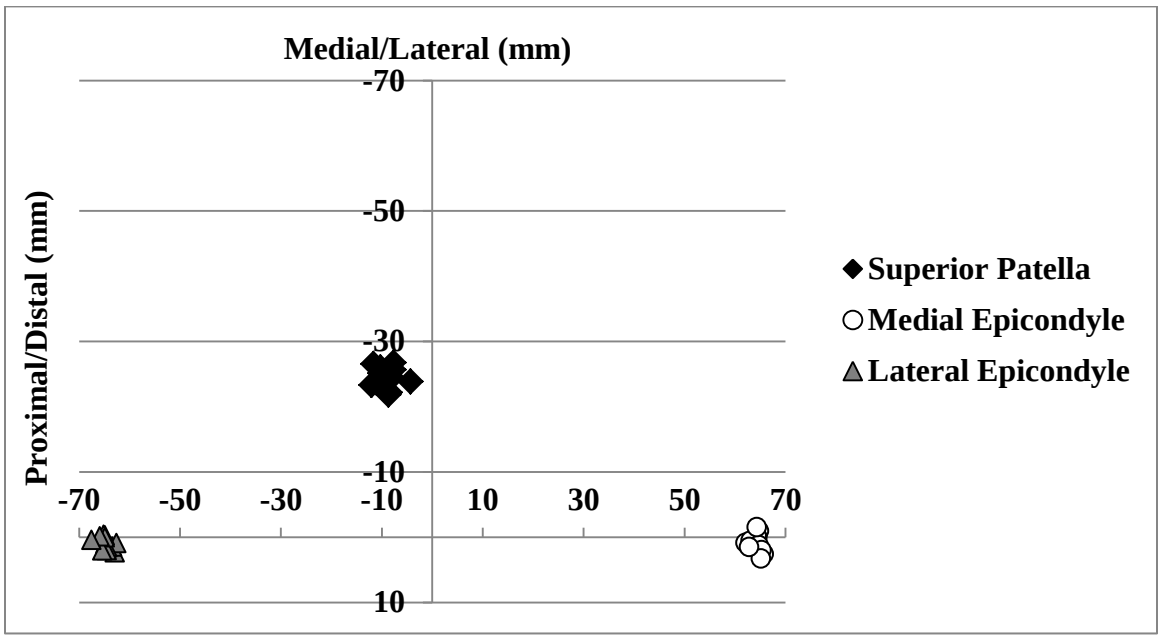

Figure 2-17: Proximal/distal (y-axis) and medial/lateral (x-axis) marker positions (mm) for the superior patella, medial epicondyle, and lateral epicondyle during 15 supine repositioning trials (30° knee flexion).

In the larger research study, kinematic motion data was integrated with the femur geometry obtained from MR scans using coordinate transformations. Singular value decomposition (SVD) residuals provide an idea of the amount of marker movement between kinematic testing and MR scanning. A previous study had an average residual of 5.76 ± 2.12 mm in the ACLD group, and 6.11 ± 1.29 mm in the healthy group (Fjeld, 2007). In the current study, the modified neutral trial (supine) resulted in average residuals reduced by 45% in the ACLD group (3.15 ± 0.85 mm), and 46% in the healthy group (3.27 ± 1.06 mm).

2.2.2 Marker Positioning

To reduce error associated with the coordinate transformation between the motion analysis lab and the MR scanner, the three markers on the femur should not be removed between locations. However, to allow for flexibility in scheduling study participants, it was desirable to have the

option to remove and replace the markers between data acquisition sessions. Two main sources of error associated with marker position were identified: 1) marker movement relative to the joint due to an altered limb position, and 2) positioning error introduced by removing and replacing the markers. Therefore, an experiment was performed to determine the magnitude of both identified sources of error.

The same marker set-up and volunteer for the supine neutral positioning experiment was used for the current experiment. To determine the influence of altered limb position, the volunteer mounted a physiotherapy bench in the centre of the motion analysis capture volume and assumed a supine position with their knees in full extension. A two second motion capture trial was taken, after which the volunteer dismounted the bench. This procedure was repeated six times.

To assess the influence of positioning error associated with marker removal, the volunteer was positioned on the physiotherapy bench in a supine position with full knee extension. The three thigh markers were traced with a fine tip Sharpie® marker to enable marker replacement. A two second motion capture trial was taken, after which the three thigh markers were removed and the volunteer dismounted the bench. The markers were then replaced, using the traced lines to guide placement, and the procedure was repeated ten times.

The coordinates of the three thigh markers were transformed into the LCS using the technique described by Soderkvist and Wedin (1993). The marker coordinates (x,y,z) for the limb repositioning and marker replacement tests were averaged across trials. The maximum standard deviation between repositioning trials was 3.76 mm for the medial/lateral (z-axis) position of the medial epicondyle marker, and between marker replacement trials was 3.34 mm for the anterior/posterior (y-axis) position of the medial epicondyle marker (Table 2-6). To assess the additional variability introduced by removing and replacing the markers, the difference in

standard deviations was calculated ($StDev_{replacement}$ - $StDev_{repositioning}$). The additional variability (standard deviation) introduced by removing and replacing the markers did not exceed 1.00 mm (Table 2-6).

Table 2-6: Average x (proximal/distal), y (anterior/posterior), and z (medial/lateral) marker coordinates in the LCS for the repositioning and marker replacement trials [mean(std)].

		Repositioning (mm)	Marker replacement (mm)	StDev Difference (mm)
Superior Patella	**x**	-20.93 (0.81)	-21.98 (0.88)	0.07
	y	47.66 (1.32)	47.50 (0.89)	-0.43
	z	-7.74 (3.22)	-9.10 (3.10)	-0.12
Medial Epicondyle	**x**	-7.92 (1.12)	-9.07 (1.61)	0.49
	y	-1.68 (2.40)	-3.56 (3.34)	0.94
	z	53.06 (3.76)	50.37 (3.17)	-0.59
Lateral Epicondyle	**x**	0.87 (1.27)	0.65 (0.70)	-0.57
	y	2.24 (0.83)	3.21 (1.84)	1.00
	z	-59.08 (3.66)	-60.51 (3.02)	-0.63

2.2.2.1 Marker Coordinate Error Propagation

Kinematic data was described using the FHA in the current study. Location x and y describe the intersection point of the FHA with the midsagittal plane of the LCS, translation describes the translation along the FHA during a dynamic task, orientation describes the angle of the FHA with the mediolateral axis of the LCS, and dispersion describes the overall rotational movement of the FHA throughout a dynamic task (see Section 3.3.3.1). To understand the combined effect of error due to repositioning and marker replacement on FHA outcome measures, a simulation was performed using kinematic data from a single participant. A matrix of normally distributed noise [M_{noise}] with known amplitude was generated in Matlab 2010b (The MathWorks Inc., Natick, MA) using the 'randn' function, and added to the coordinates of the three thigh markers (superior patella, medial and lateral epicondyles) to simulate error in marker position due to limb

repositioning and marker placement. Normally distributed noise was chosen based on previous work simulating skin motion artefacts (Alexander and Andriacchi, 2001). The FHA code (see Section 3.3.3.1) was executed ten times with no other parameters being altered. This procedure was performed with noise amplitudes of 1 mm, 2 mm, 3 mm and 4 mm. FHA variables for each task (swing/squat) and phase (flexion/extension) were calculated and averaged over five repetitions and three trials. FHA outcomes with added noise produced similar means to the original results. For example, the original FHA location y was 20.19 mm during swing flexion, and the average FHA location y with added noise ranged from 20.25 – 20.48 mm (Table 2-7). However with increasing amplitude of noise, the standard deviation between trials of the results increased. The standard deviation on the average FHA location y value during swing flexion was 0.36 mm with a noise amplitude of 1 mm, and increased to 1.33 mm with a noise amplitude of 4 mm (Table 2-7).

The minimal detectable difference (MDD) is the minimum difference that can be reliably detected given the measurement precision at the chosen alpha. A one sample t-test was used to find the MDD at a significance level of α=0.05 for each amplitude of noise and each FHA outcome measure (Equation 2-2).

$$\boldsymbol{MDD = 2.262 * \frac{std}{\sqrt{10}}} \qquad \textbf{(Eqn. 2-2)}$$

The MDD increased with increasing noise amplitude for the majority of FHA measures, with the exception of location x for swing flexion and orientation for squat flexion, which were both largest for the 3 mm noise amplitude (Table 2-7). The MDDs for the 4 mm noise amplitude were 0.67 mm for location x, 0.95 mm for location y, 0.02 mm for translation, 1.11° for orientation, and 0.01° for dispersion during swing flexion (Table 2-7). The MDDs were similar for the extension phase of the swing, and for both phases of the squat.

Table 2-7: Average FHA measures for swing flexion and squat flexion with noise amplitudes of 1 mm, 2 mm, 3 mm, and 4 mm added to the coordinates of the 3 thigh markers. Minimal detectable differences (MDD) for each noise amplitude are shown. Expected differences in FHA measures between healthy and ACLD groups are shown based on the work of Fjeld (2007).

Swing Flexion						
Noise amplitude		**Loc x (mm)**	**Loc y (mm)**	**Trans (mm)**	**Orient (°)**	**Disp (°)**
Original	**mean**	-7.04	20.19	-0.80	27.13	1.18
1 mm	**mean (std)**	-7.09 (0.29)	20.25 (0.36)	-0.81 (0.01)	27.56 (0.42)	1.19 (0.01)
	MDD	0.21	0.25	0.01	0.30	0.01
2 mm	**mean (std)**	-7.05 (0.55)	20.65 (0.70)	-0.82 (0.01)	27.48 (0.80)	1.20 (0.01)
	MDD	0.39	0.50	0.01	0.57	0.01
3 mm	**mean (std)**	-7.35 (1.32)	20.28 (0.82)	-0.81 (0.02)	27.37 (1.09)	1.19 (0.01)
	MDD	0.94	0.59	0.01	0.78	0.01
4 mm	**mean (std)**	-6.92 (0.94)	20.48 (1.33)	-0.81 (0.02)	27.38 (1.56)	1.20 (0.02)
	MDD	0.67	0.95	0.02	1.11	0.01
Expected Difference		7.63	1.91	1.70	6.00	0.58
Squat Flexion						
Noise amplitude		**Loc x (mm)**	**Loc y (mm)**	**Trans (mm)**	**Orient (°)**	**Disp (°)**
Original	**mean**	0.47	14.36	-1.93	12.59	1.49
1 mm	**mean (std)**	0.42 (0.39)	14.40 (0.42)	-1.92 (0.01)	12.55 (0.23)	1.49 (<0.01)
	MDD	0.28	0.30	0.01	0.16	<0.01
2 mm	**mean (std)**	0.37 (0.62)	14.19 (0.51)	-1.92 (0.01)	12.59 (0.34)	1.50 (0.01)
	MDD	0.45	0.37	0.01	0.25	0.01
3 mm	**mean (std)**	0.13 (0.82)	13.94 (1.16)	-1.93 (0.01)	12.38 (0.63)	1.50 (0.01)
	MDD	0.58	0.83	0.01	0.45	0.01
4 mm	**mean (std)**	0.19 (1.02)	13.86 (1.26)	-1.93 (0.01)	12.61 (0.50)	1.50 (0.02)
	MDD	0.73	0.90	0.01	0.36	0.01
Expected Difference		4.04	7.40	1.30	2.60	0.88

The variability due to repositioning the participant was the dominant source of error, as the additional variability introduced by replacing the markers was minimal. Therefore, four mm of noise overestimates the variability introduced by repositioning the participant (3.76 mm) and removing and replacing the markers (3.34 mm, Table 2-6). The MDDs with a noise amplitude of 4 mm are well below the expected differences between healthy and ACLD groups, based on the work of Fjeld (2007). Therefore, it was concluded that the error introduced by limb repositioning and marker replacement would not affect the ability to detect significant differences between healthy and ACLD groups in the current study.

2.3 Pilot Studies Summary

A series of pilot studies were conducted prior to the main data collection for this research study to validate equipment used, and to improve upon existing data collection protocols.

The KLA is a device that uses a hydraulic system to apply an anterior force to the tibia to produce ATT. Fluid pressure developed in the KLA hydraulic system was measured in Volts using a pressure transducer, and converted to force (Newtons) based on a calibration relation. The KLA hydraulic system was redesigned to achieve higher accuracy in force application. The voltage variability in the hydraulic system between piston displacements and between days was within 2% (0.1 V) of the pressure transducer voltage range, meeting the design criteria. However, the static calibration procedure did not apply to the hydraulic cylinder when it was used dynamically to apply force to a human leg. A compression load cell was used to verify measured force values from the hydraulic system, and the percent difference in hydraulic cylinder force compared to compression load cell force ranged from 103% to 414%. Therefore, a dynamic calibration procedure was developed to replace the static calibration. The percent difference in hydraulic cylinder force compared to compression load cell force ranged from 2.3%

to 8.9% in the 100 to 150 N range. These results demonstrated a marked improvement over the static calibration, and the newly designed hydraulic cylinder was deemed satisfactory for use with the current study.

A key component of the overall research study is the linkage between passive laxity measures within the MR scanner and dynamic stability measures using motion analysis. This requires a common representation of the LCS, which is achieved through the use of a transformation matrix between the motion analysis and MR scanner coordinate systems. The effect of limb positioning and marker placement on the error associated with the transformation was investigated, and the effect on FHA outcome measures was evaluated.

The error introduced by limb repositioning and marker replacement did not exceed 4 mm. Error simulations were performed and concluded that the MDDs for FHA parameters in the current study are well below the expected differences between healthy and ACLD groups. Therefore, it was concluded that the error introduced by limb repositioning and marker replacement would not affect the ability to detect significant differences between groups in the current study. Furthermore, to reduce inaccuracies associated with the coordinate transformation between MA and MR scanner coordinate systems a supine neutral trial was introduced into the MA data collection protocol for the current study, which reduced average residuals by 45% in the ACLD group and 46% in the healthy group.

Chapter Three: **Dynamic Stability in Healthy Individuals**

One of the overall research goals of this project is to understand differences in dynamic stability between healthy and ACLD individuals using movement and muscle activity patterns. Therefore, several considerations have been made in the current chapter to allow for comparisons with an ACLD group in subsequent chapters. Two dynamic tasks were chosen to investigate these differences: the single leg squat and the seated leg swing. In order to interpret changes in dynamic stability due to ACL deficiency, it was important to first characterize these tasks in a healthy population. The current chapter uses the dominant limb of the healthy group to quantify differences between dynamic tasks. Another interesting aspect of the overall research project is differences between dominant and contralateral limbs in the healthy group, which is addressed in Chapter 4. The purpose of this study was to investigate differences in movement patterns and muscle activity patterns between the single leg squat task, and the seated leg swing in a healthy group. Movement patterns are investigated using the finite helical axis, and muscle activation patterns are analysed using a wavelet analysis technique.

3.1 Literature Review

3.1.1 Finite Helical Axis

Knee joint motion is typically described using translations and rotations about three axes embedded in the articulating segments of the knee joint. However, the resulting movement is highly dependent on the definition of these axes (Blankevoort et al., 1990). Furthermore, when movement is measured with motion analysis systems based on skin mounted markers, error is introduced by locating the external landmarks on which these axes are based (Benoit et al., 2006; Leardini et al., 2005). As an alternative, joint motion can be described using a helical axis approach in which motion is expressed with respect to a coordinate system embedded in one of

the bony segments (Blankevoort et al., 1990). Helical axis motion describes the displacement of a body from one position to another as a rotation about, and a translation along a screw axis (Figure 3-1). When applied to the knee, tibial motion can be expressed as a translation along and rotation about a helical axis embedded in the femur (Bull and Amis, 1998). Using the FHA approach, knee joint motion is not constrained to three pre-defined planes of motion as it is with a joint coordinate system approach. Rather, the FHA is defined in three-dimensional space based on the relative movement of the femur and tibia throughout a dynamic movement. Therefore, it is believed that the FHA may provide a truer representation of knee joint motion, especially in an ACLD joint where the axes of motion may be altered relative to a healthy knee joint.

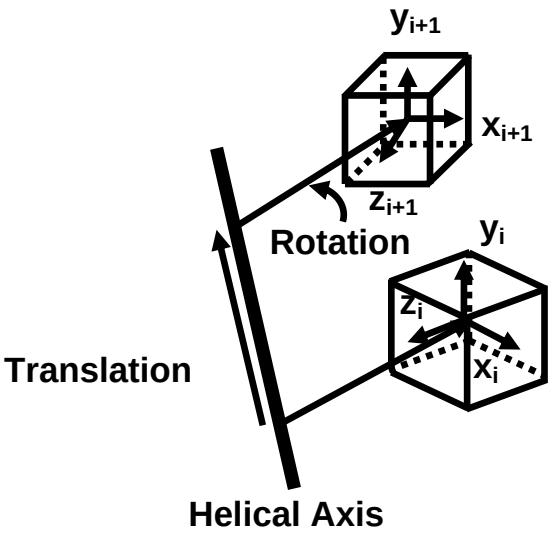

Figure 3-1: Movement of a 3D cube from postion (i) to position (i+1) described as a translation along, and a rotation about a helical axis (adapted from Kwon, 1998) with permission from Fjeld (2007)

To define the helical axis from the motion of two articulating segments, two parameters are calculated which describe the location and orientation of the FHA in 3D space. These parameters

include the unit vector ($\vec{n}$) and the radius vector of a point on the helical axis ($\mathbf{R_0}$) defined in the LCS. The following equations are used to define these parameters.

The rotation about the helical axis, ϕ can be found using the following equation, as described by Spoor and Veldpaus (1980):

$$\phi = \cos^{-1}\left(\frac{\text{trace}\,(R)\,-1}{2}\right), \qquad \textbf{(Eqn. 3-1)}$$

where **R** is the rotation matrix obtained from $\mathbf{T^{rel}}$, a transformation matrix relating the position of the tibia to the position of the femur. If this angle is negative, the vector $\vec{n}$ must be reversed so that ϕ remains positive.

The unit vector ($\vec{n}$) describes the direction of the helical axis in 3D space. It is computed from **N** which is calculated as follows:

$$N = \frac{R + R^{T}}{2} - \cos(\phi)I, \qquad \textbf{(Eqn. 3-2)}$$

where **I** is a 3 x 3 identity matrix. **N** contains three column matrices:

$$N = [\{\vec{n}_1\}\{\vec{n}_2\}\{\vec{n}_3\}], \qquad \textbf{(Eqn. 3-3)}$$

and $\{\vec{n}_1\}$, $\{\vec{n}_2\}$, and $\{\vec{n}_3\}$ are all parallel to $\vec{n}$. The normal of the unit vector along the helical axis is then calculated as follows:

$$\vec{n} = \frac{1}{|\vec{n}_{max}|}\vec{n}_{max}. \qquad \textbf{(Eqn. 3-4)}$$

The location of the helical axis in 3D space is determined as the smallest vector from the LCS origin to the helical axis. This vector (**R_0**) is perpendicular to the helical axis and is defined as follows:

$$R_0 = -\frac{1}{2}\vec{n}\times(\vec{n}\times d) + \frac{\sin\phi}{2(1-\cos\phi)}\cdot\vec{n}\times d, \qquad \textbf{(Eqn. 3-5)}$$

where **d** is the translational component of the transformation matrix, $\mathbf{T^{rel}}$. $\mathbf{R_0}$ is the radius vector of a point on the helical axis and together with the unit vector $\vec{n}$, completely defines the helical axis within the LCS. The denominator of the second term in Equation 3-5 ($1-\cos\phi$) suggests that as ϕ approaches zero (*i.e.*, for small rotations), $\mathbf{R_0}$ approaches infinity. Therefore, the FHA is not uniquely defined in the case of pure translation, and must be avoided.

FHA error is sensitive to small rotation angles (Woltring et al., 1985), which is often solved by using a larger step size between data points. The current study uses a reference position (90° of knee flexion) to calculate the FHA at each time point. This approach provides a sufficiently large angle between the angle of interest and the reference position to reduce error and to allow for a continuous calculation of the FHA. Using this approach, interpretation of the FHA must take into account the reference position, as it will affect the overall location of the FHA. However, this technique allows for robust comparison both within and between subjects.

In the current study, the FHA is used to quantify differences in knee joint stability between two dynamic tasks in a healthy population. For this purpose, seven parameters are used to quantify the FHA during dynamic movement (described in Section 3.3.3.1). The location and orientation of the helical axis within the knee joint, and how the axis translates and rotates throughout a dynamic task provides an understanding of healthy dynamic knee joint stability.

3.1.2 Wavelet Analysis

The muscular system is responsible for movement of the human body. Therefore, to understand changes in movement patterns relating to dynamic joint stability, it is of interest to understand muscle activation. Electromyography (EMG) is the study of motor unit action potentials (MUAPs) through the recording of a myoelectric signal. The EMG signal provides important information about the timing and amplitude of a muscle's activity during the dynamic tasks of interest in this study. EMG can be analysed with respect to time, often using a threshold limit, to examine the onset, offset and duration of a muscle during a task. To analyse signal amplitude, root mean squared values or a rectified signal are most often used (Basmajian and De Luca, 1985; De Luca, 1997; Farina and Merletti, 2000). The EMG signal also contains valuable information about the frequency content of the signal. It has been shown that motor units are recruited from slow to fast muscle fibres in response to muscle force requirements (J. Wakeling et al., 2002a). Therefore, information regarding EMG signal frequency may be helpful in relating muscle patterns to specific functions aimed at providing dynamic knee joint stability.

An approach developed by von Tscharner (2000) allows the signal to be analyzed simultaneously in both the time and frequency domains. The wavelet transform uses a series of wavelets of varying frequencies to separate the frequency content of the EMG signal into the frequency bands specified by the wavelet. The intensity of the wavelet transform is then calculated, representing the power of the EMG signal within the frequency band at each time point. This results in a 3D plot for each muscle with frequency band, time and intensity as the axes.

Several factors affect the magnitude of the EMG signal including electrode placement, muscle type, and thickness of tissue between the muscle and the electrode (De Luca, 1997). Therefore, in order to compare muscle intensities between muscles, individuals, and over time within

individuals, the EMG signal must be normalized. The procedure of normalizing an EMG signal involves choosing a reference contraction for the desired muscle, and dividing the magnitude of the signal for that same muscle by the magnitude of the reference contraction. The EMG signal is then expressed as a percentage of the reference value. Most commonly, it is suggested that the reference value be obtained from an isometric maximum voluntary contraction (MVC, Burden, 2010). However, it has been shown that the ability to perform a true MVC is greatly affected by pain (Benoit et al., 2003). Therefore, it is unlikely that injured (ACLD) participants could perform a true MVC following injury. Several studies involving ACLD participants have used MVCs for EMG normalization, but report using the maximum signal from either the MVC *or* the dynamic trial, indicating not all participants were able to perform a true MVC (Chmielewski et al., 2005; Hurd and Snyder-Mackler, 2007). An alternative to the MVC is to use a sub-maximal isometric contraction as the reference contraction. In fact, DeLuca (1997) suggested that using EMGs from contractions less than 80% of the MVC provide a more stable reference value.

Since the overall research study involves ACLD participants, the current study used a dynamometer (Biodex Medical Systems, Inc., New York USA) to perform sub-maximal MVCs for EMG normalization. Torque values were chosen based on isometric contractions reported by Zatterstrom (2000) for a group of ACLD individuals three months post-injury. Two levels were chosen, 50% and 80% of the reported MVCs, to ensure that all participants could perform at least one level. Torque values of 70 Nm and 105 Nm were used for extension (quadriceps), and 35 Nm and 50 Nm were used for flexion (hamstrings).

Quantitative measures were required to determine differences in muscle activation between dynamic tasks in the healthy group. The total intensity of the myoelectric signal is equal to the sum of the intensity for each wavelet, at each time point, resulting in a plot of total intensity over

time (Figure 3-2). Wavelets 1 and 13 were omitted from the analysis, as these frequency bands represent the motion artefact from the electrodes on the skin (wavelet 1), and the high frequency range that is most likely noise picked up in the system (wavelet 13). von Tscharner (2000) stated that the sum of total intensity over time approximates the usual description of power. Therefore, the area under the total intensity curve can be described as a measure of muscle power (Figure 3-2). Muscle intensity and power are used in the current study to describe the myoelectric signal in terms of muscle activation over time.

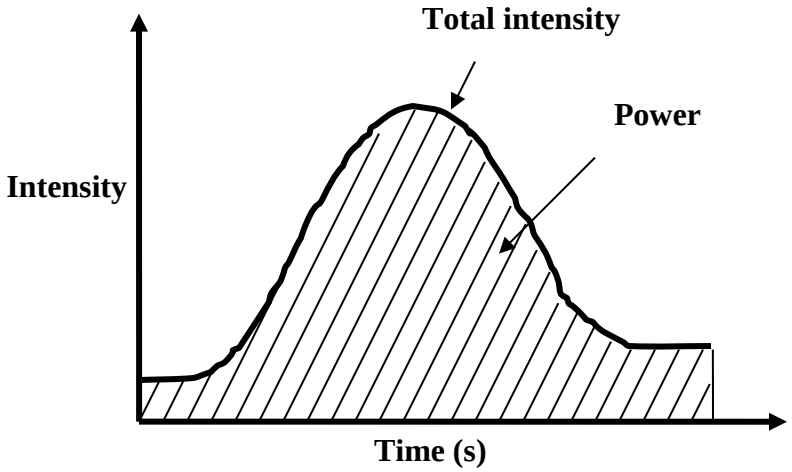

Figure 3-2: Schematic of a muscle intensity curve representing the total intensity of the signal and showing the area under the curve, which represents the integral of the total intensity over time or the muscle power, adapted from Fjeld (2007)

3.1.3 Dynamic Tasks

Typically, gait analysis is used to identify differences in movement patterns between healthy and injured individuals. As gait is an activity of daily living the advantage of using this task is that any identified differences are accountable to routine joint function (Kutzner et al., 2010; Mündermann et al., 2008; Yoshida et al., 2006). However, because walking is a relatively low demand activity with minimal rotational loading on the knee joint, 3D movement patterns during

gait may not be greatly affected following ACL injury. In support of this, a study by Sato et al. (2013) found significant correlations between passive knee laxity and maximum internal tibial rotation during a side-step cutting maneuver, but these correlations were not significant in low demand activities such as walking. Therefore, in the current study specific open and closed chain kinetic tasks were chosen for diagnostic purposes to dynamically assess the ACLD knee joint.

The term "kinetic-chain" was first applied to the human body by Steindler (1955). He observed that when a linkage (*i.e.*, arm or leg) is met with significant resistance, muscle activity and movement patterns are significantly different than when the linkage is free to move at the distal end. Therefore, the most distal limb segment being free to move defines an "open-chain" exercise, and the most distal limb being fixed defines a "closed-chain" exercise (Palmitier et al., 1991). During closed-chain exercises, the foot is fixed to the floor, and knee motion is achieved using a combination of movement at the ankle and hip joints. It has been shown that closed-chain exercises reduce anterior tibial displacement and anterior shear force on the knee, and are therefore believed to be a safer option than open-chain exercises for rehabilitation after ACL rupture (Henning et al., 1985; Lutz et al., 1993; Palmitier et al., 1991; Yack et al., 1993). Furthermore, closed-chain weight-bearing exercises are known to produce increased co-contraction of the quadriceps, hamstrings and gastrocnemius muscle groups, which is thought to reduce the strain on the ACL (Kozánek et al., 2011). Compared to closed-chain exercises, open-chain exercises exhibit decreased muscle co-contraction and increased anterior tibial shear force on the knee. Therefore, it is expected that closed-chain exercises would highlight changes in muscular control patterns due to ACL rupture, while open-chain exercises would highlight changes in joint movement patterns, both resulting in altered dynamic knee joint stability.

For the overall research study, two dynamic tasks were chosen to investigate differences in dynamic joint stability between the healthy and ACLD groups: the single legged squat and the seated leg swing. The single legged squat is a loaded, closed-chain task expected to introduce a component of stability, resulting in increased overall joint movement (*i.e.*, increased FHA translation and dispersion). In contrast, the seated leg swing is an unloaded, open-chain task with movement primarily in the sagittal plane controlled via quadriceps contraction. An extensive literature review on ACLD kinematics did not identify any studies using a single-legged squat task for investigating differences in ACLD movement patterns. Similar tasks used in related studies include: step up and step down (Brandsson et al., 2001; Gao and Zheng, 2010; Isaac et al., 2005; Jonsson and Kärrholm, 1994; Kozánek et al., 2011), double-leg supported squat (Dennis et al., 2005; M. Logan, 2004a), quasi-static lunge (Defrate et al., 2006), and supine leg press (Scarvell et al., 2005, 2004). The single legged squat task is unique because it isolates the injured limb, forcing the participant to utilize stabilization strategies and not rely on the un-injured contralateral limb for stability. For the swing task, the closest tasks found for comparison were supine passive knee extension movements (Barrance et al., 2006; Isaac et al., 2005), or the swing phase of gait. The swing task was chosen for this study to investigate a less-constrained movement compared to the squat task. It was expected to be easily performed by all ACLD participants.

The FHA method and wavelet analysis approach were applied in the current study to investigate movement and muscle activity patterns in healthy individuals. Two dynamic tasks were chosen to investigate differences in dynamic joint stability between open and closed chain exercises.

3.2 Specific Aims and Hypotheses

Based on the above literature review, the following specific aim (SA1) was achieved to test hypotheses H1a-H1b.

SA1: Determining dynamic joint stability relations in healthy knee joints using the finite helical axis method and wavelet analysis of muscle patterns

The following hypotheses (H) will be tested in accordance with the above specific aim:

H1: Healthy participants will show differences in FHA measures and muscle power between the single leg squat task and the seated leg swing

H1a: The FHA will have a more anterior location in the tibiofemoral joint, and decreased translation and dispersion during the swing task relative to the squat task in healthy participants

H1b: The swing task will be quadriceps dominant indicated by an increased ratio of quadriceps to hamstring muscle power (QH ratio), while the squat task will exhibit co-contraction of the quadriceps and hamstring muscles in healthy participants

3.3 Methods

The methods used for participant testing are described in this section along with data processing and analysis techniques. Kinematic and EMG data collection during dynamic tasks is described in detail, as well as the MR imaging protocol to obtain participant-specific knee joint geometry for LCS definition. FHA determination and wavelet analysis techniques are covered, and the statistical approaches used to test the study hypotheses are outlined.

Ethical approval for all methods was obtained from the Conjoint Health Research Ethics Board of the Faculties of Medicine, Nursing and Kinesiology, University of Calgary. Motion

assessment was performed at the Clinical Movement Assessment Laboratory of the McCaig Institute for Bone and Joint Health and MR images were collected at the Seaman Family MR Research Centre.

3.3.1 Study Participants

Twelve healthy participants were recruited through the university community via posters and website advertisements and tested for this study. Written, informed consent was obtained from each participant prior to testing (Appendix A). Only females were included in this study to control for the effects of gender on knee joint laxity and motion (Biscević et al., 2005; Hollman et al., 2003; Kerrigan et al., 1998; Malinzak et al., 2001; Park et al., 2009). Furthermore, females are two to eight times more likely to rupture their ACL compared to males participating in the same sports (Anderson et al., 2001). Therefore, it was thought that females would provide a larger pool of potential study participants to recruit from.

3.3.1.1 Participant Inclusion/Exclusion Criteria

Healthy participants were required to have bilateral intact ACLs and no history of orthopaedic diagnosis, joint injury or surgery. Participants were required to be at least eighteen years of age in order to provide their own consent and to ensure skeletal maturity, and under forty years of age as the risk of OA degenerative changes increases after forty (Roos et al., 1995).

All participants in this study were less than 185 cm in height to ensure that a knee flexion angle of 30º could be achieved in the MR scanner. Participants were excluded if they had a body mass index (BMI) greater than 30 kg/m^2 to minimize error introduced due to soft tissue movement. Participants were not permitted in the study if they were pregnant (MR scanner safety restrictions) or postpartum within one year due to hormonal changes to ligament properties

(Charlton et al., 2001). Leg dominance was determined by asking the participant with which leg they would prefer to kick a soccer ball.

3.3.2 Data Acquisition

The current study aim was to understand dynamic joint stability relations in healthy individuals. Movement patterns (FHA) and muscle activity (wavelet) were used to quantify dynamic joint stability. The FHA was described relative to a joint coordinate system in the knee, determined from participant specific knee joint geometry (MR).

Data acquisition for the study was performed in two stages in the order presented below. First, kinematic testing and muscle activation (EMG) were measured as the participant performed the swing and squat tasks. Next, knee joint geometry was imaged using MR imaging to allow for the determination of an MR based anatomical coordinate system. Typically, kinematic testing was performed on one day, followed by MR imaging on the subsequent day. However, if scheduling allowed, testing could be performed on a single day.

3.3.2.1 Kinematic Testing

3D kinematic data was acquired using an eight-camera high speed video motion capture system (Motion Analysis Corporation, Santa Rosa, CA) collected at 120 Hz. The cameras were set-up to optimize the capture volume (1.0 m wide × 3.2 m deep × 2.0 m tall) for the dynamic tasks, while ensuring that each reflective marker was visible by at least three cameras (Figure 3-3). A wand of known dimensions (500.00 mm) was used to calibrate the capture volume (residuals: 0.74 ± 0.03 mm).

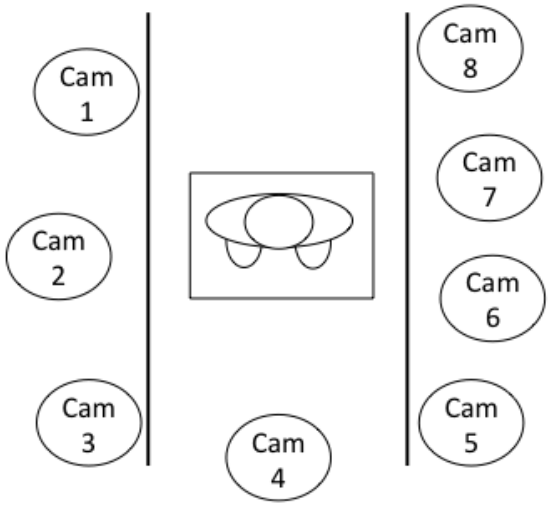

Figure 3-3: Camera set-up (overhead view).

Kinematic data was collected on both legs of all participants in order to investigate side-to-side differences within healthy participants (addressed in Chapter 4). Spherical reflective markers (20 mm diameter) were attached to the participant's skin with double-sided tape (Tesa Tape Inc., Charlotte NC, USA). Nine markers were used for dynamic trials with three markers on each segment (foot, shank and thigh). Segment markers were placed on the (a) fifth metatarsal, (b) supernavicular and (c) lateral calcaneus of the foot; (d) superior to the lateral mallelous, (e) anterior tibialis, and (f) proximal fibula of the shank; and (g) lateral femoral epicondyle, (h) anterior thigh and (i) greater trochanter for the thigh segment (Figure 3-4). The markers were placed in a manner to optimize marker distribution on each limb segment, while avoiding areas that would have large soft tissue movement relative to the bone. Four additional markers were placed around the knee to link the kinematic data with the MR images: (j) superior patella, (k) medial femoral epicondyle, (l) proximal medial tibia and (m) tibial tuberosity (Figure 3-4). These four markers along with the lateral femoral epicondyle and proximal fibula markers were used

during MR imaging to represent each segment (thigh and shank). The six markers around the knee were a smaller diameter (12 mm) to ensure adequate separation between markers (Figure 3-5). These bases of these six markers were traced following skin placement using a fine tip permanent marker to allow for marker replacement prior to MR imaging. The rubber marker material covered with reflective tape was visible in both the motion analysis and MR imaging systems.

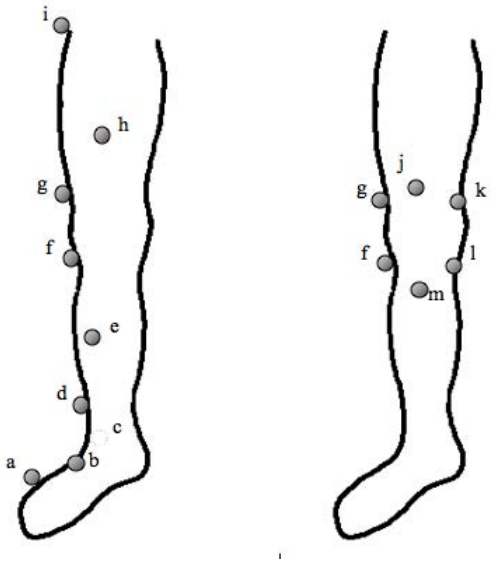

Figure 3-4: Segmental (left) and MR imaging (right) lower limb marker placement for 3D kinematic data collection. Segment markers were placed on the (a) fifth metatarsal, (b) supernavicular and (c) lateral calcaneus of the foot; (d) superior to the lateral mallelous, (e) anterior tibialis, and (f) proximal fibula of the shank; and (g) lateral femoral epicondyle, (h) anterior thigh and (i) greater trochanter for the thigh segment. An additional four markers, used with (g) and (f) for coordinate transformations between motion data and MR images, were placed around the knee on the (j) superior patella, (k) medial femoral epicondyle, (l) proximal medial tibia and (m) tibial tuberosity. Used with permission from Fjeld (2007).

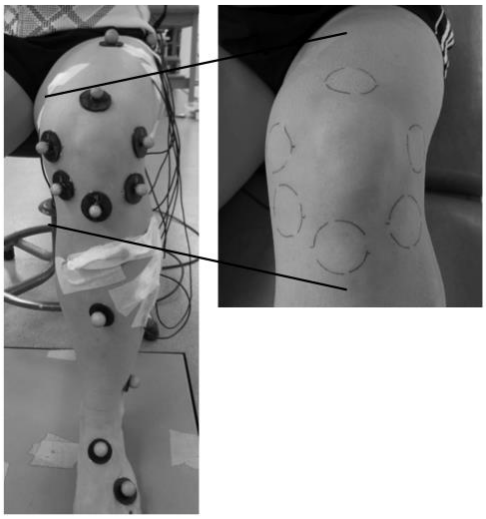

Figure 3-5: Six knee markers used to link kinematic data with MR images (left), shown with traced outlines of the markers (right) to allow for replacement prior to MR imaging.

EVaRT 4.0 software (Motion Analysis Corporation, Santa Rosa, CA) was used to collect motion data. Participants performed two dynamic tasks: a single legged squat and a seated leg swing. For the squat task, the participant stood on one foot and was told to bend at the knee to a comfortable depth while keeping their trunk upright (Figure 3-6). The depth of the squat was self-selected to ensure that the task could be completed safely within the strength and stability constraints of each individual. For the swing task, the participant was seated on an adjustable stool with their hip and knee positioned in 90º of flexion (Figure 3-7). The stool was adjusted such that the participant's foot did not touch the floor throughout the movement. Participants performed five continuous repetitions (single trial) from 90º of knee flexion to full extension (0º), and returning to 90º of knee flexion.

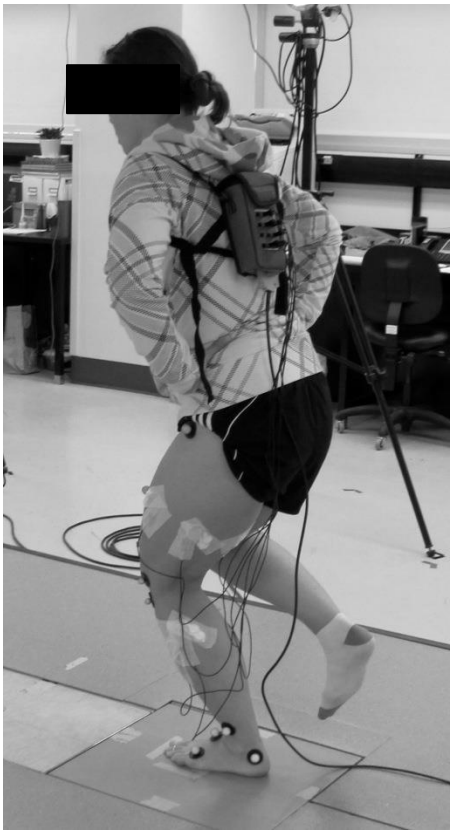

Figure 3-6: Participant performing the single-legged squat task.

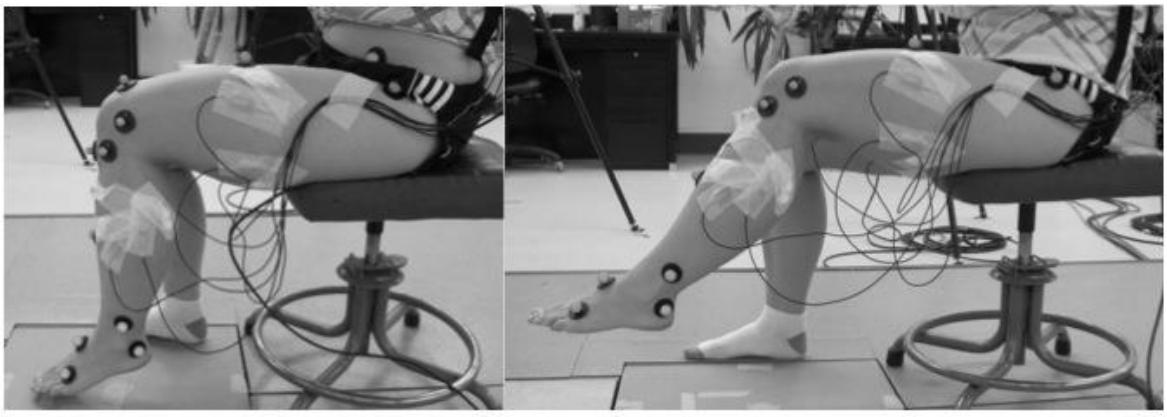

Figure 3-7: Participant preparing for swing task (left), and mid-swing (right).

For each task, three trials were completed to the beat of a metronome (1 beat/sec), resulting in one repetition (flexion and extension) every two s. One beat of rest was given between each

repetition to allow for a more controlled movement. Participants performed all tasks barefoot to eliminate the effects of different shoe types between participants.

Following the dynamic tasks, three neutral trials (two s) were acquired with all thirteen markers (Figure 3-8). The first neutral trial was obtained with the participant standing in alignment with the global coordinate system (GCS) to use as a reference for joint angle calculations. The second neutral trial was taken with the participant seated with the hip at 90º and the knee at 90º as a reference for the FHA calculations. The third neutral trial was taken with the participant lying supine with 30° of knee flexion to provide a linkage between the coordinate systems derived using the motion analysis and MR imaging systems, respectively.

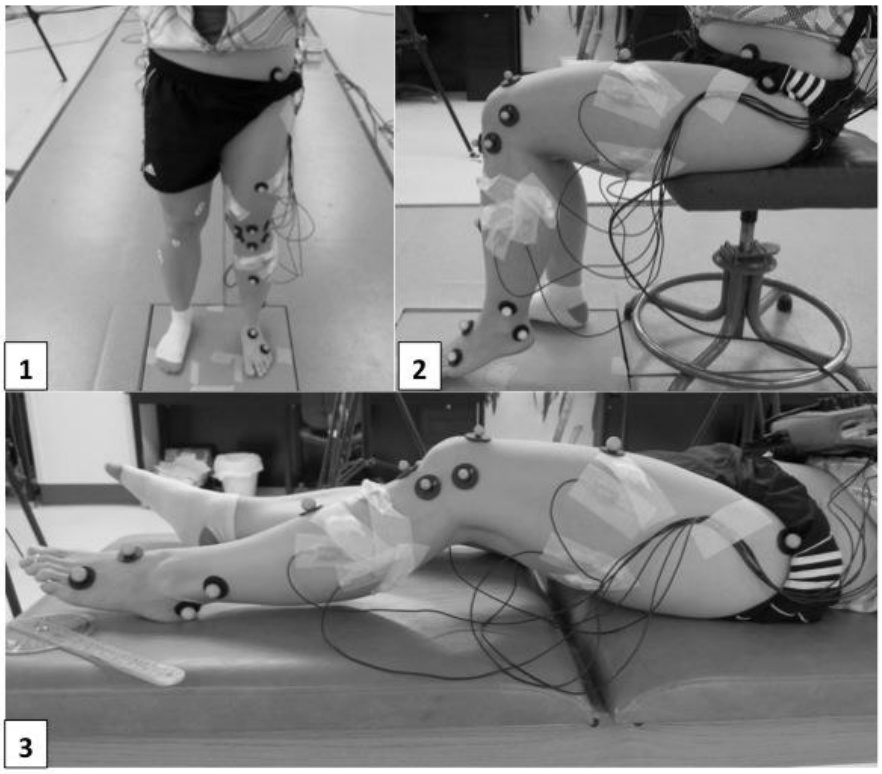

Figure 3-8: Kinematic neutral trials: 1) standing, 2) seated, 3) supine.

3.3.2.2 Electromyography

EMG was used during the dynamic tasks to record muscle activity for the tibialis anterior (TA), lateral gastrocnemius (LG), vastus medialis (VM), vastus lateralis (VL), biceps femoris long head (BF) and semitendinosus (SEM). The VM, VL, BF, and SEM were chosen to investigate the role of the medial and lateral quadriceps and hamstrings in knee stabilization (Alkjaer et al., 2003; Chmielewski et al., 2001; Rudolph et al., 2001). The gastrocnemius has also been shown to provide anterior stability to the knee (Klyne et al., 2012; Sherbondy et al., 2003), and it was expected that the TA would co-activate with the LG to provide stability.

Surface EMG was used to investigate muscle activation patterns, as it is a non-invasive method that has been used extensively in human studies. Silver/silver chloride (Ag/AgCl) electrodes (Noraxon dual electrodes, Noraxon USA Inc., Scottsdale, AZ, US) with a 10 mm diameter and an inter-electrode spacing of 20 mm were used. Electrodes were placed (Figure 3-9) in alignment with the direction of the muscle fibres on the mid belly of the muscle to ensure a strong signal (De Luca, 1997). Muscle landmarks were located using the surface EMG for non-invasive assessment of muscles (SENIAM) project guidelines (Hermens et al., 2000). The skin was prepared by shaving any hair with a razor and then rubbing with an alcohol swab. Once the skin was dry the electrodes were positioned on the desired locations and attached to the electrical leads (Biovision, Wehrheim Germany). Electrodes, amplifiers and leads were secured with medical tape (Cover-roll stretch, BSN Medical, Hamburg, Germany) to minimize movement and maintain good contact with the skin. EMG signals were locally amplified and sampled at 2.4 kHz.

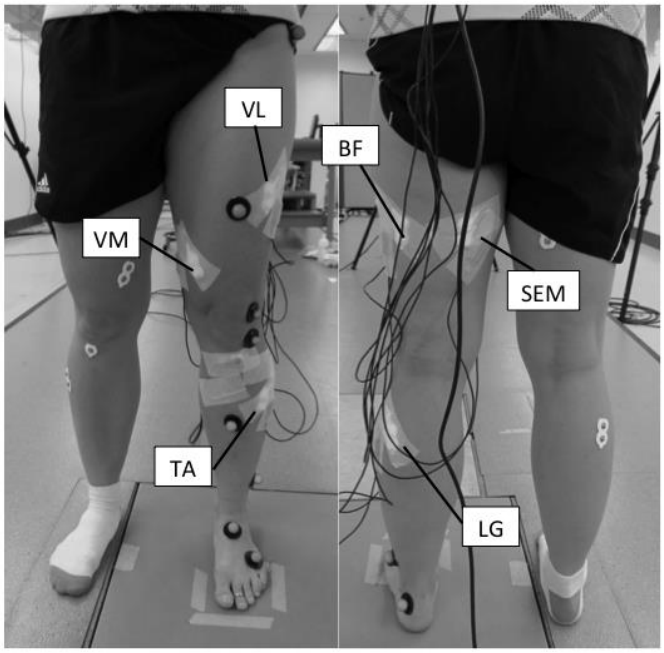

Figure 3-9: EMG electrode placement for the VM, VL, TA, BF, SEM and LG muscles.

The EMG signal was normalized using a sub-maximal isometric contraction, to provide a more stable reference value (De Luca, 1997). A dynamometer (Biodex Medical Systems, Inc., New York USA) was used to perform sub-maximal MVCs for EMG normalization. Torque values of 70 Nm and 105 Nm were used for extension (quadriceps), and 35 Nm and 50 Nm were used for flexion (hamstrings).

Trials were performed with the knee at 60° of flexion which has been shown to produce maximal isometric force (Thorstensson et al., 1976). Straps were secured on the shin, thigh, waist and chest to isolate the quadriceps and hamstring muscle groups (Figure 3-10). Participants were instructed to aim for the desired torque level and maintain as best they could for five s using visual feedback from the dynamometer system (Biodex Medical Systems, Inc., New York USA).

Participants performed three trials (five second duration) for each level of torque (flexion and extension) with thirty s of rest between trials.

Figure 3-10: Participant positioning for sub-maximal MVC testing on the Biodex dynamometer

3.3.2.3 Magnetic Resonance Imaging

The following imaging procedure was performed separately for each leg at the Seaman Family MR Research Centre (Foothills Hospital) to acquire participant-specific knee joint geometry for LCS definition. Six reflective markers (providing a linkage between MR and MA coordinate systems) were placed onto the participant's skin around the knee using the traced outlines from kinematic testing (Section 3.3.2.1), and were left in place for the imaging duration. Joint geometry images were acquired using a GE Discovery 750 3T MR scanner (General Electric Healthcare, Waukesha, WI) in conjunction with a general purpose flex coil (General Electric Healthcare, Waukesha, WI) (Figure 3-11).

Figure 3-11: Participant positioned in the KLA with a general purpose flex coil around the knee, ready for imaging.

Participants were positioned in the calibrated KLA. The compression load cell (for calibration purposes) was removed for MR imaging, and a thigh support was added to support the weight of the leg during imaging. The shank and thigh straps were secured, and the knee was positioned in 30° of flexion, confirmed with a goniometer. The general purpose flex coil was secured around the knee joint with Velcro® straps ensuring a fit that would not restrict anterior knee motion or interfere with the movement of the KLA. The flex coil improved the quality of the images, providing a better signal to noise ratio.

A fat-saturated steady-state free-precession (SSFP) imaging sequence (repetition time (TR): 7.136 ms, echo time (TE): 2.044 ms) was used to obtain high resolution sagittal and axial plane images of the knee for joint coordinate system determination (Figure 3-12). The knee was in the reference position (hydraulic system not pressurized) and imaged at a resolution of 0.31 mm x 0.31 mm x 1.0 mm [Field of View (FOV) 16 cm x 16 cm, 512 x 512 matrix].

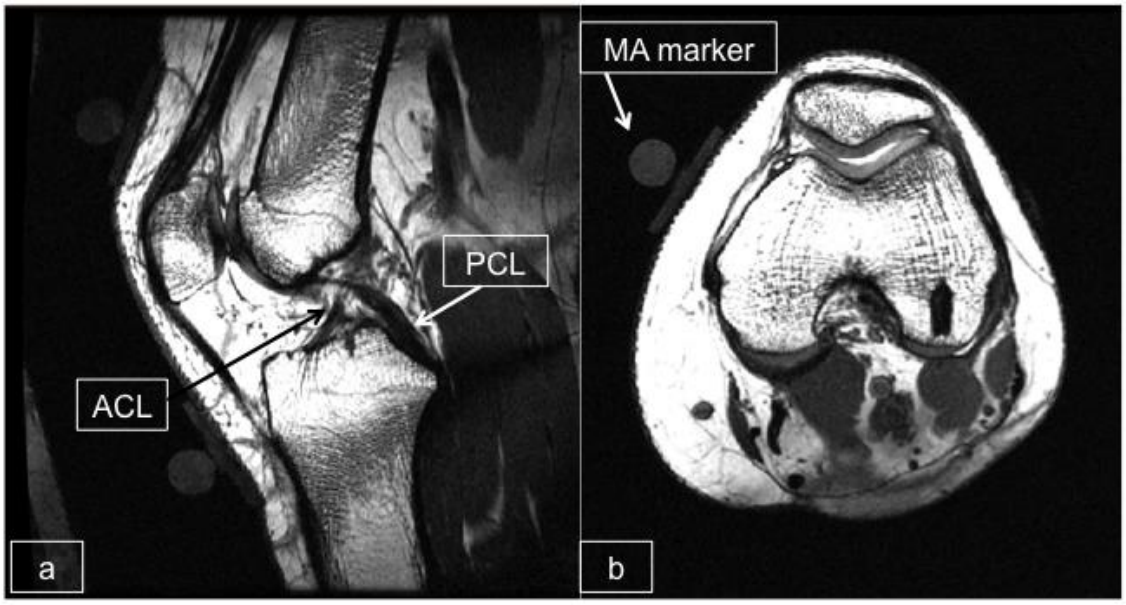

Figure 3-12: High resolution sagittal (a) and axial (b) MR images of the knee joint geometry. Sagittal image shows PCL intact; motion analysis (MA) markers are visible in the sagittal and axial images.

3.3.3 Data Processing

The techniques for data analysis are presented in the following section including treatment of raw data, LCS definition, a description of the FHA measures, a description of the EMG wavelet variables, and the statistical analysis approach.

3.3.3.1 Finite Helical Axis

Kinematic data and MR images were combined to describe the FHA within the knee. The methods used to perform this process are described in detail below.

Filters and Programs

3D marker motion data was tracked using EVaRT 4.0 (Motion Analysis Corporation, Santa Rosa, CA) and filtered using a fourth order Butterworth filter with a cut-off frequency of 10 Hz. The cut-off frequency was chosen based on values reported for the swing phase during running

(7 Hz) and walking (15 Hz) (van den Bogert et al., 1996). The swing and squat task were performed at 0.5 rep/s, which is comparable to the speed of walking (1.5 m/s) and running (3.5 m/s). Data was analysed using in house custom programs written in Matlab 7.11 (The MathWorks Inc., Natick, MA).

Image Digitization

Sagittal images of the knee were digitized using Amira 5.0 (FEI Visualization Science Group, Oregon USA). The femur, tibia and six reflective markers were digitized for each image slice (Figure 3-13a). The "lasso" tool with the "auto trace" option was used to define the edges of the bone, which corresponded to the trabecular bone/cortical bone interface. Together, the digitized MR slices created a 3D volume of the femur, tibia and marker surfaces (Figure 3-13b). A 3D point cloud was output for each bone and marker in the image coordinate system (ICS).

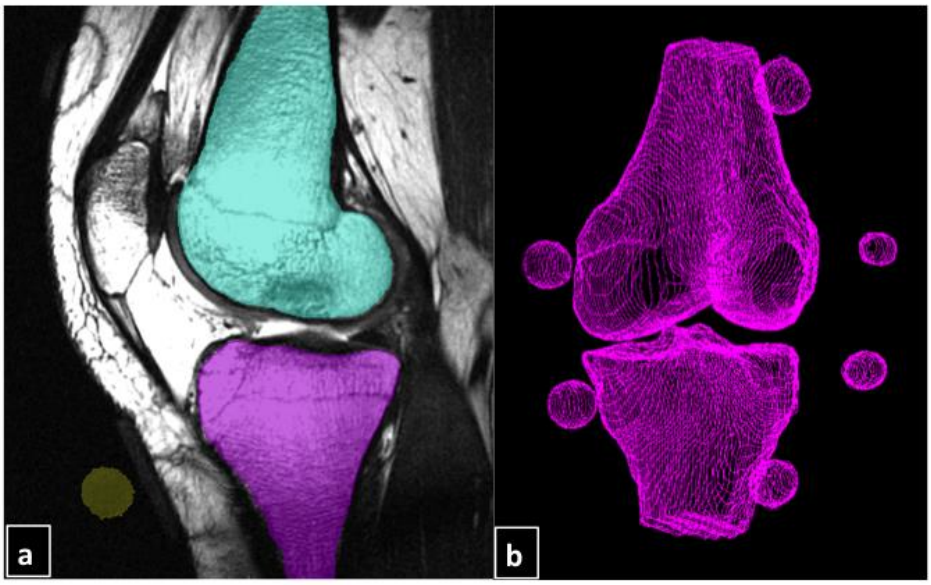

Figure 3-13: (a) Digitized sagittal MR image of the knee (single slice) (b) resulting image volume from all digitized sagittal slices

Coordinate Transformations

A transformation matrix was used to describe the digitized 3D knee model and the kinematic data in the same coordinate system. The coordinates of the six markers around the knee were known in both the ICS and the motion analysis global coordinate system (GCS). Pilot studies indicated that changes in marker location due to repositioning were the same order of magnitude for the femur and tibia markers. The standard deviation across repositioning trials for the femur marker positions ranged from 0.81 mm to 3.76 mm, and for the tibia markers ranged from 0.51 mm to 3.65 mm in the LCS (Section 2.2.2). Therefore, the three markers on the femur were chosen for this transformation due to their proximity to the femoral LCS. The transformation matrix between the two coordinate systems was calculated using the classic Soderkvist and Wedin (1993) technique, which uses a least squares approach to minimize the error associated with the marker position, such that

$$\min = \sum \left\| Rx_i + d - x_{i+1} \right\|, \qquad \textbf{(Eqn. 3-6)}$$

where x_i and x_{i+1} are the initial and subsequent marker positions, at times t_i and t_{i+1}. Single value decomposition (SVD) was used to solve Equation 3-6 since the solution is non-linear with respect to the rotation matrix, R. An algorithm based on the work of Soderkvist and Wedin (1993) was implemented and used in this study.

The x, y and z coordinates of three markers (1, 2 and 3) are known in both the global and image coordinate systems. Matrices **a** and **b** are calculated as

$$a = \begin{bmatrix} x_1 & x_2 & x_3 \\ y_1 & y_2 & y_3 \\ z_1 & z_2 & z_3 \end{bmatrix}^{global} \qquad b = \begin{bmatrix} x_1 & x_2 & x_3 \\ y_1 & y_2 & y_3 \\ z_1 & z_2 & z_3 \end{bmatrix}^{image}, \qquad \textbf{(Eqn. 3-7)}$$

where columns 1, 2 and 3 hold the x, y and z coordinates of markers 1, 2 and 3 respectively for each matrix. The mean of each row is calculated for matrices **a** ($\mathbf{a_{mean}}$) and **b** ($\mathbf{b_{mean}}$) as

$$\begin{bmatrix} \bar{x} \\ \bar{y} \\ \bar{z} \end{bmatrix} = \begin{bmatrix} (x_1 + x_2 + x_3)/3 \\ (y_1 + y_2 + y_3)/3 \\ (z_1 + z_2 + z_3)/3 \end{bmatrix}. \quad \textbf{(Eqn. 3-8)}$$

Matrices **A** and **B** are calculated as

$$A = a - a_{mean}, B = b - b_{mean}. \quad \textbf{(Eqn. 3-9)}$$

The cross dispersion matrix, **C** is determined using

$$C = BA^T. \quad \textbf{(Eqn. 3-10)}$$

SVD is used on matrix **C** resulting in three matrices **P**, **T** and **Q** such that **C**=**P**×**T**×**Q**. The rotation matrix **R** relating the initial marker position to the final marker position is determined as

$$R = PQ^T. \quad \textbf{(Eqn. 3-11)}$$

Once **R** is known, the translation vector, **d** can be calculated using Equation 3-12

$$d = x_{i+1} - Rx_i. \quad \textbf{(Eqn. 3-12)}$$

Transformation matrix, **T**, includes the rotation matrix **R** and the translation vector **d**, such that

$$T = \begin{bmatrix} R_{11} & R_{12} & R_{13} & d_1 \\ R_{21} & R_{22} & R_{23} & d_2 \\ R_{31} & R_{32} & R_{33} & d_3 \\ 0 & 0 & 0 & 1 \end{bmatrix}. \quad \textbf{(Eqn. 3-13)}$$

The marker coordinates for each segment are then transformed from the GCS to the ICS using the transformation matrix

$$[x\ y\ z]_{image} = [T][x\ y\ z]_{global}. \quad \textbf{(Eqn. 3-14)}$$

3.3.3.2 Femoral Local Coordinate System Definition

The LCS is defined using the femur geometry obtained from the high resolution sagittal MR images. The digitized femur output from Amira is input into a custom Matlab program, developed to identify each of the LCS axes (Fjeld, 2007; Kupper, 2008).

The longitudinal axis (x-axis) was defined based on the femoral shaft geometry. An ellipse was fit to each axial slice of data points along the shaft and the centroid of each ellipse was determined. A 3D least squares line was fit to these points to define the longitudinal axis (positive x-axis in the distal direction). The mediolateral axis (z-axis) was based on the circular profile of the posterior femoral condyles (Churchill et al., 1998; Coughlin et al., 2003; Freeman and Pinskerova, 2005; Iwaki et al., 2000). A sagittal image was used from approximately the centre of both the medial and lateral femoral condyles. A circle was fit to the posterior arc and the two circle centres were joined by a line defined as the mediolateral axis (z-axis) (Figure 3-14). The positive direction was defined as anatomical right (i.e. medial for left leg, lateral for right leg). The anterior-posterior y-axis was obtained with the cross product of the z and x axes (positive y-axis in the anterior direction). To ensure orthogonality, the cross product of the y and z axes was calculated again. The origin of the coordinate system was located at the intersection of the x and z axes in the centre of the femoral facets (Figure 3-14). Previously conducted intra and inter-tester repeatability tests compared the location of the LCS on the midsagittal plane, and yielded a mean of 0.79 ± 0.42 mm for within tester repeatability, and 0.85 ± 0.34 mm for between tester repeatability (Fjeld, 2007).

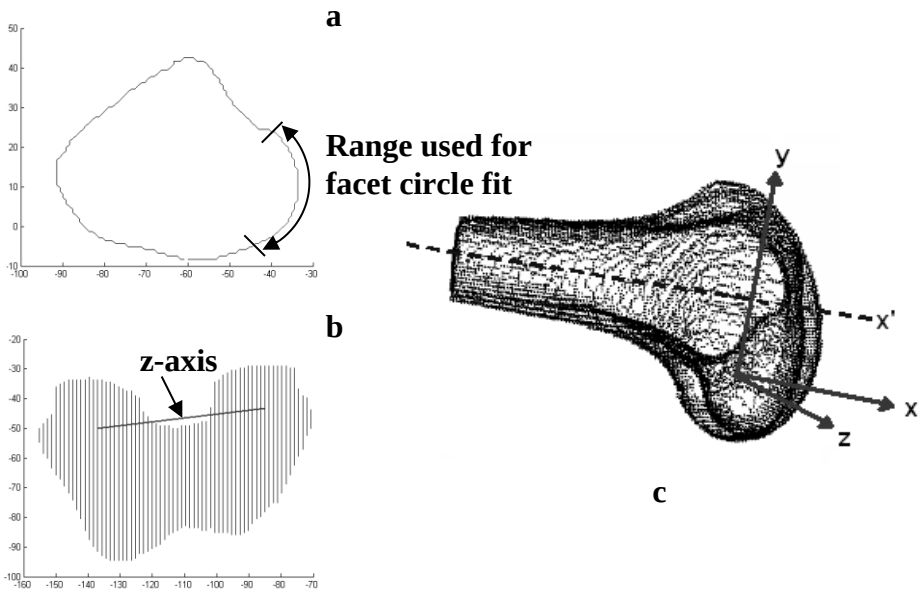

Figure 3-14: 'LCS definition: (a) outline of a sagittal slice through a femoral condyle with region selected for facet circle fit, (b) axial view from the distal end of the femur with the resulting z axis through the centres of the facet circles, (c) LCS displayed within the femur, x´ axis shown as longitudinal axis of femur shaft, origin located at projection of x´ axis on the z axis' with permission from Fjeld (2007)

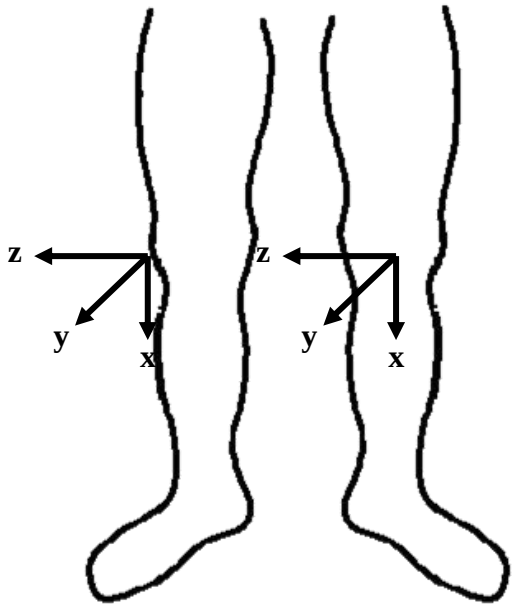

Figure 3-15: 'LCS orientation and origin for right and left legs' with permission from Fjeld (2007)

Following LCS definition, a method similar to that described in Section 3.3.3.1 was used to transform the segment marker coordinates in the ICS to the LCS, enabling all motion and image data to be described in the LCS.

Joint Angles

3D joint angles at each time point throughout the dynamic task were calculated to identify a range of interest for FHA calculations. The transformation matrix relating the position of the shank with respect to the thigh was calculated as follows:

$$\begin{aligned} [x\ y\ z]^{thigh}_{squat} &= [T]^{thigh}\,[x\ y\ z]^{thigh}_{stand} \\ [x\ y\ z]^{shank}_{squat} &= [T]^{shank}\,[x\ y\ z]^{shank}_{stand} \\ [T]^{rel} &= [T]^{thigh}\,\mathrm{inv}([T]^{shank}) \end{aligned} \quad \textbf{(Eqn. 3-15)}$$

where $\mathbf{T}^{\mathbf{thigh}}$ and $\mathbf{T}^{\mathbf{shank}}$ were found using the methods previously described (Section 3.3.3.1). A standing neutral kinematic trial (Section 3.3.2.1) was defined as 0° of knee flexion, providing a reference position to calculate knee flexion angles throughout the task.

In this study, joint angles based on a joint coordinate system approach were calculated from $\mathbf{T}^{\mathbf{rel}}$ (Eqn. 3-15) with rotation about the axes in the order flexion/extension (z-axis), ab/adduction (y-axis) and internal/external rotation (x-axis) as suggested by Cole et al. (1993). An exemplary plot of these angles during a swing task is shown in Figure 3-16. The range of interest for FHA calculations was chosen to be 20-40º of knee flexion, where full extension is 0º. This range was selected to examine 10° of motion on either side of 30° of knee flexion, which is reported to be the approximate slack/taut transition angle of the ACL (Fleming et al., 1994), and shows the greatest anterior translation (Sakane et al., 1999). Therefore, it was expected that this range would highlight the role of the ACL and show the greatest differences between the healthy and ACLD groups. All healthy participants encompassed the selected range within their motion.

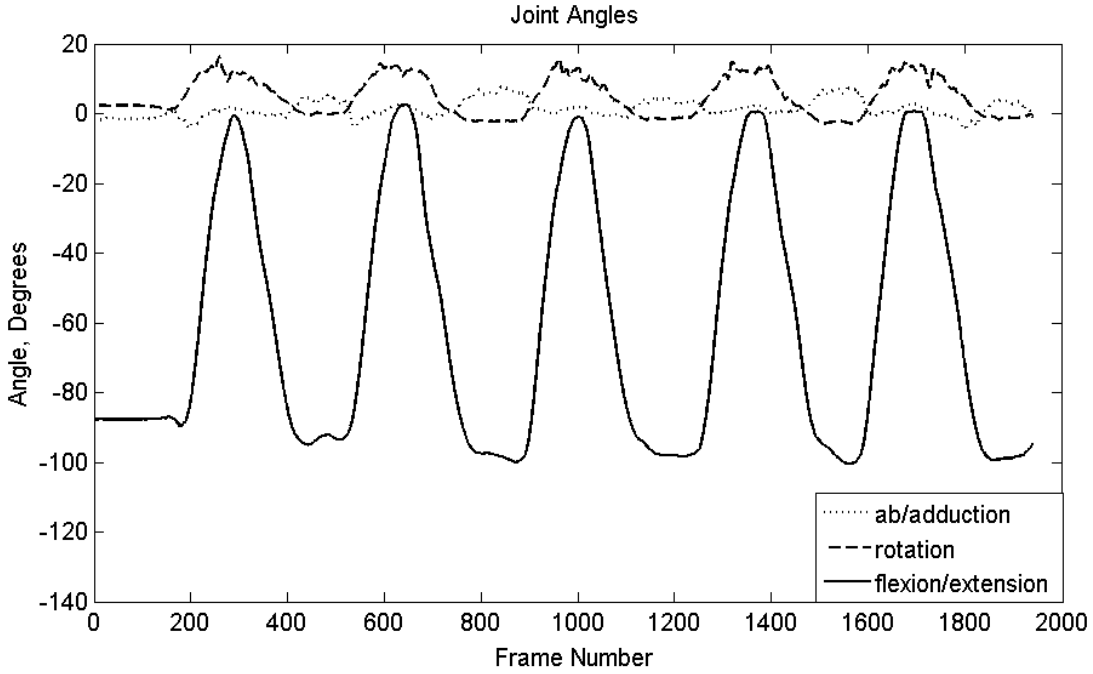

Figure 3-16: Exemplary plot of knee joint angles during a swing task

Reference Position

The FHA method is inherently sensitive to small rotations (Woltring et al., 1985). To address this issue, the current method employs a reference position such that the transformation matrix is calculated at each time point between the current position and the reference position. The reference position used was a knee flexion angle of 90°, acquired during the kinematic neutral trials (Section 3.3.2.1). This position was selected because it provided sufficient separation from the range of interest (20-40º of flexion), and it was simple to position and replicate between participants. The reference position provided a sufficiently large angle of rotation between each time point and the reference position, enabling a continuous calculation of the FHA (at each time point).

FHA Parameter Definitions

Four parameters were developed previously to describe the FHA: FHA location, translation along the FHA, FHA orientation, and FHA dispersion (Fjeld, 2007). Three novel parameters were developed to further describe FHA movement related to joint laxity for the current study: FHA path length, anterior/posterior (AP) excursion, and proximal/distal (PD) excursion. Together, these parameters were used to examine the stability within the knee.

FHA Location

FHA location describes the placement of the FHA within the knee joint. It is defined as the intersection point of the FHA, at each time point, with the midsagittal plane of the knee (x-y plane of the LCS). The series of intersection points throughout a dynamic task creates a 2D plot of the path of FHA travel through the midsagittal plane (Figure 3-17). For a single dynamic trial containing five repetitions, the FHA location plot shows ten traces (five traces for each flexion and each extension phase).

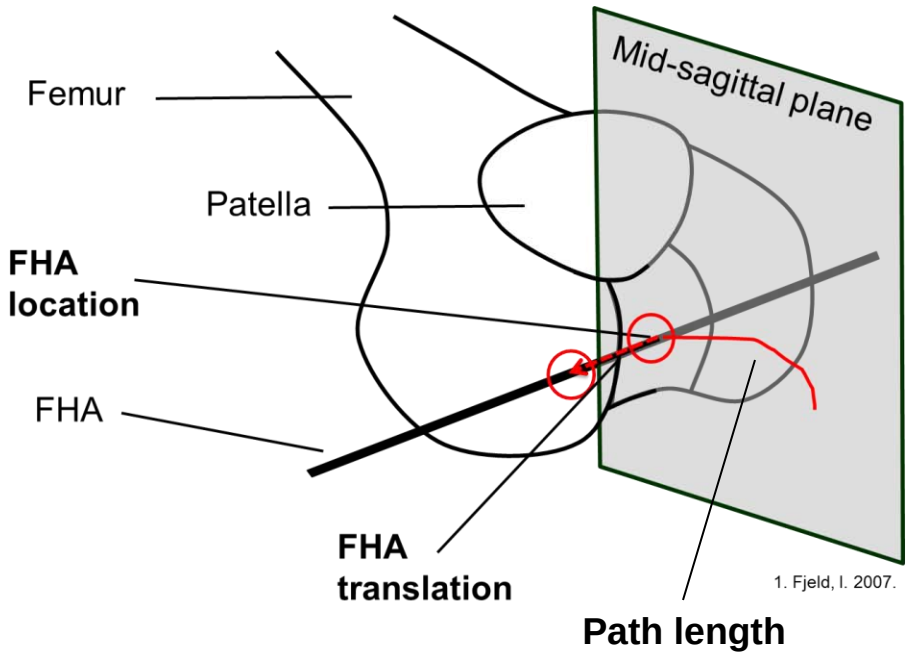

Figure 3-17: Schematic of the FHA intersection with the midsagittal plane of the knee (FHA location), resulting in a trace of the FHA path of travel during joint motion (Path length), and the translation of the tibia with respect to the femur in the direction of the FHA throughout a dynamic task (FHA translation), adapted from Fjeld (2007)

Translation Along the FHA

The translation along the FHA is calculated from the translation component of the transformation matrix (d) and the unit vector ($\vec{n}$) of the FHA (Spoor and Veldpaus, 1980):

$$t = \vec{n} \cdot d \qquad \textbf{(Eqn. 3-16)}$$

The column matrix with the largest magnitude was chosen as the unit vector ($\vec{n}$, Section 3.3.3.1**)** to reduce error (Spoor and Veldpaus, 1980). The translation was calculated between every time frame and summed for a resultant measure of the translation along the FHA during the range of knee flexion. Vector summation was used such that translation in one direction along the FHA would be subtracted from a translation in the opposite direction.

FHA translation describes translation of the tibia with respect to the femur in the direction of the FHA (Figure 3-17). Therefore, only in the case when the orientation angle is equal to zero is FHA translation equivalent to medial/lateral translation. The positive direction of the LCS was defined as anatomical right (i.e. medial for left leg, lateral for right leg, Section 3.3.3.2). To express FHA translation in terms of medial/lateral translations for both limbs, right limb translations were multiplied by negative one. This resulted in positive FHA translation towards the medial direction of the LCS, and negative FHA translation towards the lateral direction.

FHA Orientation

FHA orientation describes the orientation of the FHA within the joint. FHA orientation is defined as the angle of the FHA, at each time point, with the mediolateral axis (z-axis of the LCS) of the knee (Figure 3-18). FHA orientation is calculated using:

$$\theta_o = \cos^{-1}\left(\frac{(\vec{n}_i \cdot [0\,0\,1])}{\sqrt{\vec{n}_i^{\,2}}}\right), \qquad \textbf{(Eqn. 3-17)}$$

where θ_o is the orientation angle, and the vector **[0 0 1]** represents the z-axis of the LCS.

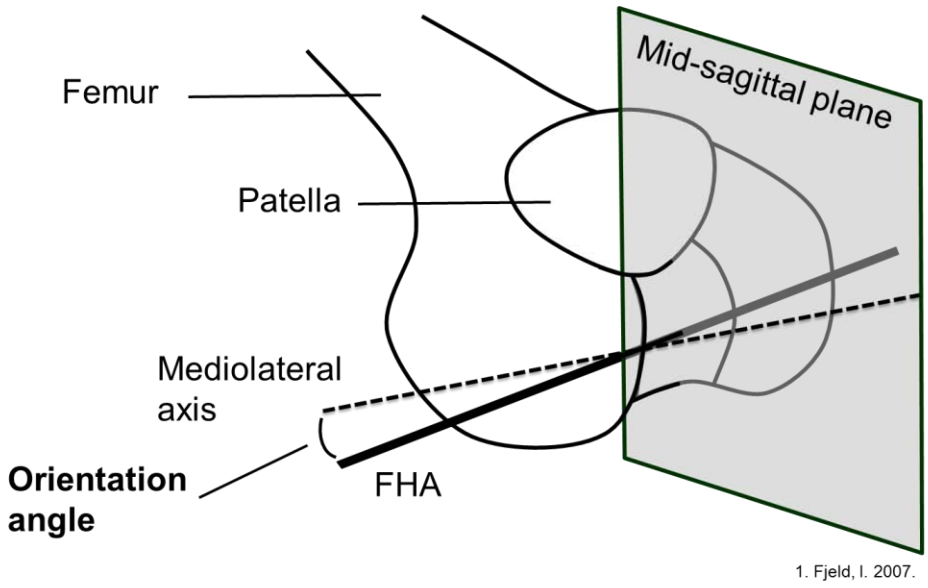

Figure 3-18: Schematic showing the orientation angle of the FHA as the angle between the FHA and the mediolateral axis of the LCS, adapted from Fjeld (2007)

FHA Dispersion

The amount of rotation of the FHA throughout a dynamic task is described by the dispersion. FHA dispersion is defined as the average angle between each individual axis and the mean helical axis:

$$\theta_{d,avg} = \frac{\sum_{i=1}^{h} \cos^{-1}\left(\frac{(\vec{n}_{mean} \cdot \vec{n}_i)}{\sqrt{\vec{n}_{mean}^{\,2}} \times \sqrt{\vec{n}_i^{\,2}}}\right)}{h}, \qquad \textbf{(Eqn. 3-18)}$$

where $\theta_{d,avg}$ is the average dispersion angle, h is the number of individual FHA axes throughout the range of interest, $\vec{n}_i$ is the unit vector of the FHA at time t_i and $\vec{n}_{mean}$ is the unit vector of the mean FHA.

FHA Path Length

FHA path length is a novel measure proposed in this study to describe the length of the FHA location trace on the midsagittal plane of the knee (Figure 3-17). It is calculated as the sum of the Euclidean distance between each pair of consecutive FHA locations (x, y) given by:

$$\mathbf{path} = \sum_{\mathbf{i=1}}^{\mathbf{n-1}} \sqrt{(\mathbf{x_{i+1}} - \mathbf{x_i})^2 + (\mathbf{y_{i+1}} - \mathbf{y_i})^2} \qquad \textbf{(Eqn. 3-19)}$$

FHA Excursion

FHA excursion is a novel measure developed for the current study to describe the range covered by the FHA location trace in the anterior/posterior (AP) direction (y-axis of the LCS) and the proximal/distal (PD) direction (x-axis of the LCS). AP excursion and PD excursion are calculated as follows:

$$\mathbf{AP_{ex}} = \mathbf{y_{max}} - \mathbf{y_{min}} \qquad \textbf{(Eqn. 3-20)}$$

$$\mathbf{PD_{ex}} = \mathbf{x_{max}} - \mathbf{x_{min}} \qquad \textbf{(Eqn. 3-21)}$$

Flexion and extension results were reported separately for all parameters to examine differences in joint motion between concentric and eccentric motions (Dyrby and Andriacchi, 2004).

3.3.3.3 EMG

The methods used to analyze the raw EMG signal are described in this section, along with the measures used to quantify muscular joint control. These measures were used to compare muscle activity between tasks within the healthy group.

Segmentation of Each Repetition

In order to average EMG data over trials and repetitions for the squat and swing tasks, cycle initiation and completion times were required for each repetition. For direct comparison with FHA measures, the cycle timing corresponding to a knee flexion angle range of 20-40° was used

for the EMG analysis presented in the current chapter. Each repetition was normalized to 100% of cycle, enabling averaging of trials and participants within the healthy group.

EMG signal normalization

Sub-maximal isometric contractions (described in Section 3.3.2.2) were used to provide a reference EMG signal for normalization of the EMG signal from dynamic trials. Submaximal isometric contractions were performed for the quadriceps and hamstring muscle groups to normalize the signals for the VM, VL, BF, and SEM muscles. Consequently, comparisons for the TA and LG muscles were limited to within leg comparisons (*i.e.*, between tasks) and qualitative assessments. Furthermore, comparisons for the VM, VL, BF and SEM muscle were limited to within group comparisons (*i.e.*, between limbs and over time) due to the normalization technique employed. Torque signals measured with the Biodex were imported into Matlab and visually assessed to determine the best trial (of three) that the participant was able to reach and maintain the desired torque value (Figure 3-19). The corresponding EMG signals for the quadriceps (VM, VL) and hamstrings (BF, SEM) were imported into Matlab (Figure 3-20). A three second window was manually selected and the mean signal amplitude for each muscle was computed. The EMG signals from the dynamic trials for the quadriceps and hamstrings were divided by the mean signal amplitude from the submaximal isometric contraction for the corresponding muscle, resulting in a normalized EMG signal.

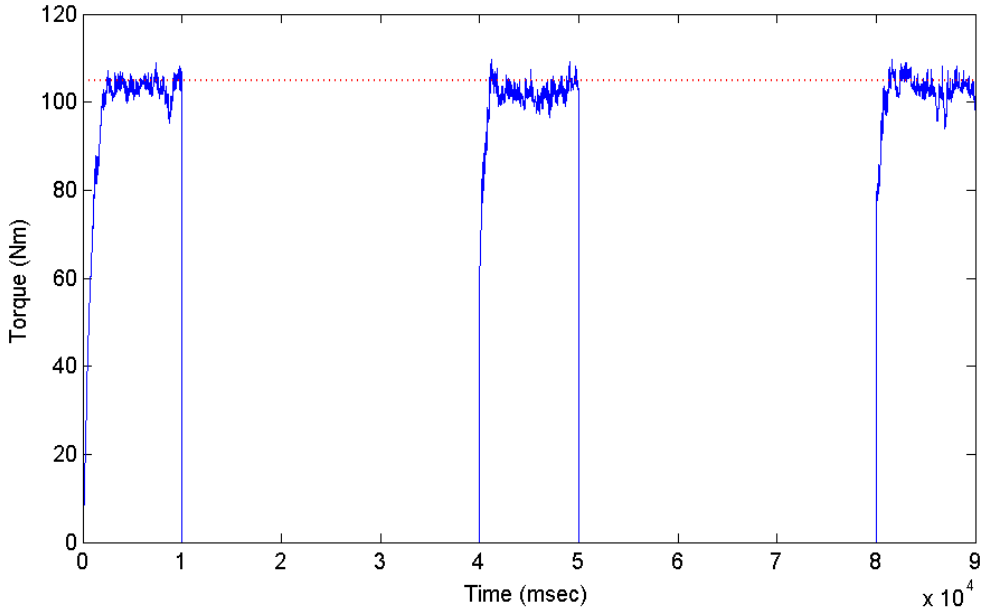

Figure 3-19: Exemplary plot of torque measured from the Biodex dynamometer during a sub-maximal isometric contraction of the quadriceps. The target of 105 Nm is indicated with a red dotted line. In this example, the second trial would be selected for EMG normalization.

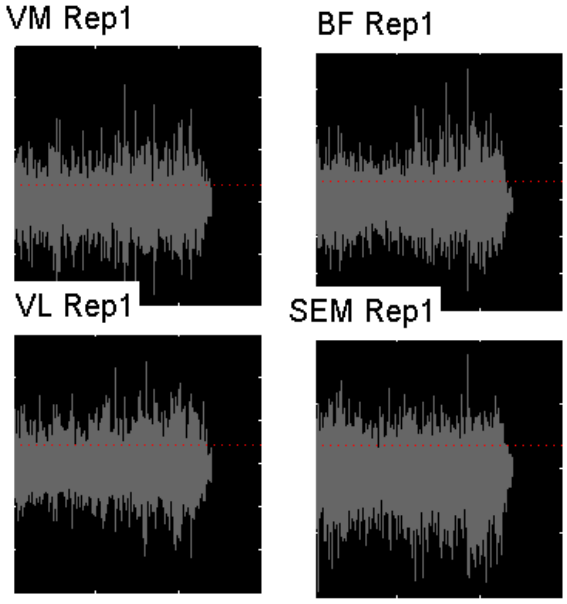

Figure 3-20: Exemplary EMG signals for VM, VL, BF, and SEM during submaximal isometric contractions

Power Analysis and Wavelet Description

The application of the wavelet analysis method to EMG signals described by von Tscharner (2000) was used in this study. Non-linearly scaled wavelets were used, with the wavelets' centre frequencies, f_c, ranging from 6.9 Hz to 542.1 Hz (Table 3-1) (von Tscharner, 2000). The maximum number of wavelets defines the extent of the frequency range covered. In the current study thirteen wavelets were used based on the EMG sampling rate of 2400 Hz.

Table 3-1: Wavelet parameters

Wavelet Number	Centre Frequency (Hz)	Band Width (Hz)	Time Resolution (ms)
1	6.9	11.7	80
2	19.3	21.1	52
3	37.7	30.5	36
4	62.1	39.8	28
5	92.4	49.2	24
6	128.5	58.6	20
7	170.4	68.0	16
8	218.1	75.0	16
9	271.5	84.4	12
10	330.6	93.8	12
11	395.4	103.1	12
12	465.9	112.5	8
13	542.1	121.9	8

The calculation of the wavelet transform was performed in three steps: (1) the normalized EMG signal was convolved with the wavelets to transform the signal, (2) the intensity of the wavelet transformed signal was computed, and (3) a Gaussian filter was applied to remove oscillations shorter than the time resolution of the signal. The signal intensity was distributed among neighbouring wavelets, causing an oscillatory pattern in each of the intensities. This was removed using a Gaussian filter with a width sufficiently large to eliminate the oscillations, but short enough to not significantly alter the time resolution (von Tscharner, 2000). The result was a

muscle intensity plot, with time on the x-axis and frequency on the y-axis, corresponding to wavelets 1-13 (Figure 3-21).

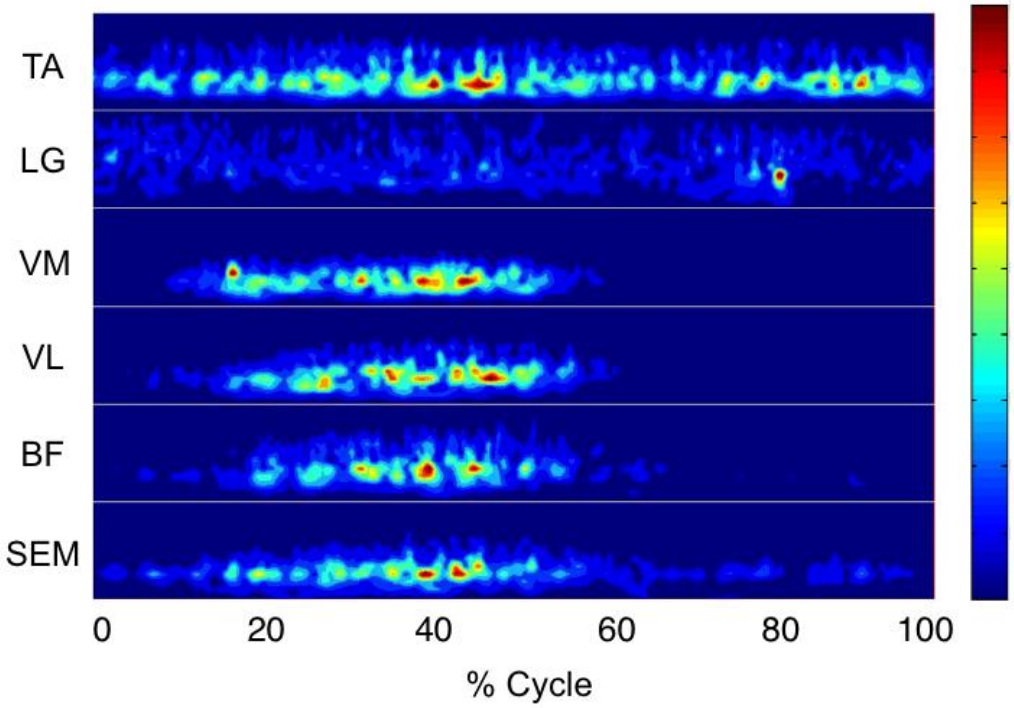

Figure 3-21: Exemplary plot of muscle intensities during a swing task with % cycle on the x-axis and frequency (Hz) on the y-axis. Wavelet patterns for each muscle (TA, LG, VM, VL, BF, SEM) are stacked in the vertical direction. The colorbar shows the intensity scale of the signal where dark blue represents minimum intensity (0), and dark red represents maximum intensity (1.0).

Wavelet Variables of Interest

Quantitative measures were required to determine differences in muscle activation between tasks within the healthy group. The variables introduced in this section describe the intensity and power of the myoelectric signal, providing insight into the co-contraction stabilization strategies of the healthy group.

Muscle Intensity and Power

Muscle intensity and power were used to describe the myoelectric signal in terms of muscle activation over time. The total intensity of the myoelectric signal was calculated as the sum of the intensity for each wavelet (2-12), at each time point (t_i) (Eqn. 3-22). Muscle power was calculated as the sum of the total intensity over time (Eqn. 3-23). The units for muscle power are arbitrary since the EMG signal was normalized in the current study. Muscle power was calculated for each cycle, and averaged across cycles for the swing and squat tasks. Differences in the power of each muscle were compared between tasks within the healthy group.

$$\textbf{Total Intensity}_{\textbf{ti}} = \int_{2}^{12} \textbf{Intensity df} \qquad \textbf{(Eqn. 3-22)}$$

$$\textbf{Power} = \int_{\textbf{i=0}}^{\textbf{i=n}} \textbf{Total intensity dt} \qquad \textbf{(Eqn. 3-23)}$$

3.3.4 Statistics

SPSS (SPSS Statistics 20, IMB, New York USA) was used for all statistical analysis in the current study. The Shapiro-Wilks test was used to check for normality in FHA and muscle power measures in the healthy group (Appendix B). Distributions of the differences between tasks were examined for use with paired T-tests. The null hypothesis that the data is normally distributed was rejected if $p<0.05$.

If the difference in FHA measures and muscle power between tasks was normally distributed in the healthy group, then paired T-tests (SPSS Statistics 20, IMB, New York USA) were used to compare between the swing and squat tasks ($\alpha=0.05$). If these variables were determined to be non-normally distributed, then non-parametric Wilcoxon Signed Ranks tests were used for comparisons between the squat and swing tasks in the healthy group ($\alpha=0.05$).

3.4 Results

3.4.1 Statistics

The percentage of non-normally distributed FHA variables was 25% in the dominant limb of the healthy group (Table B-1). The paired T-test is very robust for violations against normality (Sawilowski and Blair, 1992), therefore this test was used to compare FHA measures between tasks in the healthy group (α=0.05). The percentage of non-normally distributed muscle power variables was 64% in the dominant limb of the healthy group (Table B-3). Since the majority of muscle power variables were not normally distributed, the non-parametric Wilcoxon Signed Ranks test was used to compare muscle power between tasks in the healthy group (α=0.05).

3.4.2 Study Participants

The healthy group (Table 3-2) consisted of twelve females (24.0 ± 3.2 yrs, 165.7 ± 5.7 cm, 63.0 ± 7.8 kg). All healthy participants in the current study were right limb dominant.

Table 3-2: Study Participant Information

	Participant ID	Age (years)	Height (cm)	Weight (kg)
Healthy	H01	19	163	54.4
	H02	23	173	66.0
	H03	29	168	66.0
	H04	23	175	69.0
	H05	27	168	66.0
	H06	23	166	65.3
	H07	19	166	64.4
	H08	25	170	74.8
	H09	21	165	70.3
	H10	26	160	50.8
	H11	26	157	50.0
	H12	27	157	59.0
	Mean (std)	24.0 (3.2)	165.7 (5.7)	63.0 (7.8)

3.4.3 FHA

3.4.3.1 FHA Location

FHA location describes the intersection of the FHA with the midsagittal plane of the knee. The average FHA location in the anterior/posterior (y-axis) direction for the dominant limb of the healthy group was 25.0 mm and 24.8 mm for the flexion and extension phases of the swing task, respectively. For the squat task, the average FHA location in the anterior/posterior (y-axis) direction for the dominant limb of the healthy group was 18.2 mm and 18.6 mm for the flexion and extension phases respectively. FHA location y was significantly different between tasks during flexion ($p = 0.002$) as well as extension ($p = 0.001$) (Figure 3-22).

The average FHA location in the proximal/distal (x-axis) direction for the dominant limb of the healthy group was 1.5 mm and 0.5 mm for the flexion and extension phases of the swing task, respectively. For the squat task, the average FHA location in the proximal/distal (x-axis) direction for the dominant limb of the healthy group was 12.3 mm and 10.8 mm for the flexion and extension phases respectively. FHA location x was significantly different between tasks during flexion ($p < 0.001$) as well as extension ($p <0.001$) (Figure 3-22).

The intersection of the FHA with the midsagittal plane of the knee was located significantly more anterior and proximal during the swing task compared to the squat task.

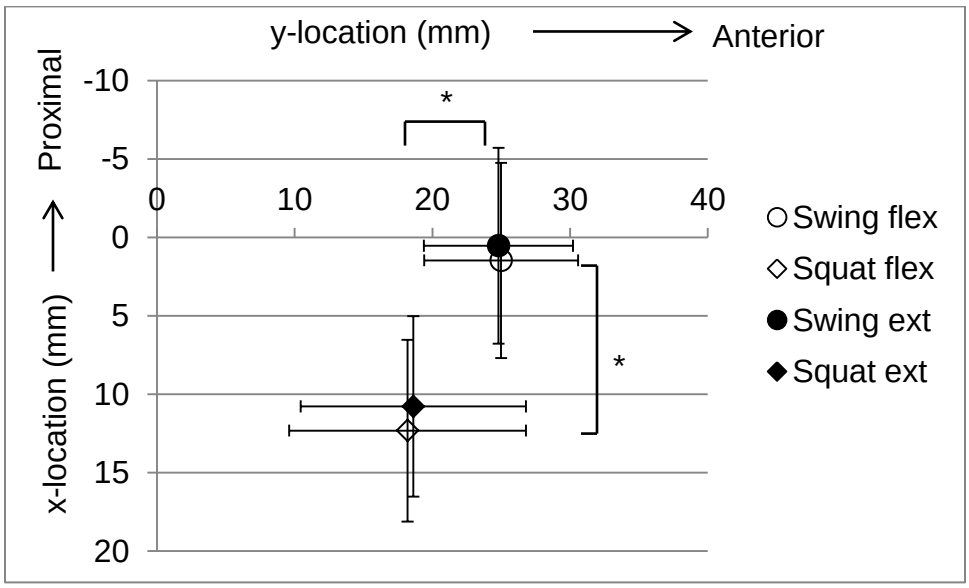

Figure 3-22: FHA location for dominant limb of healthy group during the flexion and extension phases of the squat and swing tasks (* indicates significance at α=0.05).

3.4.3.2 FHA Translation

FHA translation describes the magnitude of tibial translation along the FHA throughout a dynamic task. FHA translation was significantly greater during the squat task compared to the swing task. The average FHA translation for the dominant limb of the healthy group was 1.9 mm during swing flexion, compared to 3.4 mm during squat flexion, a difference of 1.5 mm between tasks. FHA translation was significantly different between tasks during flexion ($p = 0.019$) as well as extension ($p = 0.003$) (Figure 3-23).

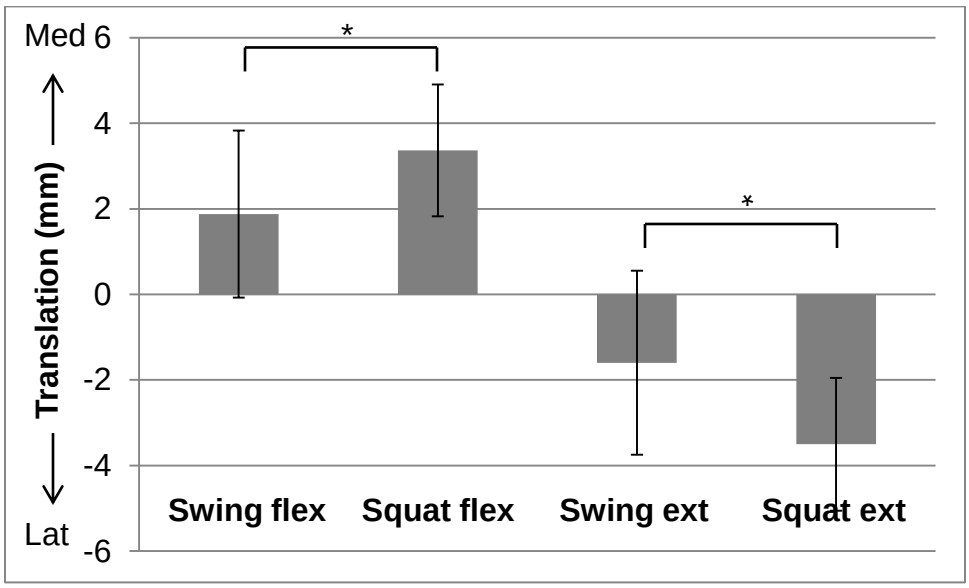

Figure 3-23: FHA translation for dominant limb of healthy group during the flexion and extension phases of the squat and swing tasks (* indicates significance at α=0.05).

3.4.3.3 FHA Orientation

FHA orientation describes the angle of the FHA with the mediolateral axis of the knee during a dynamic task. The average FHA orientation angle for the dominant limb of the healthy group was 11.5° ± 5.8° and 12.1° ± 5.7° during the flexion and extension phases of the swing task, respectively. During the squat task, the average FHA orientation angle for the dominant limb of the healthy group was 9.8° ± 3.8° and 9.5° ± 4.2° during the flexion and extension phases respectively. There were no significant differences between tasks for FHA orientation angle during flexion (p=0.483) or extension (p=0.277).

3.4.3.4 FHA Dispersion

FHA dispersion describes the deviation of the FHA from the mean FHA during a dynamic task. FHA dispersion for the dominant limb of the healthy group was 1.3° ± 0.6° and 1.2° ± 0.6° during the flexion and extension phases of the swing task, respectively. During the squat task,

FHA dispersion for the dominant limb of the healthy group was 1.5° ± 0.2° and 1.4° ± 0.4° during the flexion and extension phases respectively. There were no significant differences between tasks for FHA dispersion during flexion (p=0.254) or extension (p=0.437).

3.4.3.5 FHA Path Length

FHA path length describes the length of the FHA location trace on the midsagittal plane of the knee throughout a dynamic task. The average FHA path length for the dominant limb of the healthy group was 9.5 mm during swing flexion, compared to 6.5 mm during squat flexion. FHA path length was significantly greater during swing flexion compared to squat flexion. FHA path length was significantly different between tasks during flexion (p = 0.001), but not during extension (p = 0.115) (Figure 3-24).

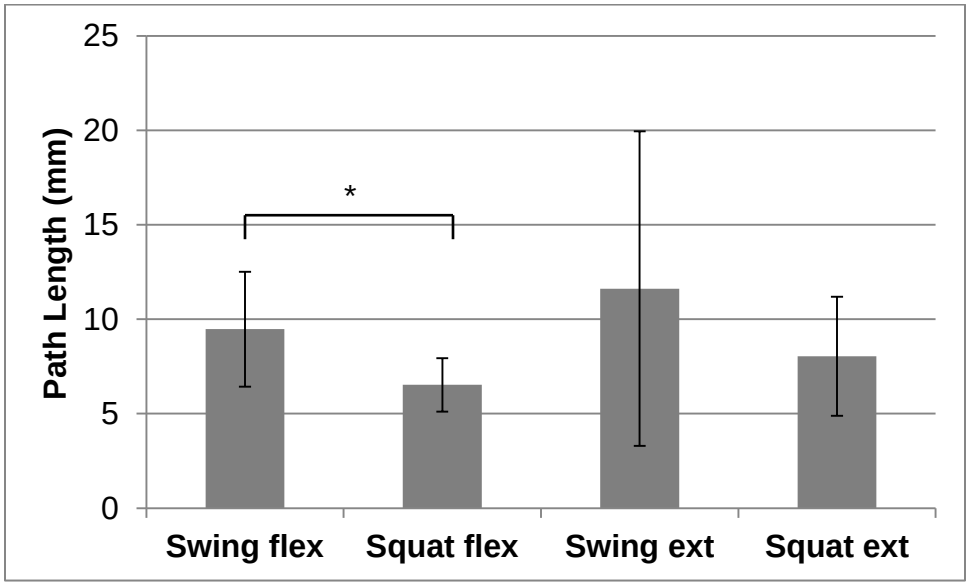

Figure 3-24: FHA path length for dominant limb of healthy group during the flexion and extension phases of the squat and swing tasks (* indicates significance at α=0.05).

AP and PD excursion further describe the FHA path length in terms of the AP and PD range of the FHA location trace on the midsagittal plane of the knee. There were no significant

differences between the squat and swing tasks in the dominant limb of the healthy group for AP excursion or PD excursion (p-value range: 0.080-0.512).

3.4.4 EMG

Quality of the EMG signal was poor in four healthy study participants (H01, H04, H07 and H11) due to significant noise artefacts. Therefore, EMG results are only presented for eight of the twelve healthy study participants.

Muscle power was significantly greater in the quadriceps during the squat compared to the swing in the healthy group. The median muscle power in the VM was 69.9 during squat flexion compared to 4.7 during swing flexion (Figure 3-25). The median muscle power in the VL was 69.9 during squat flexion compared to 8.8 during swing flexion (Figure 3-26). Muscle power was increased by factors of 14.9 and 7.9 during the squat compared to the swing for the VM and VL, respectively. Muscle power was significantly different between tasks for both flexion ($p = 0.012$) and extension ($p = 0.012$) in the VM, as well as flexion ($p=0.012$) and extension ($p=0.036$) in the VL.

Figure 3-25: VM muscle power for the dominant limb of healthy group during the flexion and extension phases of the squat and swing tasks (* indicates significance at α=0.05).

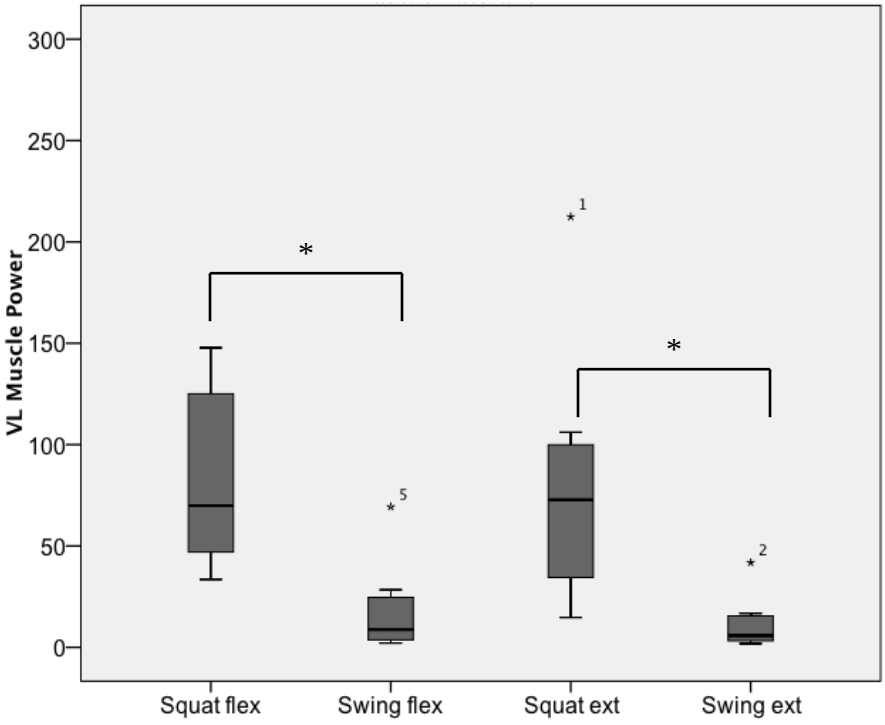

Figure 3-26: VL muscle power for the dominant limb of healthy group during the flexion and extension phases of the squat and swing tasks (* indicates significance at α=0.05).

Outliers are indicated with an asterisk and a number representing the identity of the outlier within the group.

Muscle power was also significantly greater in the hamstrings during the squat compared to the swing in the healthy group. Muscle power in the BF was 5.1 during squat flexion compared to 0.7 during swing flexion (Figure 3-27). Muscle power in the SEM was 11.9 during squat flexion compared to 0.1 during swing flexion (Figure 3-28). Muscle power was increased by factors of 7.3 and 119.0 during the squat compared to the swing for the BF and SEM, respectively. Muscle power was significantly different between tasks during both flexion ($p = 0.012$) and extension ($p = 0.012$) in the BF, and flexion ($p=0.012$) and extension ($p=0.012$) in the SEM.

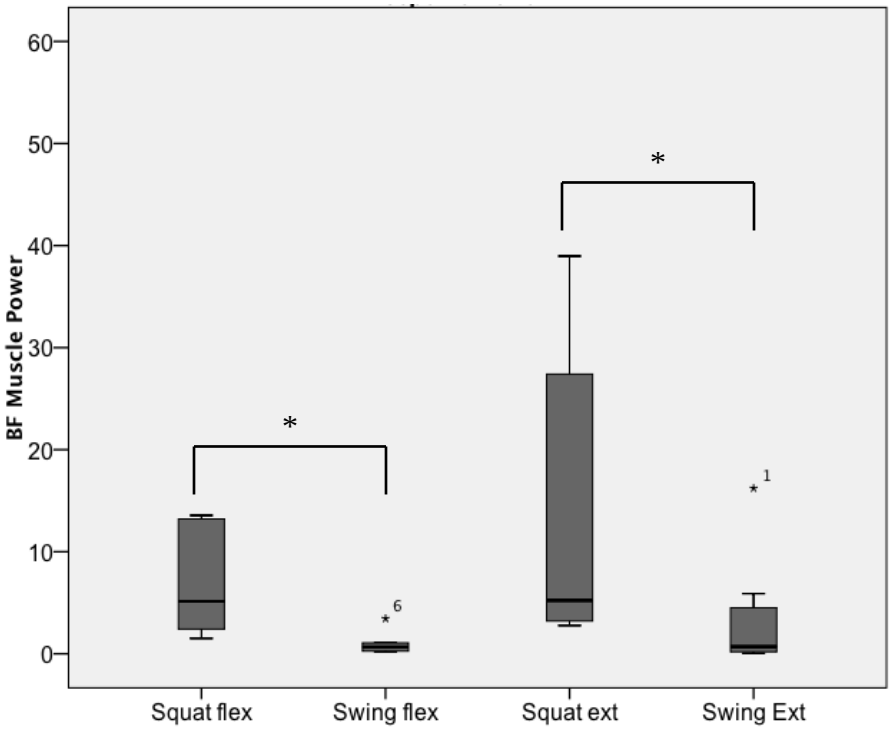

Figure 3-27: BF muscle power for the dominant limb of healthy group during the flexion and extension phases of the squat and swing tasks (* indicates significance at $\alpha=0.05$). Outliers are indicated with an asterisk and a number representing the identity of the outlier within the group.

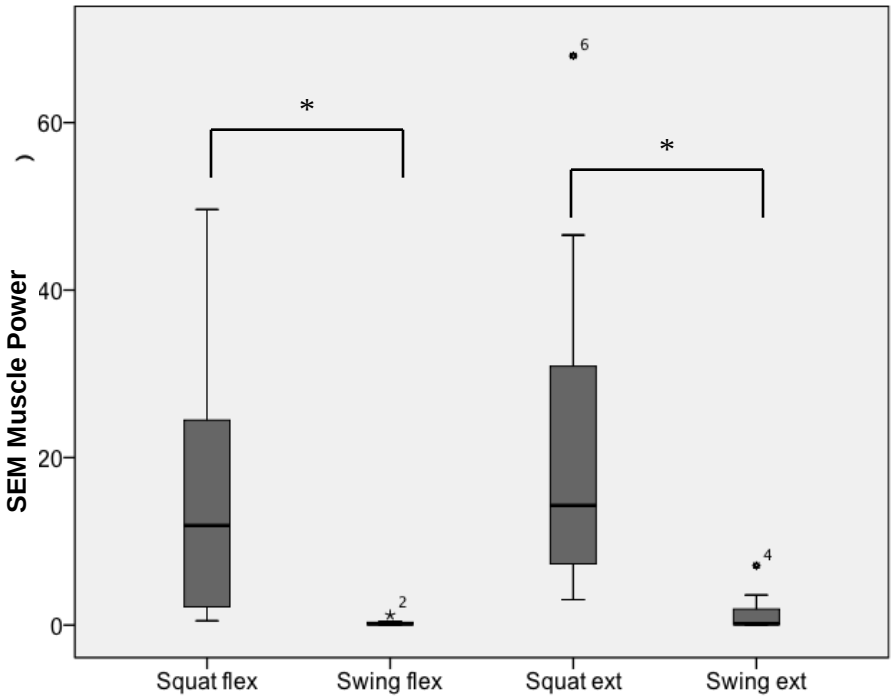

Figure 3-28: SEM muscle power for the dominant limb of healthy group during the flexion and extension phases of the squat and swing tasks (* indicates significance at α=0.05). Outliers are indicated with an asterisk and a number representing the identity of the outlier within the group.

The quadriceps to hamstring (QH) ratio was significantly greater for the swing compared to the squat in the healthy group. The median QH ratio was 7.5 during squat extension compared to 34.0 during swing extension (Figure 3-29). The QH ratio was significantly different between tasks during extension ($p = 0.012$), but not during flexion ($p=0.263$).

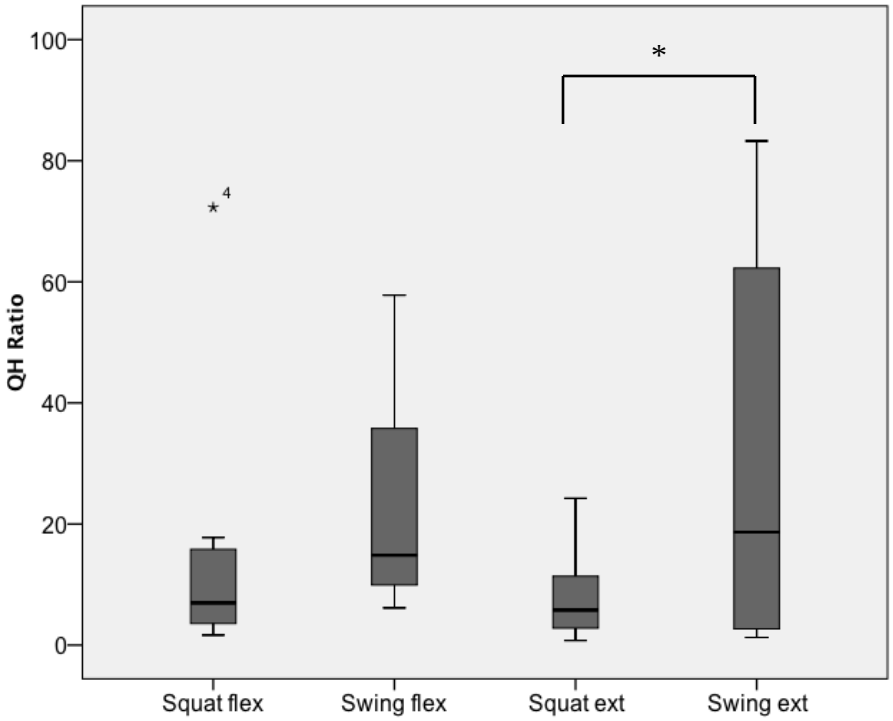

Figure 3-29: Ratio of quadriceps to hamstring muscle power for the dominant limb of healthy group during the flexion and extension phases of the squat and swing tasks (* indicates significance at α=0.05). Outliers are indicated with an asterisk and a number representing the identity of the outlier within the group.

3.4.5 Summary of Results

The main findings for the FHA and EMG results comparing the squat and swing tasks in the dominant limb of the healthy group are summarized in Table 3-3.

Table 3-3: Summary of results for FHA and EMG comparing squat and swing tasks in the dominant limb of the healthy group

Measure	Result
FHA Location	More anterior and proximal in swing task
FHA Translation	Greater in squat task
FHA Orientation	No significant differences between tasks
FHA Dispersion	No significant differences between tasks
FHA Path Length	Greater in swing task (flexion only)
FHA AP/PD Excursion	No significant differences between tasks
Quadriceps muscle power	Greater in squat task
Hamstrings muscle power	Greater in squat task
QH ratio	Greater in swing task (extension only)

3.5 Discussion

The current study used the FHA and muscle power to characterize dynamic joint stability in the seated leg swing and the single leg squat, and to investigate differences between these tasks in healthy individuals. To test the first hypothesis (H1a), differences in FHA measures were compared between the swing and squat tasks in the healthy group. It was hypothesized that the FHA would be located more anterior, and FHA translation and dispersion would be decreased in the swing compared to the squat. To test the second hypothesis (H1b), the QH ratio was compared between the swing and squat tasks in the healthy group. It was hypothesized that the swing task would be quadriceps dominant (larger QH ratio), while the squat task would exhibit co-contraction of the quadriceps and hamstrings. The results of this study are discussed in this section according to the specific tasks, and related to the specific aims and hypotheses of the study.

The open-chain swing task was characterized by lower total power and larger QH ratios than the squat. This result indicates that the swing is a quadriceps dominant task, supporting H1b. Isolated quadriceps contraction causes anterior translation of the tibia with respect to the femur (Li et al., 1999). Therefore, it is speculated that predominant quadriceps activity in the swing caused a more anterior FHA location compared to the squat in the current study, supporting H1a. The FHA was also located more proximal on the femur during the swing compared to the squat. As the knee extends from 30° of flexion to full extension, the tibia contact location moves anteriorly and proximally on the femur (Wretenberg et al., 2002). Therefore, since the FHA is shifted anteriorly on the femur during the swing, it is expected that this would be coupled with the observed proximal shift in FHA location.

FHA path length was significantly greater during the swing compared to the squat during the flexion phase of the tasks. In other words, the path of the FHA through the midsagittal plane of the knee was longer during the swing task, meaning there was increased relative movement of the tibia with respect to the femur between consecutive joint angles during the swing. This finding was unexpected, however, a possible explanation follows. There are less constraints acting on the knee joint during the open-chain swing task compared to the squat, meaning knee joint motion during the swing is largely guided by joint geometry. It is generally accepted that the compressive forces are lower, and co-contraction of the quadriceps and hamstrings is lower during open-chain kinematic exercises compared to closed-chain exercises (Lutz et al., 1993; Wilk et al., 1996). Therefore, it is speculated that the tibia can move more freely with respect to the femur during the swing, resulting in an increased FHA path length compared to the squat.

Larger muscle power and lower QH ratios in the squat reflect the greater demands of this task and the involvement of the hamstrings in knee stabilization, supporting H1b. The squat is a

weight bearing activity, which requires increased muscle power to support the weight of the body. The decreased QH ratio compared to the swing indicates a higher relative contribution from the hamstrings. The primary role of the hamstring muscles is hip extension (Palmitier et al., 1991). Hence, the hamstring muscles activate during the squat to stabilize the hip, and have a secondary effect on the knee joint motion. The quadriceps are active during the squat to stabilize the knee, thus producing co-contraction of the quadriceps and hamstrings. At the knee joint, the hamstrings help to counteract the tendency of the quadriceps to cause anterior tibia translation. During the swing, movement is isolated at the knee joint, so the stabilizing effect of the hamstring is not fully utilized.

During the squat task there was an average increase in FHA translation of 1.5 mm compared to the swing, supporting H1a. FHA translation is similar to mediolateral tibial translation, however it is in the direction of the helical axis. So, if the orientation angle was 0°, FHA translation would be equivalent to mediolateral tibial translation. FHA translation was toward the medial direction of the LCS during knee flexion, and toward the lateral direction of the LCS during knee extension for both tasks. These results align with the natural coupled motion of the knee joint, where passive knee flexion is coupled with internal tibial rotation and medial tibial translation (Wilson et al., 2000). Muscle power was increased in the quadriceps (knee extensors) during the squat compared to the swing by factors of 14.9 and 7.9 for the VM and VL respectively. Isolated quadriceps contraction causes lateral tibial translation (Li et al., 1999). Li et al. (1999) showed that application of a 200 N quadriceps load at 30° of knee flexion produced 2.4 mm of lateral tibial translation. With the addition of an 80 N hamstring load, there was a 46% reduction in lateral tibial translation, resulting in 1.3 mm of lateral tibial translation. Hence, even with hamstring co-contraction, quadriceps contraction creates lateral tibial translation. One possible

explanation for increased FHA translation during the squat compared to the swing is that increased quadriceps muscle power during the squat contributed to increased lateral translation during the extension phase of this task. These results were mirrored in the flexion phase with increased medial translation during the squat compared to the swing.

This study provides an understanding of how muscles control healthy movement in two dynamic tasks. As discussed, knee joint motion during the swing task is largely guided by joint geometry. In an ACLD population, it is expected that the less constrained swing task will isolate changes in movement patterns due to altered knee structures. The quadriceps dominant swing task is expected to produce increased anterior tibial movement in the ACLD knee due to the absence of the ACL (primary restraint to ATT). Furthermore, the stabilizing effect of the hamstrings is not fully utilized in the swing task, limiting the amount of hamstring co-contraction to counteract ATT caused by quadriceps contraction. In the squat task, movement is guided by joint geometry, but is also affected by forces generated by muscles, and joint compression from body weight. In an ACLD population, it is expected that the loaded squat task will reveal changes in movement patterns due to adaptations in muscular control following injury. It is expected that the ability to stabilize the knee using coordinated co-contraction of the quadriceps and hamstrings will be affected following ACL rupture, resulting in altered movement patterns in ACLD individuals during the squat task.

Chapter Four: **Passive Knee Laxity and Dynamic Knee Stability: Healthy versus ACLD**

The overall research goal is to develop a further understanding of changes in dynamic joint stability due to ACL deficiency, and to explore the relationship between structural joint laxity and dynamic joint stability in ACLD individuals. The current chapter investigates these relationships in a group of ACLD individuals at a sub-acute stage post injury (six weeks), and compares the relationships within this group to those within healthy individuals. Differences between groups in anterior tibial translation, FHA measures, and muscle activity are explored.

4.1 Literature Review

4.1.1 ACL Injury

The ACL is the most commonly injured ligament of the knee, with approximately 200,000 ACL ruptures annually in the United States, and 100,000 ligament reconstructions performed each year (AAOS, 2009). The risk of developing OA is greatly increased following ACL injury. The prevalence of articular cartilage lesions rises from 30% in fresh ACL injuries to approximately 70% of ACLD knees ten years post-injury (Nakamura and Shino, 2005). In a study of female soccer players, more than 50% of participants had radiographic OA in their injured knee twelve years after ACL injury (Lohmander et al., 2004). Even with ACL reconstruction, ten year follow-ups indicate the progression of OA frequently cannot be significantly prevented among athletes (Lohmander et al., 2004).

OA currently affects one in eight Canadians, and that number is expected to rise to one in four in the next thirty years (Arthritis Alliance of Canada, 2011). The need for developing a further understanding of why OA develops in ACLD individuals and how we can stop or slow the progression of this debilitating disease is evident. This study quantifies knee joint dynamics at an early stage following ACL rupture to identify early changes in the ACLD knee joint. These early

adaptations in the ACLD knee joint may be linked to the initiation of degenerative changes in the knee joint. These changes could potentially be modified with targeted rehabilitation protocols aimed at minimizing, or slowing the progression of OA.

4.1.2 Healthy Limb Symmetry

Many studies assume limb symmetry in healthy individuals to simplify data collection and analysis, or to justify pooling data from left and right limbs. Several studies investigate symmetry between limbs in healthy individuals, however the majority of these studies focus on human gait (Gundersen et al., 1989; Hannah et al., 1984; Herzog et al., 1989; Teichtahl et al., 2009). A comprehensive review by Sadeghi and colleagues (2000) highlighted several studies reporting differences between left and right limbs in healthy individuals during gait using kinematic variables including step length, foot placement angle, maximum knee flexion angle, and range of joint motion. The review concluded that human able-bodied gait is asymmetrical (Sadeghi et al., 2000). However, the kinematic variables used to quantify limb symmetry in these studies do not fully describe the 3D motion at the knee joint, which is the focus of the current study. Hannah and colleagues (1984) found asymmetries during gait in transverse and coronal plane knee motions. However, the detected asymmetries were attributed to a lower signal to noise ratio in the data in these planes. Able-bodied individuals were concluded to walk with "reasonable symmetry" at the hip and knee joints.

Other tasks used to investigate limb symmetry include sit-to-stand, and single leg hop. Lundin and colleagues (1994) reported asymmetries in peak knee and hip moments in a group of seven young healthy females (mean age: 22.9 years) during a sit-to-stand task measured via force plates and motion analysis. Van der Harst and colleagues (2007) reported asymmetries in hop distance and hip extension angle during a single leg hop in a group of nine healthy individuals

(mean age: 26.7 years) measured with an optoelectronic system. To our knowledge, there are no previous studies addressing limb symmetry for the dynamic tasks used in the current study (single leg squat and seated leg swing). In order to compare the injured limb to the contralateral limb of an ACLD group, a comparison of dominant and contralateral limbs in a healthy group is required. Therefore, outcome variables are quantified in both limbs of the healthy and ACLD groups in the current study to enable appropriate interpretation of side to side differences in an ACLD group.

4.1.3 Knee Joint Laxity

The ACL is the primary restraint to ATT, providing as much as an estimated 85% of the total restraining force (Butler et al., 1980). Hence, anterior tibiofemoral laxity is the most predictable impairment resulting from an ACL tear or complete rupture (Snyder-Mackler et al., 1997). This increase in laxity is thought to lead to knee instability and dysfunction, causing an increased risk for OA development (Snyder-Mackler et al., 1997). Numerous measures of laxity have been used to evaluate knee function following ACL rupture, and to determine stability and functional outcome following surgery (Eastlack et al., 1999).

4.1.3.1 Laxity Measurements

Traditional tests for assessing passive knee laxity in patients include the Lachman test, the anterior/posterior drawer test, the pivot shift test, the quadriceps active test, and the varus/valgus stress test (eg. Kupper et al., 2007). However, these tests produce qualitative results used primarily for diagnosis, and do not allow for quantitative comparison between participants or testers. Instrumented devices have been developed to quantify laxity; these include the KT-2000 arthrometer (MedMetric, San Diego CA, USA), the Genucom Knee Analysis System (Faro Medical Technologies, Champlain NY, USA), the Rolimeter (Aircast, Summit NJ, USA), and

the Stryker Ligament Tester (Stryker, Kalamazoo MI, USA). These devices measure tibial translation with respect to the patella under an applied load using displacement transducers and/or digitized bony landmarks. The KT-2000 is the most commonly used arthrometer in biomechanical research and clinics (Kupper et al., 2007).

The majority of laxity measurement devices are limited to measure uniaxial (tibial) displacement in the assumed anterior/posterior direction. Any out of plane motion, such as internal/external tibial rotation, which will affect the resultant laxity measure, is neglected (Logan, 2004b). Alternate measurement systems include planar stress radiography (series of 2D radiographs), radiostereometric analysis (RSA), and magnetic resonance (MR) imaging. These imaging techniques produce three-dimensional (3D) images of the knee, allowing calculation of the entire tibial displacement. MR imaging is a promising non-invasive, accurate method for measuring displacement (Logan, 2004b; Sheehan and Rebamnn, 2003), and does not expose participants to radiation. Kupper et al. (2013) developed a functional MR imaging based knee loading apparatus (KLA) to enable 3D evaluation of change in tibial position as a function of loading for understanding the functional implications of altered joint integrity. The KLA has been previously evaluated with five healthy participants, on three test days (Kupper, 2008). Anterior tibial position was evaluated at varying load levels (0N, 30N, 40N, 50N, 89N, 133N), and force-displacement curves were constructed from the anterior tibial position. The average variability of anterior displacement across days for the KLA was 0.58 mm (range 0.26 mm – 1.01 mm), compared to 1.47 mm (range 0.49 mm – 1.88 mm) for the KT-2000 (Kupper, 2008). The current study uses the KLA to quantify passive knee joint laxity.

4.1.4 ACLD Kinematics

Altered joint dynamics are speculated to contribute to the development of OA (Andriacchi et al., 2004). Several studies have investigated the kinematics of the ACLD knee in an effort to identify a specific change in knee mechanics. Increased ATT and internal tibial rotation in ACLD participants are consistently reported (Andriacchi and Dyrby, 2005; Dennis et al., 2005; Georgoulis et al., 2003; Logan, 2004a; Scarvell et al., 2004). However findings relating to varus/valgus angles remain inconsistent. A key function of the ACL is to restrict the anterior posterior motion of the femur relative to the tibia. Consequently, many studies have investigated the anterior posterior translation or contact point of the femur on the tibia. Bone imaging (e.g. MRI, CT, fluoroscopy) studies consistently report a more posterior location of the femur relative to tibia in ACLD participants compared to individuals with intact joints during a variety of load bearing activities (Barrance et al., 2006; Beynnon et al., 2002; Brandsson et al., 2001; Defrate et al., 2006; Dennis et al., 2005; Logan, 2004a; Scarvell et al., 2005, 2004). However, no consensus exists for translations within the medial and lateral femoral condyles or the knee joint kinematics of an ACLD group. These discrepancies may be attributed to differences in measurement techniques or specific tasks being investigated. Additionally, resulting joint motion is highly dependent on the definition of the LCS, making it difficult to compare results between studies.

A previous research study from our research group investigated ACLD kinematics using four parameters to describe the FHA (described in Section 3.3.3.1): location, translation, orientation, and dispersion (Fjeld, 2007). The time since injury for this group of ACLD individuals ranged from 7-61 months post injury. The ACLD knee FHA was located more anterior and proximal within the femur compared to the healthy knee FHA during both the seated leg swing and single leg squat tasks. Additionally, orientation angle and dispersion angle were decreased in the ACLD

knee during both tasks. Translation along the FHA was smaller in the ACLD group during the squat, and larger in the ACLD group in the swing compared to healthy. Overall, these results demonstrated that the healthy group had increased movement of the FHA during these tasks, while the ACLD group had less overall movement of the FHA within the knee joint. These findings were interpreted as a compensation strategy in the ACLD group to reduce movement in the injured joint.

The current study defines "dynamic joint stability" as the state of minimum deviation from healthy movement and muscle activity patterns during a given dynamic task and for a desired range of motion. We believe that ACLD individuals will show a more constrained movement pattern than healthy individuals, due to the inability to accommodate extra degrees of freedom in the knee joint following ACL rupture. This decrease in dynamic stability would be characterized by a decrease in FHA translation and dispersion in the ACLD group relative to healthy. Furthermore, we expect ACLD individuals to have an altered joint position due to the loss of the ACL, resulting in a more anterior location of the FHA and an increased orientation angle.

The current study applies the FHA technique developed by Fjeld (2007) to quantify knee kinematics in a group of ACLD individuals at six weeks post injury, addressing a sub-acute stage post injury with a more controlled time point. Kinematics are quantified in both the injured and contralateral limbs of the ACLD group allowing for within subject comparisons, while the study by Fjeld (2007) measured the injured limb only. Furthermore, measures of passive knee laxity are obtained in the current study to enable the development of relationships between dynamic knee stability and structural laxity in ACLD individuals, which has not been explored previously using the FHA. It is believed that the FHA may provide a truer representation of knee joint

motion, especially in an ACLD joint where the axes of motion may be altered relative to a healthy knee joint.

4.1.5 ACLD Muscle Activity

Mechanoreceptors present in the human ACL provide sensory feedback regarding sudden changes in ligament tension or length (Shultz et al., 2004). These mechanoreceptors include Ruffini endings, Golgi tendon organs, and Pacinian corpuscles that provide information about joint position to the central nervous system (CNS) for communication with the muscle (Adachi et al., 2002). Under low loads, the cruciate ligaments can provide proprioceptive feedback and preparatory muscle stiffening (Johansson, 1991). Under high ACL loading, there is a significant hamstring reflex arc and quadriceps inhibition (Solomonow et al., 1987). Many studies have examined the ACLD knee to understand what happens in the joint without the stabilizing effect of the ACL. Results have shown diminished proprioception (Adachi et al., 2002), delays in reflex responses to ATT (Wojtys and Huston, 1994), and altered neuromuscular control strategies (Chmielewski et al., 2002; Hurd and Snyder-Mackler, 2007; Ingersoll et al., 2008).

The contribution of the quadriceps and hamstrings to knee joint stability is altered following ACL rupture. There is general consensus that decreased quadriceps activation occurs in ACLD individuals (Chmielewski et al., 2004; Snyder-Mackler et al., 1994; Swanik et al., 1999; Urbach et al., 1999). This phenomenon is known as “arthrogenic muscle inhibition”, which is due to muscle atrophy and ongoing neural inhibition, preventing the quadriceps from fully activating (Rice and McNair, 2010). The hamstrings, also plays an important role in maintaining joint stability and preventing excessive ACL strain by preventing or decreasing anterior and rotary displacement of the tibia on the femur (Boerboom et al., 2001; Isaac et al., 2005; Liu and Maitland, 2000; MacWilliams et al., 1999).

Atrophy of the quadriceps muscle group following ACL rupture is well documented and has been associated with decreased strength and functional deficits in ACLD individuals (Baugher et al., 1984; Ingersoll et al., 2008; Lorentzon et al., 1989; Williams et al., 2005). Fjeld (2007) quantified muscle volume from MR images in healthy and ACLD groups. Muscle volume ratios were used to compare between groups. The ACLD group demonstrated lower quadriceps to hamstring ratios compared to the healthy group suggesting quadriceps atrophy in the ACLD group (Fjeld, 2007). The current study measures muscle volume from MR images in both the injured and contralateral limbs of the ACLD group, enabling between limb comparisons of muscle volume. Any changes detected in muscle morphology due to ACL rupture are speculated to contribute to altered muscular control strategies in ACLD individuals, affecting dynamic knee stability.

The gastrocnemius is one of three primary muscles spanning the knee joint (Klyne et al., 2012). Contraction of the gastrocnemius is speculated to increase knee joint stability by increasing joint stiffness and decreasing anterior tibial shear forces (Chmielewski et al., 2002; Klyne et al., 2012; Sherbondy et al., 2003). Shultz et al. (2004) found that individuals with above average knee laxity, (> 7 mm at 133 N, measured with a KT-2000) demonstrated increased levels of muscle activity in the medial gastrocnemius prior to a perturbation, potentially as a compensatory mechanism by increasing joint stability to accommodate for increased joint laxity. The tibialis anterior (TA) may also act to stabilize the knee during dynamic activities. A study by Binder-MacLeod and Buchanan found that ACLD "non-copers" had larger TA muscles in the injured limb in relation to the uninjured limb (Binder-MacLeod and Buchanan, 2006). In this study, "copers" were ACLD individuals who had returned to level one or level two activities, had not had any episodes of giving way within the last year, and had less than one episode of giving way

since the injury. "Non-copers" were ACLD individuals that did not meet the coper criteria. Increased TA activity (and TA size) in the non-coper ACLD limb was suggested to be a compensatory mechanism to provide additional knee stability by causing an outward rotation of the tibia. It can be concluded that a change in the neuromuscular control strategy of the muscles surrounding the knee joint clearly plays an important role in restoring knee joint stability after ACL rupture.

Muscular activation and timing patterns corresponding to various activities and tasks can be investigated through the use of EMG. The wavelet transform technique (Section 3.1.2) developed by von Tscharner (2000) allows the EMG signal to be analysed simultaneously in both the time and frequency domains. This provides an advantage over the traditional techniques that primarily limit analysis to the time domain. Since the development of this technique, it has been used in a number of studies to analyse EMG data (Karlsson and Gerdle, 2001; Mündermann et al., 2006; von Tscharner and Goepfert, 2003; von Tscharner et al., 2003; J. M. Wakeling et al., 2002b; Wakeling et al., 2001). Valderrabano et al. (2006) studied a group with ankle OA and found that the affected limb had a significant shift towards lower EMG frequencies for the lower limb muscles during maximal voluntary muscle contractions. It was suggested that this could be partly caused by selective muscle fiber type degradation in the affected limb. However, no published studies were found using the wavelet transform to investigate ACLD muscle activity. The current study builds on the work of Fjeld (2007) who used the wavelet transform to investigate changes in muscle activity in ACLD individuals. Fjeld (2007) found that the ACLD group had increased hamstring activity in relation to the healthy group, indicating a co-contraction strategy in the injured group. Normalization techniques (Section 3.3.3.3) are applied in the current study to allow for comparisons of muscle intensities across participants and over

time (Chapter 5). The current study aims to develop a further understanding of muscle control strategies at a sub-acute stage following ACL injury using the wavelet analysis technique.

4.1.6 Structure Function Relationship

The severity of joint laxity is commonly assumed to be directly related to the degree of instability in the knee. However, the relationships amongst knee laxity, instability, and functional outcome in the ACLD population remain unclear (Shultz et al, 2004).

Many individuals require reconstructive surgery following an ACL rupture to restore knee stability, however some elect for non-operative treatment. Some of these patients are able to return to the high level of function demonstrated before the rupture, while others experience continued knee instability. Many studies have classified ACLD patients not receiving surgery into three categories: copers, non-copers, and adapters (Shultz et al, 2004). Eastlack et al. (1999) defined copers as individuals who are able to return to function at a high level after injury without complaint of instability, while non-copers are those who are unable to return to their pre-injury level of sports play or activity because of repeated episodes of "giving way". Adapters represent the majority of ACLD individuals, who are not treated surgically, and are able to avoid evoking episodes of instability by mitigating their activity levels (Eastlack et al., 1999).

Snyder-Mackler and colleagues (1997) using a KT-2000, found no statistically or clinically significant differences in laxity, measured between copers and non-copers. Similar findings were reported by Eastlack et al. (1999) for laxity measurements obtained using the KT-2000. However, in copers the quadriceps strength of the injured side was not impaired, and in most cases it was stronger than that of the contralateral side, suggesting a link between quadriceps strength and functional outcome. Overall, the results of these studies suggest that the degree of joint laxity is not indicative of functional outcome in ACLD individuals.

Findings from recent studies investigating relationships between static and dynamic measures of knee laxity are inconclusive. Some studies concluded that these relationships do not exist (Kvist, 2005; Patel et al., 2003; Tagesson et al., 2014). Others have shown significant correlations between passive knee laxity and kinematic measures in ACLD and ACL reconstructed (ACLR) individuals (Boeth et al., 2013; Sato et al., 2013). Sato et al. (2013) found that ACLR individuals with an increased side to side difference in static ATT (measured by a KT-1000 arthrometer) had reduced maximum internal rotation during a side step cutting maneuver. However, five out of seven study participants had a side to side difference in static ATT between -2 mm and 1 mm (Figure 2, Sato et al., 2013), suggesting that the ACL reconstruction had restored or potentially even over corrected ATT in the injured limb. Side to side differences in ATT were attributed to injury. Clearly this interpretation may have benefitted from the availability of data on the side to side variability in ATT of a healthy group for comparison. Passive ATT was significantly correlated with the range of tibial AP translation during walking in a group of thirteen ACLD individuals (average time from injury: 8 ± 12 months) (Boeth et al., 2013). The ACLD individuals with increased passive ATT demonstrated an increased range of active AP translation in the knee joint. This correlation was also significant in the ACLD contralateral limb, however overall active AP translation was reduced in the injured limb compared to the contralateral (Boeth et al., 2013). A strength of this study was the inclusion of a healthy group, which showed no statistically significant differences between limbs in the range of active AP translation.

The current study uses a comprehensive approach including measurement of passive joint laxity, joint kinematics, and muscle activity in healthy and ACLD individuals, which addresses limitations identified and has not been reported to date. ACLD individuals are studied at a tightly-controlled, sub-acute stage following ACL rupture to identify early changes in the ACLD

knee joint. Both limbs are studied in each group to quantify between-limb differences in both healthy and injured individuals. It is believed that our novel approach to obtain a more precise measure of joint laxity using the KLA and imaging techniques, combined with the FHA method of analyzing kinematics during two dynamic tasks will provide excellent measures to identify correlations between passive joint laxity and dynamic joint stability. Wavelet analysis of muscle activity (EMG) provides information about movement control while measures of muscle volume reveal morphological changes. Combined these allow for further interpretation of dynamic joint stability and neuromuscular adaptations following ACL rupture.

4.2 Hypotheses and Specific Aims

The objectives of this study component are to elucidate the relations amongst passive knee laxity, joint dynamic stability and muscle activity in the ACLD group, and to compare these relations to the healthy group at the early time point of six weeks post-injury. This objective was accomplished by completing the following specific aims (SA1, SA2) and testing hypotheses H2a-H2c.

SA1: Quantifying passive laxity in healthy and ACLD knee joints *in-vivo* using MR imaging combined with a novel joint loading device

SA2: Determining dynamic joint stability relations in healthy knee joints and in joints with ACL deficiency, using the FHA method and wavelet analysis of muscle patterns.

H2: ACLD participants will have increased passive knee laxity and decreased dynamic knee stability six weeks post injury relative to healthy participants

H2a: ACLD participants will have increased side-to-side differences in passive knee laxity, FHA measures, and muscle power at six weeks post injury relative to healthy participants

H2b: ACLD participants will have decreased dynamic stability relative to healthy participants at six weeks post injury indicated by:

a. A more anterior FHA location and increased orientation angle

b. Decreased FHA translation and dispersion

H2c: ACLD participants with increased ATT will exhibit decreased dynamic knee stability at six weeks post injury, indicated by correlations between passive knee laxity and FHA measures

4.3 Methods

The methods used for participant testing are described in this section along with data processing and analysis techniques. Chapter 3 previously described kinematic and EMG data collection, the MR imaging protocol to obtain participant-specific knee joint geometry for LCS definition, and the approaches for FHA and EMG data processing. The current section covers the KLA calibration procedure and MR imaging knee loading procedure, as well as the data processing techniques to obtain measures of passive knee laxity and muscle volume. The statistical approaches to test the study hypotheses H2a-c are also outlined in this section.

Ethical approval for all methods was obtained from the Conjoint Health Research Ethics Board of the Faculties of Medicine, Nursing and Kinesiology, University of Calgary. Motion assessment was performed at the Clinical Movement Assessment Laboratory of the McCaig Institute for Bone and Joint Health and MR images were collected at the Seaman Family MR Research Centre.

4.3.1 Study Participants

Twelve healthy participants (described in Chapter 3), and ten ACLD participants were recruited and tested for this study. Written, informed consent was obtained from each participant prior to testing (Appendix A). Recruitment of the ACLD group was conducted through the Acute Knee Injury Clinic (AKIC) at the University of Calgary Sports Medicine Centre.

4.3.1.1 Participant Inclusion/Exclusion Criteria

ACLD participants were required to have a complete, isolated ACL rupture, confirmed by clinical testing at the AKIC and MR scan evaluation by a single radiologist. ACLD participants with a mild (or Grade I) medial collateral ligament (MCL) sprain, defined by less than 50% of the collagen fibres disrupted, were permitted if they had not used a knee brace. Meniscal damage was permitted if it did not affect the participants' range of motion (*i.e.*, no full thickness tears). Participants were required to be at least eighteen years of age in order to provide their own consent and to ensure skeletal maturity, and under forty years of age as the risk of OA degenerative changes increases after forty (Roos et al., 1995). The height and weight restrictions, well as restrictions for MR safety, described in Chapter 3 were applied to the ACLD group.

4.3.2 Data Acquisition

The current study aim was to understand relationships between passive knee laxity and dynamic knee stability in healthy and ACLD individuals, and to quantify differences in passive knee laxity and dynamic joint stability between groups. Movement patterns (FHA) and muscle activity (wavelet) were used to quantify dynamic joint stability. Passive knee laxity was quantified via MR imaging of the joint under loading using the KLA. FHA measures and passive knee laxity were described relative to a coordinate system located in the knee, determined from participant

specific knee joint geometry (MR). Muscle volume was measured from MR images of participant's thigh musculature to quantify changes in muscle volume due to ACL rupture.

ACLD participants were tested at six weeks post-injury. This time frame was chosen to capture changes at a sub-acute stage post-injury, but to exclude the early weeks when the joint is highly inflamed and painful. ACLD participants were tested on their non-injured limb, followed by their injured limb. Testing was performed in three stages in the order presented below. First, kinematic testing and muscle activation (EMG) were measured as the participant performed two dynamic tasks (described in Section 3.3.2.1). Next, a participant-specific calibration procedure was performed with the knee loading apparatus (KLA). Lastly, knee joint geometry was imaged under various loading conditions using MR scanning and the KLA. Typically, kinematic testing and KLA calibration were performed on one day, followed by MR imaging on the subsequent day. However, if scheduling allowed, testing could be performed on a single day. All study participants completed the IKDC and Lysholm knee function questionnaires.

4.3.2.1 KLA Calibration

A calibration procedure was performed with the KLA to determine the hydraulic force-voltage relationship for each participant (as per Section 2.1.2.3). This procedure was performed for each leg to simulate the MR testing protocol, and averaged between legs.

The participant's shank and foot were placed on the tibial platform, and the footplate was adjusted such that the end of the tibial platform was slightly distal to the knee joint line (Figure 4-1). Due to the added height of the compression load cell during calibration, extra pads were placed under the participants' gluteus maximus to obtain a knee flexion angle of 30°, confirmed with a goniometer. An elastic strap was used to secure the ankle position, and a shin pad was used to compress and secure the shank to the shank support. A proximal (elastic) and distal

(inelastic) strap secured the thigh, using a curved plastic pad to distribute the forces from the straps.

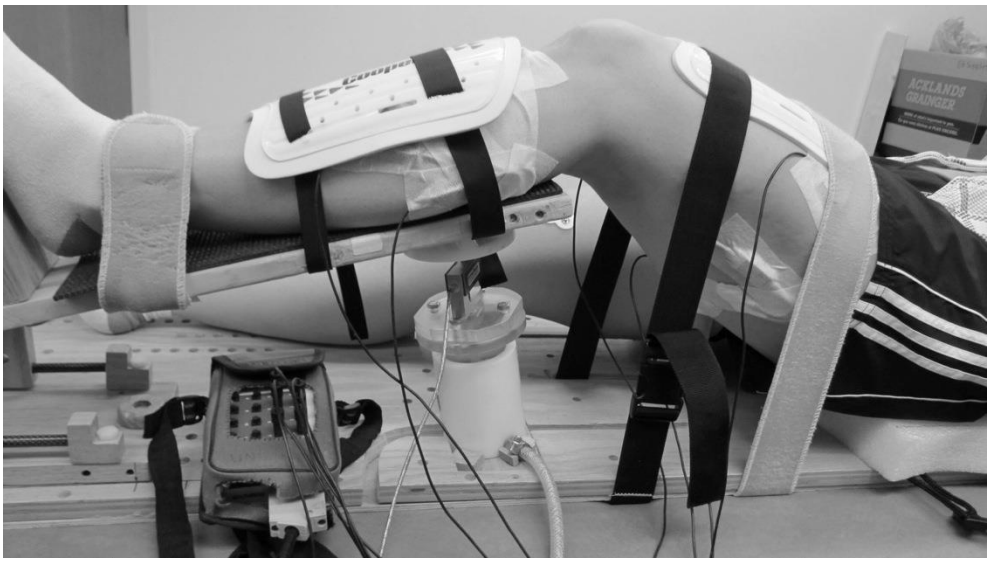

Figure 4-1: Participant secured in the KLA for calibration procedure.

Participants were instructed to relax their muscles and remain still for the duration of the calibration. The hydraulic piston was incrementally raised and lowered while the hydraulic cylinder voltage and compression load cell voltage were recorded. At each piston height, EMG was recorded for twenty s and visually monitored to identify signs of muscle guarding during loading. If muscle guarding was suspected, the participant was told to relax and the procedure was repeated.

Knee Joint Forces

The force-voltage relationship recorded in the procedure detailed above determined the voltage required to produce an applied force with the hydraulic cylinder, F_a. To resolve the forces acting on the knee joint, an indeterminate force system was solved based on Küpper et al. (2013). The known forces were the desired anterior reaction force at the knee (F_{ry}), the lower limb weight

(F_t), the counteractive mass (F_w), and the KLA mass (F_m, Figure 4-2). In the current study, a counteractive mass was not required due to the improvements made to the hydraulic system (Section 2.1.1). The lower limb mass (M_s) and center of mass location (COM) were calculated for each participant using classic anthropometric data (Winter, 1990), governed by the following equations:

$$M_s = 0.061M \quad \textbf{(Eqn. 4-1)}$$

$$COM = 0.394L \quad \textbf{(Eqn. 4-2)}$$

Where M = body mass

L = distance from femoral condyles to the medial malleolus.

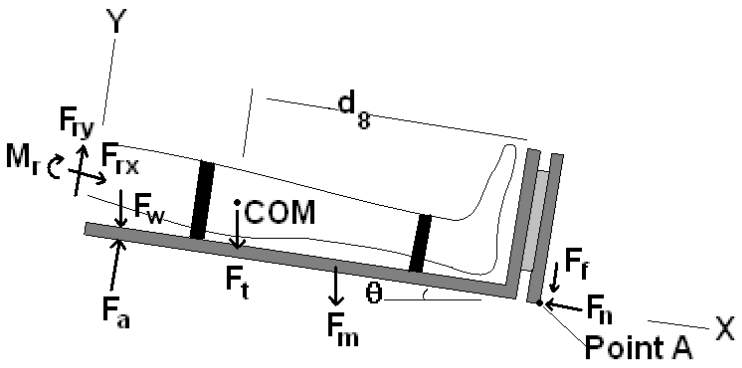

Figure 4-2 Free Body Diagram of the indeterminate force system for the KLA during testing. Forces include the applied force from the hydraulic force system (F_a), the reaction forces and moments at the knee (F_{ry}, F_{rx}, M_r), the counteractive mass (F_w), the KLA mass (F_m), and the reaction forces at the hinge (F_f, F_n). Used with permission from ASME (Küpper et al., 2013)

The unknown forces were the required applied force (F_a), the moment and axial reaction forces acting at the knee joint (M_r, F_{rx}), and the two reaction forces at the hinge (F_f, F_n). To add two

additional constraint equations, two main assumptions were made. First, the axial force F_{rx} could be neglected since the primary direction and largest magnitude of force application was in the anterior (y) direction. Second, the ratio of F_n/F_f was assumed to be 0.98, which was calculated during a static calibration of the KLA, as described by Kupper (2008). The governing equations of static equilibrium were used to calculate the target applied force (F_a) required to reach the desired anterior knee force (F_{ry}):

$\rightarrow + \sum$Fx:

$$F_{rx} + F_w \sin\theta + F_t \sin\theta + F_m \sin\theta - F_n = 0 \qquad \textbf{(Eqn. 4-3)}$$

$\uparrow + \sum$Fy:

$$F_{ry} + F_a - F_w \cos\theta - F_t \cos\theta - F_m \cos\theta - F_f = 0 \qquad \textbf{(Eqn. 4-4)}$$

$\circlearrowleft + \sum M_a z$

$$-M_r - F_{ry} d_1 + F_w d_2 \cos\theta - F_a d_2 + F_t d_8 \cos\theta + F_m d_5 \cos\theta = 0 \qquad \textbf{(Eqn. 4-5)}$$

The added constraint equations are defined by:

$$F_n = 0.98 F_f \qquad \textbf{(Eqn. 4-6)}$$

$$F_{rx} = 0 \qquad \textbf{(Eqn. 4-7)}$$

4.3.2.2 MR Imaging

The following imaging procedure was performed separately for each leg. Six reflective markers were placed onto the participant's skin around the knee using the traced outlines from kinematic testing, and were left in place for the imaging duration. Joint geometry images were acquired using a GE Discovery 750 3T MR scanner (General Electric Healthcare, Waukesha, WI) in conjunction with a general purpose flex coil (General Electric Healthcare, Waukesha, WI).

Participants were positioned in the calibrated KLA, as described in Section 4.3.2.1. The compression load cell (for calibration) was removed for MR imaging, and a thigh support was

added to support the weight of the leg during imaging. The shank and thigh straps were secured, and the knee was positioned in 30° of flexion, confirmed with a goniometer. The general purpose flex coil (General Electric Healthcare, Waukesha WI) was secured around the knee joint with Velcro® straps ensuring a fit that would not restrict anterior knee motion or interfere with the movement of the KLA. The flex coil improved the quality of the images, providing a brighter image and a better signal to noise ratio.

For assessment by a radiologist, a sagittal fast spin echo (FSE) proton density (PD) fat saturated scan (TR: 3000 ms, TE: 26.064 ms) was obtained at a resolution of 0.31 mm x 0.31 mm x 3.0 mm [FOV 16 cm x 16 cm, 512 x 512 matrix] (Figure 4-3). The purpose of this review was to assess ACL status: intact for healthy participants and completely ruptured for ACLD participants. These images were also graded for joint effusion by a single radiologist, using the MOAKS (Hunter et al., 2011) and KIMRISS (McDougall et al., 2014) effusion scores.

Figure 4-3: Diagnostic proton density (PD) MR image to assess ACL status.

A fat-saturated steady-state free-precession (SSFP) imaging sequence (TR: 7.136 ms, TE: 2.044 ms) was used to obtain high resolution sagittal and axial plane images of the knee for coordinate system determination for the joint (Section 3.3.2.3). The knee was in the reference position (hydraulic system not pressurized) at a resolution of 0.31 mm x 0.31 mm x 1.0 mm [FOV 16 cm x 16 cm, 512 x 512 matrix].

Next, knee joint geometry was obtained at a knee angle of 30^{o} with applied anterior load levels of 0, 30, 50, 89, and 133 N, during loading and unloading phases. The load was applied with the KLA loading apparatus (described in Section 2.1). Forces were applied and monitored from the control room via the hydraulic system. No active participation was required from the participant, they were required to lie still and relax. Low resolution sagittal images of the knee joint were obtained during loading, at a resolution of 0.31 mm x 0.31 mm x 3.0 mm (FOV 16 cm x 16 cm, 512 x 512 matrix) using a balanced SSFP sequence.

The MR scan sequences were chosen based on the work of Kupper (2008). The high resolution images provided detailed joint geometry at the expense of longer scan times (2 minutes and 38 s). During joint loading, low resolution images minimized scan time (1 minute and 3 s) resulting in loss of image quality. The high resolution images were used to define accurate coordinate systems from bony landmarks that were then applied to the lower resolution images using a custom registration technique (Habib et al., 2001).

Once the loading protocol was complete for both legs, the KLA was removed from the MR scanner and a muscle volume scan of the participant's thighs was acquired using the same MR scanner (without the flex coil). The participant was positioned supine on the scanner bed in full knee extension with their toes taped together to prevent movement during the scan. A spoiled gradient (SPGR) muscle volume sequence (TR: 2500 ms, TI: 0 ms, TE: 21.216 ms) was used to

obtain axial images of the VL, VM, BF and ST (Figure 4-4). Images had a slice thickness of 10 mm and an image resolution of 0.7813 mm × 0.7813 mm (512 × 512 matrix and field of view of 40 cm × 40 cm). The participant was in full extension and relaxed for the duration of the scan (approximately 5 minutes).

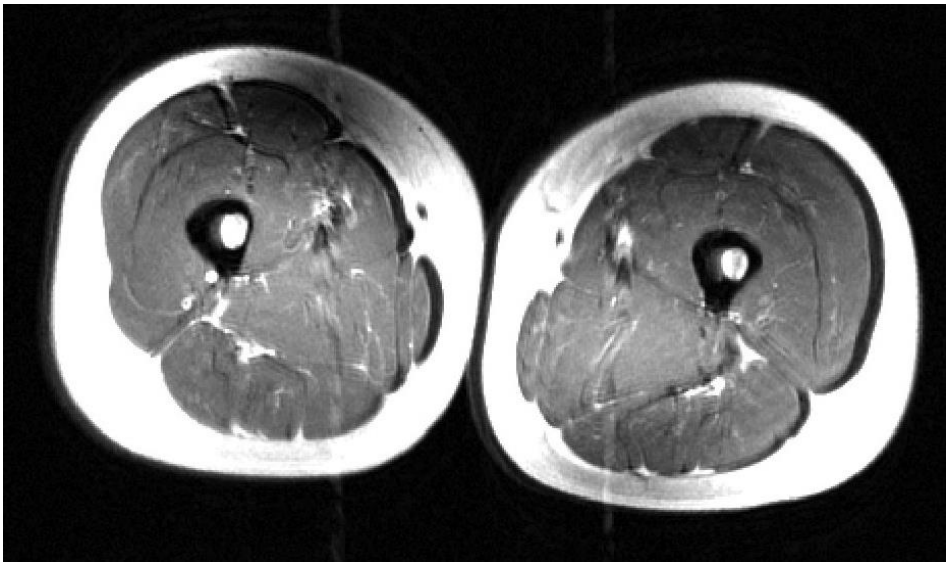

Figure 4-4: Muscle volume MR image of thigh muscles.

4.3.3 Data Processing

Techniques for analysing kinematic (FHA) and EMG data, including LCS definition, are described in Chapter 3. Data analysis techniques to calculate joint laxity from MR images under loading (KLA) and muscle volume are presented in the following section.

4.3.3.1 Joint Laxity

ATT resulting from force application to the tibia with the KLA during MR imaging (described in Section 4.3.2.2) is a key study variable relating to joint laxity. The following section describes the analysis techniques used to calculate this variable, based on the work of Kupper (2008). The

processes to provide the 3D joint displacement of the femur with respect to the tibia (in the tibia LCS) under loading, specifically ATT, are described in the following sections (Figure 4-5).

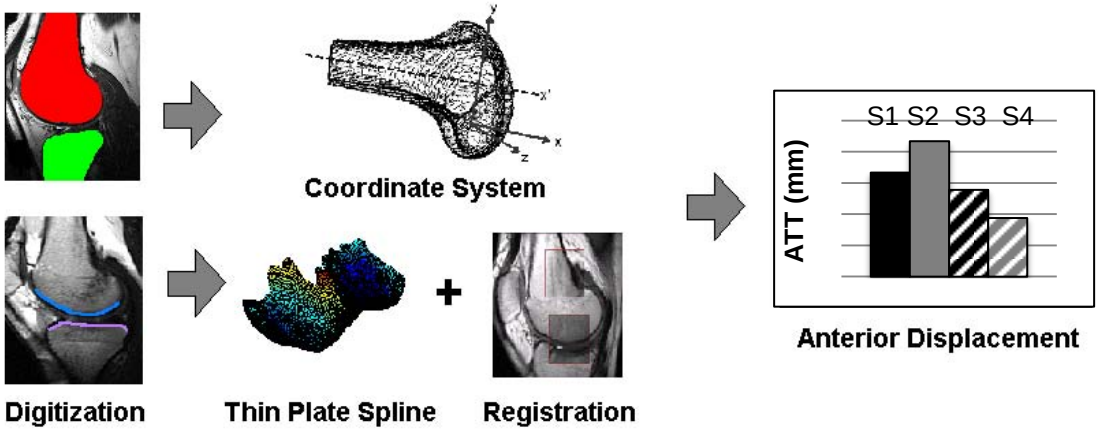

Figure 4-5: 'Flow Chart depicting the image data analysis process through digitization to obtain local joint coordinate systems, thin plate spline mappings of joint surfaces, registration to match surfaces, combined to find anterior joint displacement' (adapted from Kupper, 2008)

Image Digitization

High resolution (unloaded) and low resolution (loaded) sagittal MR images were digitized using Amira 5.0 software (FEI Visualization Science Group, Oregon USA), as described in Section 3.3.3.1. A 3D point cloud was output for the femur and tibia bones in the image coordinate system (ICS).

For coordinate system definition, the entire volume of the femur and tibia bones were used from the sagittal high resolution MR images (Figure 4-6 a). For joint surface registration (between high and low resolution images) only the articulating surfaces of the femur and tibia were required. In Amira, the "Cluster Filter" function was used to define the region of interest for joint

image registration. A 3D cloud of points in the ICS for the femur and tibia surfaces was output for both high resolution and low resolution sagittal images (Figure 4-6 b,c).

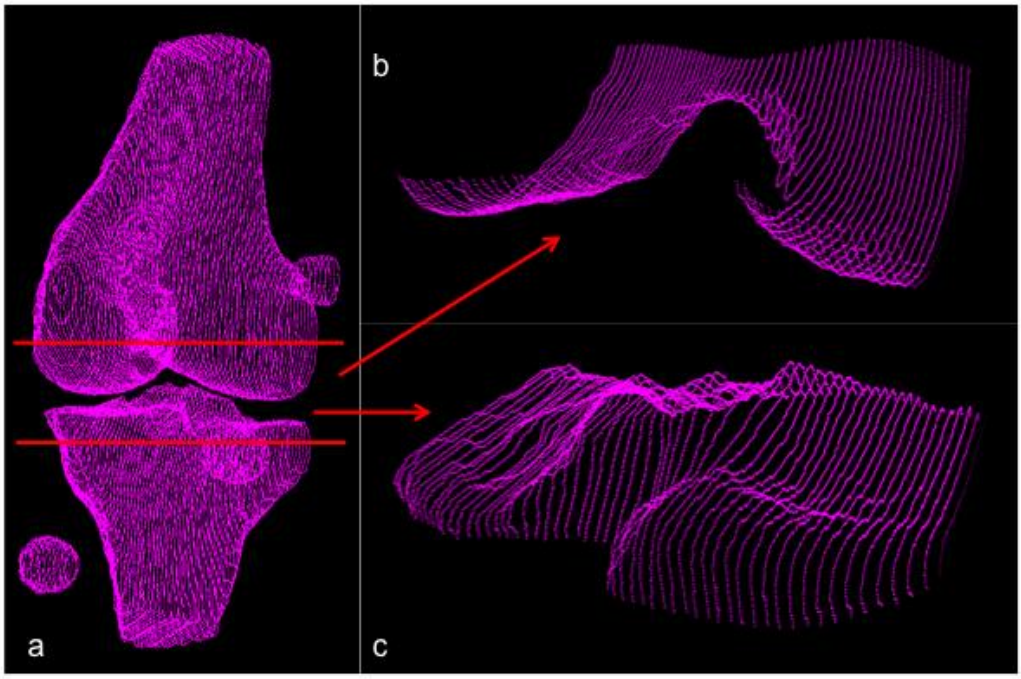

Figure 4-6: Image Digitization resulting in a 3D point cloud for the femur and tibia bones (a) for LCS definition. Cutting planes were applied in Amira (red lines) to isolate the femur (b) and tibia (c) surfaces for joint surface registration.

Local Coordinate System Definition

The digitized 3D high resolution femur and tibia volumes were used to define the coordinate systems based on bony geometry. For a right knee, the ICS is oriented with the x-axis positive in the medial direction, y-axis positive in the posterior direction, and z-axis positive in the superior/proximal direction. Both the local coordinate systems (LCS) for the femur and tibia were oriented with the x-axis positive in the distal direction, y-axis positive in the anterior direction, and z-axis positive in the anatomical right direction.

The femoral LCS was defined as described in Section 3.3.3.2. The LCS for the tibia was defined using the method developed by Kupper (2008). The ellipse-fit technique used to define the femur LCS longitudinal axis (x-axis) was also used for the tibia LCS longitudinal axis (x-axis). Kupper (2008) determined that the ellipse fit technique underestimated the 30^{o} knee flexion angle (confirmed with a goniometer) due to the cut-off point for tibial geometry in the MR image field of view. Accordingly, a 30^{o} rotation of the tibia LCS with respect to the femur LCS in the z-y plane of the ICS was applied as a correction factor.

The mediolateral axis (z-axis) of the tibia LCS was defined using the posterior tibial condylar line (PTCL), defined by the most posterior points of each tibial condyle. A sixth order polynomial was fit to the axial view of the data set to detect these points. The local maxima of the sixth order polynomial were determined, corresponding to the most posterior points of the medial and lateral tibial condyles. The line connecting these two points was defined as the mediolateral axis (z-axis) of the tibia LCS (Figure 4-7a).

The mathematical cross product of the z-axis with the x-axis produced the anterior/posterior axis (y-axis) of the tibia LCS. The z-axis was then redefined by taking the cross product of the x-axis and the y-axis to ensure that the coordinate system was orthogonal. The origin of the tibia LCS was defined as the point along the longitudinal x-axis with the shortest perpendicular distance to the mediolateral z-axis (Figure 4-7b), corresponding to the approximate centre and surface of the tibial plateau. Tests were performed previously to compare the root mean square (RMS) error between the locations of the tibia LCS origin for both the midsagittal plane projection and the 3D coordinate. For multiple repetitions of defining the origin, intra-tester repeatability was found to be 0.47 mm in the midsagittal plane and 0.23 mm in 3D (Kupper, 2008).

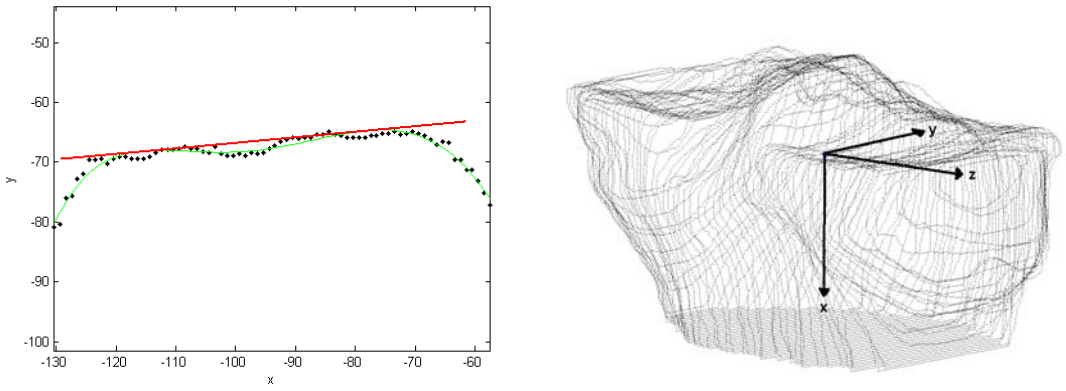

(a) **(b)**

Figure 4-7: (a) Medial/Lateral z-axis definition (red) based on the PTCL using a sixth order polynomial (green) and (b) the tibia LCS with permission from Kupper (2008)

Surface Reconstruction

A Thin Plate Spline (TPS) algorithm was used to fit a surface to the 3D cloud of points for the femur and tibia, generated from the digitization of high and low resolution sagittal MR images (Section 4.3.3.1) (Figure 4-8). This custom Matlab algorithm (version 7.11, The MathWorks Inc., Natick, USA) has been used previously to generate 3D surfaces from MR data (Kupper, 2008). The application of the TPS to joint surface modelling is described in detail by Boyd et al. (1999).

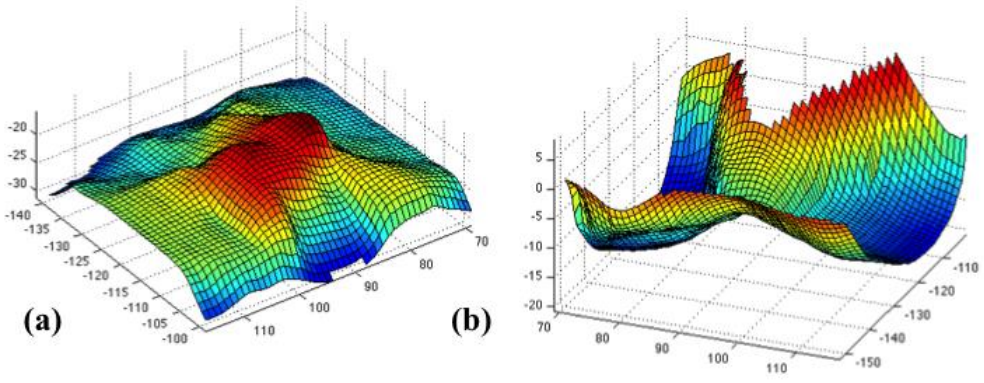

Figure 4-8: TPS Surfaces for high resolution (a) tibia and (b) femur

The TPS deforms an infinite thin plate with bending and without shear to pass through a set of data points while minimizing bending energy. The bending energy E(*f*) for a surface z=*f*(x,y) is given by:

$$E(f) = \iint_{R^2} \left\{ \left[\frac{\partial^2 f}{\partial x^2} \right]^2 + 2 \left[\frac{\partial^2 f}{\partial x \partial y} \right]^2 + \left[\frac{\partial^2 f}{\partial y^2} \right]^2 \right\} dxdy \qquad \textbf{(Eqn. 4-8)}$$

where R^2 is the x-y plane, and z describes the deflected height of the surface data points. Smoothing can be applied to the TPS surface S(x,y) such that

$$S(x, y) = \sum_{i=1}^{n} c_i f_i(x_i, y_i) + c_{n+1} + c_{n+2} x + c_{n+3} y \qquad \textbf{(Eqn. 4-9)}$$

where c_i are constants, and the functions f_i relate the data points to the base surface for *n* data points. Smoothing is performed using a least squares criterion where the function J(*f*) is minimized when *f* = S:

$$J(f) = E(f) + \sum_{n=1}^{n} w_i \left[f(x_i, y_i) - z_i \right]^2 \qquad \textbf{(Eqn. 4-10)}$$

where w_i are the weights that determine the amount of smoothing. As the value of w_i increases towards infinity, the surface becomes interpolated with minimal smoothing. Conversely, as w_i decreases towards zero, oversmoothing results in a planar surface. For the current study, a smoothing factor of 0.275 was used for the rougher tibial surface, and 0.6 was used for the relatively smooth femur, based on the work of Kupper (2008).

To achieve an evenly distributed point set for surface registration, high resolution femoral and tibial data were resampled at 1 mm by 1 mm intervals using the TPS algorithm. Low resolution images were resampled at 3 mm by 1 mm intervals to preserve the in-plane resolution.

Registration Technique

Registration is a surface matching technique that solves for the parameters required to transform one surface to match another. The current project used a custom registration technique (Habib et al., 2001), implemented in Matlab 7.11 (The Mathworks Inc., Natick, USA). The advantages of this technique include the ability to handle randomly distributed data sets, multiple coordinate systems, and varying levels of point density. These features make this technique suitable for MR image analysis since the data may be collected at different image resolutions, in different body positions, and over multiple days. Previous work performed registration of femoral MR image data with a pixel size of 0.6 mm, and found that the average root mean square distance was 0.217 ± 0.035 mm (Cheng, 2006). This value was less than the size of the image pixel, indicating a high quality fit of the surface.

For this registration technique, the first surface (S_1) is defined by points, and the reference surface (S_2) is defined by triangular patches. A 3D similarity transformation is used to match the two surfaces. This assumes that the transformation between surfaces is rigid, which is appropriate for the current application since the bone surfaces are assumed to be rigid. A coplanarity condition requires that the volume between a point and corresponding patch must be equal to zero (Figure 4-9).

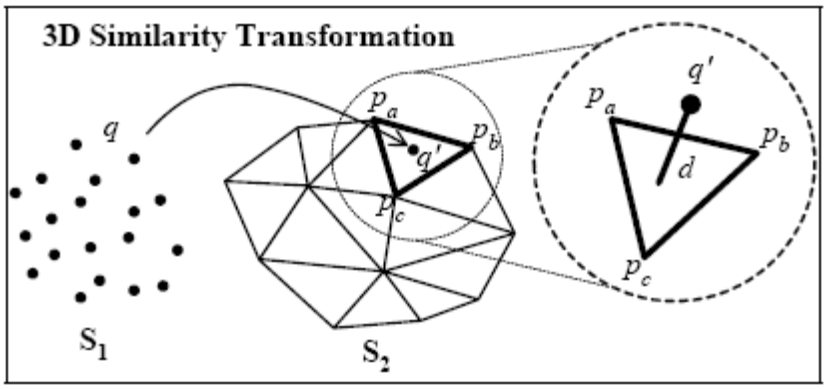

Figure 4-9: 'Coplanarity condition describes the correspondence between a point in S1 and a patch in S2 after performing 3D similarity transformation' (used with permission from Cheng, 2006)

The primary output from the registration algorithm is the transformation function that describes the relationship between the reference frames of S_1 and S_2. The transformation function is described by seven parameters: three translations (X_T, Y_T, Z_T), three rotations (ω, φ, κ), and one scaling factor (S). The equation describing the transformation of points from surface one (X, Y, Z) to surface two (X', Y', Z') is given by:

$$\begin{bmatrix} X' \\ Y' \\ Z' \end{bmatrix} = \begin{bmatrix} X_T \\ Y_T \\ Z_T \end{bmatrix} + S \times R(\omega, \varphi, \kappa) \begin{bmatrix} X \\ Y \\ Z \end{bmatrix} \qquad \textbf{(Eqn. 4-11)}$$

For the current study, S_2 was defined using high resolution data, and S_1 was defined using low resolution data. The distance threshold between S_1 and S_2 to identify a match was set to 0.5 mm based on the work of Kupper (2008). The scaling constant S was equal to one in all cases. The remaining six output parameters were used to create transformation matrices for the femur

(T_l2hfem) and tibia (T_l2htib) at each load level. The transformation matrices described the transformation from low resolution (loaded) image space to high resolution (unloaded) image space. The transformation matrix was used in a series of coordinate transformations to determine tibial displacement under loaded conditions.

Coordinate Transformations to obtain Gross Joint Displacement

Coordinate transformations were used to determine the relative movement of the femur with respect to the tibia at each load level, as described previously by Kupper (2008). The method described in Section 3.3.3.1 was used to compute the transformation matrix between two coordinate systems (Soderkvist and Wedin, 1993).

For the current study, a series of transformation matrices were required to determine the relative displacement between the femur and tibia in the tibia LCS (Figure 4-10). Transformation matrices for the femur and tibia (T_l2hfem and T_l2htib) mapping the low resolution bone to the high resolution bone in the ICS were found using a registration technique. The local coordinate system definition was used to apply the Soderkvist and Wedin (1993) technique. The transformation matrix for the femur and tibia (T_bonefem and T_bonetib) was calculated from the femur LCS and tibia LCS points in the ICS (x_1, x_2, x_3) to the unit vectors y_1 = (1,0,0), y_2 = (0,1,0), and y_3 = (0,0,1).

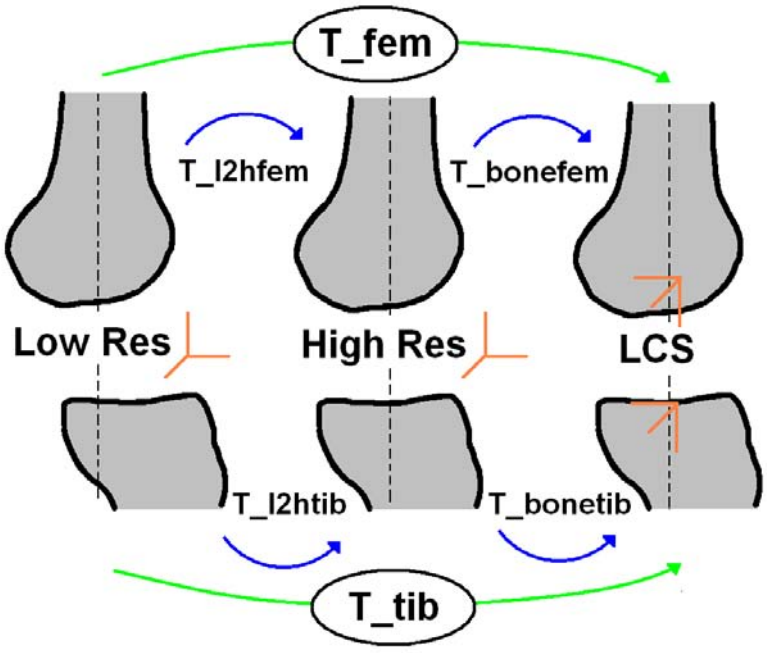

Figure 4-10: 'Transformation matrices for conversion from low resolution images (applied load) to high resolution images (T_l2hfem, T_l2htib) to LCS (T_bonefem, T_bonetib). Cumulative transformation matrices from low resolution images to LCS (T_fem, T_tib) are used to obtain relative motion between tibia and femur' with permission from Kupper (2008)

The transformation matrix (T_{rel}) describing the relative motion of the femur with respect to the tibia in the tibia LCS was determined by:

$$T_{rel} = (T_{bonetib} * T_{l2htib}) * (T_{bonefem} * T_{l2hfem})^{-1} \quad \textbf{(Eqn. 4-12)}$$

Cardan angles (described in Section 3.3.3.1) were used to determine the joint angles and displacements of the femur with respect to the tibia from T_{rel}. For this calculation, the angles of rotation were minimal and the order of rotation was selected as: flexion/extension, internal/external rotation, and ab/adduction (z, x, y). Three rotations and three translations about the tibia LCS axes were calculated from the transformation matrix. The main output variable was anterior displacement of the tibia. Knee flexion angle and internal/external rotation were also of interest but were not considered primary outcome measures.

4.3.3.2 EMG Segmentation of Each Repetition

To examine muscular control in the current study, the entire cycle was of interest, as opposed to the finite range of 20-40° of knee flexion used for FHA determination. Cycle initiation and completion times were required for each repetition to allow averaging of EMG data over trials and repetitions for the squat and swing tasks. Kinematic marker locations were used to determine the initiation and completion times for each cycle. For the swing task, the marker located superior to the lateral malleolus was used. The greater trochanter marker was used for the squat task (marker placement described in Section 3.3.2.1). For the squat task, the initiation of the cycle was defined as the time point when the greater trochanter marker moved more than 0.1 mm in the vertical direction (global coordinate system) between successive frames. Cycle completion was defined as the time point when the marker moved less than 0.1 mm between successive frames (Figure 4-11). Initiation and completion times were determined in a similar manner for the swing task, using the marker superior to the malleolus. Each repetition was normalized to 100% of cycle, enabling averaging of trials and participants within the ACLD and healthy groups.

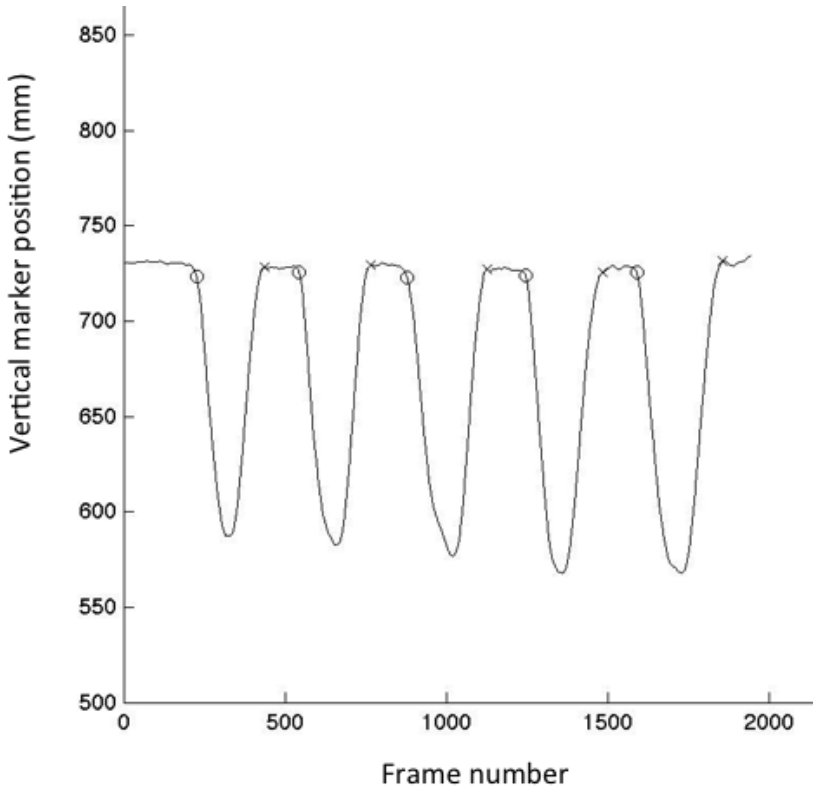

Figure 4-11: Initiation (o) and completion (x) times for each repetition selected from marker position data for the squat task

4.3.3.3 Muscle Volume

Muscle volume was quantified to investigate changes in muscle size due to ACL injury. The muscle anatomical MR data was input into Amira (FEI Visualization Science Group, Oregon USA) and each muscle was manually digitized throughout the length of the thigh, from the proximal patella to the hip joint centre (Figure 4-12). A corresponding volume was calculated for the VM, VL, BF and SEM muscles by multiplying the muscle area on each image slice by the slice thickness, and summing over all image slices. Since muscle volume is highly dependent on individual participant height and weight, comparisons were limited to within participant comparisons between legs.

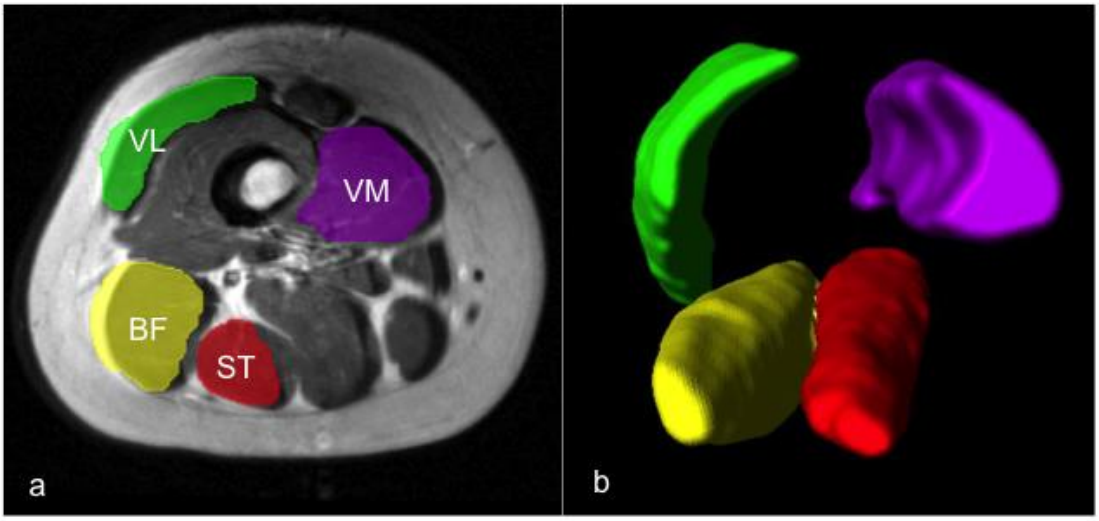

Figure 4-12: Digitization of the VM, VL, BF, and ST (a) and the resulting image muscle volume (b) obtained in Amira software

4.3.4 Statistics

SPSS (SPSS Statistics 20, IMB, New York USA) was used for all statistical analysis in the current study. The Shapiro-Wilks test was used to check for normality in laxity, FHA, muscle power and muscle volume measures in the healthy and ACLD groups (Appendix B). Group distributions for each leg were examined (to check for use with the T-test), as well as the distribution of the side to side differences (Δ_{leg}) (for use with paired T-tests). The null hypothesis that the data is normally distributed is rejected if $p<0.05$.

FHA measures, muscle power and Δ_{leg} ATT were evaluated for normal distribution in the healthy and ACLD groups. The precise test applied depended on the result of the normal distribution test. The T-test is very robust for violations against normality (Sawilowski and Blair, 1992). Therefore, if the majority of variables were normally distributed then the T-test was used for comparisons between healthy and ACLD groups to enable comparison and discussion of group means ($\alpha=0.05$). However, equal variance between groups is critical (Sawilowski and Blair,

1992). Levene's test for equality of variance was applied, and if the groups did not exhibit equal variance, the p-value was reported for the case that equal variances were not assumed. If the majority of variables were non-normally distributed, then non-parametric Mann-Whitney U-tests were used to compare between the healthy and ACLD groups (α=0.05).

Side to side differences in FHA measures, muscle power and muscle volume were evaluated for normal distribution in the healthy and ACLD groups. The precise test applied depended on the result of the normal distribution test. The paired T-test is very robust for violations against normality (Sawilowski and Blair, 1992). Therefore, if the majority of variables were normally distributed then the paired T-test was applied to compare between dominant and contralateral limbs in the healthy group, and injured and contralateral limbs in the ACLD group (α=0.05). If the majority of variables were non-normally distributed, then non-parametric Wilcoxon Signed Ranks tests were used to compare between dominant and contralateral limbs in the healthy group, and injured and contralateral limbs in the ACLD group (α=0.05).

Spearman's Rank-Order Correlation test was used to determine significant correlations between ATT and FHA measures in the healthy and ACLD groups. Select correlations were explored based on the understanding of the physical meaning of FHA measures (location y, FHA translation, FHA dispersion, FHA path length and AP excursion). The non-parametric Spearman's correlation was chosen instead of the parametric equivalent (Pearson's correlation). This decision was taken because Spearman's correlation does not assume that the data is linearly related, instead it assumes that there is a monotonic relationship between the two variables. A monotonic relationship means that the variables either increase in value together, or as one variable value increases, the other variable value decreases. Since there is no evidence to suggest that FHA measures should be linearly correlated with ATT, the non-parametric test was chosen.

The Spearman correlation coefficient provides a measure of the strength of the relationship, where 0-0.19 is very weak, 0.2-0.39 is weak, 0.4-0.59 is moderate, 0.6-0.79 is strong, and 0.8-1.0 is considered very strong.

4.4 Results

4.4.1 Statistics

IKDC and Lysholm scores were normally distributed for the ACLD group (p value range: 0.340-0.992), but not for the healthy group ($p \leq 0.002$, Table B-5). The T-test was chosen to compare IKDC and Lysholm scores between groups, reporting the p-value for non-equal distributions.

The side to side difference in ATT was normally distributed for both the healthy (p=0.494) and ACLD (p=0.522, Table B-2) group, therefore the T-test was used to compare Δ_{leg} ATT between groups (α=0.05).

The majority of FHA variables were normally distributed for both limbs of the ACLD group (range of non-normally distributed = 9%-22% for a given limb), and for the healthy group (range of non-normally distributed = 19%-28% for a given limb, Table B-2). Therefore, T-tests were used for between group comparisons of FHA measures to enable comparison and discussion of group means (α=0.05). The percentage of non-normally distributed side to side differences in FHA variables was 16%, and 13%, for the healthy and ACLD groups, respectively. Therefore, the paired T-test was used to compare FHA measures between dominant and contralateral limbs in the healthy group, and injured and contralateral limbs in the ACLD group (α=0.05).

The percentage of non-normally distributed side to side differences in muscle power was 75%, and 33%, for the healthy and ACLD groups, respectively (Table B-3). Therefore, non-parametric Wilcoxon Signed Ranks tests were used to compare muscle power between dominant and contralateral limbs in the healthy group, and injured and contralateral limbs in the ACLD group

(α=0.05). Muscle power data from some participants was excluded due to poor quality, therefore participant numbers were low (n=8 for healthy, n=6 for ACLD), which could contribute to the non-normal distribution. Furthermore, the EMG normalization technique employed for this study (Section 3.3.3.3) was designed for within subject comparisons, which may also have affected the distribution of the data.

The percentage of non-normally distributed side to side differences in muscle volume was 25% for the ACLD group (Table B-4). Therefore, the paired T-test was used to compare muscle volume between injured and contralateral limbs in the ACLD group (α=0.05).

4.4.2 Study Participants

One of the ACLD participants was excluded due to a high BMI that resulted in poor quality kinematic and EMG data. The ACLD group (Table 4-1) consisted of nine females (28.8 ± 7.2 yrs, 166.9 ± 5.0 cm, 65.6 ± 11.5 kg). Average time from injury for the ACLD group was 45.6 ± 5.9 days for the six week testing session.

Table 4-1: Study Participant Information

	Participant ID	Age (years)	Height (cm)	Weight (kg)	Injured Limb	6 weeks (days)
ACLD	A01	27	163	54.9	Right	40
	A02	23	159	57.6	Left	50
	A03	37	175	90.7	Left	41
	A04	22	168	61.2	Left	36
	A05	29	165	60.3	Right	50
	A06	37	167	61.2	Right	51
	A07	28	170	68.0	Right	46
	A08	18	163	59.0	Right	53
	A09	38	172	77.5	Right	43
	Mean (std)	28.8 (7.2)	166.9 (5.0)	65.6 (11.5)		45.6 (5.9)

The ACLD group had statistically significantly lower scores for both the IKDC and Lysholm questionnaires compared to the healthy group (Table 4-2). The ACLD group had an average score of 50.8 ± 15.1 for the IKDC, compared to 97.8 ± 4.9 for the healthy group ($p<0.001$). For the Lysholm questionnaire, the ACLD group had an average score of 68.1 ± 18.8, compared to 97.5 ± 3.4 for the healthy group ($p=0.002$).

Table 4-2: IKDC and Lysholm knee function questionnaire scores (out of 100) for the healthy and ACLD groups

Healthy			**ACLD**		
Participant ID	**IKDC**	**Lysholm**	**Participant ID**	**IKDC**	**Lysholm**
H01	n/a	100.0	A01	49.4	82.0
H02	100.0	100.0	A02	64.4	69.0
H03	100.0	90.0	A03	58.2	85.0
H04	94.3	95.0	A04	50.6	59.0
H05	100.0	100.0	A05	51.7	51.0
H06	98.9	100.0	A06	18.4	34.0
H07	100.0	100.0	A07	39.1	64.0
H08	98.9	100.0	A08	55.2	73.0
H09	100.0	95.0	A09	69.9	96.0
H10	100.0	100.0			
H11	83.9	95.0			
H12	100.0	95.0			
Mean	97.8	97.5	**Mean**	50.8	68.1
Std	4.9	3.4	**Std**	15.1	18.8

The ACLD injured limb had a significantly higher KIMRISS effusion score compared to the healthy dominant limb, indicating increased joint effusion (Table 4-3). The ACLD injured limb had an average KIMRISS score of 3.22 ± 2.73, compared to 0.5 ± 0.67 for the healthy dominant limb ($p=0.017$). For the MOAKS joint effusion score, the ACLD injured limb had an average of 0.44 ± 0.73, while the healthy dominant limb had an average of 0 ± 0 ($p=0.104$). There were no

significant differences between limbs in the healthy group for MOAKS (p=0.339) or KIMRISS (p=0.166) scores, or in the ACLD group for MOAKS (p=0.282) or KIMRISS (p=0.073) scores.

Table 4-3: MOAKS (0-3) and KIMRISS (0-12) joint effusion scores for the dominant and contralateral limbs of the healthy group, and the injured and contralateral limbs of the ACLD group

Healthy					ACLD				
	Dominant		Contralateral			Injured		Contralateral	
ID	MOAKS	KIM RISS	MOAKS	KIM RISS	ID	MOAKS	KIM RISS	MOAKS	KIM RISS
H01	0	1	0	2	A01	2	9	0	0
H02	0	1	0	0	A02	1	5	0	0
H03	0	0	0	2	A03	0	3	0	1
H04	0	0	0	0	A04	1	5	0	1
H05	0	0	0	1	A05	0	1	0	1
H06	0	0	0	1	A06	0	1	0	0
H07	0	1	0	1	A07	0	3	0	1
H08	0	2	1	2	A08	0	1	0	0
H09	0	1	0	1	A09	0	1	1	4
H10	0	0	0	0					
H11	0	0	0	0					
H12	0	0	0	0					
Mean	0.00	0.50	0.08	0.83	**Mean**	0.44	3.22	0.11	0.89
Std	0.00	0.67	0.29	0.83	**Std**	0.73	2.73	0.33	1.27

4.4.3 Laxity

Laxity values (ATT) are reported for an anterior reaction force (F_{ry}) of 89 N at the knee joint. This load was chosen for comparison purposes because it is clinically relevant (Daniel et al., 1985), and the maximum applied load of 133 N was not achieved in every participant due to height limitations in the MR scanner and the technique used to secure the participant's thigh during loading.

The reaction force (F_{ry}) at the proximal tibia resulting from KLA loading during MR imaging was within 12.9% of the target F_{ry} for the dominant limb of the healthy group, and within 43.4% of the target F_{ry} for the contralateral limb of the healthy group (Table 4-4). The between limb

difference for the reaction force was within 33.8% for the healthy group. For the ACLD group, F_{ry} was within 11.3% of the target F_{ry} for the injured limb, and within 9.4% of the target F_{ry} for the contralateral limb (Table 4-4). The between limb difference for the reaction force was within 13.1% for the ACLD group. In general, F_{ry} during MR imaging was less than the target F_{ry}, indicated by a negative percent difference.

Table 4-4: Target reaction force at the knee joint (F_{ry},89 N) and F_r applied during MR imaging for healthy and ACLD study participants. Percent difference from target shown for each limb, as well as percent difference between limbs.

Healthy						
		Dominant		**Contra**		
Participant ID	**Target F_{ry} (N)**	**Actual F_{ry} (N)**	**% diff**	**Actual F_{ry} (N)**	**% diff**	**% diff b/w limb**
H01	89	n/a		n/a		
H02	89	82	-7.4	69	-22.9	-15.4
H03	89	79	-10.8	71	-20.4	-9.6
H04	89	81	-8.5	71	-20.7	-12.1
H05	89	78	-12.9	50	-43.4	-30.5
H06	89	87	-2.0	87	-2.0	0.1
H07	89	84	-5.4	89	-0.3	5.1
H08	89	89	0.1	60	-33.1	-33.2
H09	89	88	-1.6	84	-5.6	-4.0
H10	89	88	-1.4	58	-35.2	-33.8
H11	89	89	0.2	90	1.5	1.3
H12	89	86	-3.7	85	-4.0	-0.3
ACLD						
		Injured		**Contra**		
	Target F_{ry} (N)	**Actual F_{ry} (N)**	**% diff**	**Actual F_{ry} (N)**	**% diff**	**% diff b/w limb**
A01	89	85	-4.2	88	-1.6	2.6
A02	89	84	-5.8	86	-2.9	3.0
A03	89	79	-11.3	91	1.8	13.1
A04	89	91	2.7	89	-0.4	-3.2
A05	89	86	-3.9	87	-2.5	1.4
A06	89	89	-0.1	81	-9.4	-9.4
A07	89	88	-1.3	86	-3.2	-1.9
A08	89	84	-5.9	90	1.4	7.3
A09	89	87	-1.9	86	-3.8	-1.9

Generally, the ACLD group demonstrated increased ATT in the injured limb compared to the contralateral limb, and compared to the healthy group (Figure 4-13). Side to side differences in ATT were calculated as Δ_{leg} ATT=$ATT_{Injured}$-$ATT_{Contralateral}$ for the ACLD group, and Δ_{leg} ATT=$ATT_{Dominant}$-$ATT_{Contralateral}$ for the healthy group. The average Δ_{leg} ATT at 89 N was 2.83 ± 4.39 mm in the ACLD group, and 0.26 ± 0.86 mm in the healthy group, however the difference between groups was not significant ($t(8.46) = -2.084$, $p = 0.069$). In the ACLD group, some participants (n=3) had an increased ATT in the contralateral limb compared to the injured limb, resulting in a negative value for Δ_{leg}ATT. The ACLD group had an average of 5.13 ± 4.13 mm of ATT in the injured limb, while the healthy dominant limb had 1.86 ± 0.76 mm of ATT (p=0.046). Levene's test indicated that there were significant differences in variance between groups (p=0.003), therefore equal variances were not assumed for the T-test.

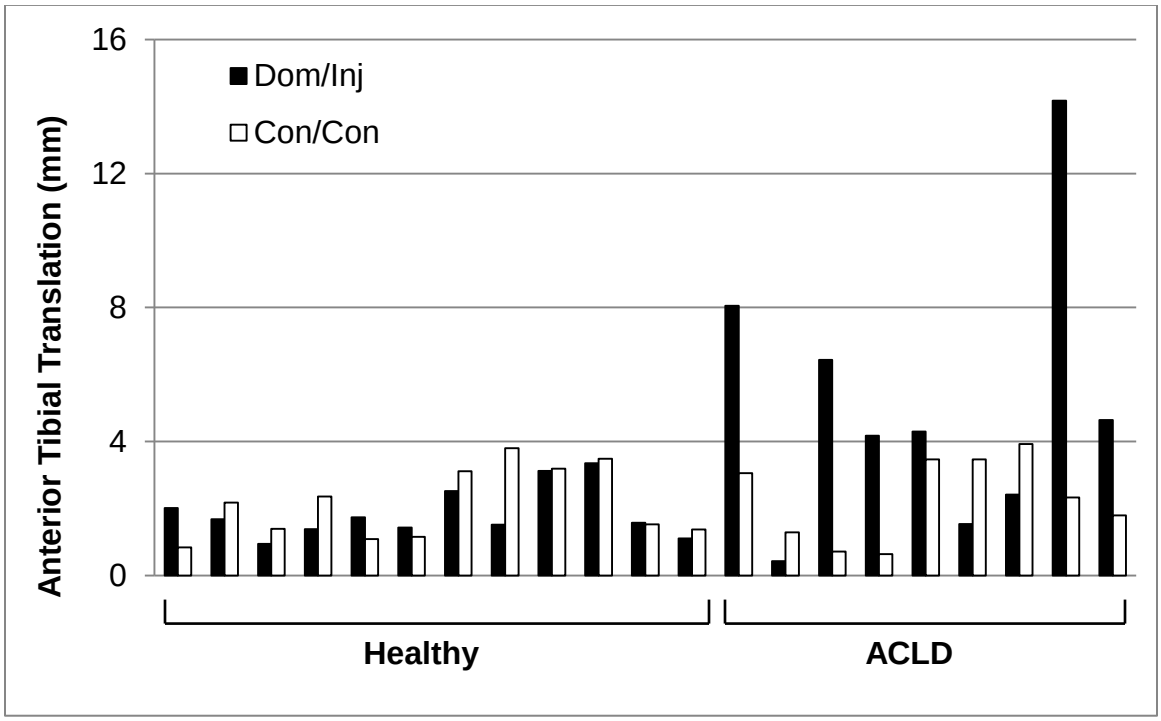

Figure 4-13: Anterior tibial translation for each study participant in the healthy group (n=12) and each study participant in the ACLD group (n=9). Black bars represent ATT for

the dominant limb of the healthy group and the injured limb of the ACLD group, while white bars represent ATT for the contralateral limb of both groups.

4.4.4 FHA

Healthy Group: FHA location describes the intersection of the FHA with the midstagittal (x-y) plane of the knee during a dynamic task. In the healthy group, the FHA was located significantly more anterior (increased location y) in the dominant limb compared to the contralateral during the flexion (p=0.038) and extension (p=0.048) phases of the swing task (Table 4-5, Figure 4-14). The average FHA location y was 24.98 mm in the dominant limb, compared to 21.77 mm in the contralateral limb during swing flexion. During the extension phase of the squat task, PD excursion was significantly greater in the dominant limb of the healthy group compared to the contralateral (p=0.017, Table 4-5), indicating increased movement of the FHA in the PD direction on the midsagittal plane of the LCS. Average PD excursion was 3.04 mm in the dominant limb compared to 2.11 mm in the contralateral limb during squat extension.

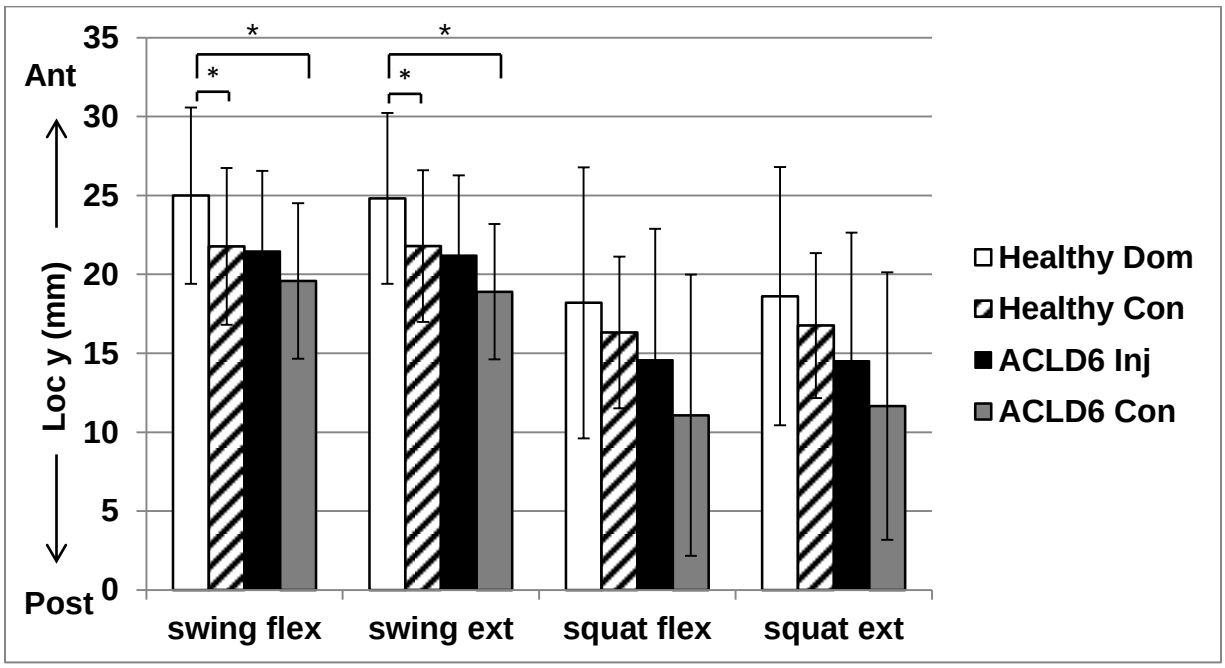

Figure 4-14: Average FHA location y (mm) for the dominant (dom) and contralateral (con) limbs of the healthy group, and for the injured (inj) and contralateral (con) limbs of the ACLD group during the flexion and extension phases of the squat and swing tasks. (* indicates significance at α=0.05).

ACLD Group: In the ACLD group, FHA orientation angle was significantly larger in the injured limb compared to the contralateral limb during squat flexion (p=0.04, Table 4-5), and the FHA was oriented toward internal tibial rotation in the ACLD injured limb (Figure 4-15). The average FHA orientation angle was 12.21° in the injured limb compared to 8.30° in the contralateral limb during the flexion phase of the squat task.

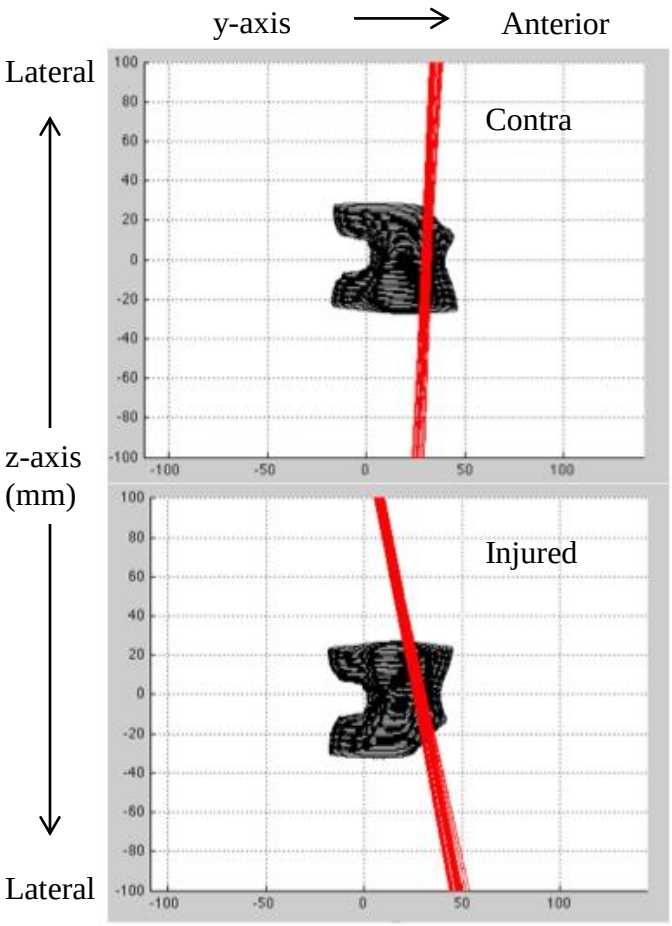

Figure 4-15: Finite helical axes throughout the squat task shown in the y-z (axial) plane (mm) of the LCS for the injured and contralateral limb of an example ACLD participant.

Table 4-5: Average FHA measures for the dominant (dom) and contralateral (con) limbs of the healthy group, and for the injured (inj) and contralateral (con) limbs of the ACLD group during the flexion and extension phases of the squat and swing tasks.

Task	Phase	Measure	Healthy					ACLD				
			Dom mean (std)	Con mean (std)	t	df	p-value	Inj mean (std)	Con mean (std)	t	df	p-value
Swing	flex	loc x (mm)	1.46 (6.22)	0.64 (3.83)	.390	11	.704	-1.76 (4.82)	-1.75 (9.72)	-.003	8	.998
		loc y (mm)	24.98 (5.58)	21.77 (4.97)	2.350	11	.038*	21.46 (5.09)	19.57 (4.92)	1.391	8	.202
		trans (mm)	1.87 (1.95)	2.16 (1.3)	-.474	11	.645	1.88 (0.99)	1.83 (1.07)	.128	8	.902
		orient (°)	11.54 (5.77)	14.97 (8.57)	-1.367	11	.199	12.85 (5.61)	13.33 (5.37)	-.327	8	.752
		disp (°)	1.33 (0.56)	1.34 (0.64)	-.057	11	.956	1.39 (0.49)	1.42 (0.52)	-.175	8	.865
		path (mm)	9.47 (3.04)	10.14 (4.44)	-.947	11	.364	10.5 (8.46)	12.01 (6.17)	-1.391	8	.202
		APex (mm)	3.39 (1.49)	2.68 (1.19)	1.786	11	.102	4.05 (1.84)	3.69 (2.04)	.704	8	.502
		PDex (mm)	2.56 (1.05)	2.35 (0.77)	.569	11	.581	2.6 (1.9)	2.75 (1.14)	-.260	8	.802
	ext	loc x (mm)	0.52 (6.24)	-0.26 (3.94)	.371	11	.718	-2.01 (4.57)	-3.07 (9.14)	.377	8	.716
		loc y (mm)	24.8 (5.41)	21.79 (4.8)	2.228	11	.048*	21.2 (5.06)	18.89 (4.28)	1.900	8	.094
		trans (mm)	-1.59 (2.15)	-2.48 (1.25)	1.438	11	.178	-1.9 (0.84)	-1.97 (1.06)	.153	8	.882
		orient (°)	12.11 (5.71)	16.05 (8.37)	-1.528	11	.155	13.31 (5.32)	13.1 (4.49)	.119	8	.908
		disp (°)	1.22 (0.56)	1.2 (0.5)	.116	11	.910	1.12 (0.68)	1.16 (0.28)	-.161	8	.876
		path (mm)	11.62 (8.32)	7.94 (3.12)	1.821	11	.096	10.42 (9.41)	12.43 (6.86)	-.731	8	.486
		APex (mm)	3 (1.28)	2.24 (1.1)	1.469	11	.170	3.82 (1.81)	3.15 (2.08)	.859	8	.415
		PDex (mm)	2.66 (1.75)	2.14 (0.46)	1.119	11	.287	2.31 (1.5)	2.69 (0.94)	-.849	8	.421

Squat	**flex**	**loc x (mm)**	12.31 (5.79)	10.19 (5.61)	1.180	11	.263	11.49 (5.88)	8.68 (6.85)	1.085	8	.309
		loc y (mm)	18.19 (8.58)	16.3 (4.8)	.905	11	.385	14.56 (8.32)	11.07 (8.9)	1.466	8	.181
		trans (mm)	3.36 (1.53)	3.61 (1.33)	-.568	11	.581	3.78 (0.66)	3.4 (0.87)	1.132	8	.291
		orient (°)	9.79 (3.81)	12.87 (6.13)	-1.260	11	.234	12.21 (2.52)	8.3 (4.17)	2.452	8	.040*
		disp (°)	1.49 (0.24)	1.52 (0.53)	-.183	11	.858	1.76 (0.47)	1.67 (0.41)	.427	8	.681
		path (mm)	6.52 (1.42)	6.73 (1.64)	-.438	11	.670	7.78 (2.43)	8.06 (1.76)	-.303	8	.770
		APex (mm)	2.54 (1.28)	1.85 (0.81)	1.548	11	.150	2.56 (1.33)	3.18 (1.28)	-1.598	8	.149
		PDex (mm)	2.87 (1.54)	2.6 (0.96)	.618	11	.549	3.31 (1.88)	2.74 (1.12)	.860	8	.415
	ext	**loc x (mm)**	10.77 (5.75)	8.54 (5.1)	1.244	11	.239	9.54 (5.98)	7.18 (6.54)	.875	8	.407
		loc y (mm)	18.61 (8.17)	16.75 (4.59)	.918	11	.378	14.51 (8.13)	11.64 (8.47)	1.286	8	.234
		trans (mm)	-3.5 (1.55)	-3.79 (1.53)	.621	11	.547	-3.92 (0.64)	-3.48 (0.81)	-1.361	8	.210
		orient (°)	9.45 (4.16)	12.8 (6.48)	-1.266	11	.232	10.59 (1.82)	7.58 (3.95)	1.999	8	.081
		disp (°)	1.36 (0.37)	1.37 (0.4)	-.102	11	.921	1.59 (0.47)	1.51 (0.45)	.318	8	.759
		path (mm)	8.04 (3.15)	6.61 (1.45)	1.715	11	.114	7.18 (2.44)	7.74 (1.81)	-.469	8	.651
		APex (mm)	2.22 (1.53)	1.63 (0.75)	1.229	11	.245	2.5 (1.35)	2.49 (1.27)	.010	8	.992
		PDex (mm)	3.04 (1.68)	2.11 (0.79)	2.820	11	.017*	2.62 (1.25)	2.37 (0.99)	.432	8	.677

Healthy versus ACLD: The healthy dominant limb was chosen for comparison with the injured and contralateral limbs of the ACLD group because it was thought to be more representative of healthy movement patterns, as it was the limb that the participants' felt most comfortable kicking a soccer ball with. The dominant limb also showed higher variability (indicated with increased

standard deviations) than the contralateral limb, which is consistent with healthy biomechanics data (Georgoulis et al., 2006; Moraiti et al., 2007). Therefore, all comparisons between the healthy and ACLD groups used the healthy dominant limb (referred to hereinafter as the "healthy limb").

There were no significant differences in FHA measures between the healthy limb and the ACLD injured limb. However, compared to the ACLD contralateral limb, the FHA was located significantly more anterior in the healthy limb during swing flexion ($p=0.033$) and extension ($p=0.014$, Figure 4-14). The average FHA location y was 24.99 mm in the healthy limb, compared to 19.58 mm in the ACLD contralateral limb during swing flexion. Additionally, FHA path length was significantly greater in the ACLD contralateral limb compared to the healthy limb during squat flexion ($p=0.039$). The ACLD contralateral limb had an average path length of 8.01 mm, compared to 6.53 mm in the healthy limb.

4.4.5 Correlations

FHA location y describes the intersection of the FHA on the anterior/posterior (y) axis of the midsagittal plane of the knee. In the ACLD injured limb, individuals with higher ATT exhibited a more anterior FHA location (increased location y) (Figure 4-16). FHA location y was significantly correlated with ATT in the ACLD injured limb during both swing flexion ($r_s(9)=0.700$, $p=0.036$) and extension ($r_s(9)=0.733$, $p=0.025$). However, during the squat, the correlation between FHA location y and ATT was not significant during flexion ($r_s(9)=0.633$, $p=0.067$) or extension ($r_s(9)=0.617$, $p=0.077$, Table 4-6). FHA location y was also not significantly correlated with ATT in the healthy limb, or the contralateral limb of the ACLD group for either dynamic task.

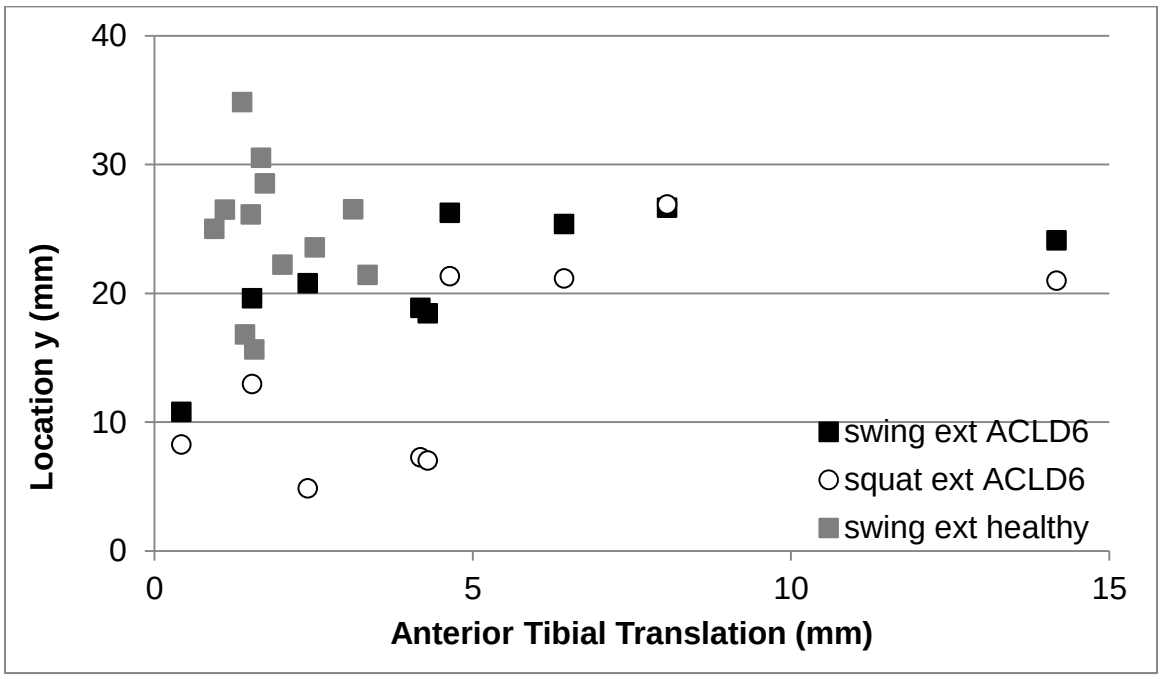

Figure 4-16: FHA location y (mm) versus anterior tibial translation (mm) for the ACLD injured limb (ACLD6) during swing extension (swing ext, p=0.025*) and squat extension (squat ext, p=0.077)), and for the healthy limb during swing extension (swing ext, p=0.633). (* indicates significance at α=0.05).

FHA translation describes the translation of the tibia with respect to the femur along the FHA during a dynamic task. In the ACLD injured limb, individuals with increased ATT exhibited decreased FHA translation during the swing task (Figure 4-17). FHA translation was significantly correlated with ATT in the ACLD injured limb during swing extension ($r_s(9)=0.783$, p=0.013), but was not significant during swing flexion ($r_s(9)=-0.617$, p=0.077, Table 4-6). In the contralateral limb of the ACLD group, ATT and FHA translation were significantly correlated during only the extension phase of the squat ($r_s(9)=0.667$, p=0.050, Table 4-6). FHA translation was not significantly correlated with ATT in the healthy limb (Figure 4-17).

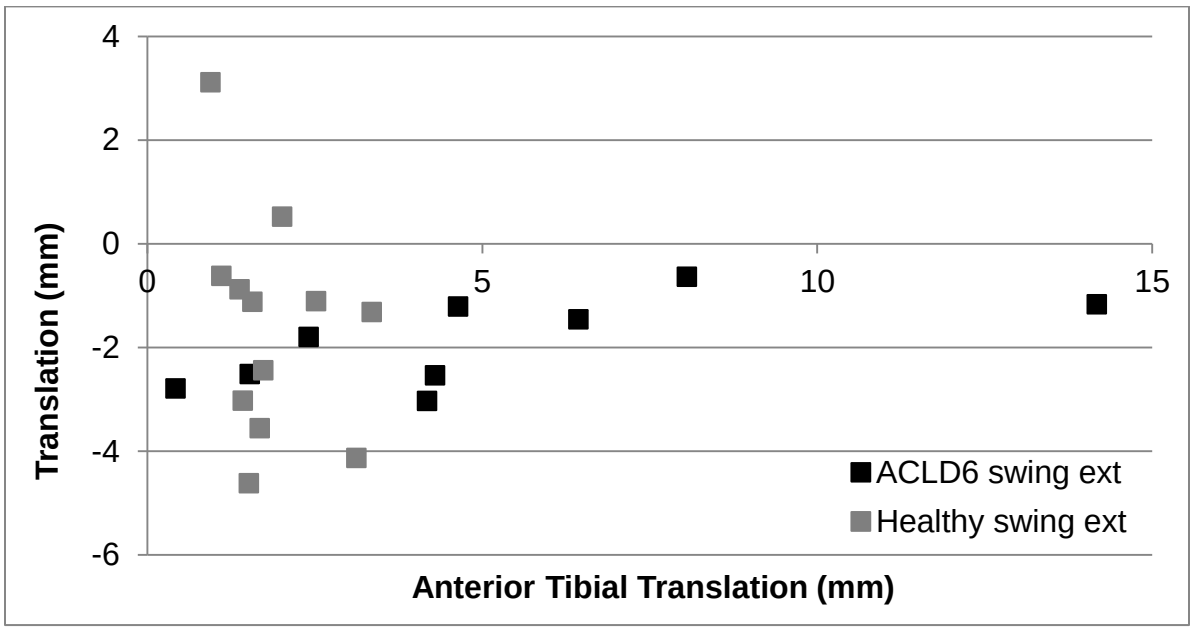

Figure 4-17: FHA translation (mm) versus anterior tibial translation (mm) for the ACLD injured limb (ACLD6) during swing extension (swing ext, p=0.013*), and for the healthy limb during swing extension (swing ext, p=0.255). (* indicates significance at α=0.05).

In the ACLD injured limb, individuals with increased ATT exhibited decreased FHA path length during the swing task (Figure 4-18). FHA path length was significantly correlated with ATT in the ACLD injured limb during swing flexion ($r_s(9)$=-0.717, p=0.030) and swing extension ($r_s(9)$=-0.817, p=0.007, Table 4-6). In contrast, for the healthy limb, there was a significant relationship between ATT and path length, whereby individuals with increased ATT showed increased path length (Figure 4-18). ATT was significantly correlated with FHA path length during the flexion phase of the swing task ($r_s(9)$=0.622, p=0.031, Table 4-6) in the healthy limb. FHA path length was not significantly correlated with ATT in the contralateral limb of the ACLD group.

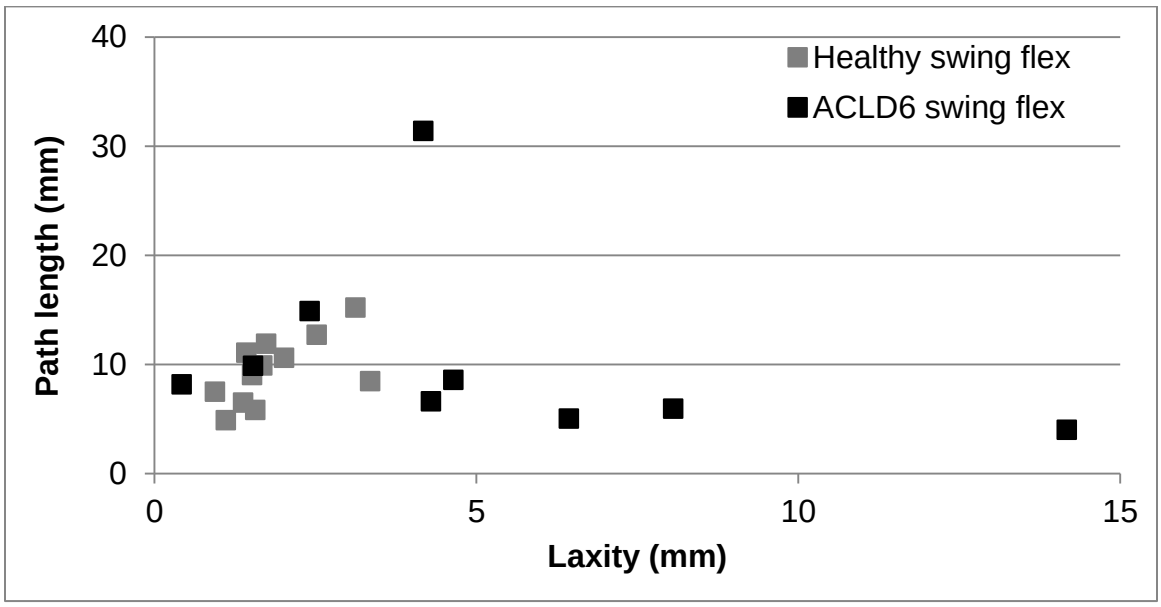

Figure 4-18: FHA path length (mm) versus anterior tibial translation (mm) for the ACLD injured limb (ACLD6) during swing flexion (swing flex, p=0.030*), and for the healthy limb during swing flexion (swing flex, p=0.031). (* indicates significance at α=0.05).

In the healthy limb, a significant correlation was detected between ATT and FHA dispersion for the extension phase of the swing ($r_s(9)=0.594$, p=0.042, Table 4-6). No significant correlations were detected between ATT and AP excursion for the healthy limb or the ACLD group.

Table 4-6: Spearman's correlation coefficients and significance values between anterior tibial translation and FHA measures for the healthy dominant limb (Healthy Dom), and the injured (Inj) and contralateral (Con) limbs of the ACLD group. (* indicates significance at α=0.05)

			Healthy Dom		ACLD Inj		ACLD Con	
Task	**Phase**	**Measure**	**Corr Coeff**	**Sig.**	**Corr Coeff**	**Sig.**	**Corr Coeff**	**Sig.**
Swing	**flex**	loc y (mm)	-.175	.587	.700	.036*	-.183	.637
		Trans (mm)	.140	.665	-.617	.077	.517	.154
		Disp (°)	.210	.513	-.333	.381	0.000	1.000
		Path (mm)	.622	.031*	-.717	.030*	-.050	.898
		Apex (mm)	.434	.159	-.417	.265	.433	.244
	ext	loc y (mm)	-.154	.633	.733	.025*	-.283	.460
		Trans (mm)	-.357	.255	.783	.013*	-.600	.088
		Disp (°)	.594	.042*	-.467	.205	.067	.865
		Path (mm)	-.021	.948	-.817	.007*	-.500	.170
		Apex (mm)	.238	.457	-.367	.332	-.167	.668
Squat	**flex**	loc y (mm)	.014	.966	.633	.067	.100	.798
		Trans (mm)	.231	.471	.250	.516	-.450	.224
		Disp (°)	-.301	.342	.133	.732	-.200	.606
		Path (mm)	.350	.265	.100	.798	-.567	.112
		Apex (mm)	-.042	.897	0.000	1.000	-.117	.765
	ext	loc y (mm)	.014	.966	.617	.077	-.017	.966
		Trans (mm)	-.301	.342	-.300	.433	.667	.050*
		Disp (°)	-.448	.145	-.017	.966	-.133	.732
		Path (mm)	-.028	.931	-.067	.865	.383	.308
		Apex (mm)	-.126	.697	.233	.546	-.200	.606

4.4.6 EMG

Quality of the EMG signal was poor in four healthy study participants (H01, H04, H07 and H11) and three ACLD study participants (A01, A02, A06) due to significant noise artefacts. Therefore, EMG results are only presented for eight of the twelve healthy study participants, and six of the nine ACLD study participants.

An exemplary multi-muscle pattern for the dominant limb of a healthy participant during the swing task shows coordinated activity of the quadriceps (VM, VL) and hamstrings (BF, SEM) between 30% and 50% of the swing cycle, corresponding to raising the shank (knee extension) (Figure 4-19). The TA has minimal activity throughout the task to maintain foot plantar flexion.

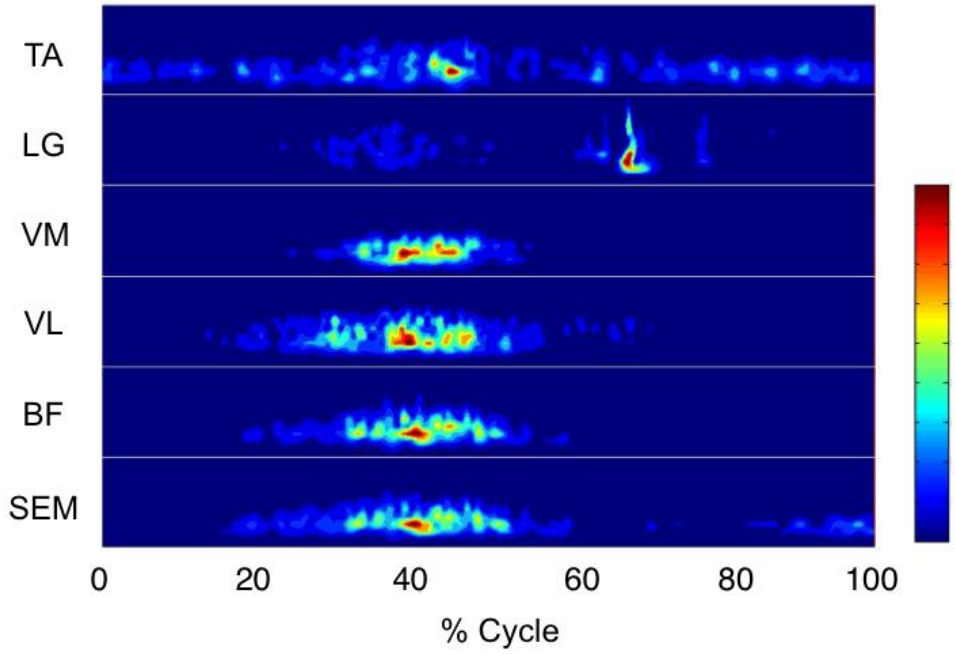

Figure 4-19: Exemplary plot of muscle intensities for the dominant limb of a healthy participant during a swing task with % cycle on the x-axis and frequency (Hz) on the y-axis. Wavelet patterns for each muscle (TA, LG, VM, VL, BF, SEM) are stacked in the vertical direction. The colorbar shows the intensity scale of the signal where dark blue represents minimum intensity (0), and dark red represents maximum intensity (1.0).

An exemplary multi-muscle pattern for the dominant limb of a healthy participant during the squat task shows coordinated activity of the quadriceps (VM, VL) and hamstrings (BF, SEM) between 20% and 60% of the squat cycle, corresponding to lowering (knee flexion) and the transition to raising (knee extension) (Figure 4-20). The TA and LG are active throughout the squat cycle to control ankle flexion and contribute to knee stability.

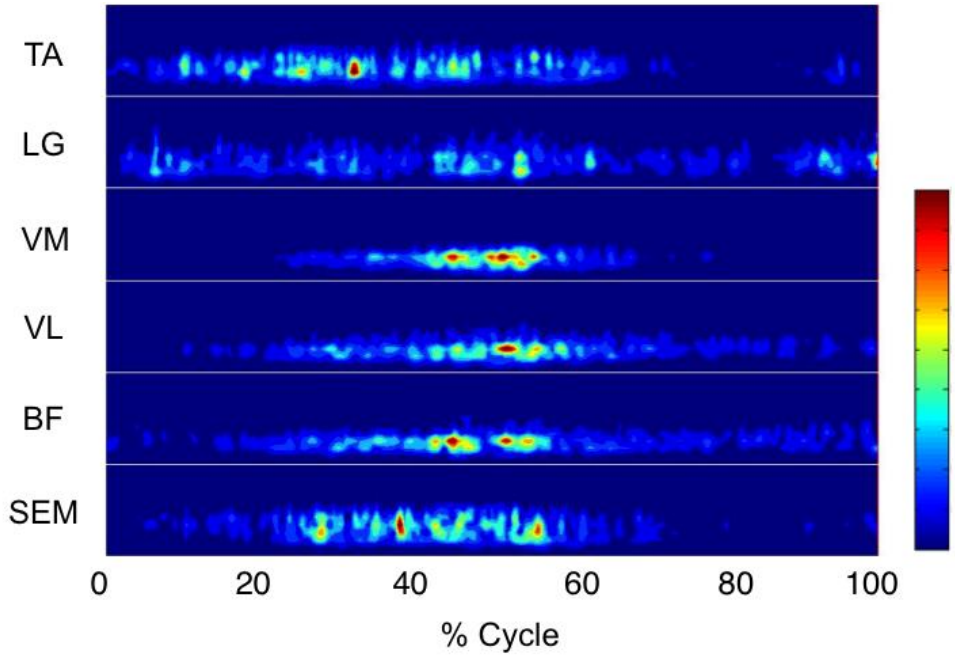

Figure 4-20: Exemplary plot of muscle intensities for the dominant limb of a healthy participant during a squat task with % cycle on the x-axis and frequency (Hz) on the y-axis. Wavelet patterns for each muscle (TA, LG, VM, VL, BF, SEM) are stacked in the vertical direction. The colorbar shows the intensity scale of the signal where dark blue represents minimum intensity (0), and dark red represents maximum intensity (1.0).

An exemplary multi-muscle pattern for the injured limb of an ACLD participant during the swing task shows coordinated activity of the quadriceps (VM, VL) and lateral hamstring (BF) between 20% and 50% of the swing cycle, corresponding to raising the shank (knee extension) (Figure 4-21). The hamstrings (BF, SEM) are also active between 80% and 100% of the swing

cycle, while the shank is lowered to 90° of knee flexion. The TA is active throughout the task to maintain foot plantar flexion.

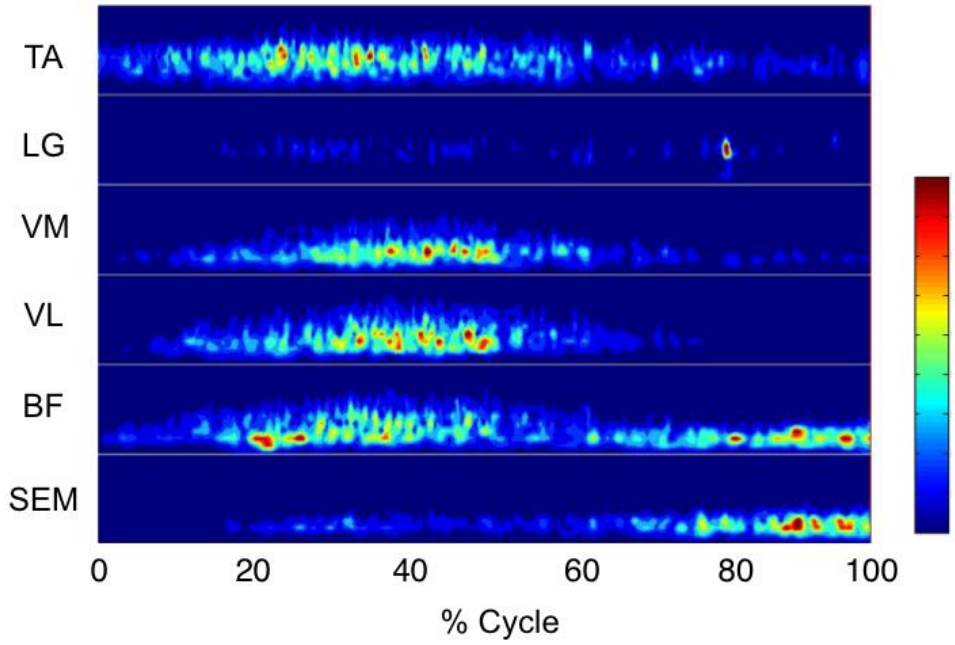

Figure 4-21: Exemplary plot of muscle intensities for the injured limb of an ACLD participant during a swing task with % cycle on the x-axis and frequency (Hz) on the y-axis. Wavelet patterns for each muscle (TA, LG, VM, VL, BF, SEM) are stacked in the vertical direction. The colorbar shows the intensity scale of the signal where dark blue represents minimum intensity (0), and dark red represents maximum intensity (1.0).

An exemplary multi-muscle pattern for the injured limb of an ACLD participant during the squat task shows less coordinated activity of the quadriceps (VM, VL) and hamstrings (BF, SEM) throughout the task (Figure 4-22). The VM and VL are active between 30% and 80% of the squat cycle, corresponding to the lowering (knee flexion) and raising (knee extension) portions of the squat. The BF and SEM are active throughout the entire duration of the squat with higher intensity observed between 50% and 70% of the cycle, corresponding to the raising (knee extension) portion of the squat. The TA is active throughout most of the squat cycle, while the

LG is most active between 60% and 80% of the cycle, corresponding to the raising (knee extension) portion of the squat.

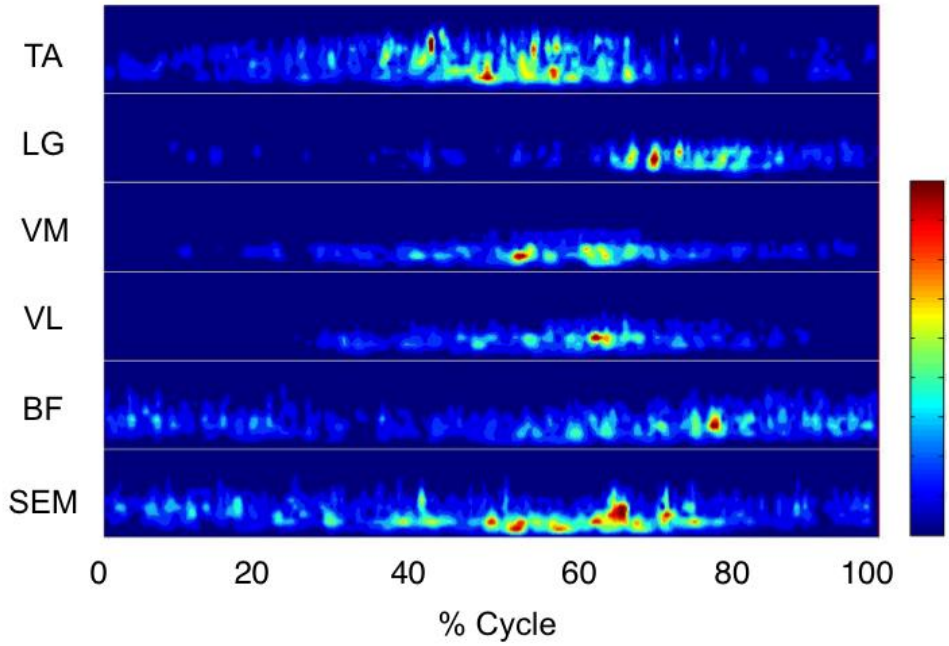

Figure 4-22: Exemplary plot of muscle intensities for the injured limb of an ACLD participant during a squat task with % cycle on the x-axis and frequency (Hz) on the y-axis. Wavelet patterns for each muscle (TA, LG, VM, VL, BF, SEM) are stacked in the vertical direction. The colorbar shows the intensity scale of the signal where dark blue represents minimum intensity (0), and dark red represents maximum intensity (1.0).

Muscle power for the VM, VL, BF and SEM was compared between dominant and contralateral limbs for the healthy group. No significant differences were detected in muscle power between limbs in the healthy group for the swing or the squat task (Table 4-7). In the ACLD group, muscle power was significantly lower in the injured limb compared to the contralateral for the VM, VL, and SEM during both the squat and swing tasks (Table 4-7).

Table 4-7: Muscle power medians and interquartile ranges (IQR) for the VM, VL, BF and SEM muscles during the swing and squat tasks for the dominant (Dom) and contralateral (Con) limbs of the healthy group, and the injured (Inj) and contralateral (Con) limbs of the ACLD group. (* indicates significance at α=0.05)

				VM	VL	BF	SEM
Healthy	Swing	Dom	Median	194.4	200.4	13.5	2.7
			IQR	324.3	432.1	12.5	8.0
		Con	Median	207.9	161.1	8.8	1.2
			IQR	241.2	184.0	60.9	21.9
		p-value		0.779	0.208	0.401	1.000
	Squat	Dom	Median	1593.6	925.3	72.7	46.8
			IQR	775.1	494.7	156.2	144.6
		Con	Median	1249.3	873.1	81.3	68.8
			IQR	1625.2	1756.6	525.0	256.8
		p-value		0.674	0.889	0.263	0.484
ACLD	Swing	Inj	Median	36.3	66.6	1.9	0.2
			IQR	82.1	78.0	36.1	1.3
		Con	Median	212.7	225.6	5.7	1.2
			IQR	422.0	205.2	8.8	1.9
		p-value		0.028*	0.028*	0.345	0.028*
	Squat	Inj	Median	495.6	297.3	23.7	15.5
			IQR	996.3	603.3	284.4	11.4
		Con	Median	1688.8	539.5	33.2	51.4
			IQR	1603.5	1098.2	48.1	47.5
		p-value		0.046*	0.028*	0.753	0.046*

The median muscle power in the VM during the swing was 36.3 in the injured limb compared to 212.7 in the contralateral limb (p = 0.028). During the squat, median muscle power in the VM was 495.6 in the injured limb compared to 1688.8 in the contralateral limb (p = 0.046, Figure 4-23).

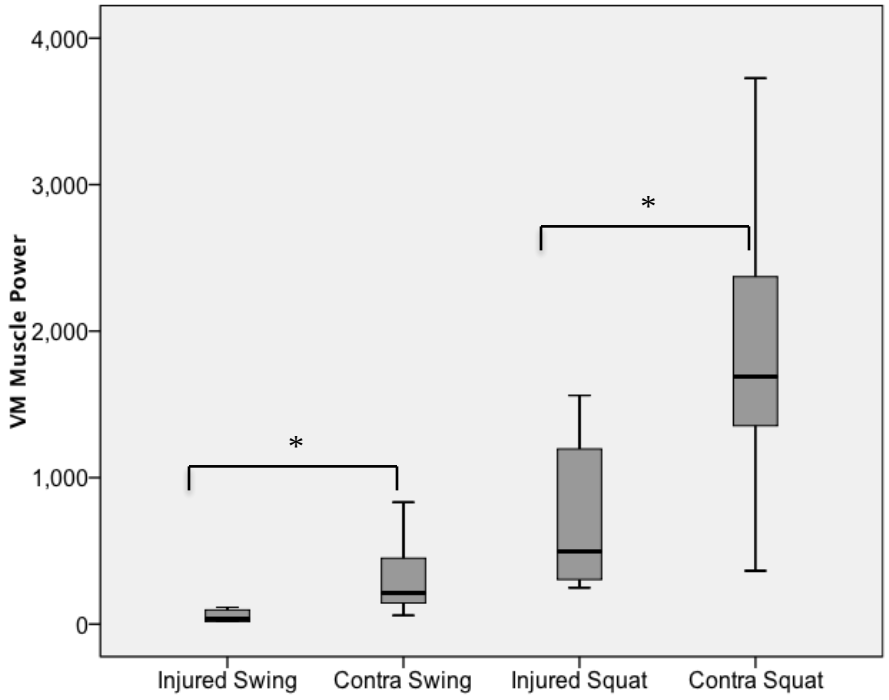

Figure 4-23: VM muscle power for the injured and contralateral limb of the ACLD group during the squat and swing tasks (* indicates significance at α=0.05)

The median muscle power in the VL during the swing was 66.6 in the injured limb compared to 225.6 in the contralateral limb (p = 0.028). During the squat, median muscle power in the VL was 297.3 in the injured limb compared to 539.5 in the contralateral limb (p = 0.028, Figure 4-24).

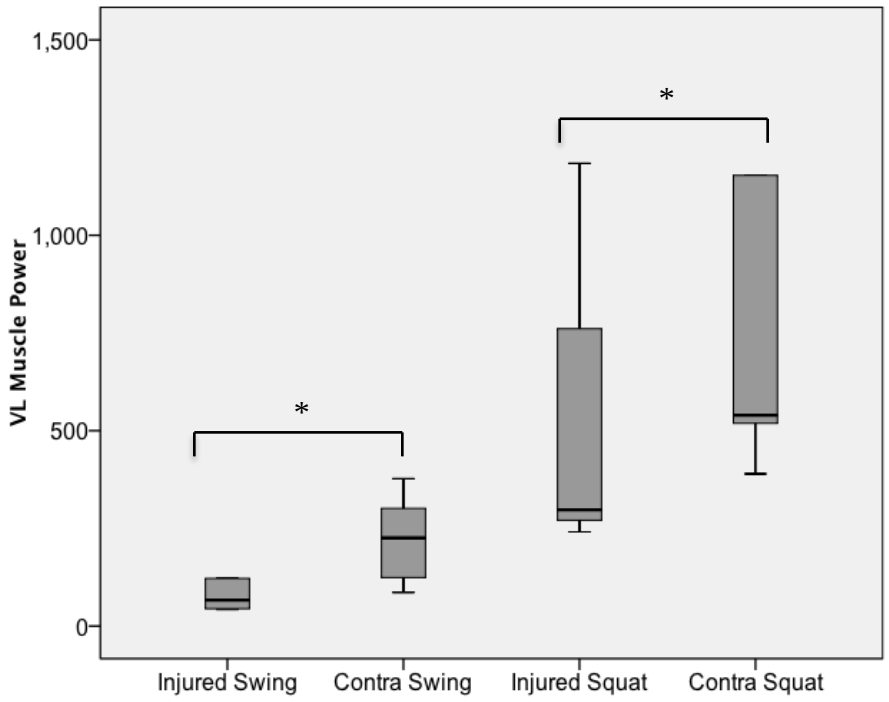

Figure 4-24: VL muscle power for the injured and contralateral limb of the ACLD group during the squat and swing tasks (* indicates significance at α=0.05)

The median muscle power in the SEM during the swing was 0.2 in the injured limb compared to 1.2 in the contralateral limb (p = 0.028). During the squat, median muscle power in the SEM was 15.5 in the injured limb compared to 51.4 in the contralateral limb (p = 0.046, Figure 4-25).

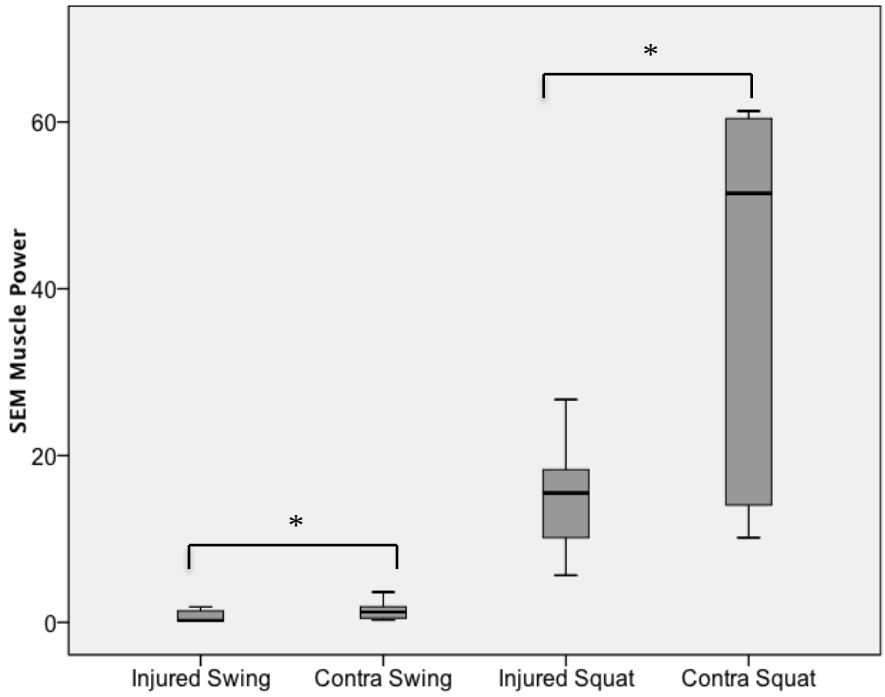

Figure 4-25: SEM muscle power for the injured and contralateral limb of the ACLD group during the squat and swing tasks (* indicates significance at α=0.05)

4.4.7 Muscle Volume

The muscle volume for the VM was significantly lower in the ACLD injured limb (165.2 ± 37.8 cm^3) compared to the contralateral limb (198.4 ± 29.5 cm^3) (p=0.002, Figure 4-26). The muscle volume for the VL was also significantly lower in the ACLD injured limb (265.2 ± 46.3 cm^3) compared to the contralateral limb (314.6 ± 40.8 cm^3) (p=0.001, Figure 4-26). There were no statistically significant differences between limbs in the ACLD group for the BF (p=0.798), or SEM (p=0.978) muscle volumes.

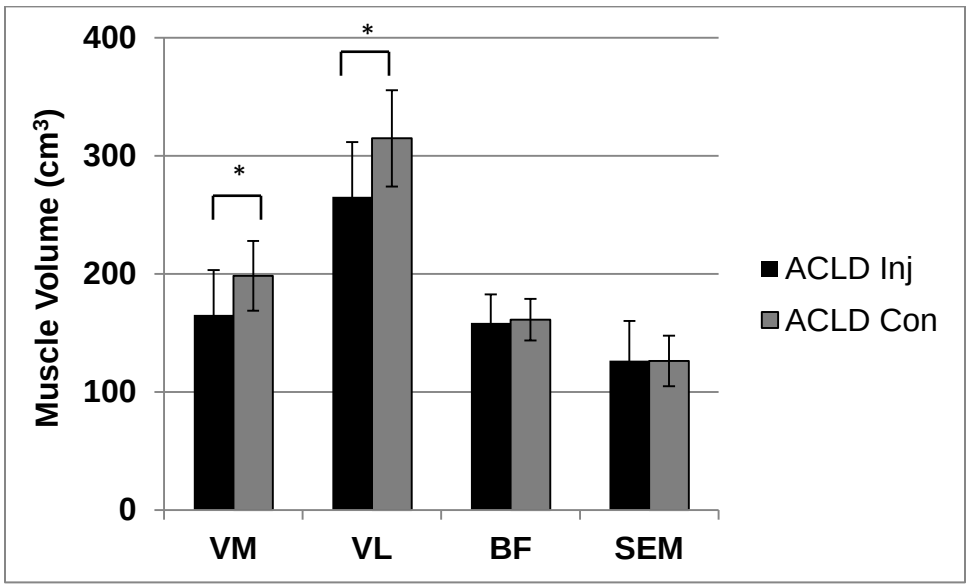

Figure 4-26: Muscle volume for the VM, VL, BF and SEM muscles of the injured and contralateral limbs of the ACLD group at six weeks post injury (* indicates significance at α=0.05)

4.4.8 Summary of Results

4.4.8.1 Laxity

- Average side to side difference in ATT at 89 N was 2.83 ± 4.39 mm in the ACLD group, and 0.26 ± 0.86 mm in the healthy group (p = 0.069)
- ACLD group had an average of 5.13 ± 4.13 mm of ATT in the injured limb, while the healthy dominant limb had 1.86 ± 0.76 mm of ATT (p=0.046)

4.4.8.2 FHA

A list of the key statistically significant findings in FHA measures for the healthy and ACLD group at six weeks post injury is presented below:

- FHA was located more anterior in the healthy dominant limb compared to the healthy contralateral limb during swing flexion and extension

- PD excursion was greater in the healthy dominant limb compared to the healthy contralateral limb during squat extension
- Orientation angle was greater in the ACLD injured limb compared to the ACLD contralateral limb during squat flexion
- No significant differences in FHA measures between the ACLD injured limb and the healthy dominant limb
- FHA was located more anterior in the healthy dominant limb compared to the ACLD contralateral limb during swing flexion and extension
- Path length was greater in the ACLD contralateral limb compared to the healthy dominant limb during squat flexion

4.4.8.3 Correlations

The key correlations between ATT and FHA measures in the healthy and ACLD group at six weeks post injury is presented below (Table 4-8).

Table 4-8: Key relationships between increased ATT and FHA measures in the healthy dominant limb and the ACLD group at six weeks post injury for the injured and contralateral limbs. ↑ indicates an increase in the FHA measure with increased ATT, and ↓ indicates a decrease in the FHA measure with increased ATT.

FHA measure	Task	Healthy	ACLD 6 weeks	
		Dominant	Injured	Contra
Location y (mm)	Swing		↑	
	Squat			
Translation (mm)	Swing		↓	
	Squat			↑
Dispersion (°)	Swing	↑		
	Squat			
Path (mm)	Swing	↑	↓	
	Squat			
AP ex (mm)	Swing			
	Squat			

4.4.8.4 EMG

A list of the key statistically significant findings in EMG muscle power for the healthy and ACLD group at six weeks post injury is presented below:

- No significant differences in muscle power between limbs in the healthy group during the swing or squat
- Quadriceps (VM, VL) and medial hamstring (SEM) muscle power was lower in the ACLD injured limb compared to the ACLD contralateral limb during the squat and swing

4.4.8.5 Muscle Volume

A list of the key statistically significant findings in muscle volume for the ACLD group at six weeks post injury is presented below:

- Quadriceps (VM and VL) muscle volume was lower in the ACLD injured limb compared to the ACLD contralateral limb
- No significant differences in muscle volume for the hamstrings (BF and SEM) between the ACLD injured and ACLD contralateral limbs

4.5 Discussion

The current study used the FHA, combined with an MR based measure of laxity to investigate the structure function relationship in ACLD individuals, and to examine differences in these measures between healthy and ACLD groups. Muscular control was investigated to enable interpretation of changes in movement patterns due to ACL deficiency. The results of this study and their interpretation are discussed in this section as they relate to the specific aims and hypotheses.

To test the first hypothesis (H2a), side-to-side differences in laxity, FHA measures, and muscle power were compared between healthy and ACLD groups. The hypothesis that the ACLD group would have increased side-to-side differences in these measures was supported by FHA orientation angle, and quadriceps and hamstring muscle power. The ACLD group did not show statistically increased side-to-side differences in ATT compared to the healthy group, which was unexpected. However, the ACLD injured limb had significantly increased ATT relative to the healthy dominant limb. Daniel et al. (1985) suggested that a side-to-side difference of 3 mm in ATT with an 89 N load is indicative of an ACL rupture. In the current study, the ACLD group had an average side to side difference of 2.83 mm, which is approaching the clinically significant value of 3 mm. Although measures were taken to avoid muscle guarding during knee loading with the KLA, this could not be completely controlled for during MR imaging. Therefore, it is possible that some participants were activating muscles surrounding the knee during the test on the injured limb, which would reduce the side-to-side difference in ATT. Levene's test indicated that the groups did not have equal variances, therefore the p-value for unequal variances was reported. Three ACLD participants displayed larger ATT in the contralateral limb compared to the healthy limb, resulting in a negative difference between limbs. This increased the variance of the ACLD group, and may have affected the ability to detect a significant difference between groups. A power calculation revealed that fourteen participants in each group would be required to achieve a significant difference (α=0.05) in the side to side difference in ATT between groups with a power of 0.8. Therefore, future studies examining this measure between healthy and ACLD groups should have a sample size of at least fourteen participants in each group.

FHA measures showed a significant side-to-side difference in FHA orientation angle in the ACLD group during squat flexion, which was not detected in the healthy group, supporting H2a.

In the ACLD group, FHA orientation angle was larger in the injured limb relative to the contralateral limb by approximately 4° on average. FHA orientation angle is the angle of the FHA with the mediolateral axis of the knee joint. Orientation angle encompasses both internal/external rotation and varus/valgus. In a study by Andriacchi and Dyrby (2005), they reported an average 2.9° offset toward internal rotation during the gait cycle in the ACLD injured limb compared to the contralateral limb. An offset in tibial rotation in ACLD limbs has been reported in numerous studies (Dennis et al., 2005; Georgoulis et al., 2003; Logan, 2004a; Scarvell et al., 2004). This finding is consistent with the pivot-shift phenomenon observed in ACLD patients, which demonstrates combined ATT and internal tibial rotation (Noyes et al., 1991). Therefore, the increased orientation angle in the ACLD limb observed in the current study is likely due to increased internal tibial rotation in the injured limb, as visualized in Figure 4-15. The occurrence of this difference during the squat task but not the swing task may indicate that it is related to a joint loading phenomenon needing to support partial body weight, or muscle activation patterns not utilized as much during the swing. Results from Chapter 3 provided evidence that the swing task is quadriceps dominant while the squat task requires control from both the quadriceps and hamstrings. Therefore, it is speculated that altered hamstring activity in the ACLD injured limb during the squat may play a role in the observed increased orientation angle.

The ACLD group had significantly lower muscle power in the quadriceps (VM, VL) and the medial hamstring (SEM) in the injured limb relative to the contralateral limb during both tasks, while the healthy group did not demonstrate significant side-to-side differences in muscle power, supporting H2a. This result is likely due to muscle inhibition of the thigh muscles following ACL rupture. Synder-Mackler et al. (1994) showed that individuals with a sub-acute ACL

rupture (average three months post-injury) had significant reflex inhibition of the quadriceps femoris muscle. A quadriceps inhibition or "avoidance" pattern to reduce ATT in ACLD participants has also been demonstrated by others (Andriacchi, 1990; Wexler et al., 1998). In the current study, the ACLD group did not display significant differences between limbs in the anterior location of the FHA (location y) during either dynamic task. This result may have been accomplished via the observed decrease in quadriceps muscle power in the ACLD injured limb to avoid excessive anterior translation of the tibia. The majority of literature supports the idea of increased hamstring activation, or "hamstring facilitation" following ACL rupture to compensate for the loss of the ACL (Alkjaer et al., 2012; Boerboom et al., 2001; Hurd and Snyder-Mackler, 2007; Wexler et al., 1998). However, a recent study by Gardinier et al. (2012) used an EMG-driven musculoskeletal model to estimate muscle forces and demonstrated decreased muscle force from both the quadriceps and hamstrings during gait in individuals with acute ACL rupture (average eight weeks post-injury). It was suggested these individuals accomplished decreased peak knee moment by reducing the force from both the knee flexor and extensor muscles, which could be related to muscle weakness after injury (Gardinier et al., 2012). Furthermore, the SEM functions as an internal tibial rotator, therefore individuals with an ACL rupture may reduce SEM muscle power in an attempt to reduce excessive internal tibial rotation. However, the ACLD group in the current study demonstrated an increased FHA orientation angle in the injured limb compared to the contralateral limb during the squat. Therefore, the reduced SEM muscle power observed in the ACLD injured limb was not able to fully compensate for the decreased rotational stability in the knee joint due to the loss of the ACL.

The ACLD group also demonstrated significant atrophy of the quadriceps (VM and VL) in the injured limb relative to the contralateral limb. Atrophy of the quadriceps muscle group following

ACL rupture is well documented and has been associated with decreased strength and functional deficits in ACLD individuals (Baugher et al., 1984; Ingersoll et al., 2008; Lorentzon et al., 1989; Williams et al., 2005). It has been suggested that the VM is the key muscle responsible for lower limb strength deficits in ACLD individuals (Okada, 1989; Stockmar et al., 2006). Okada (1989) demonstrated significant atrophy of the VM muscle at four weeks post ACL transection, and significant atrophy of the VL muscle at twelve weeks post ACL transection in a rat model. Stockmar and colleagues (2006) found significantly decreased VM muscle fibre diameters in a group of chronic ACLD individuals, indicating VM muscle fibre atrophy due to ACL deficiency. It is suggested that muscle atrophy of the VM and VL in the current study is partially responsible for the observed reduction in quadriceps muscle power in the injured limb relative to the contralateral limb of the ACLD group during dynamic tasks.

In the healthy group, the FHA was located significantly more anterior in the dominant limb compared to the contralateral limb during the swing task, suggesting limb asymmetry. During the swing task, movement is primarily controlled by activation of the quadriceps. Therefore, one possible explanation is that the dominant limb has stronger quadriceps than the contralateral limb, causing a more anterior FHA position. The current study did not quantify muscle strength, and little support was found in the literature to support the theory that quadriceps muscle strength is greater in the dominant limb. However, future studies could quantify differences in muscle strength between legs in study participants by having them perform an MVC on the Biodex dynamometer with each leg.

PD excursion was significantly larger in the dominant limb compared to the contralateral limb in the healthy group during squat extension. This finding suggests that the FHA covers a larger range in the proximal/distal direction on the midsagittal plane of the dominant healthy knee

during the extension phase of the squat. It is suggested that healthy participants are less confident performing the single leg squat with the contralateral limb, and therefore exhibit tighter control resulting in less movement of the FHA in the contralateral limb. PD excursion is affected by joint position as well as joint loading due to compression and muscular forces. The results of the current study are not able to confirm the proposed explanation, as there were no significant side to side differences in muscle power or FHA position during the squat in the healthy group.

Side-to-side differences in FHA measures were present in the healthy group that were not present in the ACLD group. This finding reveals that movement patterns were not symmetrical in healthy group. This is a very important finding for the current study, because in order to interpret side to side differences in an ACLD population, we must first understand side to side differences in a healthy population.

To test the second hypothesis (H2b), FHA measures were compared between the healthy and ACLD group. The hypothesis that ACLD participants would have decreased dynamic stability relative to healthy participants was not supported. It was hypothesized that the ACLD injured limb would have a) a more anterior FHA location and increased orientation angle, and b) decreased FHA translation and dispersion. There were no significant differences detected between ACLD and healthy groups in the FHA measures. This finding was surprising. The results may be attributed to several potential explanations including ongoing pain and effusion, increased capsular tension, and reflex inhibition of the quadriceps in the injured joint at six weeks post-injury. A significantly increased KIMRISS score in the injured limb of the ACLD group relative to the dominant limb of the healthy group supports the theory of increased joint effusion in the ACLD limb. It is thought that ongoing pain and effusion in the ACLD joint could prevent the development of an adaptation strategy. Joint effusion is common after acute trauma,

and is thought to provide additional stability to the joint. Increased capsular tension, which has been reported with joint effusion, has been suggested to increase proprioceptive control, thereby increasing joint stability (Palmieri et al., 2003). Reflex inhibition of the quadriceps related to knee joint effusion has also been well documented (Palmieri et al., 2003). Therefore, it is speculated that that kinematic differences between ACLD injured limbs and the healthy group in the current study are not present at six weeks post injury due to ongoing joint effusion. In a study by Rudolph et al. (2001), it was suggested that ACLD "non-copers" attempt to shift control away from the unstable knee to the stable hip during gait. This may also be a strategy for the ACLD individuals in the current study, and could help to explain the lack of kinematic differences between the healthy and ACLD groups.

FHA measures were also compared between the ACLD contralateral limb and the dominant limb of the healthy group, to understand whether there were adaptations in the contralateral limb following ACL injury. The FHA was located significantly more anterior in the healthy limb compared to the contralateral limb of the ACLD group during the swing task. Additionally, FHA path length was significantly greater in the ACLD contralateral limb relative to the healthy limb during squat flexion. The majority of FHA variables exhibited no differences between the ACLD contralateral limb and the healthy limb at this early time point. Furthermore, similar behaviours were displayed between healthy versus ACLD contralateral limbs, and healthy dominant versus contralateral limbs. However, as there were some differences between the healthy limb and the contralateral limb of the ACLD group, the ACLD contralateral limb is not considered as the 'control' for the current study.

To test the third hypothesis (H2c), correlations between ATT and FHA measures were examined in both groups. The hypothesis that ACLD participants with increased ATT would exhibit

decreased dynamic knee stability at six weeks post injury was supported by the results for the swing task. The ACLD injured limb showed significant correlations between ATT and the anterior/posterior location of the FHA (location y), FHA translation, and FHA path length. ACLD individuals with increased ATT showed a more anterior FHA location in the joint during the swing task, supporting H2c. This finding was expected because increased ATT in the joint allows the tibia to translate anteriorly, resulting in a more anterior position of the tibia with respect to the femur. This relationship was not present in the ACLD contralateral limb, or the healthy group. ACLD individuals with increased ATT also showed decreased FHA translation and path length during the swing task, supporting H2c. This finding suggests that ACLD individuals with increased joint laxity attempt to reduce translation and rotational movement within the knee. This aligns with the stabilization strategy suggested by Rudolph et al. (2001), whereby non-copers reduce their range of motion and increase co-contraction to stiffen the knee. However, this finding was only true in the swing task. The wavelet analysis multi muscle pattern (MMP) plots reveal that ACLD individuals tend to activate the quadriceps and hamstrings earlier and longer during the swing in the injured limb (Figure 4-21) compared to healthy individuals (Figure 4-19), supporting the theory of joint stiffening using a co-contraction strategy. As suggested, during the squat ACLD individuals may transfer control to the hip, and can also take advantage of hamstring contraction for stabilization. The wavelet analysis MMP plots show that ACLD individuals tend to activate the hamstrings during the entire squat task in the injured limb (Figure 4-22), while healthy individuals display a more strategic hamstring control pattern (Figure 4-20). Along with joint compression, these mechanisms might reduce the effect of increased ATT on movement patterns during the squat task.

The healthy group demonstrated significant correlations between joint laxity and FHA dispersion and path length during the swing. Healthy individuals with more ATT showed increased path length during swing flexion, and increased dispersion during swing extension. These relationships are opposite to those demonstrated by the ACLD group. This highlights and reinforces the ability of the swing task to identify differences in movement patterns due to joint structure, discussed in Chapter 3.

Within the ACLD group there is a spectrum of laxity values, which correlate with measures of dynamic movement at a sub-acute stage post injury. These correlations are only present during the swing task at six weeks post injury. The same relationships are not present in the contralateral limb or the healthy group. These findings highlight that there is a range of laxity values and FHA measures in the ACLD group, which may affect the ability to detect differences between injured and healthy limbs. We have shown that dynamic movement patterns are affected, or perhaps even dictated by the amount of laxity in the ACLD joint at six weeks post injury. It is speculated that that these relationships will change over time in ACLD individuals due to adaptations to cope with the loss of the ACL. This idea will be explored in Chapter 5.

Chapter Five: **Passive Knee Laxity and Dynamic Knee Stability: ACLD over time**

The current chapter evaluates changes in passive knee laxity and dynamic knee stability over time in ACLD individuals to understand how the joint is adapting to the loss of the ACL. Investigating changes over time in anterior tibial translation, FHA measures, and muscle activation will provide insight into adaptation strategies in ACLD individuals, and may help to identify mechanisms leading to the development of OA. Furthermore, relationships amongst FHA measures and anterior tibial translation are compared between six and twelve weeks post-injury to improve understanding of how structural laxity influences movement patterns within the ACLD group.

5.1 Literature Review

5.1.1 Joint Structure

Joint structures have been reported to adapt following ACL rupture. The secondary stabilizing structures of the knee are thought to adapt to the loss of the ACL to provide additional joint stability (Atarod et al., 2013; Daniel et al., 1994; Jackson et al., 1999; Maitland et al., 1998). Secondary restraint to ATT is provided by the collateral ligaments, the middle third of the joint capsule, and the iliotibial tract and band (Butler et al., 1980). The meniscus has also been shown to play a role in anterior joint stabilization (Allen et al., 2000). The majority of studies use animal models to quantify these changes over time, due to the invasive nature of measuring structural changes and ethical limitations associated with human studies. A study by Maitland et al. (1998) quantified changes in passive tibial displacement relative to the femur in a cat model prior to and following ACL transection. Anterior tibial translation significantly increased by 6 mm immediately following transection, and subsequently decreased by 4 mm four months following transection. Stiffness during ATT decreased significantly by 6 N/mm immediately

following ACL transection, and increased by 5 N/mm four months after transection. These results suggest that the feline increases anterior stability in the knee with secondary restraints four months after ACL transection. Jackson at el. (1999) showed a 35-40% reduction in anterior-posterior tibial translation eight months following ACL transection in a goat model. This reduction in ATT corresponded with enlarged medial menisci and capsule thickening. The meniscus and capsule remodelling was suggested to result from increased loading following ACL transection, thus contributing to the reduced ATT in the joint (Jackson et al., 1999). The work of Lopez et al. (2003) in ACL deficient canines also supported the role of the joint capsule in maintaining AP joint stability. While limited, there is evidence in ACLD humans of decreased ATT over time. In a study by Daniel et al. (1994), 39% of individuals with a side-to-side ATT difference of more than 3 mm immediately following ACL injury, had a side-to-side difference of less than 3 mm at follow-up testing (average 64 months post-injury). The reduction in ATT over time was suggested to be attributed either to healing of the ACL, or to secondary stabilizing structures (Daniel et al., 1994). However, the time course in human studies is generally long-term, and does not capture acute changes in the joint.

Altered loading in the remaining joint ligaments following ACL rupture would support the role of the ligaments as secondary stabilizers to anterior tibial translation. Atarod et al. (2013) quantified changes in loading in the MCL, LCL and PCL following ACL transection in an ovine model. At twenty weeks post-transection, the average loads in the PCL and LCL were significantly decreased compared to the intact state. Over time, the LCL demonstrated a significant decrease in loading between four and twenty weeks post-transection, however loading in the MCL and PCL did not significantly change during this period (Atarod et al., 2013). Increased loading in the MCL following ACL transection has been reported in cadaveric studies

(Sakane et al., 1999; Shelburne et al., 2004). Altered loading in the collateral and posterior cruciate ligaments after ACL transection may have a long-term effect on the mechanical properties of the ligaments and their ability to control joint motion.

The above studies provide evidence to support the concept that secondary structures can provide anterior stability to the knee following ACL rupture, and that these structures have the ability to remodel over time. However, it is not clear how early these changes occur in the human knee joint after ACL rupture. In the current study, it is expected that the period between six and twelve weeks post injury may be too brief to detect structural adaptations within the joint.

5.1.2 Kinematic changes

There are very few studies in humans quantifying kinematic changes over time after ACL rupture. This is likely due to challenges recruiting participants at an acute stage post-injury, difficulties in controlling confounding variables, and because a large percentage of ACLD individuals undergo surgical repair (Lohmander et al., 2004). Consequently, the majority of studies quantifying serial kinematic changes following ACL rupture use an animal model. Tashman et al. (2004b) used a canine model to quantify changes in kinematics before and serially for two years after ACL transection (2, 4, 6, 8, 10, 12, 16, 20 and 24 months post ACL transection). Following ACL transection, peak ATT was increased in the ACLD limb by 10 mm on average, but did not change over time. ATT at pre-pawstrike was not significantly different from intact between two and four months post ACL transection. However, it significantly increased by 3.5 mm over time, with the majority of change happening in the first year. It was speculated that initially, the meniscus may function like a spring to restore ATT after stance phase, however over time it is no longer able to resist the increased ATT due to repetitive loading (Tashman et al., 2004b). The tibia in the ACLD canines was also shifted 0.75 mm

medially relative to the femur during the first year post-transection. This change could be related to capsular thickening or osteophyte development (Tashman et al., 2004b). The ACL/MCL transected ovine stifle joint provides an alternative to the canine model. Tapper et al. (2008) quantified serial changes in 3D walking kinematics in ACL/MCL transected sheep between intact, two and twenty weeks post transection. After injury, average joint flexion at hoof strike was increased, and tibial position relative to the femur was shifted anteriorly during midstance (Tapper et al., 2008). Over time, the tibial position shifted toward internal rotation, as well as anterior and medial translation in the transected joint between two and twenty weeks. Anterior tibial position during the swing phase of gait was not different from intact immediately following ACL/MCL transection. However, tibial position became significantly more anterior at twenty weeks post transection. This finding agrees with the findings of Tashman and colleagues (2004b) in the canine model. Tapper et al. (2008) supported the potential role of the meniscus in maintaining tibial joint position at the early stages after injury. Development of an anterior tibial shift during the pre-swing phase over time was also suggested as an adaptation strategy to reduce sliding between joint surfaces. The findings of these animal studies suggest that secondary joint stabilizers initially provide AP knee stability after ACL rupture, but over time these structures become damaged from repeated loading and ATT increases in the ACLD knee.

5.1.3 Neuromuscular adaptations

In addition to passive joint stabilizers, active joint stabilizers (*i.e.*, muscles) also play a role in maintaining joint stability in ACLD individuals. The muscular system is responsible for movement of the human body, therefore neuromuscular adaptations greatly contribute to the changes observed in movement patterns following ACL rupture. While changes in quadriceps and hamstring muscle activation the injured limb of ACLD individuals are clear, there is

growing evidence to suggest that neuromuscular adaptation occurs bilaterally (Konishi et al., 2003; Urbach et al., 1999). Urbach et al. (1999) used a combination of maximal voluntary contraction and supermaximal electrical stimulation (twitch interpolation technique), to demonstrate that the ability to fully activate the quadriceps muscle was significantly decreased in both the ACLD injured and contralateral limbs compared to a healthy control group. Therefore, central mechanisms are speculated to be responsible for changes in muscle activation following unilateral ACL rupture.

The central nervous system (CNS) communicates directly with the musculoskeletal system to produce a motor response. The ascending afferent information from the mechanoreceptors in the peripheral joints is processed at three levels of the CNS (spinal cord, brain stem, and motor cortex) and provides information about body position and balance. An ACL rupture causes modifications of ascending afferent pathways, which may cause reorganization of the central nervous system (Kapreli et al., 2009). The ability of the CNS to adapt and change based on the stimulus it receives from the ascending afferent pathways is called "neuroplasticity" (Kapreli et al., 2009). Kapreli et al. (2009) performed a study to determine whether an ACL rupture is capable of causing changes in CNS organization and function. The ACLD group showed diminished activation in several sensorimotor cortical areas relative to the healthy control group, likely due to modifications of ascending afferent pathways from the injured joint (Kapreli et al., 2009). The ACLD group also showed increased activation in three sensorimotor cortical areas, one being the contralateral presupplementary motor area (pre-SMA), a region responsible for the preparation of movement. Increased activation in this area could be due to the increased need to plan movement in ACLD individuals, resulting in more organized movement patterns compared to healthy individuals (Kapreli et al., 2009).

Muscle weakness in the quadriceps can be referred to as arthrogenic muscle inhibition, or AMI. The lost ability to fully activate the quadriceps after ACL rupture can be attributed to muscle atrophy and ongoing neural inhibition (Rice and McNair, 2010). The gamma loop is a spinal reflex circuit formed when motoneurons innervate primary muscle spindles. Normal function of the gamma loop is required to achieve full muscle activation during voluntary contractions. Rice and McNair (2010) suggest that ACL injury results in a loss of excitatory feedback from ligament mechanoreceptors to quadriceps gamma motoneurons, which diminishes coactivation during strong muscle contractions (Rice and McNair, 2010). Konishi and colleagues suggested that gamma loop dysfunction in both the injured and contralateral limbs of ACLD individuals could lead to bilateral muscle weakness (Konishi et al., 2003, 2002). The consequences of ongoing quadriceps weakness include decreased dynamic knee stability, a risk of re-injury to the knee, and a risk of developing OA (Rice and McNair, 2010).

The results of these studies support the theory that ACLD individuals demonstrate alterations in the CNS following injury, which would cause bilateral changes in muscular control and affect movement patterns in both the injured and contralateral limbs.

5.1.4 Acute ACLD kinematics

Studies examining kinematic changes in ACLD individuals at an acute stage post injury are limited. Furthermore, the definition of "acute" varies greatly between studies. Hurd and Snyder-Mackler (2007) studied a group of ACLD individuals with an average time from injury of 11.4 weeks during walking. The ACLD injured limb exhibited a more flexed knee and a lower knee moment at peak knee extension, increased hamstring activity, and decreased soleus activity compared to the contralateral limb during the mid-stance phase of the gait cycle (Hurd and Snyder-Mackler, 2007). Gardinier et al. (2012) recruited ACLD individuals with a mean time

from injury of 7.9 ± 7.4 weeks, defining the acute phase as the first seven months after injury. They found decreased peak knee flexion angle and internal knee extensor moment in the injured limb compared to the contralateral during the stance phase of gait, similar to the findings of Hurd and Snyder-Mackler (2007). They also found decreased flexor and extensor muscle force in the injured limb, which was thought to be due to muscle weakness (Gardinier et al., 2012). Chmielewski et al. (2001) tested a group of ACLD "potential copers", defined as candidates for non-operative rehabilitation (Fitzgerald et al., 2000), at an average time from injury of 3.4 weeks (range 1-9 weeks). The potential copers had decreased knee flexion, a lower vertical ground reaction force at loading, and a decreased knee support moment at peak knee flexion during walking in the injured limb (Chmielewski et al., 2001).

The presence of kinematic adaptations at an "acute" stage following ACL rupture is evident from the studies above. However the studies are limited to walking, and the primary kinematic outcomes are in the sagittal plane only. Clearly, there is a need to quantify ACLD kinematics at a well-defined acute time point post injury, and to track kinematic changes over time to understand early adaptations in this population. Applying the FHA to quantify kinematics during open and closed chain tasks in a group of acute ACL injured individuals may provide a truer representation of knee motion in injured joints, and is expected to reveal adaptations in dynamic joint stability due to ACL deficiency over time.

5.1.5 Mechanisms of OA development

ACL injury is associated with an increased risk of developing knee OA, which is not decreased following ACL reconstruction (Daniel et al., 1994; Lohmander et al., 2007; Roos et al., 1995). The causes for cartilage breakdown leading to the development of OA are multifactorial and interrelated, including biological, mechanical and structural pathways. Increased anterior-

posterior (AP) laxity is a primary outcome of ACL rupture, along with increased rotational tibial laxity. ACL reconstruction is able to restore normal AP laxity (Daniel et al., 1994). However several studies have reported abnormal tibial rotation following ACL reconstruction, especially during high load activities such as step down and pivoting tasks (Georgoulis et al., 2003; Ristanis et al., 2003; Tashman et al., 2004a; Zampeli et al., 2012). These studies highlight the important role of rotational instability in the development of OA in ACLD and ACLR individuals.

Andriacchi et al. (2004) proposed a framework for the initiation of OA, suggesting that a condition (i.e. ACL rupture) that causes a shift in contact position of the joint to an area not accustomed to frequent loading causes articular surface damage. Evidence exists for early matrix consolidation, loss of proteoglycans at the articular cartilage surface layer, and fibrillation with OA (Guilak et al., 1994; Maniwa et al., 2001). Therefore, it is likely that both rotational and translational changes in joint movement patterns due to ACL rupture causes a shift in the load bearing joint contact location, thus initiating cartilage degradation. This theory was also suggested by Stergiou et al. (2007) who focused on the role of abnormal rotational movements in the knee resulting in load application on areas of cartilage not commonly loaded in healthy knees.

Articular cartilage adapts to the loads that it experiences. For example, during walking the medial compartment of the knee is estimated to experience higher loading, which correlates with thicker medial femoral cartilage (Andriacchi et al., 2004). However, ACL rupture causes a rapid shift in joint loading. A biological response to stop the cycle of cartilage damage does not exist. This results in a cascade of events leading to progressive cartilage breakdown and gross cartilage failure (Chaudhari et al., 2012). Cartilage surface fibrillation causes increased friction, which leads to cartilage fibril fracture and additional fibrillation (Chaudhari et al., 2012). This

damaging cycle eventually results in the desensitization of cartilage to increased loading, as compressive stresses turn into cartilage-degenerating shear stresses in the tissue due to friction (Chaudhari et al., 2012). Once the cartilage experiences this change in response to loading, the progression phase of OA begins. OA progression is then characterized by further cartilage degradation caused by increased joint loading on damaged cartilage (Andriacchi et al., 2004; Chaudhari et al., 2012).

Evidence of structural adaptations within the ACLD joint over time, and alterations in kinematics and muscular control over time following ACL rupture has been presented. However, human studies quantifying these outcomes in an ACLD population are generally longer term, while the majority of studies quantifying acute changes in the ACLD joint primarily rely on animal models. To address this gap in literature, the current study investigates changes over time in passive knee laxity, kinematics, and muscular control in ACLD individuals over a tightly controlled time frame to capture adaptations during a sub-acute stage post injury (*i.e.*, six and twelve weeks post injury). Furthermore, both limbs of the ACLD individuals are tested to investigate bilateral adaptations following injury, due to evidence for adaptations to the CNS. Adaptations and relations amongst passive knee laxity and dynamic knee stability in relation to understanding mechanisms for OA development and progression are explored.

5.2 Specific Aims and Hypotheses

The objectives of this study component were to identify changes over time between six and twelve weeks post injury in passive knee laxity, dynamic joint stability, and the relations between these measures following ACL rupture. This objective was accomplished by completing the following specific aims (SA1, SA2) and testing hypotheses H3a-H3c.

Based on the above literature review, the following specific aims (SA1, SA2) were achieved to test hypotheses H3a-H3c.

SA1: Quantifying passive laxity in ACL deficient knee joints over time *in-vivo* using MR imaging combined with a novel joint loading device

SA2: Determining dynamic joint stability relations in joints with ACL deficiency over time, using the finite helical axis method and wavelet analysis of muscle patterns.

H3: ACLD participants will not show a change in passive knee laxity between six and twelve weeks post-injury, but will show changes in dynamic knee stability during this period

H3a: ACLD participants will not show a significant change in passive knee laxity between six and twelve weeks post injury

H3b: ACLD participants will demonstrate changes between six and twelve weeks post injury in dynamic knee stability in both the injured and contralateral limbs, affecting limb symmetry

H3c: At twelve weeks post injury, ACLD participants will show altered correlations (compared to six weeks post injury) between passive knee laxity and FHA measures

5.3 Methods

Chapters 3 and 4 previously described the data collection protocols and approaches for data processing to obtain measures of passive knee laxity and dynamic knee stability. Data collection protocols remained identical for the ACLD group at twelve weeks post injury. However, modifications were made to the data analysis approach for ATT and FHA measures to ensure high repeatability within participants over time. The current section details these modifications and outlines the statistical approaches used to test the study hypotheses H3a-c.

Ethical approval for all methods was obtained from the Conjoint Health Research Ethics Board of the Faculties of Medicine, Nursing and Kinesiology, University of Calgary.

5.3.1 Study Participants

Twelve healthy participants (described in Chapter 3), and ten ACLD participants (described in Chapter 4) were recruited and tested for this study. Written, informed consent was obtained from each participant prior to testing (Appendix A).

5.3.2 Data Acquisition

ACLD participants were tested at six and twelve weeks post-injury. This time frame was chosen to capture changes at a sub-acute stage post-injury, but to exclude the early weeks when the joint is highly inflamed and painful. The protocol for kinematic, EMG and MR data acquisition described in Chapters 3 and 4 was performed for the ACLD group at twelve weeks post-injury.

5.3.3 Data Processing

The data processing and analysis techniques for FHA, EMG and laxity described in Chapters 3 and 4 were applied to the twelve week ACLD data. However, to ensure consistency in LCS definition for the six and twelve week ACLD data, methods were developed to enable the application of the LCS definition from the six week data to the twelve week data. These methods are described below.

5.3.3.1 Laxity

Low resolution MR images with 89 N of applied anterior force to the tibia (KLA) were digitized in Amira 5.0 (FEI Visualization Science Group, Oregon USA), resulting in a 3D cloud of points in the image coordinate system (ICS) for the femur and tibia. The thin plate spline method (Section 4.3.3.1) was used to fit a surface to the 3D cloud of points for the femur and tibia. The registration technique described in Section 4.3.3.1 was used to transform the low resolution

(loaded) femur and tibia surfaces from the twelve week MR images to the high resolution (unloaded) femur and tibia surfaces generated from the six week MR images. However, the surface registration program requires an initial guess of the transformation. At six weeks post-injury, the high and low resolution MR images were acquired with the participant in the same position within the scanner. Therefore, the initial guess for the transformation matrix was based on the small movement expected from KLA load application to the tibia. Therefore, the 3D surface matching tool in Amira was used to provide an initial guess of the transformation matrix required to match the joint position at twelve weeks to the joint position at six weeks. High resolution (six weeks) and low resolution (twelve weeks) tibia and femur surfaces were created in Amira from the digitized bones. Rigid surface matching was applied to the femur and tibia surfaces independently using fifteen iterations and an RMS of 0.001 mm. The resulting 3D transformation matrices for the femur and tibia were used in the surface registration program as an initial guess of the transformation.

The tibia LCS and femur LCS were defined based on boney geometry from high resolution MR images acquired at six weeks post injury (Section 4.3.3.1). Therefore, the adjusted registration technique described above enabled 3D joint movement resulting from KLA loading to be described with respect to the six week LCS definition.

5.3.3.2 FHA

In order to describe the FHA in terms of the six week LCS, an additional transformation matrix was required describing the transformation from the six week ICS to the twelve week ICS. This transformation matrix was determined using the Amira 3D surface matching tool, as described in Section 5.3.3.1.

5.3.4 Statistics

SPSS (SPSS Statistics 20, IMB, New York USA) was used for all statistical analysis in the current study. The Shapiro-Wilks test was used to check for normality in laxity, FHA, muscle power and muscle volume measures in the healthy and ACLD groups (Appendix B). The approach described in Section 4.3.4 was used to determine the appropriate statistical tests for comparisons of ATT, FHA measures, muscle power, and muscle volume between groups and within groups (between limbs).

Differences over time in Δ_{leg} ATT, FHA measures, muscle power and muscle volume were evaluated for normal distribution in the ACLD group. The precise test applied depended on the result of the normal distribution test. The paired T-test is very robust for violations against normality (Sawilowski and Blair, 1992). Therefore, if the majority of variables were normally distributed then the paired T-test was applied to compare between the six and twelve week post injury time points in the ACLD group (α=0.05). If the majority of variables were non-normally distributed, then non-parametric Wilcoxon Signed Ranks tests were used to compare between the six and twelve week post injury time points in the ACLD group (α=0.05).

5.4 Results

5.4.1 Statistics

IKDC and Lysholm scores were normally distributed for the ACLD group at twelve weeks post injury (p-value range: 0.404-0.473), but were not normally distributed for the healthy group ($p \leq$ 0.002, Table B-5). The T-test was chosen to compare IKDC and Lysholm scores between groups, reporting the p-value for non-equal distributions (α=0.05). The difference between days was normally distributed for the IKDC and Lysholm scores (p-value range: 0.718-0.961, Table

B-5) for the ACLD group. Therefore, paired T-tests were used to compare scores between six and twelve weeks post injury for the ACLD group (α=0.05).

The side to side difference (Δ_{leg}) in laxity was normally distributed in the ACLD group at six (p=0.522) and twelve weeks (p=0.325) post injury (Table B-2). Therefore, paired T-tests were used to compare Δ_{leg} laxity between six and twelve weeks post injury within the ACLD group (α=0.05).

The majority of FHA variables were normally distributed for both limbs of the ACLD group at six and twelve weeks post injury (range of non-normally distributed = 3%-22% for a given limb), and for the healthy group (range of non-normally distributed = 19%-28% for a given limb, Table B-2). Therefore, T-tests were used for between group comparisons of FHA measures to enable comparison and discussion of group means (α=0.05).

The percentage of non-normally distributed side to side differences in FHA variables was 16%, 13% and 6% for the healthy, ACLD six week, and ACLD twelve week groups respectively (Table B-2). The percentage of non-normally distributed differences over time in FHA variables was 19% and 6% for the ACLD injured and contralateral limbs respectively (Table B-2). Therefore, the paired T-test was used to compare FHA measures between dominant and contralateral limbs in the healthy group, injured and contralateral limbs in the ACLD group, and differences between six and twelve weeks post injury for the injured and contralateral limbs of the ACLD group (α=0.05).

The percentage of non-normally distributed side to side differences in muscle power was 17% for the ACLD group at twelve weeks post injury (Table B-3). The percentage of non-normally distributed day to day differences in muscle power was 33% and 0% for the injured and contralateral limbs of the ACLD groups (Table B-3). Non-parametric Wilcoxon Signed Ranks

tests were used to compare muscle power between injured and contralateral limbs in the ACLD group, and differences between six and twelve weeks post injury for the injured and contralateral limbs of the ACLD group (α=0.05). Muscle power data from some participants was excluded due to poor quality, therefore participant numbers were low (n=6 for ACLD), which could contribute to the non-normally distributed data. Furthermore, the EMG normalization technique employed for this study (Section 3.3.3.3) was designed for within subject comparisons, which may have affected the distribution of the data.

The percentage of non-normally distributed side to side differences in muscle volume was 25% for the ACLD group at twelve weeks post injury (Table B-4). Therefore, the paired T-test was used to compare muscle volume between injured and contralateral limbs in the ACLD group (α=0.05).

5.4.2 Study Participants

One of the ACLD participants was excluded due to a high BMI that resulted in poor quality kinematic and EMG data, and one ACLD participant did not complete the twelve week follow-up testing (A06). The ACLD group consisted of nine females (28.8 ± 7.2 yrs, 166.9 ± 5.0 cm, 65.6 ± 11.5 kg). Average time from injury for the ACLD group was 83.5 ± 3.9 days for the twelve week testing session. Further participant information is shown in Table 5-1.

Table 5-1: ACLD Participant Information

Participant ID	Age (years)	Height (cm)	Weight (kg)	Injured Limb	6 weeks (days)	12 weeks (days)
A01	27	163	54.9	Right	40	87
A02	23	159	57.6	Left	50	83
A03	37	175	90.7	Left	41	87
A04	22	168	61.2	Left	36	83
A05	29	165	60.3	Right	50	79
A06	37	167	61.2	Right	51	
A07	28	170	68.0	Right	46	84
A08	18	163	59.0	Right	53	77
A09	38	172	77.5	Right	43	88
mean (std)	28.8 (7.2)	166.9 (5.0)	65.6 (11.5)		45.6 (5.9)	83.5 (3.9)

The ACLD group had significantly lower scores for both the IKDC and Lysholm questionnaires compared to the healthy group at twelve weeks post injury (Table 5-2). The ACLD group had an average score of 69.2 ± 7.6 for the IKDC, compared to 97.8 ± 4.9 for the healthy group ($p<0.001$). For the Lysholm questionnaire, the ACLD group had an average score of 78.1 ± 8.8, compared to 97.5 ± 3.4 for the healthy group ($p<0.001$). The IKDC score significantly increased over time in the ACLD group (Table 5-2). The IKDC score for the ACLD group was 50.8 ± 15.1 at six weeks post injury, and increased to 69.2 ± 7.6 at twelve weeks post injury ($p=0.007$). The Lysholm score did not significantly change over time ($p=0.293$).

Table 5-2: IKDC and Lysholm knee function questionnaire scores (out of 100) for the healthy and ACLD group at 6 and 12 weeks post injury

Healthy			ACLD				
				6 weeks		12 weeks	
Participant ID	**IKDC**	**Lysholm**	**Participant ID**	**IKDC**	**Lysholm**	**IKDC**	**Lysholm**
H01	n/a	100	A01	49.4	82.0	67.8	67.0
H02	100.0	100.0	A02	64.4	69.0	65.1	74.0
H03	100.0	90.0	A03	58.2	85.0	67.8	78.0
H04	94.3	95.0	A04	50.6	59.0	58.6	69.0
H05	100.0	100.0	A05	51.7	51.0	83.9	80.0
H06	98.9	100.0	A06	18.4	34.0		
H07	100.0	100.0	A07	39.1	64.0	65.5	76.0
H08	98.9	100.0	A08	55.2	73.0	69.0	90.0
H09	100.0	95.0	A09	69.9	96.0	75.9	91.0
H10	100.0	100.0					
H11	83.9	95.0					
H12	100.0	95.0					
Mean	97.8	97.5	**Mean**	50.8	68.1	69.2	78.1
Std	4.9	3.4	**Std**	15.1	18.8	7.6	8.8

The injured limb of the ACLD group had a significantly higher KIMRISS effusion score at twelve weeks post injury relative to both the ACLD contralateral limb ($p=0.020$) at twelve weeks and the dominant limb of the healthy group ($p=0.025$) indicating increased joint effusion in the ACLD injured limb (Table 5-3). The ACLD group had an average KIMRISS score of 1.88 ± 1.36 in the injured limb and 0.50 ± 1.07 in the contralateral limb at twelve weeks post injury. The healthy group had an average KIMRISS score of 0.50 ± 0.67 in the dominant limb. The KIMRISS score significantly decreased over time in the ACLD contralateral limb from 1.00 ± 1.31 at six weeks post injury to 0.50 ± 1.07 at twelve weeks post injury ($p=0.033$), indicating a decrease in joint effusion in the contralateral limb over time. The KIMRISS score in the ACLD injured limb did not significantly change over time ($p=0.129$). There were no significant

differences between groups (p=0.170), between limbs in the ACLD group (p=0.351), or over time in the ACLD group (p=0.451) for the MOAKS score.

Table 5-3: MOAKS (0-3) and KIMRISS (0-12) joint effusion scores for the dominant and contralateral limbs of the healthy group, and the injured and contralateral limbs of the ACLD group at 6 and 12 weeks post injury

Healthy					ACLD								
						6 weeks				12 weeks			
	Dom		Contra			Injured		Contra		Injured		Contra	
ID	MOAKS	KIMRISS	MOAKS	KIMRISS	ID	MOAKS	KIMRISS	MOAKS	KIMRISS	MOAKS	KIMRISS	MOAKS	KIMRISS
H01	0	1	0	2	A01	2	9	0	0	0	3	0	0
H02	0	1	0	0	A02	1	5	0	0	0	1	0	0
H03	0	0	0	2	A03	0	3	0	1	0	2	0	0
H04	0	0	0	0	A04	1	5	0	1	1	3	0	0
H05	0	0	0	1	A05	0	1	0	1	0	0	0	1
H06	0	0	0	1	A06	0	1	0	0				
H07	0	1	0	1	A07	0	3	0	1	0	1	0	0
H08	0	2	1	2	A08	0	1	0	0	0	1	0	0
H09	0	1	0	1	A09	0	1	1	4	1	4	1	3
H10	0	0	0	0									
H11	0	0	0	0									
H12	0	0	0	0									
Mean	0.00	0.50	0.08	0.83	**Mean**	0.44	3.22	0.11	0.89	0.25	1.88	0.13	0.50
Std	0.00	0.67	0.29	0.83	**Std**	0.73	2.73	0.33	1.27	0.46	1.36	0.35	1.07

5.4.3 Laxity

Laxity values (ATT) are reported for an anterior reaction force (F_{ry}) of 89 N at the knee joint. The reaction force (F_{ry}) at the proximal tibia resulting from KLA loading during MR imaging was within 8.8% of the target F_{ry} for the injured limb of the ACLD group, and within 4.4% of the target F_{ry} for the contralateral limb of the ACLD group (Table 5-4). The between limb difference for the reaction force was within 6.0% for the ACLD group. In general, F_{ry} during MR imaging was less than the target F_{ry}, indicated by a negative percent difference.

Table 5-4: Target reaction force at the knee joint (F_{ry}, 89 N) and F_r applied during MR imaging for ACLD study participants at 12 weeks post injury. Percent difference from target shown for each limb, as well as percent difference between limbs.

	ACLD 12 weeks					
		Injured		Contra		
Participant ID	Target F_{ry} (N)	Actual F_{ry} (N)	% diff	Actual F_{ry} (N)	% diff	% diff b/w limb
A01	89	85	-4.8	87	-1.7	3.1
A02	89	88	-0.7	88	-0.9	-0.2
A03	89	86	-2.9	85	-4.4	-1.5
A04	89	86	-3.6	89	0.5	4.1
A05	89	89	0.4	87	-2.4	-2.8
A07		n/a		n/a		
A08	89	81	-8.8	87	-2.8	6.0
A09	89	86	-3.4	87	-2.5	0.9

Five out of eight ACLD study participants showed a decrease in ATT in the injured limb between six and twelve weeks post injury (Figure 5-1). Side to side differences in ATT were calculated as Δ_{leg} ATT=$ATT_{Injured}$-$ATT_{Contralateral}$ for the ACLD group. The average Δ_{leg} ATT at 89N in the ACLD group at six weeks post injury was 3.43 ± 4.28 mm, and at twelve weeks post-injury was 1.29 ± 2.47 mm. The difference in Δ_{leg} ATT between six and twelve weeks post injury in the ACLD group was not statistically significant ($t(7) = 1.346$, $p = 0.220$).

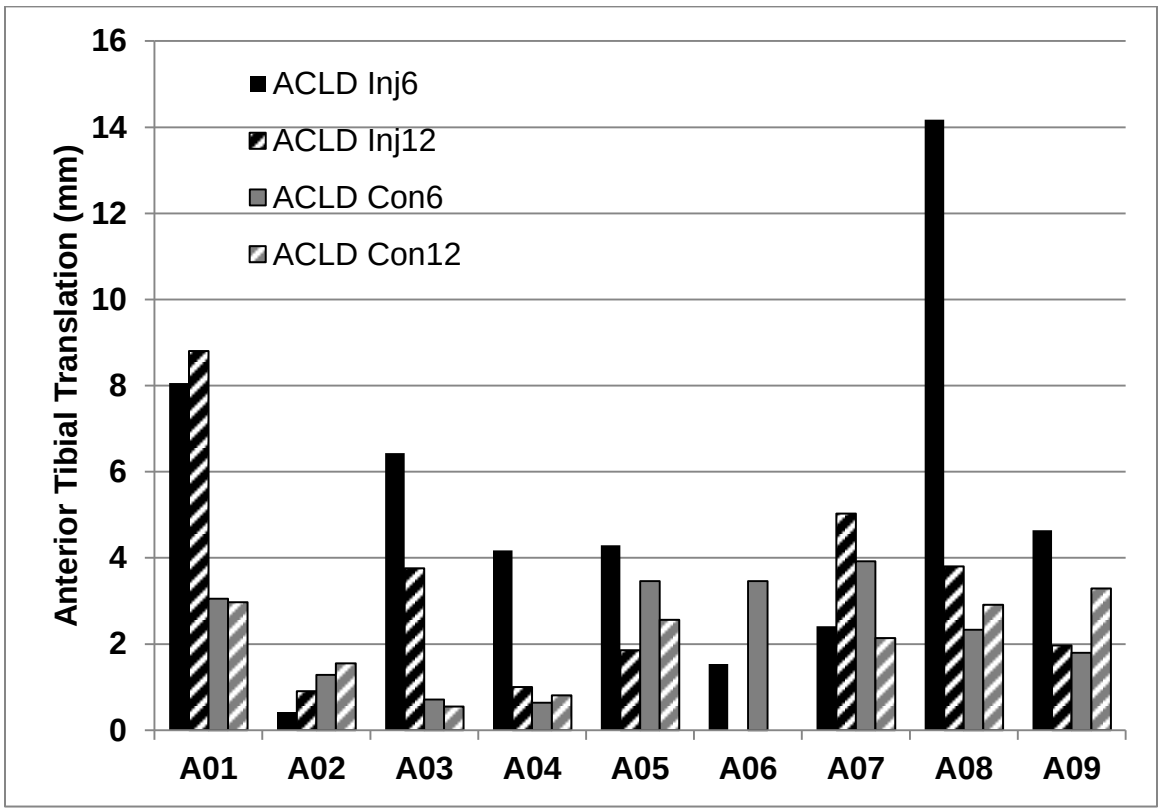

Figure 5-1: Anterior tibial translation (mm) at 89 N for individual participants in the ACLD group at six weeks post injury for the injured (ACLD Inj6) and contralateral (ACLD Con6) limbs, and at twelve weeks post-injury for the injured (ACLD Inj12) and contralateral (ACLD Con12) limbs

5.4.4 FHA

5.4.4.1 Location

The FHA was located significantly more anterior in the ACLD injured limb compared to contralateral during the flexion ($p=0.035$) and extension ($p=0.017$) phases of the swing task at twelve weeks post injury. During swing flexion average FHA location y was 21.62 ± 5.62 mm in the injured limb, compared to 19.04 ± 6.51 mm in the contralateral limb (Figure 5-2). This difference was not significant during the squat task, and was not significant at six weeks post

injury (Chapter 4). No significant differences in FHA location were detected over time in the ACLD group, p values ranged from 0.299-0.945.

The FHA was located significantly more posterior in the ACLD contralateral limb at twelve weeks post-injury compared to the healthy group during swing flexion (p=0.042) and swing extension (p=0.025). During swing flexion the average FHA location y was 19.04 ± 6.51 mm in the contralateral limb, compared to 24.99 ± 5.59 mm in the healthy group (Figure 5-2). This finding was also significant at six weeks post-injury (Chapter 4).

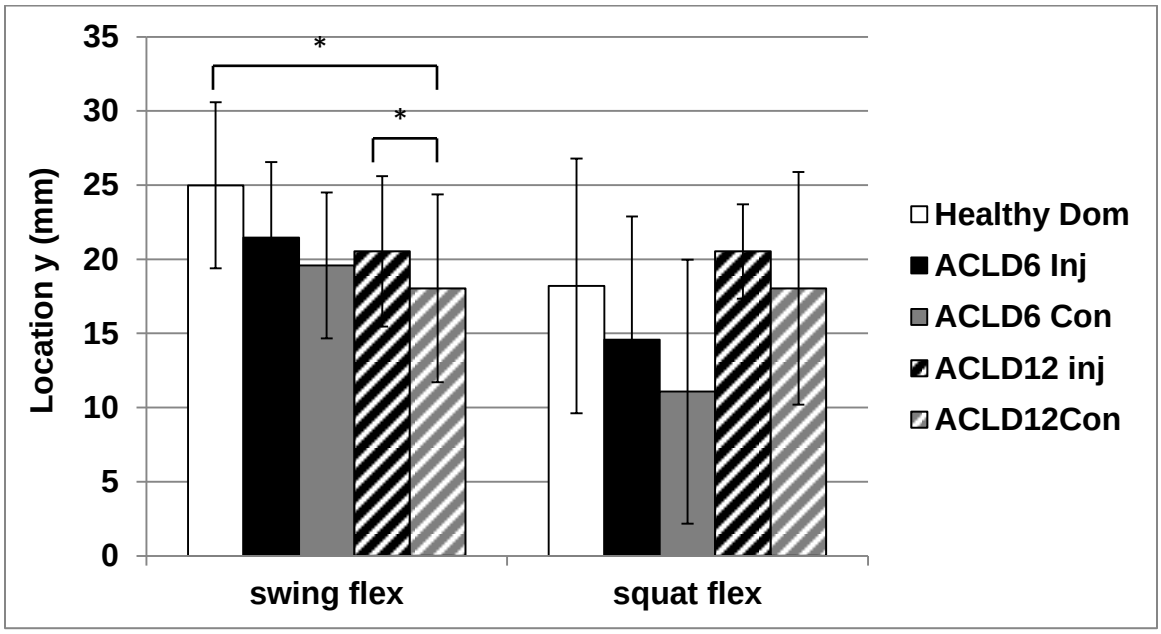

Figure 5-2: Average FHA location y (mm) for the healthy group, and for the injured (inj) and contralateral (con) limbs of the ACLD group at 6 and 12 weeks post injury during the flexion and phase of the squat (squat flex) and swing (swing flex) tasks. (* indicates significance at α=0.05).

5.4.4.2 Translation

FHA translation was significantly decreased in the ACLD injured limb at twelve weeks post-injury compared to six weeks post-injury during squat flexion (p=0.005) and extension (p=0.010). During the flexion phase of the squat, translation was 3.79 ± 0.71 mm at six weeks

post injury, and decreased to 2.97 ± 0.58 mm at twelve weeks post injury in the ACLD group (Figure 5-3). There were no significant differences over time in FHA translation during the swing task.

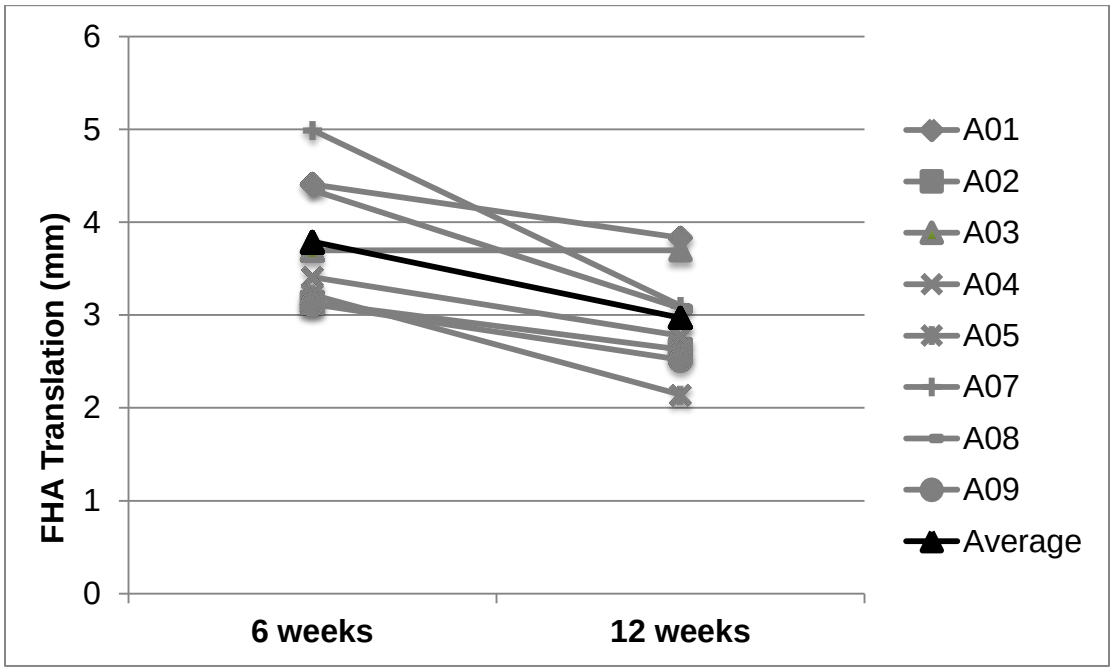

Figure 5-3: FHA translation (mm) during squat flexion for the ACLD injured limb at 6 and 12 weeks post-injury. Grey lines represent individual participants, black line represents group average.

FHA translation was also significantly lower in the ACLD injured limb compared to the contralateral during squat flexion (p=0.034), however was not significant during squat extension (p=0.072) at twelve weeks post-injury. During the flexion phase of the squat, translation was 2.97 ± 0.58 mm in the ACLD injured limb, compared to 3.84 ± 1.39 mm in the contralateral limb (Figure 5-4). There were no significant side to side differences in FHA translation during the swing task for the ACLD group at twelve weeks post injury.

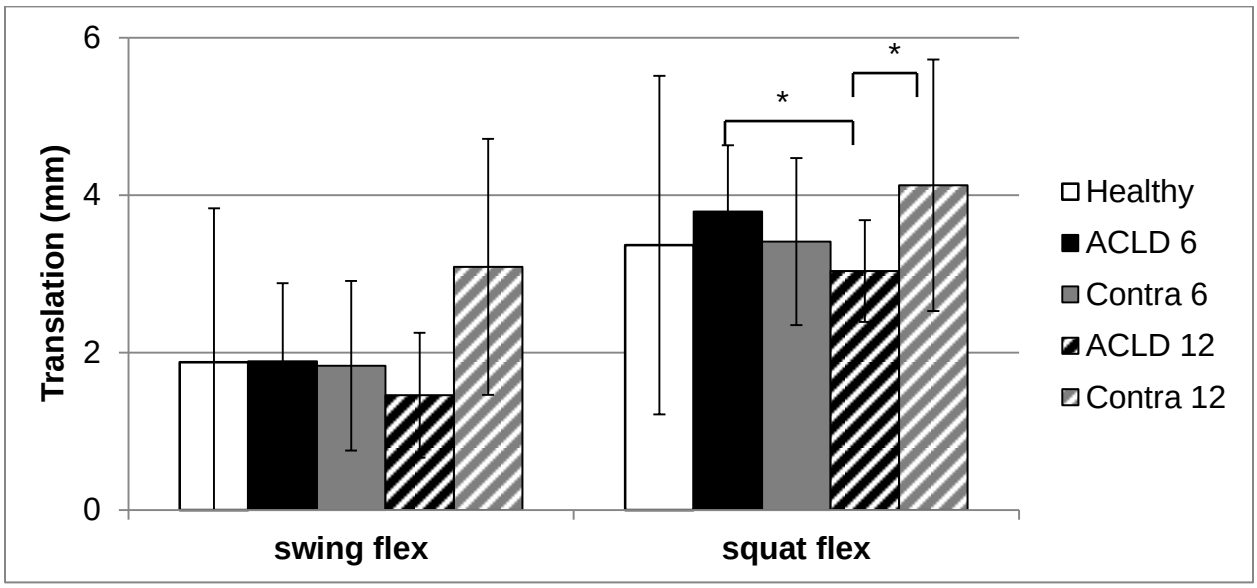

Figure 5-4: Average FHA translation (mm) for the healthy group, and for the injured (ACLD) and contralateral (Contra) limbs of the ACLD group at 6 and 12 weeks post-injury during the flexion phase of the squat (squat flex) and swing (swing flex) tasks. (* indicates significance at α=0.05).

The side to side difference in FHA translation (Δ_{leg}=ACLD-Contra) significantly increased over time in the ACLD group during squat flexion (p=0.015), squat extension (p=0.010), and swing flexion (p=0.026), indicating decreased limb symmetry at twelve weeks post-injury. During the flexion phase of the squat, Δ_{leg} increased from 0.32 ± 1.06 mm at six weeks post-injury, to -0.87 ± 0.93 mm at twelve weeks post-injury (Figure 5-5). The change in sign indicates that at six weeks post injury the ACLD limb had larger translation, while at twelve weeks post injury the contralateral had larger translation.

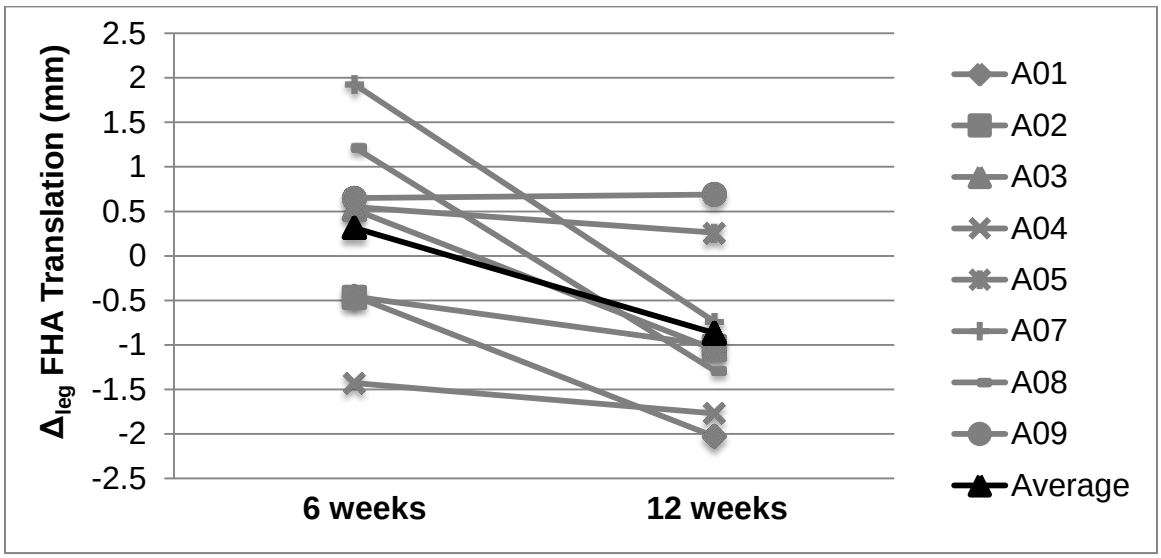

Figure 5-5: Side to side difference (Δ_{leg}) in FHA translation (mm) during squat flexion for the ACLD group at 6 and 12 weeks post-injury. Grey lines represent individual participants, black line represents group average.

5.4.4.3 Orientation

There were no significant differences in FHA orientation angle between legs in the ACLD group, or between groups at twelve weeks post injury. Average orientation angle ranged from 9.45°-12.11° in the healthy group, 9.18°-13.17° in the ACLD injured limb, and 7.99°-16.53° in the ACLD contralateral limb during the swing and squat tasks. P-values ranged from 0.147-0.571 for side to side differences, and 0.101-0.881 for between group differences.

5.4.4.4 Dispersion

The side to side difference in FHA dispersion (Δ_{leg}=ACLD-Contra) significantly increased over time in the ACLD group during squat flexion (p=0.047), however did not significantly change during squat extension (p=0.091), indicating decreased limb symmetry at twelve weeks post-injury. During the flexion phase of the squat, Δ_{leg} increased from 0.11 ± 0.68° at six weeks post-injury, to 0.67 ± 0.29° at twelve weeks post-injury (Figure 5-6). The side to side difference in

FHA dispersion was also significantly greater in the ACLD group at twelve weeks post injury compared to the healthy group during squat flexion (p=0.007) and squat extension (p=0.005). In the healthy group, Δ_{leg} dispersion was -0.03 ± 0.60° during the flexion phase of the squat compared to 0.67 ± 0.29° in the ACLD group at twelve weeks post injury.

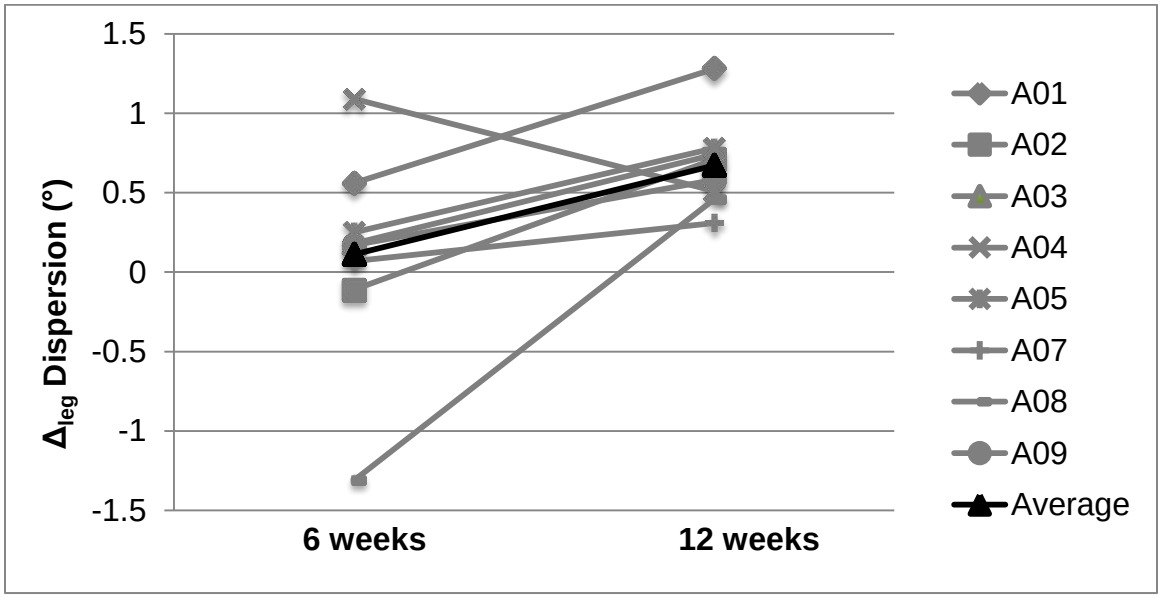

Figure 5-6: Side to side difference (Δ_{leg}) in FHA dispersion (°) during squat flexion for the ACLD group at 6 and 12 weeks post-injury. Grey lines represent individual participants, black line represents group average.

FHA dispersion was significantly greater in the ACLD injured limb compared to contralateral during squat flexion (p<0.001) and extension (p=0.006) at twelve weeks post injury, and compared to healthy during squat flexion (p<0.001) and extension (p=0.018). Average dispersion was 1.85 ± 0.46° in the ACLD injured limb, 1.13 ± 0.34° in the contralateral limb, and 1.36 ± 0.38° in the healthy group during squat extension (Figure 5-7). In the ACLD contralateral limb, dispersion significantly decreased over time during squat extension (p=0.041), however did not significantly change during squat flexion (p=0.059). At six weeks post-injury, dispersion was

1.51 ± 0.49° in the contralateral limb, compared to 1.13 ± 0.34° at twelve weeks post-injury during squat extension (Figure 5-7).

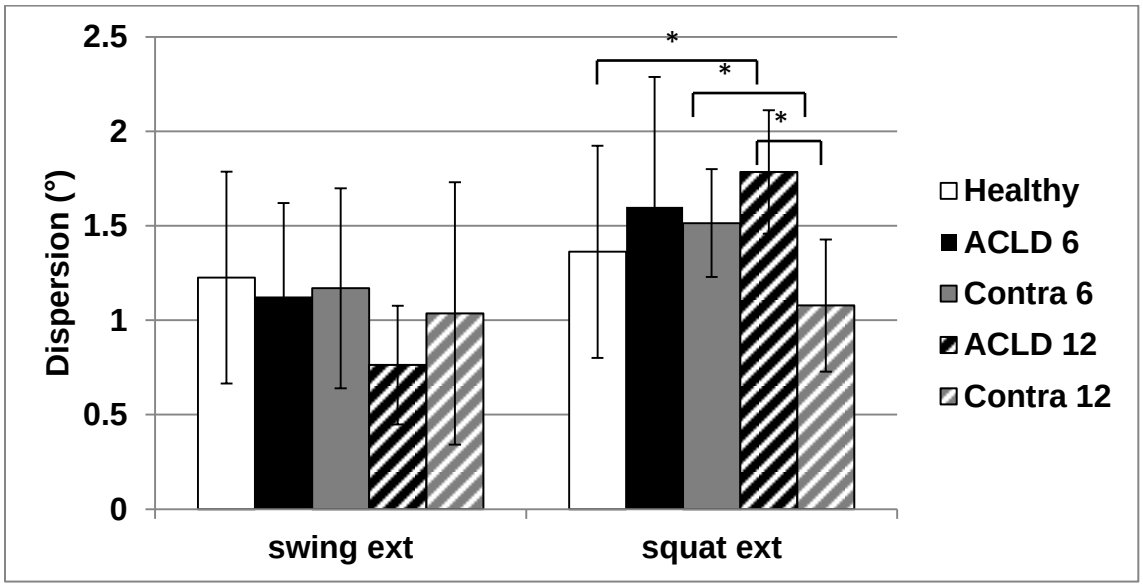

Figure 5-7: Average FHA dispersion (°) for the healthy group, and for the injured (ACLD) and contralateral (Contra) limbs of the ACLD group at 6 and 12 weeks post-injury during the extension phase of the squat (squat ext) and swing (swing ext) tasks. (* indicates significance at α=0.05).

5.4.4.5 Path

FHA path length significantly decreased over time in the ACLD contralateral limb during squat extension (p=0.002), however did not significantly change during squat flexion (p=0.072). Path length during the extension phase of the squat was 7.34 ± 1.43 mm at six weeks post-injury, and reduced to 5.62 ± 1.61 mm at twelve weeks post injury in the ACLD contralateral limb (Figure 5-8). There were no significant differences in path length over time in the ACLD injured limb.

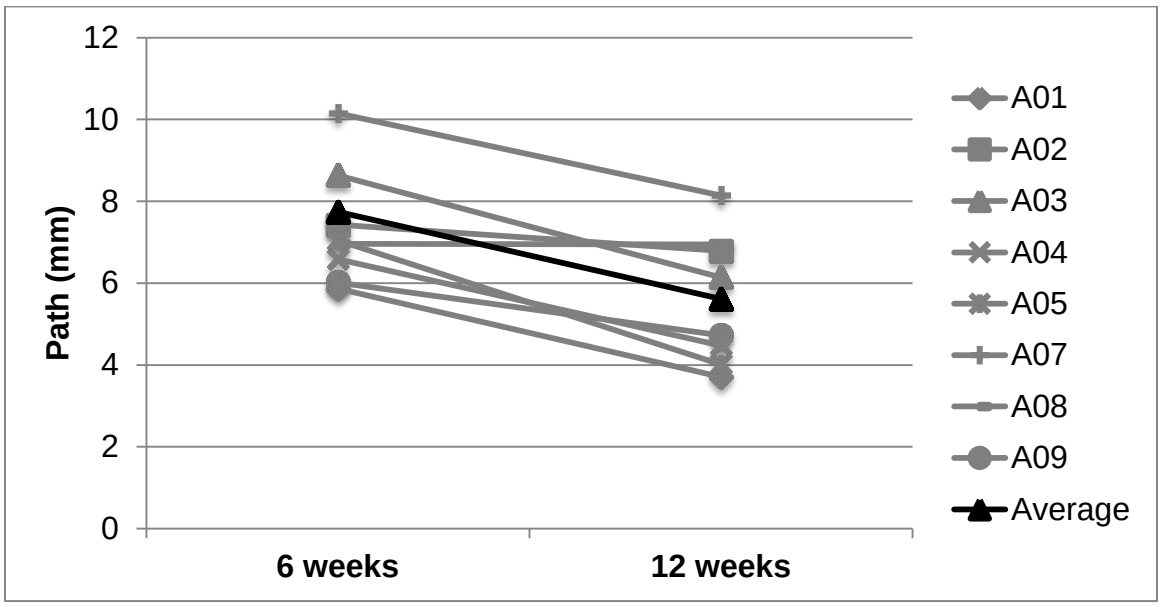

Figure 5-8: FHA path length (mm) during squat extension for the ACLD contralateral limb at 6 and 12 weeks post-injury. Grey lines represent individual participants, black line represents group average.

5.4.4.6 Excursion

FHA AP excursion significantly decreased over time in the ACLD contralateral limb during swing extension (p=0.033), however did not significantly change during squat flexion (p=0.076). AP excursion during the extension phase of the swing was 3.37 ± 2.12 mm at six weeks post-injury, and reduced to 1.81 ± 1.05 mm at twelve weeks post injury in the ACLD contralateral limb (Figure 5-9). There were no significant differences in AP excursion over time in the ACLD injured limb.

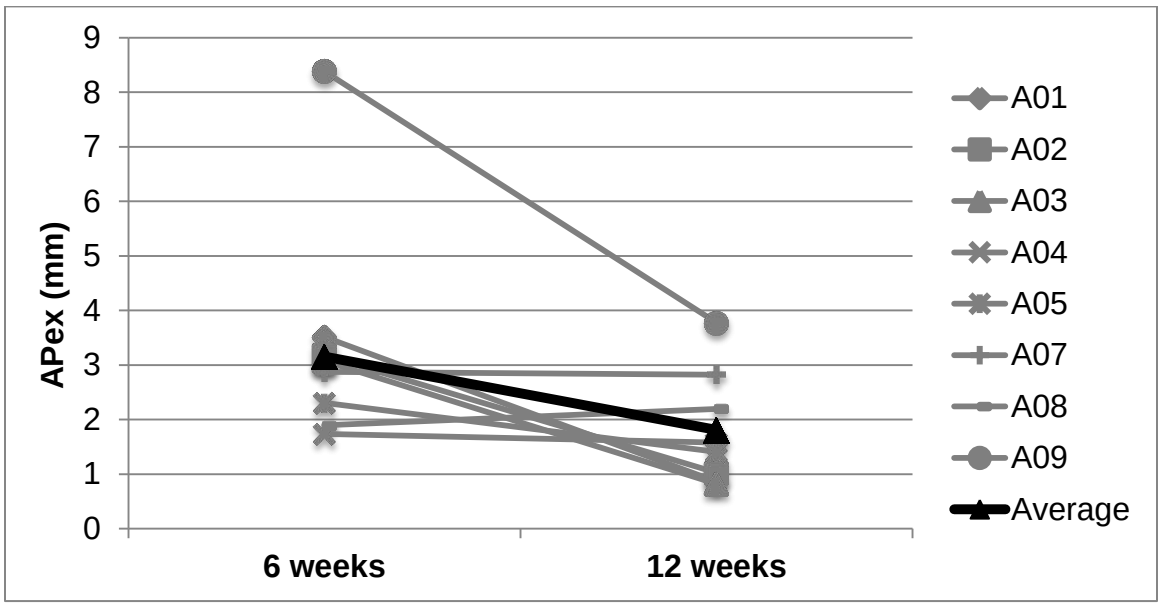

Figure 5-9: FHA AP excursion (AP ex) (mm) during swing extension for the ACLD contralateral limb at 6 and 12 weeks post-injury. Grey lines represent individual participants, black line represents group average.

AP excursion was also significantly decreased in the ACLD contralateral limb compared to the ACLD injured limb during swing flexion ($p=0.010$) and extension ($p=0.042$), and compared to healthy during swing extension ($p=0.043$). Average AP excursion was 1.81 ± 1.05 mm in the ACLD contralateral limb, 2.80 ± 1.21 mm in the injured limb, and 3.00 ± 1.29 mm in the healthy group (Figure 5-10).

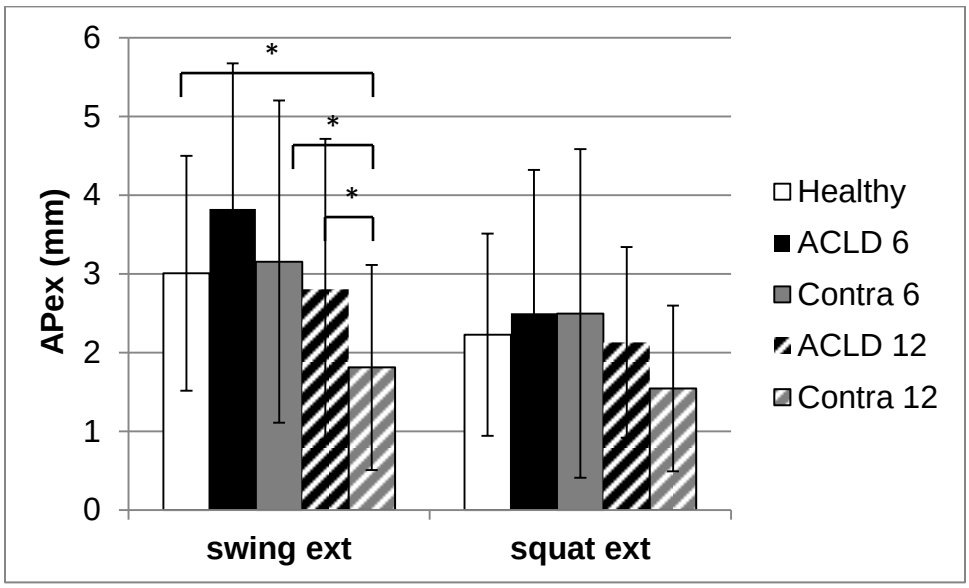

Figure 5-10: Average FHA AP excursion (AP ex) (mm) for the healthy group, and for the injured (ACLD) and contralateral (Contra) limbs of the ACLD group at 6 and 12 weeks post-injury during the extension phase of the squat (squat ext) and swing (swing ext) tasks. (* indicates significance at α=0.05).

PD excursion was significantly decreased in the ACLD contralateral limb compared to the injured limb at twelve weeks post injury during squat extension (p=0.004). Average PD excursion was 1.84 ± 0.64 mm in the contralateral limb, compared to 2.58 ± 0.72 mm in the injured limb during the extension phase of the squat.

5.4.5 Correlations

In the ACLD injured limb at twelve weeks post injury, individuals with higher anterior tibial translation (ATT) exhibited a more anterior FHA location (Figure 5-11). FHA location y was correlated with ATT in the ACLD injured limb during swing flexion ($r_s(8)=0.690$, p=0.058) and extension ($r_s(8)=0.7690$, p=0.058), although this relationship did not reach statistical significance. In the ACLD contralateral limb, FHA location y was significantly correlated with ATT during squat flexion ($r_s(8)=0.857$, p=0.007, Figure 5-11) and extension ($r_s(8)=0.857$,

p=0.007). FHA location y was not significantly correlated with ATT in the healthy group (Chapter 4).

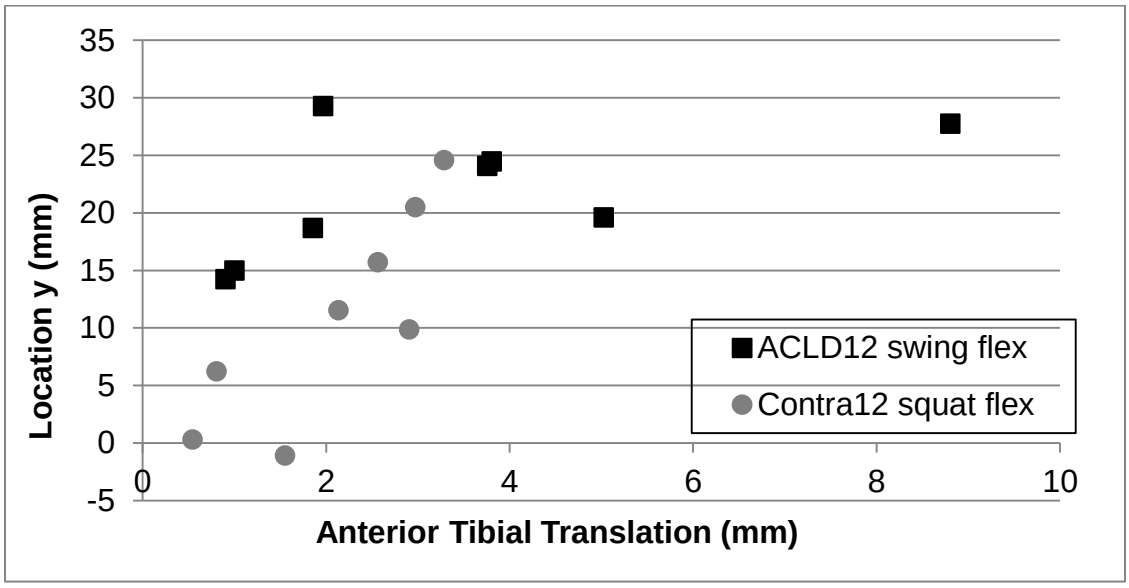

Figure 5-11: FHA location y versus anterior tibial translation for the ACLD injured limb during swing flexion (p=0.058), and for the contralateral limb during squat flexion (p=0.007*) at 12 weeks post injury. (* indicates significance at α=0.05).

In the ACLD injured limb, individuals with higher ATT exhibited decreased translation during the swing task, and increased translation during the squat task (Table 5-5, Figure 5-12). FHA translation was correlated with ATT in the ACLD injured limb during swing flexion ($r_s(8)$=-0.714, p=0.047) and extension ($r_s(8)$=0.714, p=0.047), and during squat flexion ($r_s(8)$=0.738, p=0.037) and extension ($r_s(8)$=-0.667, p=0.071). There were no significant correlations in the ACLD contralateral limb at twelve weeks post injury (Table 5-5), or in the healthy group (Chapter 4).

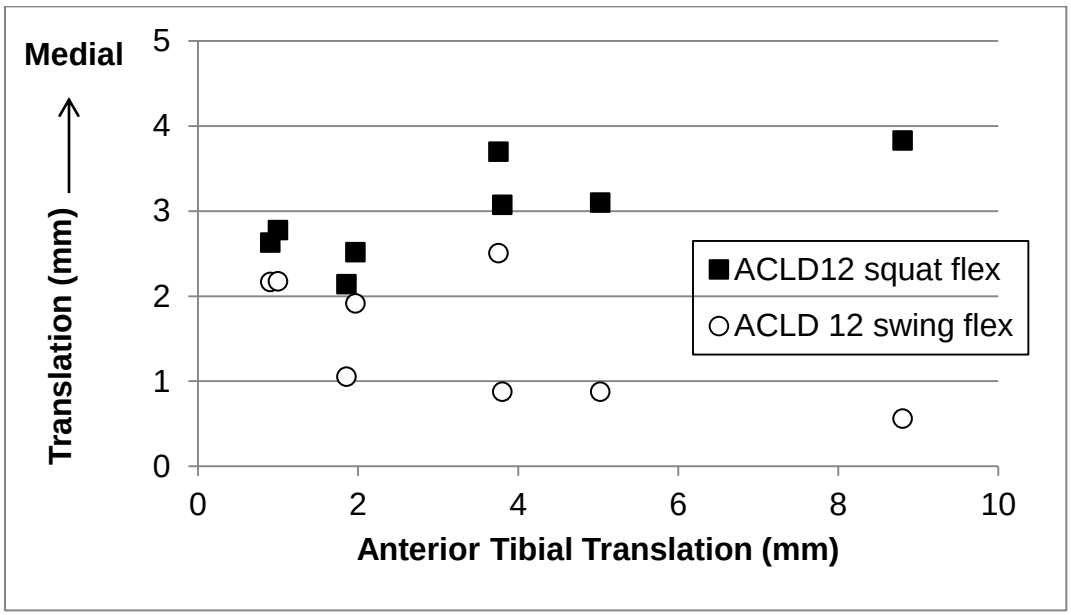

Figure 5-12: FHA translation versus anterior tibial translation for the ACLD injured limb during swing flexion (p=0.047*), and squat flexion (p=0.037*) at 12 weeks post injury. (* indicates significance at α=0.05).

In the ACLD injured limb, individuals with higher ATT also exhibited decreased dispersion during the swing task, and increased dispersion during the squat task (Table 5-5, Figure 5-13). FHA dispersion was correlated with ATT in the ACLD injured limb during swing extension ($r_s(8)$=-0.786, p=0.021) and during squat flexion ($r_s(8)$=0.762, p=0.028).

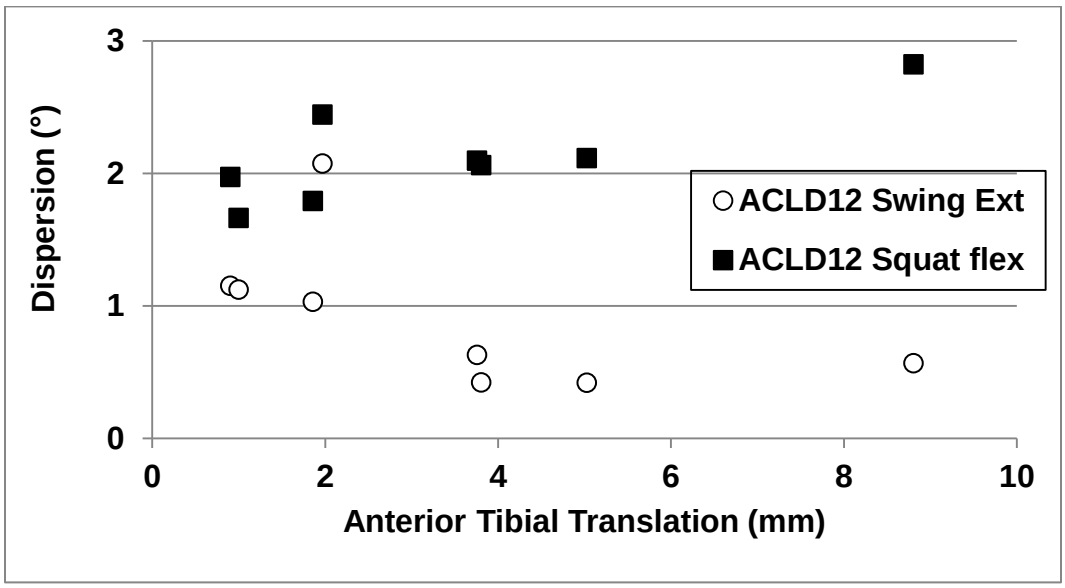

Figure 5-13: FHA dispersion (°) versus anterior tibial translation (mm) for the ACLD injured limb (ACLD12) during swing extension (p=0.021*), and squat flexion (p=0.028*) at 12 weeks post injury. (* indicates significance at α=0.05).

In the injured limb of the ACLD group, individuals with larger ATT exhibited increased path length and AP excursion during the squat (Table 5-5). Conversely, in the ACLD contralateral limb, individuals with larger ATT exhibited decreased path length and AP excursion during the squat. FHA path length was correlated with ATT during squat flexion in the ACLD injured limb ($r_s(8)=0.762$, p=0.028), and the contralateral limb ($r_s(8)=-0.762$, p=0.028, Figure 5-14). FHA AP excursion was correlated with ATT during squat flexion in the ACLD injured limb ($r_s(8)=0.810$, p=0.015), and the contralateral limb ($r_s(8)=-0.690$, p=0.058, Figure 5-15).

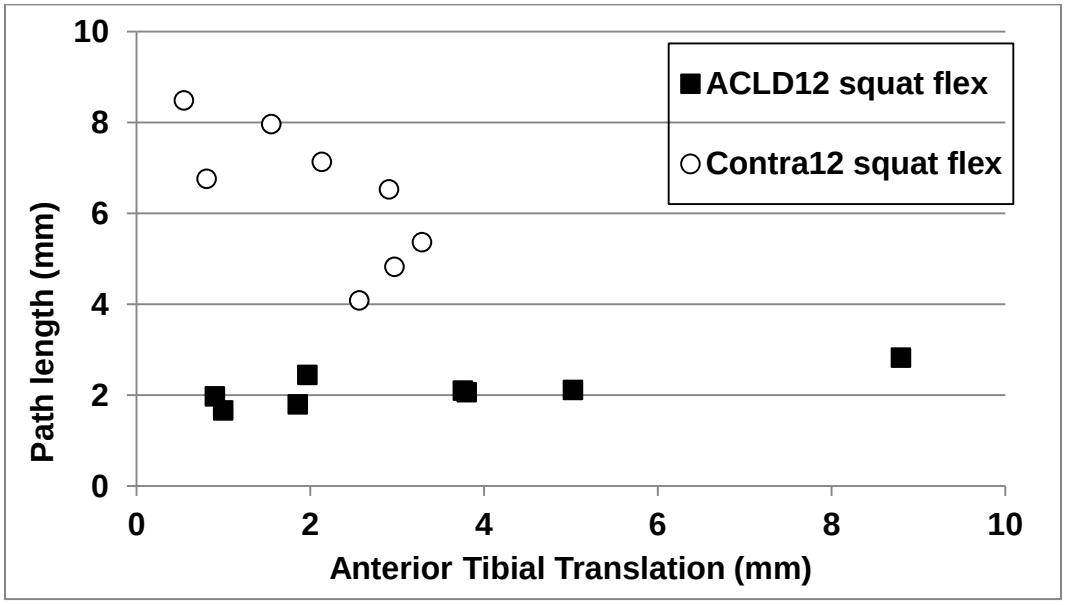

Figure 5-14: FHA path length (mm) versus anterior tibial translation (mm) for the ACLD injured (ACLD12, p=0.028*) and contralateral (Contra12, p=0.028*) limbs during squat flexion at 12 weeks post injury. (* indicates significance at α=0.05).

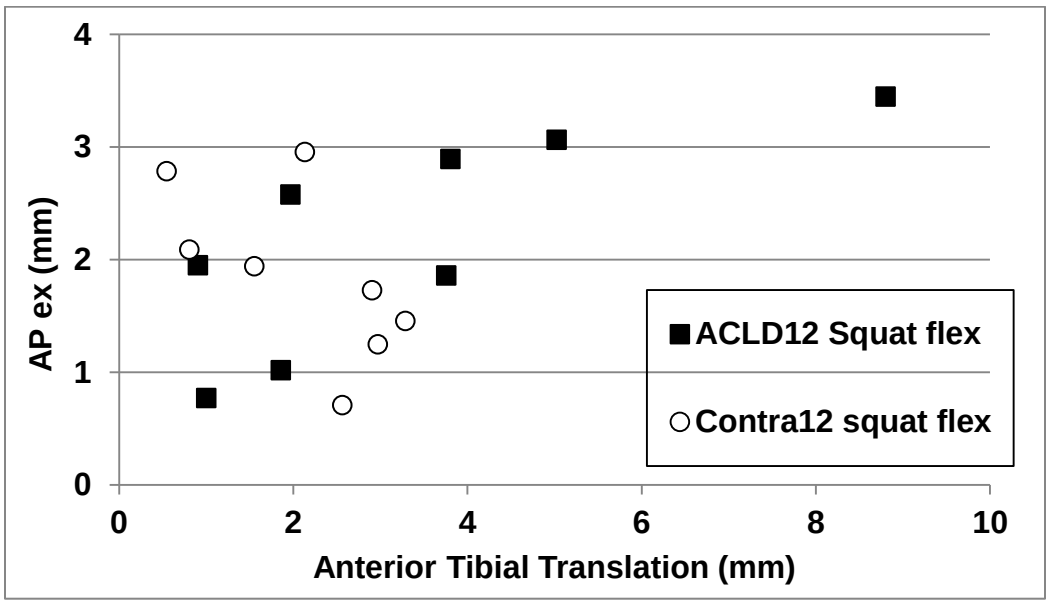

Figure 5-15: FHA AP excursion (mm) versus anterior tibial translation (mm) for the ACLD injured (ACLD12, p=0.015*) and contralateral (Contra12, p=0.058) limbs during squat flexion at 12 weeks post injury. (* indicates significance at α=0.05).

Table 5-5: Spearman's correlation coefficients and significance values between anterior tibial translation and FHA measures for the injured and contralateral limbs of the ACLD group at 6 and 12 weeks post injury. (* indicates significance at α=0.05).

			ACLD Inj 6 weeks		ACLD Con 6 weeks		ACLD Inj 12 weeks		ACLD Con 12 weeks	
task	phase	Measure	Corr Coeff	Sig.	Corr Coeff	Sig.	Corr Coeff	Sig.	Corr Coeff	Sig.
swing	flex	loc y (mm)	.700	.036*	-.183	.637	.690	.058	.548	.160
		trans (mm)	-.617	.077	.517	.154	-.714	.047*	.024	.955
		disp (°)	-.333	.381	0.000	1.000	-.167	.693	.286	.493
		path (mm)	-.717	.030*	-.050	.898	-.286	.493	-.595	.120
		APex (mm)	-.417	.265	.433	.244	.357	.385	.548	.160
	ext	loc y (mm)	.733	.025*	-.283	.460	.690	.058	.405	.320
		trans (mm)	.783	.013*	-.600	.088	.714	.047*	-.190	.651
		disp (°)	-.467	.205	.067	.865	-.786	.021*	.333	.420
		path (mm)	-.817	.007*	-.500	.170	-.619	.102	-.143	.736
		APex (mm)	-.367	.332	-.167	.668	.286	.493	.476	.233
squat	flex	loc y (mm)	.633	.067	.100	.798	.048	.911	.857	.007*
		trans (mm)	.250	.516	-.450	.224	.738	.037*	-.333	.420
		disp (°)	.133	.732	-.200	.606	.762	.028*	.548	.160
		path (mm)	.100	.798	-.567	.112	.762	.028*	-.762	.028*
		APex (mm)	0.000	1.000	-.117	.765	.810	.015*	-.690	.058
	ext	loc y (mm)	.617	.077	-.017	.966	.167	.693	.857	.007*
		trans (mm)	-.300	.433	.667	.050*	-.667	.071	.357	.385

		disp (°)	-.017	.966	-.133	.732	.190	.651	.286	.493
		path (mm)	-.067	.865	.383	.308	.333	.420	-.238	.570
		APex (mm)	.233	.546	-.200	.606	.833	.010*	-.405	.320

5.4.6 EMG

Quality of the EMG signal was poor in two ACLD study participants (A01, A02) due to significant noise artifacts. Therefore, EMG results are only presented for six of the eight ACLD study participants at twelve weeks post injury.

5.4.6.1 Quadriceps

Median VL muscle power was significantly decreased in the ACLD injured limb (330.30) compared to the contralateral limb (801.97) at twelve weeks post injury during the squat (p=0.028). This result was also true at six weeks post injury (Chapter 4).

The side to side differences (Δ_{leg}=ACLD-Contra) in VM and VL muscle power decreased over time during the swing in the ACLD group, indicated increased symmetry in the quadriceps muscles. At six weeks post injury median Δ_{leg} for the VM was -133.33, and decreased to -73.36 at twelve weeks post injury (p=0.028). For the VL, median Δ_{leg} was -142.36 at six weeks post injury, and decreased to -34.42 at twelve weeks post injury (p=0.028, Figure 5-16). In the ACLD injured limb, quadriceps muscle power increased over time during the swing, although this observation did not reach significance. Median quadriceps power ranged from 36.29-66.59 at six weeks post injury, compared to 107.33-119.18 at twelve weeks post injury (p=0.075-0.116). In the ACLD contralateral limb, the opposite trend was observed, with the quadriceps muscle power decreasing over time during the swing (also not statistically significant). Median quadriceps power ranged from 212.71-225.60 at six weeks post injury, compared to 162.39-

193.76 at twelve weeks post injury (p=0.075). Therefore, muscle power in the quadriceps increased over time in the ACLD injured limb, and decreased over time in the contralateral limb to increase limb symmetry at twelve weeks post-injury.

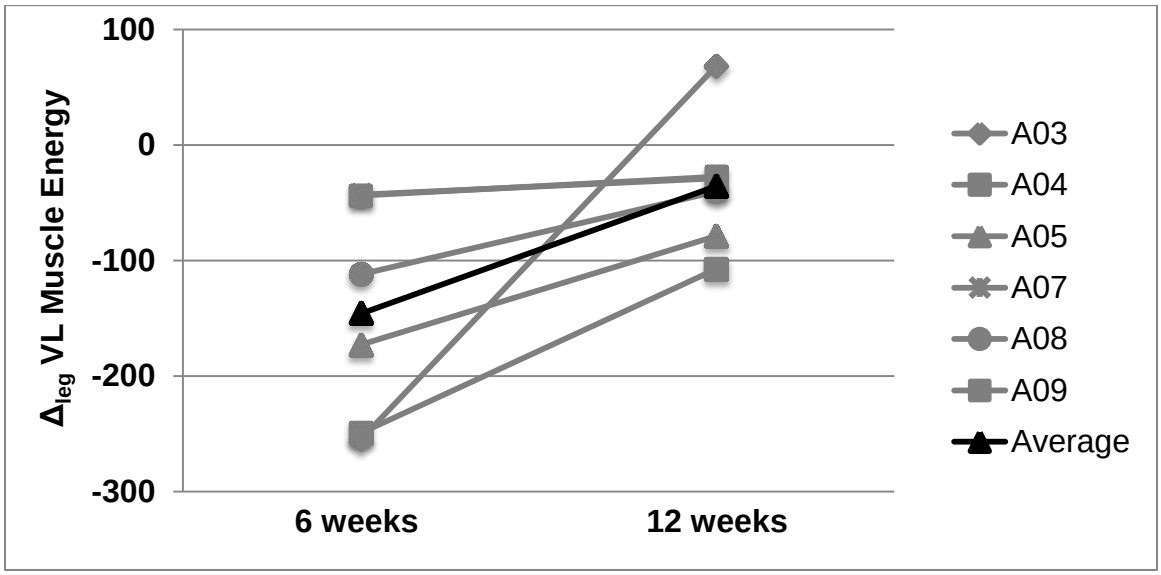

Figure 5-16: Side to side difference (Δ_{leg}) in VL muscle power during the swing task for the ACLD group 6 and 12 weeks post-injury. Grey lines represent individual participants, black line represents group average.

5.4.6.2 Hamstrings

Muscle power in the SEM significantly increased over time in the ACLD contralateral limb during the squat (p=0.028), however did not significantly change during the swing (p=0.075). Median SEM muscle power during the squat was 51.44 at six weeks post injury, and increased to 152.22 at twelve weeks post injury in the ACLD contralateral limb (Figure 5-17). SEM muscle power was also significantly greater in the ACLD contralateral limb (152.22) compared to the injured limb (24.18) at twelve weeks post injury during the squat (p=0.028).

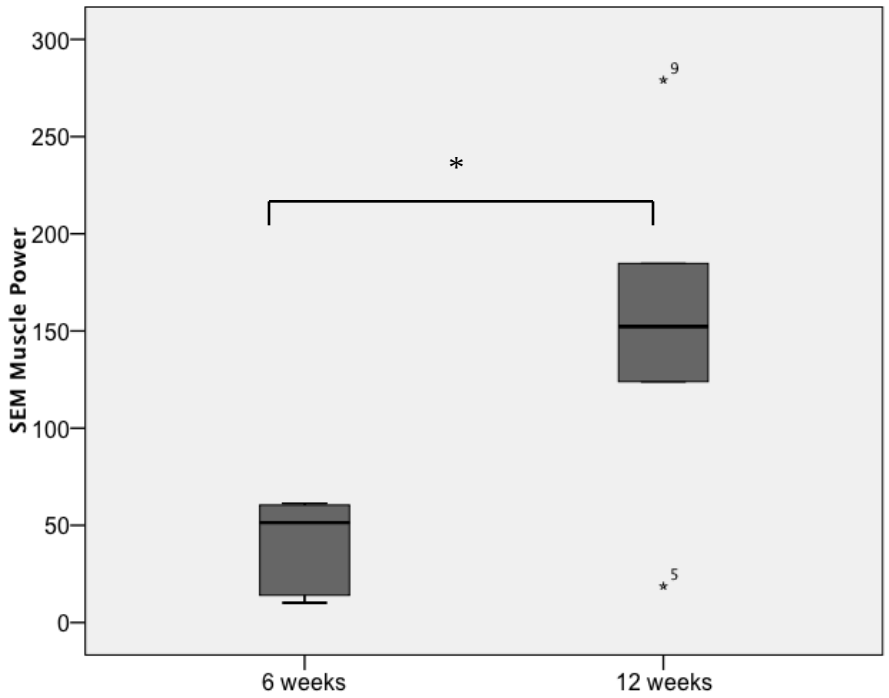

Figure 5-17: SEM muscle power in the ACLD contralateral limb during the squat at 6 and 12 weeks post injury (* indicates significance at α=0.05). Outliers are indicated with an asterisk and a number representing the identity of the outlier within the group.

The side to side difference (Δ_{leg}=ACLD-Contra) in SEM muscle power significantly increased over time in the ACLD group during the squat task (p=0.028), indicating decreased limb symmetry in the hamstrings at twelve weeks post injury. At six weeks post injury median Δ_{leg} for the SEM was -30.92, and decreased to -109.36 at twelve weeks post injury (Figure 5-18). The increased side to side difference is related to the increase in SEM muscle power in the ACLD contralateral limb over time.

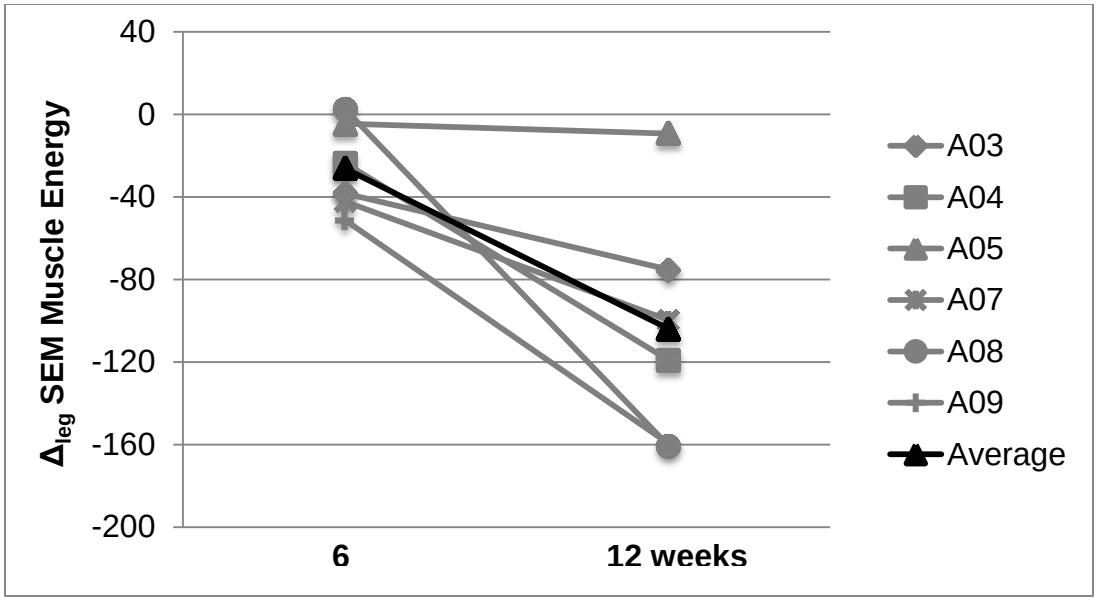

Figure 5-18: Side to side difference (Δ_{leg}) in SEM muscle power during the squat task for the ACLD group 6 and 12 weeks post-injury. Grey lines represent individual participants, black line represents group average.

In the ACLD injured limb, SEM muscle power significantly increased over time during the swing task (p=0.046). At six weeks post injury, median SEM muscle power was 0.24, and increased to 3.76 at twelve weeks post injury (Figure 5-19).

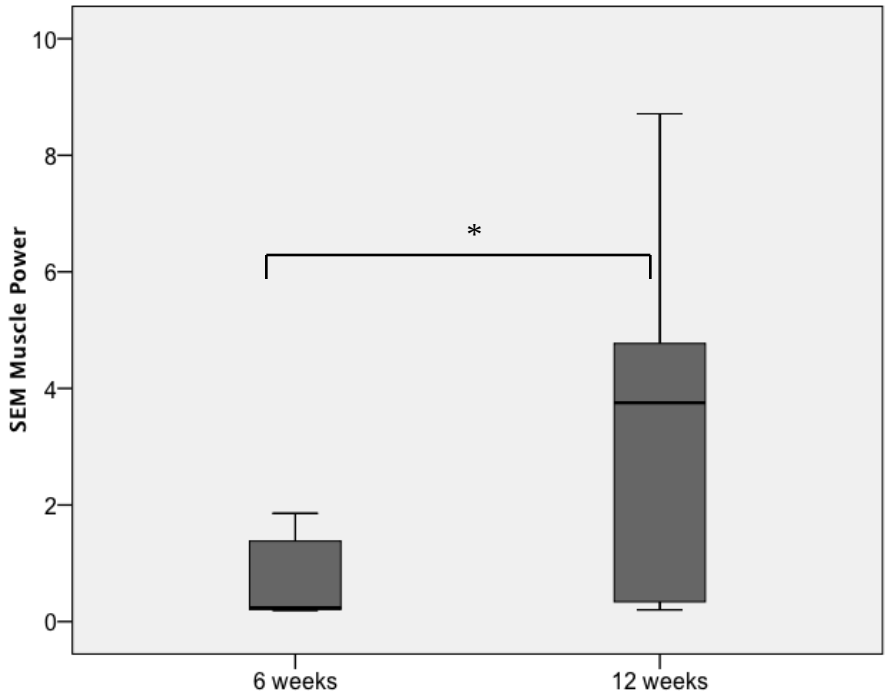

Figure 5-19: SEM muscle power in the ACLD injured limb during the swing at 6 and 12 weeks post injury (* indicates significance at α=0.05).

5.4.7 Muscle Volume

The muscle volume for the VM was significantly lower in the ACLD injured limb (208.6 ± 32.9 cm^3) compared to the contralateral limb (231.0 ± 27.3 cm^3) at twelve weeks post injury (p=0.008, Figure 5-20). The muscle volume for the VL was also significantly lower in the ACLD injured limb (294.2 ± 45.7 cm^3) compared to the contralateral limb (338.0 ± 40.0 cm^3) (p=0.007, Figure 5-20) at twelve weeks post injury. There were no statistically significant differences between limbs in the ACLD group for the BF (p=0.859), or SEM (p=0.193) muscle volumes. This result was also true at six weeks post injury.

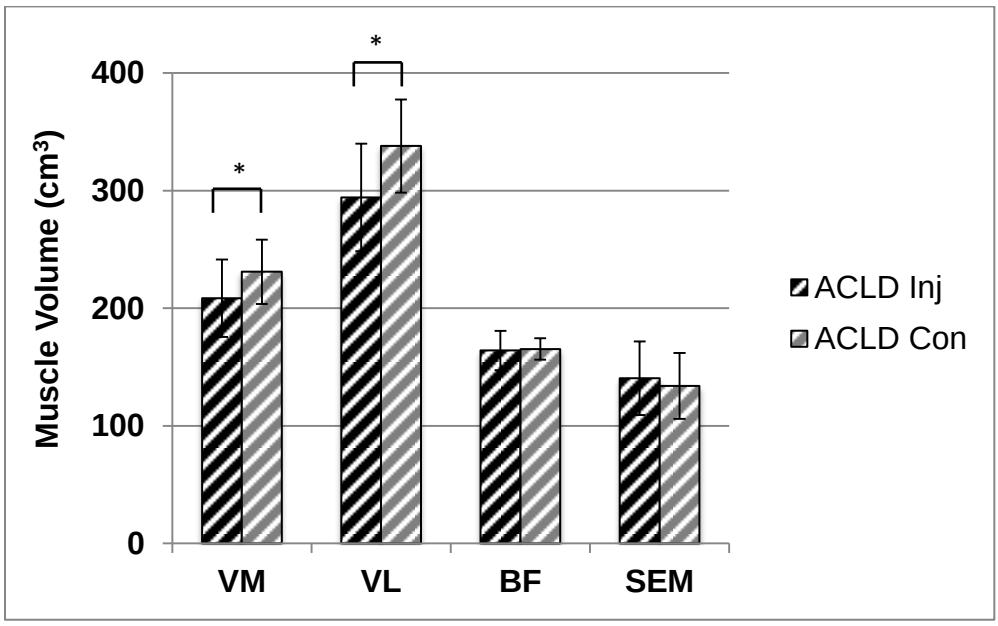

Figure 5-20: Muscle volume for the VM, VL, BF and SEM muscles of the injured and contralateral limbs of the ACLD group at twelve weeks post injury (* indicates significance at α=0.05).

5.4.8 Summary of Results

5.4.8.1 Laxity

The side to side difference in ATT at 89N in the ACLD group at six weeks post injury was 3.43 ± 4.28 mm, and at twelve weeks post-injury was 1.29 ± 2.47 mm (p=0.220).

5.4.8.2 FHA

A list of the key statistically significant findings in FHA measures for the ACLD group over time, and compared to healthy is presented below:

- FHA was located more anterior in the ACLD injured limb compared to the contralateral limb during the swing task at twelve weeks post injury
- Translation decreased over time in the ACLD injured limb during the squat task

    - Translation was lower in ACLD injured compared to contralateral at twelve weeks post injury
    - Side to side difference in translation increased over time in ACLD group
- Dispersion decreased over time in the ACLD contralateral limb during the squat
    - Dispersion was significantly greater in the ACLD injured limb at twelve weeks post injury compared to contralateral and healthy
    - Side to side difference in dispersion increased over time in the ACLD group
- Path length decreased over time in the ACLD contralateral limb during the squat
- AP excursion decreased over time in the ACLD contralateral limb during the swing
    - AP excursion decreased in the ACLD contralateral at twelve weeks post injury compared to both ACLD injured and healthy
- PD excursion decreased in the ACLD contralateral limb at twelve weeks post injury compared to the injured limb during the squat task

5.4.8.3 Correlations

The key statistically significant correlations between ATT and FHA measures in the ACLD group at twelve weeks post injury are presented below (Table 5-6).

Table 5-6: Key relationships between ATT and FHA measures in the ACLD group at 12 weeks post injury for the injured and contralateral limbs. ↑ indicates an increase in the FHA measure with increased ATT, and ↓ indicates a decreased in the FHA measure with increased ATT.

FHA measure	Task	ACLD 12 weeks	
		Injured	Contra
Location y (mm)	Swing	↑	
	Squat		↑
Translation (mm)	Swing	↓	
	Squat	↑	
Dispersion (°)	Swing	↓	
	Squat	↑	
Path (mm)	Swing		
	Squat	↑	↓
AP ex (mm)	Swing		
	Squat	↑	↓

5.4.8.4 EMG

A list of the key statistically significant findings in EMG muscle power for the ACLD group between limbs at twelve weeks post injury and over time is presented below:

- Quadriceps (VM, VL) muscle power was decreased in the ACLD injured limb compared to the ACLD contralateral limb during the squat task at twelve weeks post injury
- Side to side difference in quadriceps muscle power decreased over time in the ACLD group during the swing task
    - Quadriceps (VM, VL) muscle power increased over time in the ACLD injured limb, and decreased over time in the contralateral limb during the swing task
- Side to side difference in hamstring (SEM) muscle power increased over time in the ACLD group during the squat task
    - SEM muscle power increased over time in the ACLD contralateral limb

- SEM muscle power was greater in the contralateral limb compared to the injured limb at twelve weeks post injury

- SEM muscle power increased over time in the ACLD injured limb during the swing task

5.4.8.5 Muscle Volume

A list of the key statistically significant findings in muscle volume for the ACLD group at twelve weeks post injury is presented below:

- Quadriceps (VM and VL) muscle volume was lower in the ACLD injured limb compared to the ACLD contralateral limb at twelve weeks post injury
- No significant differences in muscle volume for the hamstrings (BF or SEM) between the ACLD injured and ACLD contralateral limbs at twelve weeks post injury

5.5 Discussion

The current study investigated changes over time in laxity and dynamic stability in ACLD individuals using the FHA combined with wavelet analysis of muscle patterns, and an MR based measure of laxity. The structure function relationship was examined at twelve weeks post-injury to identify alterations in these relationships with time from injury. The results of this study and their interpretations are discussed in this section as they relate to the specific aims and hypotheses.

To test the first hypothesis (H3a), the side to side difference in passive laxity in the ACLD group was compared between six and twelve weeks post injury. The average side to side difference in ATT in the ACLD group did not significantly change over time, supporting H3a. However, five out of eight ACLD study participants showed a decrease in ATT in the injured limb between six and twelve weeks post injury. A reduction in ATT over time could be a sign of stiffening within

the ACLD joint after injury due to adaptations in the joint structures (*i.e.*, capsule, ligaments, meniscus), which has been demonstrated previously in animal and human studies (Daniel et al., 1994; Maitland et al., 1998). MOAKS and KIMRISS scores did not reveal a significant change in joint effusion in the injured limb of the ACLD group between six and twelve weeks post injury. Other factors that could affect ATT include limb positioning and securement in the KLA, as well as muscle guarding. A power calculation revealed that twenty-one participants would be required to achieve a significant difference (α=0.05) in the side to side difference in ATT between six and twelve weeks post injury in the ACLD group with a power of 0.8. Therefore, future studies examining differences over time in this measure within an ACLD group should have a sample size of at least twenty-one participants.

To test the second hypothesis (H3b), changes in FHA measures and muscle power between six and twelve weeks post injury were examined for the injured and contralateral limbs of the ACLD group. The ACLD group demonstrated changes over time in FHA measures as well as muscle power in both limbs, supporting the H3b. In the ACLD injured limb, FHA translation decreased over time during the squat task. In the contralateral limb, FHA dispersion decreased over time during the squat task. Together, these changes resulted in an increase in the side to side difference in both translation and dispersion between six and twelve weeks post-injury, indicating decreased limb symmetry over time during the squat. This finding is interesting because changes in both the injured and contralateral limb had an effect on limb symmetry. Changes over time in FHA measures were only significant in the squat, which is suggestive of neuromuscular adaptations. The ACLD contralateral limb also showed decreased path length over time in the squat, and decreased AP excursion over time in the swing. The injury in the

ACLD group was unilateral, however these results clearly demonstrate that both limbs are adapting over time following ACL injury.

Changes over time in muscular control were also demonstrated in both limbs of the ACLD group, supporting H3b. During the swing task, quadriceps muscle power increased over time in the ACLD injured limb, and decreased over time in the contralateral limb. These adaptations resulted in a decreased side to side difference in quadriceps muscle power in the ACLD group during the swing, indicating increased limb symmetry. The medial hamstring muscle power also increased over time in the ACLD injured limb during the swing. This may be an attempt to counteract the increase in anterior tibial shear force caused by the increased quadriceps muscle activity observed in the injured limb. During the squat task, medial hamstring muscle power increased over time in the ACLD contralateral limb, and was greater than the injured limb at twelve weeks post injury. As a result, the side to side difference in SEM muscle power increased over time in the ACLD group, indicating decreased limb symmetry during the squat.

It is thought that increasing limb symmetry may be a stabilization strategy following injury. These results suggest that between six and twelve weeks post-injury, both limbs of the ACLD group are adapting in terms of both movement patterns (FHA) and muscle activity. During the swing task, quadriceps activity changed in both limbs in the ACLD group to increase symmetry at twelve weeks post injury. The only significant differences between limbs during the swing task in the ACLD group at twelve weeks post injury were anterior FHA location (location y) and AP excursion. There were no significant differences in muscle activity. It is expected that the quadriceps would be the primary mechanism used to modify AP location of the tibia with respect to the femur. Therefore, increasing quadriceps limb symmetry during the swing may be an attempt to correct side to side differences in AP excursion and anterior FHA location.

However, during the squat, changes over time in FHA measures and muscle power were unilateral, resulting in divergence between legs and therefore decreased symmetry. In the squat task, there were significant side to side differences in FHA translation and dispersion at twelve weeks post injury in the ACLD group. There were also significant differences between limbs in quadriceps (VL) and hamstring (SEM) muscle power. The inability to achieve symmetry in movement and muscle activity patterns, as well as divergence in symmetry in these measures points to the challenging nature of the squat task for ACLD individuals. Furthermore, the ACLD group demonstrated ongoing quadriceps atrophy (VM, VL) in the injured limb at twelve weeks post injury, likely causing decreased quadriceps strength. Perhaps an ideal adaptation strategy has not yet been developed for tasks involving single leg balance, and highlights the importance of developing an appropriate strategy to avoid early joint damage.

To test the third hypothesis (H3c), relationships between ATT and FHA measures were examined at twelve weeks post injury in the ACLD group and compared to the relationships detected at six weeks post injury. The ACLD group exhibited several relationships that did not exist at six weeks post injury, supporting the H3c. In the ACLD injured limb, individuals with increased ATT showed a more anterior FHA location during the swing task, which was also the case at six weeks post injury. Also during the swing task, ACLD individuals with increased ATT in their injured limb showed decreased FHA translation and dispersion. This latter relationship was not present at six weeks post injury. A possible explanation for this result is during the swing task, individuals with increased ATT have a more anterior tibial position which causes the tibia to be further restricted by the secondary restraints (*i.e.*, meniscus and posterior capsule), resulting in reduced translation and dispersion.

During the squat task, ACLD individuals with increased ATT in their injured limb exhibited increased translation, dispersion, path length, and AP excursion. These relationships in the squat task were only present at twelve weeks post injury, supporting H3c. The anterior position of the FHA in the ACLD limb was not significantly different from the contralateral limb during the squat, so the tibia was not in a position where the secondary restraints were able to limit translational and rotational movement, as observed in the swing. Therefore, additional structural laxity in ACLD individuals likely resulted in increased FHA translation and dispersion due to lack of additional stability provided by secondary passive restraints. This finding also suggests that the active joint stabilizers (*i.e.*, muscles) were not able to control for additional movement in the joint in the ACLD injured limb at twelve weeks post injury during the squat. Increased path length and AP excursion in those with increased ATT may be due to the weight-bearing nature of the squat whereby gravity causes the femur to translate posteriorly on the tibial plateau (Kvist, 2005), and increased muscle activity is required to support body weight. In the ACLD contralateral limb, individuals with increased ATT demonstrated a more anterior FHA location, and decreased path length and AP excursion during the squat task. In the contralateral limb, AP FHA location (location y) was sensitive to the amount of ATT in the joint. A more anterior location of the tibia may have caused decreased FHA path length and AP excursion, due to additional stability provided by secondary restraints. These relationships in the ACLD contralateral limb were not present at six weeks post injury.

This is the first study to quantify relationships between passive knee laxity (using an MR based measure of laxity) and dynamic movement patterns (using FHA) in a sub-acute group of ACLD individuals. Relationships between passive ATT and dynamic FHA measures identified at twelve weeks post injury in the ACLD injured limb were not present in the contralateral limb.

Furthermore, several of these relationships were not present at six weeks post injury. For example, the FHA dispersion pattern was very random in the ACLD group during the swing and squat tasks at six weeks post injury (not correlated with ATT). However, at twelve weeks post injury, the amount of dispersion was dependent on the amount of passive joint laxity. It would appear that the ACLD individuals exhibited a more random control strategy at six weeks post injury, and adapted over time to modify movement based on the amount of passive laxity in the joint.

Therefore, in the ACLD injured limb, movement patterns are affected, or perhaps even dictated by the amount of passive laxity in the knee joint, while the contralateral limb does not display these same relationships. Open and closed chain tasks were used to evaluate these relationships, and showed opposite relationships in the ACLD limb. ACLD individuals with increased ATT demonstrated a more constrained movement in the swing task, and a less constrained movement in the squat task. There is a spectrum of ATT within an ACLD group. Depending where an individual lies along that spectrum, their movement patterns will differ. Therefore, rehabilitation protocols need to address individual needs based on both passive and dynamic measures.

A key finding in this study was evidence of adaptation in the ACLD contralateral limb. This confirms that kinematic and muscular adaptations occur bilaterally following ACL rupture, which can be partially attributed to central control mechanisms. Furthermore, the contralateral limb is not an appropriate healthy control, and may mask changes from healthy in the ACLD limb. However, the contralateral limb does serve as a measure to evaluate joint symmetry. Adaptations in the ACLD contralateral limb may also contribute to an increased rate of ACL rupture to the contralateral limb, therefore it is suggested that rehabilitation protocols address the contralateral limb as well as the injured limb.

The results of the current study showed that ACLD individuals reduced FHA translation over time, while FHA dispersion remained larger in the ACLD limb at twelve weeks post-injury suggesting ongoing rotational instability during the weight-bearing squat task. It has been suggested that a shift in joint contact position to an area not accustomed to high loads leads to the initiation of cartilage damage and the development of osteoarthritis (Andriacchi et al., 2004; Stergiou et al., 2007). There is evidence to suggest that increased tibial rotation in the joint causes loading of areas not typically loaded (Stergiou et al., 2007). Therefore, the movement patterns observed at twelve weeks post-injury may be detrimental to the joint at this sub-acute stage. While there are components of the single leg squat that are performed repeatedly throughout the day, such as stair climbing and sit to stand, the single leg squat is not an activity of daily living. The number of repetitive joint loading cycles typically performed during a day with a single leg squat type movement is small in comparison to walking, for example. Therefore, the connection between rotational instability during the single leg squat and OA development must be carefully interpreted. However, the period between six and twelve weeks post injury may be a critical time to train healthy adaptation strategies that do not result in altered loading of the joint.

Chapter Six: **Discussion and Summary**

The overall research goal was to develop a further understanding of the relations amongst joint structure, joint function, and the development of degenerative changes associated with ligament injury. The current study objective was to investigate relations amongst structural joint laxity and dynamic joint stability in healthy and ACLD individuals over time. This chapter presents a summary and discussion of the key findings of this study. The significance of this research towards the understanding of mechanisms for OA development and progression are explored. Limitations associated with this research are also addressed.

6.1 Key Findings and Contributions

6.1.1 Acute adaptation in ACLD individuals

The timing of testing the ACLD group and the choice of test subjects (humans) was of great importance for this research study. Numerous studies in the literature address acute changes in ACLD individuals. However, the definition of "acute" varies greatly from study to study and the range of timing post injury generally covers a reasonably large time frame. Furthermore, the majority of studies quantifying changes over time in the ACLD joint use an animal model, which is highly informative, but cannot be directly applied to humans. The current study tested ACLD human subjects at six and twelve weeks post injury to investigate a sub-acute stage post injury, prior to reconstructive surgery. Interestingly, the ACLD group showed minimal kinematic differences from the healthy group at six weeks post injury. However, between six and twelve weeks post injury ACLD individuals demonstrated adaptations in both kinematics and muscular control. Therefore, it is suggested that this period may be a critical time to intervene and train healthy adaptation strategies that do not result in altered loading of the joint.

6.1.2 Bilateral adaptation following ACL rupture

There is growing evidence to suggest that neuromuscular adaptation occurs bilaterally following ACL rupture (Konishi et al., 2003; Urbach et al., 1999). However, few studies such as the current one have captured adaptations at a sub-acute stage post injury. Adaptations in the contralateral limb are important to identify, firstly because they have implications for using the contralateral limb as a control in studies. Secondly, and equally importantly, they may have implications on recovery, rehabilitation and repair following ACL rupture. The current study revealed adaptations in the ACLD contralateral limb over time in FHA dispersion, path length, AP excursion, and SEM muscle power. These findings confirm that kinematic and muscular adaptations occur bilaterally following ACL rupture, which can be partially attributed to central neuromotor control mechanisms. Identifying adaptations that occur early after injury in the contralateral limb provides evidence to inform rehabilitation protocols targeting both the injured and contralateral limb in ACLD individuals. Furthermore, there is a high incidence of rupturing the contralateral limb after primary ACL rupture (Kvist et al., 2005; Lohmander et al., 2004). Perhaps contralateral adaptations contribute to this increased risk, and could be mitigated with proper rehabilitation.

6.1.3 Rotational instability

In the ACLD group, FHA translation reduced over time in the injured limb, while FHA dispersion increased over time in the injured limb during the squat. These results suggest ongoing rotational instability in the ACLD injured limb at twelve weeks post-injury during the weight-bearing squat task. It is thought that rotational instability plays a key role in the dynamic stability of ACLD individuals. FHA dispersion provides an excellent measure to quantify this rotational instability. Dispersion is a unique FHA measure that has a low minimal detectable

difference and is not dependent on the definition of the local coordinate system in the knee, making it a very reliable measure. Rotational instability may result in a shift in joint contact position to an area not accustomed to high loads, which has been suggested to lead to the initiation of cartilage damage and the development of OA. However, the number of repetitive joint loading cycles typically performed during a day with a single leg squat type movement is small in comparison to walking, for example. Therefore the connection between rotational instability during the single leg squat and OA development must be carefully interpreted. Nonetheless, it is suggested that restoring rotational instability in ACLD individuals should be a primary focus for rehabilitation programs prior to reconstructive surgery. The squat is a common rehabilitation task that challenges neuromuscular control during weight bearing. However, this task may be putting the joint at risk of early damage if performed with ongoing rotational instability, as demonstrated in the ACLD limb at twelve weeks post injury. Therefore, it is suggested that modified or assisted squats be performed during the early stages following ACL rupture in order to reduce loading on the knee joint whilst developing appropriate control strategies. Rotational stability (quantified with FHA dispersion) could also play a role in evaluating the outcome of reconstructive surgery. It is speculated that the overall goal is likely to keep the loads on the knee as similar as possible to before injury in order to avoid overloading the cartilage in areas not habituated to loading. One approach to accomplish this could be the use of targeted rehabilitation protocols aimed at restoring healthy joint loading patterns.

6.1.4 Limb symmetry

One of the key contributions of this work was the integrated quantification of kinematics, passive knee laxity, and muscle activity in both limbs of a group of healthy individuals. Measuring these variables in both limbs provided the advantage of allowing quantification of "healthy

variability", or typical side to side differences in healthy individuals. This knowledge enabled us to forgo the typical assumption of symmetry within the healthy population. Further, by quantifying the extent of asymmetry within the healthy population, a baseline for variability was established for comparison with non-healthy groups. This knowledge then allowed us to compare side to side differences in healthy individuals to side to side differences in ACLD individuals. The comparisons led to new insights about whether differences between limbs in the ACLD group were in fact due to ACL rupture, or merely due to healthy variability between limbs. For example, the dominant limb of the healthy group had a significantly more anterior location of the FHA within the knee joint compared to the contralateral limb during the swing task. This was also true for the ACLD group at twelve weeks post injury, where the injured limb had a more anterior location than the contralateral limb during the swing. If we had not identified this side to side difference in the healthy group, it would have been assumed that the difference in FHA location between injured and contralateral limbs of the ACLD group was due to injury. The importance of using this approach was clear for measures of passive knee laxity, as it has been well documented that the side to side difference within an individual indicates whether the ACL is ruptured or not (*i.e.*, side to side difference greater than 3 mm). However, kinematic studies often neglect the importance of quantifying between limb differences in healthy individuals. Further, while comparing the injured limb to the contralateral limb in an injured group provides a strong within subject comparison, it remains critical to also compare with a healthy group to enable appropriate interpretation of differences. This is particularly relevant as the non-injured limb may not be a true representation of a healthy limb.

Another advantage of measuring both limbs in the healthy and ACLD groups is that it enabled the quantification of limb symmetry. The healthy group demonstrated small differences between

limbs, with only one significant difference in FHA location during the swing task. Otherwise, there were no significant differences between limbs for passive knee laxity, FHA measures, or muscle power. The injured limb of the ACLD group demonstrated decreased limb symmetry over time between six and twelve weeks post injury during the squat task due to bilateral changes in FHA translation and dispersion, and unilateral changes in hamstring muscle activity (contralateral only). During the swing task, limb symmetry increased over time due to bilateral changes in quadriceps muscle activity. There were no significant differences in these measures between limbs in the healthy group, indicating symmetry within the healthy group. Over time, the ACLD group was able to increase limb symmetry during the swing. However, during the squat the limbs became less symmetrical over time. This begs the question, what is better for long term joint health, limb symmetry or healthy dynamics? Furthermore, from a long term joint health perspective, is one strategy preferable to the other? ACLD individuals may adopt differing strategies to optimize dynamic joint stability, and perhaps limb symmetry is a coping mechanism. It is speculated that limb symmetry may be an indicator of how well an individual is able to adapt to ACL rupture in the short term. Although the limbs may not fall within the range of a healthy individual, perhaps ACLD individuals reach a new normal that allows them to maintain dynamic stability. Furthermore, perhaps ACLD individuals who become more symmetrical over time following injury will have a better long term joint health outcome than those who become more asymmetrical over time following injury. Change in symmetry over time following injury could provide a measure to evaluate risk of joint damage and/or dysfunction, however this hypothesis needs to be evaluated in the longer term. Regardless, movement patterns outside the range of a healthy individual may have negative effects on joint health in the long term.

6.1.5 Relationships between passive knee laxity and dynamic knee stability

The link between passive knee laxity and measures of dynamic function in ACLD individuals is yet to be clarified in the literature. This research study identified relationships amongst passive knee laxity and dynamic knee stability by applying novel techniques and tools to quantify these key variables. Furthermore, two dynamic tasks (open and closed chain) were specifically chosen to highlight differences in the dynamics of the ACLD joint. At twelve weeks post injury, ACLD individuals with increased ATT in the injured limb demonstrated a more constrained movement during the swing task, and a less constrained movement during the squat task. These same relationships did not exist in the healthy group or the ACLD contralateral limb. This valuable finding confirms the hypothesis that the amount of laxity in an injured (ACLD) joint does in fact impact the way that the joint moves dynamically. In the current study, it is too early to know whether the amount of passive laxity in the joint is predictive of the ability to dynamically stabilize the knee in the long term, with or without reconstructive surgery. However, it would be interesting to follow these subjects over time to determine whether these relationships hold true in the longer term. Furthermore, these findings could be used to work towards a simpler and more cost-effective technology to evaluate dynamic joint stability clinically. Perhaps measures of dynamic stability assessed during the single leg squat and seated leg swing tasks could augment diagnostics to better inform knee joint status and evaluate risk of future joint damage following ACL rupture. It would be interesting to perform a similar study with ACL reconstructed individuals, to determine whether the same relationships found in the current study exist between passive knee laxity and dynamic knee stability in an ACLR group, or whether these relationships are altered following ACL reconstruction.

6.2 Study Limitations

One of the limitations of this study was that activity level of the ACLD participants was not controlled between six and twelve weeks post injury. It is acknowledged that the exact rehabilitation program and compliance to a program would have an effect on dynamic movement control. However the effect of rehabilitation was not a primary question in this study. Participants were asked to log their activity between testing sessions to have as additional information to review for confounding variables in the case of major discrepancies between ACLD participants. Another study limitation was that the healthy group was tested only once. It was assumed that the healthy group would not display changes over time in measures of passive knee laxity or dynamic knee stability. Pilot studies were conducted to address the repeatability and error associated with the techniques and devices used in the current study to ensure that the study design requirements were achieved. Furthermore, an error propagation analysis determined minimal detectable differences (MDD) for FHA outcome measures. In the current study, differences observed between healthy and ACLD groups, and within the ACLD group over time were greater than the MDDs.

The small sample size of the ACLD group (n=9) was a limitation in this study. This was primarily due to strict study inclusion criteria, the time commitment involved for participants and the study timeline and scope, which hindered recruitment of additional ACLD participants into the study. An informed approach was taken for statistical analysis to ensure appropriate use of statistical tests (*i.e.*, parametric versus non-parametric). A significance level of $\alpha=0.05$ was chosen for the current study to minimize the occurrence of Type I errors. Due to the number of outcome variables (*i.e.*, ATT, FHA, muscle power, muscle volume) and factors (*i.e.*, group, limb, task, phase) in the current study, a large number of statistical comparisons were made. Therefore,

it must be acknowledged that there is an increased chance of a type I error, and a risk that some comparisons are significant due to chance. Traditional adjustments for multiple comparisons, such as the Bonferroni correction, were considered to address these Type I errors however were not applied. While they reduce the number of type I errors, they also increase the number of type II errors. The significance level was not adjusted because of the exploratory nature of the study, which aimed to identify key variables for use in larger future studies. Several comparisons in the current study had a significance level between 0.05 and 0.10, which could be seen as a trend. However, due to low subject numbers, the study was not powered to detect these differences (*i.e.* Type II error). The means and variances presented in the current study can be used to identify the sample size required to achieve significance in future studies.

The participants in this study were females less than 185 cm in height, and with a BMI less than thirty due to requirements for the KLA and dynamic testing. Therefore, it must be considered that the findings of this study may not be generalizable to a larger population, including males as well as overweight females. In particular, joint loads may differ in females with a higher body weight, which could affect the ability to dynamically stabilize the knee. Future studies are required in a larger more diverse group to fully understand to the relationships between passive joint laxity and dynamic knee stability following ACL rupture in the general population.

A limitation associated with the KLA was that the maximum desired load at the knee joint (133 N) was not achieved in all study participants. Therefore, ATT with an anterior load of 89 N was used for comparisons between healthy and ACLD groups. It is expected that an applied load of 133 N would produce increased ATT in the ACLD injured limb, which may have provided a stronger comparison between groups in the current study. This was primarily due to the rigidity of securing the femur position during anterior knee loading. However, a balance between

participant comfort and rigidity of thigh strapping was required to ensure participant comfort during MR imaging. Measures were taken in the current study to improve the strapping method for the thigh, but the highest loading level (133 N) was still not achieved in all study participants. Future studies should address this issue. A potential solution is to create a rigid plastic cuff for the thigh to distribute pressure from the thigh straps enabling a more rigid femur position.

An additional limitation associated with the KLA is the risk of muscle guarding during load application in the MRI, which would reduce anterior tibial translation. There was no evidence of muscle guarding during the KLA calibration procedure, and no signs of muscle guarding during MR imaging (*i.e*. image artefacts due to movement) with the ACLD participants in the current study. However, muscle guarding is a very common problem when testing knee laxity in a clinical setting. Therefore, future studies should explore options for directly monitoring muscle guarding during MR imaging.

Participant EMG signals were normalized to a sub-maximal MVC with a set torque value in the current study. It was thought that ACLD participants would not be able to perform a true MVC at the sub-acute stage tested post injury due to pain and muscle inhibition. Therefore, comparisons of muscle power in the current study were limited to within subject comparisons, and comparisons between healthy and ACLD groups were not performed. Muscle volumes for the ACLD group were analysed by two independent testers, one performed the analysis for six weeks post injury, and a second performed the analysis for twelve weeks post injury. Therefore, comparisons within the ACLD group were limited to between limb comparisons at each time point. Comparisons between six and twelve weeks post injury were not performed, as the repeatability between testers was unknown. This analysis was beyond the scope of the current

study. Future work will determine the inter-rater repeatability for this measure, to determine whether the comparison over time can be performed.

Finally, the FHA was only evaluated for the range of interest (20°-40° of knee flexion) chosen for the current study. This range was selected to examine 10° of motion on either side of 30° of knee flexion, which is reported to be the approximate slack/taut transition angle of the ACL (Fleming et al., 1994), and shows the greatest anterior translation (Sakane et al., 1999). Therefore, it was expected that this range would highlight the role of the ACL and show the greatest differences between the healthy and ACLD groups. However, studies have shown that ACL strain increases as the knee approaches full extension (Beynnon et al., 1995; Markolf et al., 1995). Therefore, it is possible that there are important differences in the range of 0° to 20° of knee flexion that the current study did not capture. Future studies should investigate the applicability of the FHA calculation technique used in the current study to a larger range of interest for application to other study populations and for use with additional dynamic tasks.

6.3 Summary

Ultimately, the goal of this research study was to provide a further understanding of early adaptations in the knee joint following ACL rupture. A comprehensive approach including quantification of passive knee laxity and dynamic knee stability was applied to ACLD individuals at a well-controlled sub-acute stage post-injury. Adaptations in both the injured and contralateral limbs of an ACLD group were identified, suggesting bilateral adaptations to ACL rupture. Furthermore, relationships between passive knee laxity and measures of dynamic knee stability were established in the ACLD group, providing an understanding of how structural joint laxity directly influences dynamic movement patterns. Early adaptations in the ACLD knee joint are speculated to contribute to the initiation of degenerative changes in the knee joint, which may

be modifiable with targeted rehabilitation protocols aimed at minimizing or slowing the progression of OA.

Chapter Seven: **Future Directions**

Several recommendations for future research in this area are presented in this chapter to inspire future work building on the findings of this research project.

The group of ACLD individuals from the current study should be followed longer term, to evaluate dynamic stability at a longer time point (1-3 years) post ACL rupture, to understand whether the current study findings are indicative of longer term outcomes. Measures of passive knee laxity and dynamic knee stability could be compared between a sub-acute and a longer term time point following ACL rupture. Perhaps measures of passive knee laxity and dynamic knee stability at a sub-acute stage post injury are predictive of dynamic knee stability in the longer term. Furthermore, it would be interesting to understand who requires surgery and who doesn't, and to quantify changes in passive knee laxity and dynamic knee stability following ACL reconstruction to evaluate the effect of surgery.

The dynamic tasks used in the current study were specifically chosen to highlight changes in the ACLD knee joint for diagnostic purposes. However, the number of repetitive joint loading cycles typically performed during a day with a single leg squat or seated leg swing type movement is small in comparison to walking, for example. Therefore, the link between dynamic stability in these tasks and development and progression of OA must be carefully interpreted. Walking is a task of daily living and results in repetitive joint loading. Therefore, in addition to the two dynamic tasks used in the current study, future studies should consider evaluating dynamic stability during walking to strengthen links between alterations in dynamic stability due to ACL rupture and the development and progression of OA.

The current study revealed variability between dynamic trials for the healthy and ACLD groups. A potentially valuable future study to evaluate this variability relates to the definition of dynamic knee stability, whereby it is thought that the ACLD group may perform dynamic tasks in a more repeatable manner relative to the healthy group due to a reduced ability to deal with additional degrees of freedom in the joint. Furthermore, a comparison between limbs in the ACLD group would reveal whether the contralateral limb also performs dynamic tasks in a highly repeatable manner following ACL rupture.

Motion analysis technology quantifies kinematics with an accuracy of less than 1 mm. Dual fluoroscopy (DF) has an accuracy of less than 0.1 mm, however participants are exposed to radiation, thus the amount of data collected is limited. In order to validate the findings of the current study, a combined project using both motion analysis and dual fluoroscopy technologies to calculate the FHA within the knee joint is proposed to enable a comparison of FHA outcome measures between the two systems. The results of this proposed study could be used to determine the accuracy (with a high resolution) of the current FHA approach using motion analysis linked with MR images to quantify the FHA in relation to the participant specific knee joint.

Developing and applying techniques to quantify temporal changes in wavelet muscle intensity is viewed as the next step in the application of the wavelet analysis approach to ACLD groups. This would enable statistical comparisons of muscle intensity timing between and within groups, providing an improvement over visual assessment of wavelet muscle intensity plots. Furthermore, the application of classification techniques to discriminate between groups (*i.e.*, healthy versus ACLD) and to identify sub-groups within the ACLD group would benefit from muscle intensity and timing information.

FHA orientation angle encompasses both internal/external rotation and varus/valgus. Currently, the FHA is plotted within the participant-specific knee joint to visually assess the orientation of the FHA with respect to the medio-lateral axis of the knee in both the axial and frontal planes. However, quantification of the orientation angle in the axial and frontal planes of the knee LCS is suggested to enable further interpretation of differences in FHA orientation between groups.

The current study used ATT at an anterior tibial force of 89 N to compared passive knee laxity between healthy and ACLD groups. However, data was collected for several additional loading levels (*i.e.*, 0, 30, 50, 89 and 133 N). It is suggested that this data be used to create force-displacement curves to quantify the effect of a range of loading on the tibiofemoral joint, and to understand alterations in joint stiffness due to ACL rupture.

Several anatomical features have been identified that are speculated to contribute to an increased risk for sustaining an ACL rupture including tibial slope (Marouane et al., 2014; Voos et al., 2012; Webb et al., 2013) and intercondylar notch width (Shelbourne et al., 1998). It is suggested that the high resolution MR images collected in the current study be used to evaluate tibial slope and intercondylar notch width in healthy and ACLD study participants to determine whether the ACLD group possessed anatomical features that increased their risk for ACL rupture.

The 3D registration mapping technique to match boney surface geometries employed in the current study requires several steps and is very time consuming. Therefore, future studies performing 3D surface matching should compare the 3D surface-matching tool in Amira software to the 3D registration mapping technique to evaluate whether the 3D surface-matching tool in Amira provides sufficient accuracy for detecting tibial displacement from MR images.

The MRI Osteoarthritis Knee Score (MOAKS, Hunter et al., 2011) is a tool used to perform multi- feature joint assessments including grading of articular cartilage, subchondral bone

marrow lesions and cysts, osteophytes, menisci, anterior and posterior cruciate ligaments, collateral ligaments, synovitis, joint effusion, bone attrition, intra- articular loose bodies, and periarticular cysts/bursitis. It is suggested that the MOAKS score be evaluated for the healthy and ACLD participants in the current study to explore relationships between joint degeneration, dynamic stability measures and OA development.

The current work provided significant progress towards understanding sub-acute adaptations in the knee joint following ACL rupture, and developing relations amongst passive knee laxity and dynamic knee stability in ACLD individuals. With these combined future advances, the important goal of understanding the relations amongst joint structure, joint function, and the development of degenerative changes associated with ligament injury will be closer to being achieved.

References

AAOS, 2009. ACL Injury: Does it require surgery? [WWW Document].

Adachi, N., Ochi, M., Uchio, Y., Iwasa, J., Ryoke, K., Kuriwaka, M., 2002. Mechanoreceptors in the anterior cruciate ligament contribute to the joint position sense. Acta Orthop. Scand. 73, 330–4.

Alexander, E.J., Andriacchi, T.P., 2001. Correcting for deformation in skin-based marker systems. J. Biomech. 34, 355–361.

Alkjaer, T., Simonsen, E.B., Jørgensen, U., Dyhre-Poulsen, P., 2003. Evaluation of the walking pattern in two types of patients with anterior cruciate ligament deficiency: copers and non-copers. Eur. J. Appl. Physiol. 89, 301–8.

Alkjaer, T., Simonsen, E.B., Magnusson, S.P., Dyhre-Poulsen, P., Aagaard, P., 2012. Antagonist muscle moment is increased in ACL deficient subjects during maximal dynamic knee extension. Knee 19, 633–9.

Allen, C.R., Wong, E.K., Livesay, G. a, Sakane, M., Fu, F.H., Woo, S.L., 2000. Importance of the medial meniscus in the anterior cruciate ligament-deficient knee. J. Orthop. Res. 18, 109–15.

Anderson, A.F., Dome, D.C., Gautam, S., Awh, M.H., Rennirt, G.W., 2001. Correlation of anthropometric measurements , strength , anterior cruciate ligament size , and intercondylar notch characteristics to sex differences in anterior cruciate ligament tear rates. Am. J. Sports Med. 29, 58–66.

Andriacchi, T.P., 1990. Dynamics of pathological motion: Applied to the anterior cruciate deficient knee. J. Biomech. 23, 99–105.

Andriacchi, T.P., Dyrby, C.O., 2005. Interactions between kinematics and loading during walking for the normal and ACL deficient knee. J. Biomech. 38, 293–8.

Andriacchi, T.P., Mündermann, A., Smith, R.L., Alexander, E.J., Dyrby, C.O., Koo, S., 2004. A framework for the in vivo pathomechanics of osteoarthritis at the knee. Ann. Biomed. Eng. 32, 447–57.

Arthritis Alliance of Canada, 2011. The impact of arthritis in canada: today and over the next 30 years.

Atarod, M., Frank, C.B., Shrive, N.G., 2013. Decreased posterior cruciate and altered collateral ligament loading following ACL transection: A longitudinal study in the ovine model. J. Orthop. Res. 22, 1–8.

Barrance, P.J., Williams, G.N., Snyder-Mackler, L., Buchanan, T.S., 2006. Altered knee kinematics in ACL-deficient non-copers: a comparison using dynamic MRI. J. Orthop. Res. 24, 132–40.

Basmajian, J., De Luca, C., 1985. Description and Analysis of the EMG Signal. In: Butler, J. (Ed.), Muscles Alive: Their Functions Revealed by Electromyography. Williams & Wilkins, Baltimore, pp. 19–167.

Baugher, W., Warren, R., Marshall, J., Joseph, A., 1984. Quadriceps atrophy in the anterior cruciate insufficient knee. Am. J. Sports Med. 12, 192–195.

Benoit, D.., Lamontagne, M., Cerulli, G., Liti, a, 2003. The clinical significance of electromyography normalisation techniques in subjects with anterior cruciate ligament injury during treadmill walking. Gait Posture 18, 56–63.

Benoit, D.L., Ramsey, D.K., Lamontagne, M., Xu, L., Wretenberg, P., Renström, P., 2006. Effect of skin movement artifact on knee kinematics during gait and cutting motions measured in vivo. Gait Posture 24, 152–64.

Beynnon, B.D., Fleming, B.C., Johnson, R.J., Nichols, C.E., Renstr, P.A., Pope, M.H., 1995. Anterior cruciate ligament strain behavior during rehabilitation exercises in vivo. Am. J. Sports Med. 23, 24–34.

Beynnon, B.D., Fleming, B.C., Labovitch, R., Parsons, B., 2002. Chronic anterior cruciate ligament deficiency is associated with increased anterior translation of the tibia during the transition from non-weightbearing to weightbearing. J. Orthop. Res. 20, 332–7.

Binder-MacLeod, B., Buchanan, T.S., 2006. Tibialis anterior volumes and areas in ACL-injured limbs compared with unimpaired. Med. Sci. Sports Exerc. 38, 1553–1557.

Biscević, M., Tomić, D., Starc, V., Smrke, D., 2005. Gender differences in knee kinematics and its possible consequences. Croat. Med. J. 46, 253–60.

Blankevoort, L., Huiskes, R., de Lange, A., 1990. Helical axes of passive knee joint motions. J. Biomech. 23, 1219–1229.

Boerboom, A., Hof, A., Halbertsma, J., Raaij, J., Schenk, W., Diercks, R., Horn, J., 2001. Atypical hamstrings electromyographic activity as a compensatory mechanism in anterior cruciate ligament deficiency. Knee Surgery, Sport. Traumatol. Arthrosc. 9, 211–216.

Boeth, H., Duda, G.N., Heller, M.O., Ehrig, R.M., Doyscher, R., Jung, T., Moewis, P., Scheffler, S., Taylor, W.R., 2013. Anterior cruciate ligament-deficient patients with passive knee joint laxity have a decreased range of anterior-posterior motion during active movements. Am. J. Sports Med. 41, 1051–1057.

Boyd, S.K., Ronsky, J.L., Lichti, D.D., Salkauskas, D., Chapman, M.A., 1999. Joint Surface Modeling With Thin-Plate Splines. J. Biomech. Eng. 121, 525–532.

Brandsson, S., Karlsson, J., Eriksson, B.I., Kärrholm, J., 2001. Kinematics after tear in the anterior cruciate ligament: dynamic bilateral radiostereometric studies in 11 patients. Acta Orthop Scand 72, 372–378.

Burden, A., 2010. How should we normalize electromyograms obtained from healthy participants? What we have learned from over 25 years of research. J. Electromyogr. Kinesiol. 20, 1023–1035.

Butler, D.L., Noyes, F.R., Grood, E.S., 1980. Ligamentous restraints to anterior-posterior drawer in the human knee. A biomechanical study. J. Bone Jt. Surg. 62, 259–270.

Charlton, W., Coslett-Charlton, L., Ciccotti, M., 2001. Correlation of estradiol in pregnancy and anterior cruciate ligament laxity. Clin. Orthop. Relat. Res. 165–170.

Chaudhari, A.M.W., Schmitt, L.C., Andriacchi, T.P., 2012. Effects of Alterations in Gait Mechanics on the Development of Osteoarthritis in the ACL-Deficient Knee. In: Noyes, F.R., Barber-Westin, S. (Eds.), ACL Injuries in the Female Athlete. Springer Berlin Heidelberg, Berlin, Heidelberg, pp. 137–147.

Cheng, R.W.T., 2006. Registration for the In-Vivo Studies of Osteoarthritis based on Magnetic Resonance Imaging (Thesis). University of Calgary Department of Geomatics Engineering.

Chmielewski, T.L., Hurd, W.J., Snyder-Mackler, L., 2005. Elucidation of a potentially destabilizing control strategy in ACL deficient non-copers. J. Electromyogr. Kinesiol. 15, 83–92.

Chmielewski, T.L., Rudolph, K.S., Fitzgerald, G.K., Axe, M.J., Snyder-Mackler, L., 2001. Biomechanical evidence supporting a differential response to acute ACL injury. Clin. Biomech. (Bristol, Avon) 16, 586–91.

Chmielewski, T.L., Rudolph, K.S., Snyder-Mackler, L., 2002. Development of dynamic knee stability after acute ACL injury. J. Electromyogr. Kinesiol. 12, 267–74.

Chmielewski, T.L., Stackhouse, S., Axe, M.J., Snyder-Mackler, L., 2004. A prospective analysis of incidence and severity of quadriceps inhibition in a consecutive sample of 100 patients with complete acute anterior cruciate ligament rupture. J. Orthop. Res. 22, 925–30.

Churchill, D.L., Incavo, S.J., Johnson, C.C., Beynnon, B.D., 1998. The transepicondylar axis approximates the optimal flexion axis of the knee. Clin. Orthop. Relat. Res. 111–8.

Cole, G.K., Nigg, B.M., Ronsky, J.L., Yeadon, M.R., 1993. Application of the joint coordinate system to three-dimensional joint attitude and movement representation: a standardization proposal. J. Biomech. Eng. 115, 344–9.

Coughlin, K.M., Incavo, S.J., Churchill, D.L., Beynnon, B.D., 2003. Tibial axis and patellar position relative to the femoral epicondylar axis during squatting. J. Arthroplasty 18, 1048–1055.

Daniel, D.M., Stone, M. Lou, Sachs, R., Malcom, L., 1985. Instrumented measurement of anterior knee laxity in patients with acute anterior cruciate ligament disruption. Am. J. Sports Med. 13, 401–407.

Daniel, D.M., Stone, M.L., Dobson, B.E., Fithian, D.C., Rossman, D.J., Kaufman, K.R., 1994. Fate of the ACL-injured patient: a prospective outcome study. Am. J. Sports Med. 22, 632–644.

De Luca, C.J., 1997. The use of surface electromyography in biomechanics. J. Appl. Biomech. 13, 135–163.

Defrate, L.E., Papannagari, R., Gill, T.J., Moses, J.M., Pathare, N.P., Li, G., 2006. The 6 degrees of freedom kinematics of the knee after anterior cruciate ligament deficiency: an in vivo imaging analysis. Am. J. Sports Med. 34, 1240–6.

Dennis, D.A., Mahfouz, M.R., Komistek, R.D., Hoff, W., 2005. In vivo determination of normal and anterior cruciate ligament-deficient knee kinematics. J. Biomech. 38, 241–53.

Dyrby, C.O., Andriacchi, T.P., 2004. Secondary motions of the knee during weight bearing and non-weight bearing activities. J. Orthop. Res. 22, 794–800.

Eastlack, M.E., Axe, M.J., Snyder-Mackler, L., 1999. Laxity, instability, and functional outcome after ACL injury: copers versus noncopers. Med. Sci. Sports Exerc. 210–215.

Farina, D., Merletti, R., 2000. Comparison of algorithms for estimation of EMG variables during voluntary isometric contractions. J. Electromyogr. Kinesiol. 10, 337–349.

Fitzgerald, G.K., Axe, M.J., Snyder-Mackler, L., 2000. A decision-making scheme for returning patients to high-level activity with nonoperative treatment after anterior cruciate ligament rupture. Knee surgery, Sport. Traumatol. Arthrosc. 8, 76–82.

Fjeld, I., 2007. In-vivo Dynamic Joint Stability Quantified in Intact and ACL Deficient Knees (Thesis). University of Calgary Department of Mechanical and Manufacturing Engineering.

Fleming, B.C., Beynnon, B.D., Tohyama, H., Johnson, R.J., Nichols, C.E., Renstrom, P., Pope, M.H., 1994. Determination of a zero strain reference for the anteromedial band. J. Orthop. Res. 12, 789–795.

Freeman, M.A.R., Pinskerova, V., 2005. The movement of the normal tibio-femoral joint. J. Biomech. 38, 197–208.

Gao, B., Zheng, N.N., 2010. Alterations in three-dimensional joint kinematics of anterior cruciate ligament-deficient and -reconstructed knees during walking. Clin. Biomech. (Bristol, Avon) 25, 222–9.

Gardinier, E.S., Manal, K., Buchanan, T.S., Snyder-Mackler, L., 2012. Gait and neuromuscular asymmetries after acute ACL rupture. Med. Sci. Sports Exerc. 44, 1490–6.

Georgoulis, A.D., Moraiti, C., Ristanis, S., Stergiou, N., 2006. A novel approach to measure variability in the anterior cruciate ligament deficient knee during walking: the use of the approximate entropy in orthopaedics. J. Clin. Monit. Comput. 20, 11–8.

Georgoulis, A.D., Papadonikolakis, A., Papageorgiou, C.D., Mitsou, A., Stergiou, N., 2003. Three-dimensional tibiofemoral kinematics of the anterior cruciate ligament-deficient and reconstructed knee during walking. Am. J. Sports Med. 31, 75–9.

Guilak, F., Ratcliffe, A., Lane, N., Rosenwasser, M.P., Mow, V.C., 1994. Mechanical and biochemical changes in the superficial zone of articular cartilage in canine experimental osteoarthritis. J. Orthop. Res. 12, 474–84.

Gundersen, L.A., Valle, D.R., Barr, A.E., Danoff, J. V, Stanhope, J., Snyder-Mackler, L., 1989. Bilateral analysis of the knee and ankle during gait : an examination of the relationship between lateral dominance and symmetry. J. Am. Phys. Ther. Assoc. 69, 640–650.

Habib, A.F., Lee, Y.-R., Morgan, M., 2001. Surface matching and change detection using a modified hough transformation for robust parameter estimation. Photogramm. Rec. 17, 303–315.

Hannah, R., Morrison, J., Chapman, A., 1984. Kinematic symmetry of the lower limbs. Arch. Phys. Med. Rehabil. 65, 155–158.

Henning, C.E., Lynch, M.A., Glick, K.R., 1985. An in vivo strain gage study of the anterior cruciate ligament elongation of. Am. J. Sports Med. 13, 22–26.

Hermens, H.J., Freriks, B., Disselhorst-Kulg, C., Rau, G., 2000. Development of recommendations for SEMG sensors and sensor placement procedures. J. Electromyogr. Kinesiol. 10, 361–374.

Herzog, W., Nigg, B., Read, L., Olsson, E., 1989. Asymmetries in ground reaction force patterns in normal human gait. Med. Sci. Sport. Exerc. 21, 110–114.

Hollman, J.H., Deusinger, R.H., Van Dillen, L.R., Matava, M.J., 2003. Gender differences in surface rolling and gliding kinematics of the knee. Clin. Orthop. Relat. Res. 208–21.

Hunter, D.J., Guermazi, a, Lo, G.H., Grainger, a J., Conaghan, P.G., Boudreau, R.M., Roemer, F.W., 2011. Evolution of semi-quantitative whole joint assessment of knee OA: MOAKS (MRI Osteoarthritis Knee Score). Osteoarthritis Cartilage 19, 990–1002.

Hurd, W.J., Snyder-Mackler, L., 2007. Knee instability after acute ACL rupture affects movement patterns during the mid-stance phase of gait. J. Orthop. Res. 1369–1377.

Ingersoll, C.D., Grindstaff, T.L., Pietrosimone, B.G., Hart, J.M., 2008. Neuromuscular consequences of anterior cruciate ligament injury. Clin. Sports Med. 27, 383–404.

Isaac, D.L., Beard, D.J., Price, a J., Rees, J., Murray, D.W., Dodd, C. a F., 2005. In-vivo sagittal plane knee kinematics: ACL intact, deficient and reconstructed knees. Knee 12, 25–31.

Iwaki, H., Pinskerova, V., Freeman, M.A.R., 2000. Tibiofemoral movement 1 : the shapes and relative movements of the femur and tibia in the unloaded cadaver knee. J. Bone Jt. Surg. 82, 1189–95.

Jackson, D.W., Schreck, P., Jacobson, S., Simon, T.M., 1999. Reduced anterior tibial translation associated with adaptive changes in the anterior cruciate ligament-deficient joint: goat model. J. Orthop. Res. 17, 810–816.

Johansson, H., 1991. Role of knee ligaments in proprioception and regulation of muscle stiffness. J. Electromyogr. Kinesiol. 1, 158–79.

Jonsson, H., Kärrholm, J., 1994. Three-dimensional knee joint movements during a step-up: evaluation after anterior cruciate ligament rupture. J. Orthop. Res. 12, 769–79.

Kapreli, E., Athanasopoulos, S., Gliatis, J., Papathanasiou, M., Peeters, R., Strimpakos, N., Van Hecke, P., Gouliamos, A., Sunaert, S., 2009. Anterior cruciate ligament deficiency causes brain plasticity: a functional MRI study. Am. J. Sports Med. 37, 2419–26.

Karlsson, S., Gerdle, B., 2001. Mean frequency and signal amplitude of the surface EMG of the quadriceps muscles increase with increasing torque — a study using the continuous wavelet transform. J. Electromyogr. Kinesiol. 11, 131–140.

Kerrigan, D.C., Todd, M.K., Della, C.U., 1998. Gender differences in joint biomechanics during walking: normative study in young adults. Am. J. Phys. Med. Rehabil. 77, 2–7.

Klyne, D.M., Keays, S.L., Bullock-Saxton, J.E., Newcombe, P.A., 2012. The effect of anterior cruciate ligament rupture on the timing and amplitude of gastrocnemius muscle activation: A study of alterations in EMG measures and their relationship to knee joint stability. J. Electromyogr. Kinesiol. 22, 446–55.

Konishi, Y., Fukubayashi, T., Takeshita, D., 2002. Possible mechanism of quadriceps femoris weakness in patients with ruptured anterior cruciate ligament. Med. Sci. Sports Exerc. 34, 1414–8.

Konishi, Y., Konishi, H., Fukubayashi, T., 2003. Gamma loop dysfunction in quadriceps on the contralateral side in patients with ruptured ACL. Med. Sci. Sports Exerc. 35, 897–900.

Kozánek, M., Hosseini, A., Van de Velde, S.K., Moussa, M.E., Li, J.S., Gill, T.J., Li, G., 2011. Kinematic evaluation of the step-up exercise in anterior cruciate ligament deficiency. Clin. Biomech. 26, 950–954.

Kupper, J., 2008. A Novel Measure of In-Vivo Knee Joint Laxity (Thesis). University of Calgary Department of Mechanical and Manufacturing Engineering.

Kupper, J., Loitz-Ramage, B., Corr, D., Hart, D., Ronsky, J., 2007. Measuring knee joint laxity: a review of applicable models and the need for new approaches to minimize variability. Clin. Biomech. 22, 1–13.

Küpper, J.C., Robu, I., Frayne, R., Ronsky, J.L., 2013. The knee loading apparatus: axial, anterior, and compressive loading with magnetic resonance imaging. J. Mech. Des. 135, 024501.

Kutzner, I., Heinlein, B., Graichen, F., Bender, a, Rohlmann, a, Halder, a, Beier, a, Bergmann, G., 2010. Loading of the knee joint during activities of daily living measured in vivo in five subjects. J. Biomech. 43, 2164–73.

Kvist, J., 2005. Sagittal tibial translation during exercises in the anterior cruciate ligament-deficient knee. Scand. J. Med. Sci. Sports 15, 148–158.

Kvist, J., Ek, A., Sporrstedt, K., Good, L., 2005. Fear of re-injury: a hindrance for returning to sports after anterior cruciate ligament reconstruction. Knee Surg. Sports Traumatol. Arthrosc. 13, 393–7.

Leardini, A., Chiari, L., Della Croce, U., Cappozzo, A., 2005. Human movement analysis using stereophotogrammetry. Part 3. Soft tissue artifact assessment and compensation. Gait Posture 21, 212–25.

Li, G., Rudy, T.W., Sakane, M., Kanamori, A., Ma, C.B., Woo, S.L., 1999. The importance of quadriceps and hamstring muscle loading on knee kinematics and in-situ forces in the ACL. J. Biomech. 32, 395–400.

Liu, W., Maitland, M.E., 2000. The effect of hamstring muscle compensation for anterior laxity in the ACL-deficient knee during gait. J. Biomech. 33, 871–9.

Logan, M., Dunstan, E., Robinson, J., Williams, A., Gedroyc, W., Freeman, M., 2004a. Tibiofemoral kinematics of the anterior cruciate ligament (ACL)-deficient weightbearing, living knee employing vertical access open "interventional" multiple resonance imaging. Am. J. Sports Med. 32, 720–726.

Logan, M., Williams, A., Lavelle, J., Gedroyc, W., Freeman, M., 2004b. What really happens during the lachman test?: a dynamic MRI analysis of tibiofemoral motion. Am. J. Sports Med. 32, 369–375.

Lohmander, L.S., Englund, P.M., Dahl, L.L., Roos, E.M., 2007. The long-term consequence of anterior cruciate ligament and meniscus injuries: osteoarthritis. Am. J. Sports Med. 35, 1756–69.

Lohmander, L.S., Ostenberg, A., Englund, M., Roos, H., 2004. High prevalence of knee osteoarthritis, pain, and functional limitations in female soccer players twelve years after anterior cruciate ligament injury. Arthritis Rheum. 50, 3145–52.

Lopez, M.J., Kunz, D., Vanderby, R., Heisey, D., Bogdanske, J., Markel, M.D., 2003. A comparison of joint stability between anterior cruciate intact and deficient knees : a new canine model of anterior cruciate ligament disruption. J. Orthop. Res. 21, 224–230.

Lorentzon, R., Elmqvist, L., Sjostrom, M., Fagerlund, M., Fugl-Meyer, A., 1989. Thigh musculature in relation to chronic anterior cruciate ligament tear : Muscle size , morphology , and mechanical output before reconstruction. Am. J. Sports Med. 17, 423–429.

Lundin, T., Grabiner, M., Jahnigen, D., 1994. Technical Note: On the assumtion of bilateral lower extremity joint moment symmetry during the sit-to-stand task. J. Biomech. 28, 109–112.

Lutz, G., Palmitier, R., An, K., Chao, E., 1993. Comparison of tibiofemoral joint forces during open-kinetic-chain and closed-kinetic-chain exercises. J Bone Jt. Surg Am 75, 732–739.

MacWilliams, B. a, Wilson, D.R., DesJardins, J.D., Romero, J., Chao, E.Y., 1999. Hamstrings cocontraction reduces internal rotation, anterior translation, and anterior cruciate ligament load in weight-bearing flexion. J. Orthop. Res. 17, 817–22.

Maitland, M.E., Leonard, T., Frank, C.B., Shrive, N.G., Herzog, W., 1998. Longitudinal measurement of tibial motion relative to the femur during passive displacements in the cat before and after anterior cruciate ligament transection. J. Orthop. Res. 16, 448–54.

Malinzak, R.A., Colby, S.M., Kirkendall, D.T., Yu, B., Garrett, W.E., 2001. A comparison of knee joint motion patterns between men and women in selected athletic tasks. Clin. Biomech. 16, 438–45.

Maniwa, S., Nishikori, T., Furukawa, S., Kajitani, K., Ochi, M., 2001. Alteration of collagen network and negative charge of articular cartilage surface in the early stage of experimental osteoarthritis. Arch. Orthop. Trauma Surg. 121, 181–185.

Mannel, H., Marin, F., Claes, L., Durselen, L., 2004. Anterior cruciate ligament rupture translates the axes of motion within the knee. Clin. Biomech. 19, 130–135.

Markolf, K.L., Burchfield, D.M., Shapiro, M.M., Shepard, M.F., Finerman, G. a, Slauterbeck, J.L., 1995. Combined knee loading states that generate high anterior cruciate ligament forces. J. Orthop. Res. 13, 930–5.

Marouane, H., Shirazi-Adl, A., Adouni, M., Hashemi, J., 2014. Steeper posterior tibial slope markedly increases ACL force in both active gait and passive knee joint under compression. J. Biomech. 47, 1353–9.

McDougall, D.R., Jaremko, J.L., Lambert, R.G., Maksymowych., W.P., 2014. Comparative validation of an electronic overlay enhanced target-lesion based methodology (KIMRISS) with the volumetric based MRI Osteoarthritis Knee Score (MOAKS) for scoring bone marrow lesions in the knee in osteoarthritis: Data from the Osteoarthritis. In: ISS Edinburgh 2014 Scientific Paper Presentations. p. 1344.

Moraiti, C., Stergiou, N., Ristanis, S., Georgoulis, A.D., 2007. ACL deficiency affects stride-to-stride variability as measured using nonlinear methodology. Knee surgery, Sport. Traumatol. Arthrosc. 15, 1406–1413.

Mündermann, A., Dyrby, C.O., D'Lima, D.D., Colwell, C.W., Andriacchi, T.P., 2008. In vivo knee loading characteristics during activities of daily living as measured by an instrumented total knee replacement. J. Orthop. Res. 26, 1167–72.

Mündermann, A., Wakeling, J.M., Nigg, B.M., Humble, R.N., Stefanyshyn, D.J., 2006. Foot orthoses affect frequency components of muscle activity in the lower extremity. Gait Posture 23, 295–302.

Nakamura, N., Shino, K., 2005. The clinical problems of ligament healing of the knee. Sports Med. Arthrosc. 13, 118–126.

Noyes, F., Grood, E., Cummings, J., Wroble, R., 1991. An analysis of the pivot shift phenomenon: the knee motions and subluxations induced by different examiners. Am. J. Manag. Care 19, 148–155.

Okada, Y., 1989. Histochemical study on the atrophy of the quadriceps femoris muscle caused by knee joint injuries of rats. Hiroshima J. Med. Sci. 38, 13–21.

Palmieri, R.M., Ingersoll, C.D., Cordova, M.L., Kinzey, S.J., Stone, M.B., Krause, B.A., 2003. The effect of a simulated knee joint effusion on postural control in healthy subjects. Arch. Phys. Med. Rehabil. 84, 1076–1079.

Palmitier, R.A., Kai-nan, A., Scott, S.G., Chao, E.Y.S., 1991. Kinetic chain exercise in knee rehabilitation. Sport. Med. 11, 402–413.

Park, S.-K., Stefanyshyn, D.J., Ramage, B., Hart, D.A., Ronsky, J.L., 2009. Relationship between knee joint laxity and knee joint mechanics during the menstrual cycle. Br. J. Sports Med. 43, 174–9.

Patel, R.R., Hurwitz, D.E., Bush-Joseph, C.A., Bach, B.R., Andriacchi, T.P., 2003. Comparison of clinical and dynamic knee function in patients with anterior cruciate ligament deficiency. Am. J. Sports Med. 31, 68–74.

Rice, D.A., McNair, P.J., 2010. Quadriceps arthrogenic muscle inhibition: neural mechanisms and treatment perspectives. Semin. Arthritis Rheum. 40, 250–66.

Ristanis, S., Giakas, G., Papageorgiou, C.D., Moraiti, T., Stergiou, N., Georgoulis, a D., 2003. The effects of anterior cruciate ligament reconstruction on tibial rotation during pivoting after descending stairs. Knee Surg. Sports Traumatol. Arthrosc. 11, 360–5.

Roos, H., Adalberth, T., Dahlberg, L., Lohmander, L.S., 1995. Osteoarthritis of the knee after injury to the anterior cruciate ligament or meniscus: the influence of time and age. Osteoarthr. Cartil. 3, 261–267.

Rudolph, K.S., Axe, M.J., Buchanan, T.S., Scholz, J.P., Snyder-Mackler, L., 2001. Dynamic stability in the anterior cruciate ligament deficient knee. Knee Surgery, Sport. Traumatol. Arthrosc. 9, 62–71.

Sadeghi, H., Allard, P., Prince, F., Labelle, H., 2000. Symmetry and limb dominance in able-bodied gait: a review. Gait Posture 12, 34–45.

Sakane, M., Livesay, G.A., Fox, R.J., Rudy, T.W., Runco, T.J., Woo, S.L.-Y., 1999. Relative contribution of the ACL, MCL, and bony contact to the anterior stability of the knee. Knee surgery, Sport. Traumatol. Arthrosc. 7, 93–97.

Sato, K., Maeda, A., Takano, Y., Matsuse, H., Ida, H., Shiba, N., 2013. Relationship between static anterior laxity using the KT-1000 and dynamic tibial rotation during motion in patients with anatomical anterior cruciate ligament reconstruction. Kurume Med. J. 60, 1–6.

Sawilowski, S., Blair, R., 1992. A more realistic look at the robustness and type II error properties of the t test to departures from population normality. Phychological Bull. 111, 352–360.

Scarvell, J.M., Smith, P.N., Refshauge, K.M., Galloway, H., Woods, K., 2005. Comparison of kinematics in the healthy and ACL injured knee using MRI. J. Biomech. 38, 255–262.

Scarvell, J.M., Smith, P.N., Refshauge, K.M., Galloway, H.R., Woods, K.R., 2004. Comparison of kinematic analysis by mapping tibiofemoral contact with movement of the femoral condylar centres in healthy and anterior cruciate ligament injured knees. J. Orthop. Res. 22, 955–62.

Sheehan, F., Rebamnn, A., 2003. Non-invasive, in vivo measures of anterior cruciate ligament strains. In: 49th Annual Meeting of the Orthopaedic Research Society. p. 240.

Shelbourne, K.D., Davis, T.J., Klootwyk, T.E., 1998. The relationship between intercondylar notch width of the femur and the incidence of anterior cruciate ligament tears: a prospective study. Am. J. Sports Med. 26, 402–408.

Shelburne, K.B., Pandy, M.G., Torry, M.R., 2004. Comparison of shear forces and ligament loading in the healthy and ACL-deficient knee during gait. J. Biomech. 37, 313–319.

Sherbondy, P., Queale, W., McFarland, E., Mizuno, Y., Cosgarea, A., 2003. Soleus and gastrocnemius muscle loading decreases anterior tibial translation in anterior cruciate ligament intact and deficient knees. J. Knee Surg. 16, 152–158.

Shultz, S.J., Carcia, C.R., Perrin, D.H., 2004. Knee joint laxity affects muscle activation patterns in the healthy knee. J. Electromyogr. Kinesiol. 14, 475–483.

Snyder-Mackler, L., De Luca, P.F., Williams, P.R., Eastlack, M.E., Bartolozza, A.R., 1994. Reflex inhibition of the quadriceps femoris muscle after injury or reconstruction of the anterior cruciate ligament. J. Bone Jt. Surg. 76-A, 555–560.

Snyder-Mackler, L., Fitzgerald, G.K., Bartolozzi, A.R., Ciccotti, M.G., 1997. The relationship between passive joint laxity and functional outcome after anterior cruciate ligament injury. Am. J. Sports Med. 25, 191–195.

Soderkvist, I., Wedin, P., 1993. Determining the movements of the skeleton using well-configured markers. J. Biomech. 26, 1473–1477.

Solomonow, M., Baratta, R., Zhou, B., Shoji, E., Bose, W., Beck, C., D'Ambrosia, R., 1987. The synergistic action of the anterior cruciate ligament and thigh muscles in maintaining joint stability. Am. J. Sports Med. 15, 207–213.

Spoor, C.W., Veldpaus, F.E., 1980. Rigid body motion calculated from spatial co-ordinates of markers. J. Biomech. 13, 391–393.

Steindler, A., 1955. Kinesiology of the Human Body Under Normal and Pathological Conditions. Thomas, Springfield IL.

Stergiou, N., Ristanis, S., Moraiti, C., Georgoulis, A.D., 2007. Tibial rotation in anterior cruciate ligament (ACL)-deficient and ACL-reconstructed knees: a theoretical proposition for the development of osteoarthritis. Sports Med. 37, 601–13.

Stockmar, C., Lill, H., Trapp, A., Josten, C., Punkt, K., 2006. Fibre type related changes in the metabolic profile and fibre diameter of human vastus medialis muscle after anterior cruciate ligament rupture. Acta Histochem. 108, 335–42.

Stratford, P., Miseferi, D., Ogilvie, R., Binkley, J., Wuori, J., 1991. Assessing the responsiveness of five KT1000 knee arthrometer measures used to evaluate anterior laxity at the knee joint. Clin. J. Sport. Med. 1, 225–228.

Swanik, C.B., Lephart, S.M., Giraldo, J.L., DeMont, R.G., Fu, F.H., 1999. Reactive muscle firing of anterior cruciate ligament-injured females during functional activities. J. Athl. Train. 34, 121–129.

Tagesson, S., Oberg, B., Kvist, J., 2014. Static and dynamic tibial translation before, 5 weeks after, and 5 years after anterior cruciate ligament reconstruction. Knee surgery, Sport. Traumatol. Arthrosc.

Tapper, J.E., Fukushima, S., Azuma, H., Sutherland, C., Marchuk, L., Thornton, G.M., Ronsky, J.L., Zernicke, R., Shrive, N.G., Frank, C.B., 2008. Dynamic in vivo three-dimensional (3D) kinematics of the anterior cruciate ligament/medial collateral ligament transected ovine stifle joint. J. Orthop. Res. 26, 660–72.

Tashman, S., Anderst, W., Kolowich, P., Havstad, S., Arnoczky, S., 2004a. Kinematics of the ACL-deficient canine knee during gait: serial changes over two years. J. Orthop. Res. 22, 931–41.

Tashman, S., Collon, D., Anderson, K., Kolowich, P., Anderst, W., 2004b. Abnormal rotational knee motion during running after anterior cruciate ligament reconstruction. Am. J. Sports Med. 32, 975–983.

Teichtahl, A.J., Wluka, A.E., Morris, M.E., Davis, S.R., Cicuttini, F.M., 2009. The associations between the dominant and nondominant peak external knee adductor moments during gait in healthy subjects: evidence for symmetry. Arch. Phys. Med. Rehabil. 90, 320–4.

Thorstensson, A., Grimby, G., Karlsson, J., 1976. Force-velocity relations and fibre composition in human knee extensor muscles. J. Appl. Physiol. 40, 12–16.

Urbach, D., Nebelling, W., Weiler, H.-T., Amiszus, F., 1999. Bilateral Deficit of voluntary muscle activation after unilateral ACL tear. Med. Sci. Sport. Exerc. 31, 1691–1696.

Valderrabano, V., Tscharner, V. Von, Nigg, B.M., Hintermann, B., Goepfert, B., Fung, T.S., Frank, C.B., Herzog, W., 2006. Lower leg muscle atrophy in ankle osteoarthritis. J. Orthop. Res. 24, 2159–69.

Van den Bogert, A., Read, L., Nigg, B.M., 1996. A method for inverse dynamic analysis using accelerometry. J. Biomech. 29, 949–954.

Van der Harst, J.J., Gokeler, A., Hof, a L., 2007. Leg kinematics and kinetics in landing from a single-leg hop for distance. A comparison between dominant and non-dominant leg. Clin. Biomech. (Bristol, Avon) 22, 674–80.

Von Tscharner, V., 2000. Intensity analysis in time-frequency space of surface myoelectric signals by wavelets of specified resolution. J. Electromyogr. Kinesiol. 10, 433–445.

Von Tscharner, V., Goepfert, B., 2003. Gender dependent EMGs of runners resolved by time/frequency and principal pattern analysis. J. Electromyogr. Kinesiol. 13, 253–272.

Von Tscharner, V., Goepfert, B., Nigg, B.M., 2003. Changes in EMG signals for the muscle tibialis anterior while running barefoot or with shoes resolved by non-linearly scaled wavelets. J. Biomech. 36, 1169–1176.

Voos, J.E., Suero, E.M., Citak, M., Petrigliano, F.P., Bosscher, M.R.F., Citak, M., Wickiewicz, T.L., Pearle, A.D., 2012. Effect of tibial slope on the stability of the anterior cruciate ligament-deficient knee. Knee Surg. Sports Traumatol. Arthrosc. 20, 1626–31.

Wakeling, J., M., S., Kaya, M., Temple, G.K., Johnston, I.A., Herzog, W., 2002a. Determining patterns of motor recruitment during locomotion. J. Exp. Biol. 205, 359–369.

Wakeling, J.M., Pascual, S.A., Nigg, B.M., 2002b. Altering muscle activity in the lower extremities by running with different shoes. Med. Sci. Sports Exerc. 34, 1529–1532.

Wakeling, J.M., Von Tscharner, V., Nigg, B.M., Stergiou, P., 2001. Muscle activity in the leg is tuned in response to ground reaction forces. J. Appl. Physiol. 91, 1307–1317.

Webb, J.M., Salmon, L.J., Leclerc, E., Pinczewski, L. a, Roe, J.P., 2013. Posterior tibial slope and further anterior cruciate ligament injuries in the anterior cruciate ligament-reconstructed patient. Am. J. Sports Med. 21, 2800–2804.

Wexler, G., Hurwitz, D., Bush-Joseph, C., Andriacchi, T., Bach, B., 1998. Functional gait adaptations in patients with anterior cruciate ligament deficiency over time. Clin. Orthop. … 166–175.

Wilk, K.E., Escamilla, R.F., Fleisig, G.S., Barrentine, S.W., Andrews, J.R., Boyd, M.L., 1996. A comparison of tibiofemoral joint forces and electromyographic activity during open and closed kinetic chain exercises. Am. J. Sports Med. 24, 518–527.

Williams, G.N., Snyder-Mackler, L., Barrance, P.J., Buchanan, T.S., 2005. Quadriceps femoris muscle morphology and function after ACL injury: a differential response in copers versus non-copers. J. Biomech. 38, 685–93.

Wilson, D.R., Feikes, J.D., Zavatsky, A.B., O'Connor, J.J., 2000. The components of passive knee movement are coupled to flexion angle. J. Biomech. 33, 465–473.

Winter, D.A., 1990. Biomechanics and Motor Control of Human Movement, Second Edi. ed. Wiley-Interscience, Waterloo, Ontario, Canada.

Wojtys, E.M., Huston, J., 1994. Neuromuscular performance in normal and anterior cruciate ligament-deficient lower extremities. Am. J. Sports Med. 22, 89–104.

Woltring, H.J., Huiskes, R., de Lange, A., Veldpaus, F.E., 1985. Finite centroid and helical axis estimation from noisy landmark measurements in the study of human joint kinematics. J. Biomech. 18, 379–89.

Wretenberg, P., Ramsey, D.K., Nemeth, G., 2002. Tibiofemoral contact points relative to flexion angle measured with MRI. Clin. Biomech. 17, 477–485.

Yack, J.H., Collins, C.E., Whieldon, T.J., 1993. Comparison of closed and open kinetic chain exercise in the anterior cruciate ligament-deficient knee. Am. J. Sports Med. 21, 49–54.

Yoshida, H., Faust, a, Wilckens, J., Kitagawa, M., Fetto, J., Chao, E.Y.-S., 2006. Three-dimensional dynamic hip contact area and pressure distribution during activities of daily living. J. Biomech. 39, 1996–2004.

Zampeli, F., Pappas, E., Giotis, D., Hantes, M.E., Georgoulis, A.D., 2012. Kinematic predictors of subjective outcome after anterior cruciate ligament reconstruction: an in vivo motion analysis study. Knee surgery, Sport. Traumatol. Arthrosc. 20, 785–92.

Zätterström, R., Fridén, T., Lindstrand, a, Moritz, U., 2000. Rehabilitation following acute anterior cruciate ligament injuries--a 12-month follow-up of a randomized clinical trial. Scand. J. Med. Sci. Sports 10, 156–63.

APPENDIX A: SUBJECT CONSENT FORM

TITLE: Knee Joint Laxity and Functional Stability in Healthy and ACL Deficient Individuals

INVESTIGATORS: **Dr. Janet Ronsky**

Canada Research Chair in Biomedical Engineering
Department of Mechanical Engineering
[redacted]

CO-INVESTIGATORS: Emily Bishop
PhD Student
Department of Mechanical Engineering
[redacted]

Richard Frayne, PhD
Canada Research Chair in Image Science
Faculty of Medicine, Departments of Radiology and Clinical Neurosciences
[redacted]

Cy Frank, MD
Department of Surgery, Division of Orthopaedics
[redacted]

This consent form is only part of the process of informed consent. It should give you the basic idea of what the research is about and what your participation will involve. If you would like more detail about something mentioned here, or information not included here, please ask. Take the time to read this carefully and to understand any accompanying information. You will receive a copy of this form.

BACKGROUND

The loss of the anterior cruciate ligament (ACL) within the knee results in increased joint movement (laxity) and may be related to later degeneration of the cartilage surfaces inside the knee joint (osteoarthritis). We have developed a functional MRI based knee joint laxity device that enables 3D evaluation of change in ligament length as a function of loading. As well, we have developed a way of measuring knee joint movement in the laboratory and we think that this will lead us to better ways of measuring joint motion in the clinic. The long-term research goal is to better understand and diagnose relations amongst joint function, joint structure and degenerative joint disease.

You have been asked to participate (as one of approximately 30 subjects) in this study because you have either recently ruptured your ACL (ACLD), or because you have no lower extremity injuries and you will serve as a control subject. Your participation will involve 1 (control) or 2 (ACLD) testing sessions lasting approximately 6 hours.

WHAT IS THE PURPOSE OF THE STUDY?

The purpose of this study is to investigate the role that ligament deficiency plays in altered joint structure, joint mechanics and joint instability. In this study, we will be measuring how the axis around which the knee joint moves changes and compare between 10 ACL-deficient adults versus 10 subjects who have not had a knee injury. This will be done through functional testing (walking, leg squats and swings) in the laboratory as well as through the use of magnetic resonance imaging (MRI) to examine the underlying structures of the knee joint. A knee loading apparatus will be used in the MRI to measure knee laxity under varying loads.

WHAT WOULD I HAVE TO DO?

Before the measurements, the participant will complete a questionnaire to examine, firstly, any reasons why magnetic resonance imaging (MRI) would not be safe, such as if the subject has metal in the limb, and, secondly, about the functional status of the knee.

Motion Analysis Data Collection

For the functional knee tests you will wear shorts so that small reflective markers can be taped to various locations on your lower limbs. Disposable surface electrodes will be taped to your skin over the several muscles of your calf and thigh in order to record the electrical activity of some muscles that cross your knee joint. You will be asked to do three movements: walking, knee bending (flexion) and straightening (extension) while sitting with your foot dangling, and a single leg squat where you will stand on one leg and squat down until your knee is bent about 60 degrees. Each movement will be repeated 5 times. The movements will be recorded with video motion cameras that record only the position of the reflective markers; your image is not recorded. The force that you place on your foot during the squat will be recorded by a force platform embedded in the floor. This testing will take approximately 2 hours.

MR Imaging

The following day, you will arrive at the Seaman MRI Centre. You will lie on a special loading device that slides into the MRI machine. MRI scans of both knees will be made at varying loads. This requires no active participation, you will just be asked to lie still and relax. The duration of one scan will last between 1 and 3 minutes. The total duration of the measurements is approximately 90 minutes. There will be no follow-up measurements.

You will be requested to attend an MRI training session at the University of Calgary Health Science Center lasting approximately 2 hours. The purpose of this training session is to familiarize you with the set-up that will be used during the MR scans. Following successful training, you will complete various MRI scans conducted at the Seaman Family MR Research Centre. The training session will be on the same day as the motion analysis session.

WHAT ARE THE RISKS?

MR imaging is non-invasive and there are no known health risks associated with MR imaging for participants who complete the questionnaire that asks about possible risks. You will be asked to lie on a narrow table that slides into a large tunnel-like tube within the scanner. There is no pain associated with MR imaging. Some people feel somewhat claustrophobic from being inside the scanner. The machine produces loud thumping and humming noises during normal operation. You will be given ear plugs to reduce the noise. A licensed technologist will observe you during the entire procedure and you may speak to her/him during the procedure through an intercom in the scanner.

The muscle surface electrode application procedure may cause a slight stinging of the skin before the electrodes are applied. You may experience a reddening of the skin after the electrodes are removed; this usually resolves in a few hours. There are no other risks associated with surface EMG testing.

During the squatting activity, there is a slight chance that you will lose your balance. We will minimize this risk by having a researcher stand right next to you and to whom you can easily reach or who can easily reach you to provide stability.

ARE THERE ANY REPRODUCTIVE RISKS?

There are no reproductive risks associated with this study.

WILL I BENEFIT IF I TAKE PART?

If you agree to participate in this study there may not be a direct medical benefit to you. The information we get from this study may help us provide better treatments in the future for

patients with a rupture of the anterior cruciate ligament. You will be provided with the overall findings of the study, as available.

DO I HAVE TO PARTICIPATE?

Participation in this study is voluntary and you may withdraw from the study at any time. You will be asked if you want to continue before each new scan is made.

Subjects will agree to participate on a volunteer basis only. You may withdraw from the study at any time without jeopardizing your healthcare. To withdraw, you must contact either Dr. Janet Ronsky or Emily Bishop to inform them of your decision.

WILL I BE PAID FOR PARTICIPATING, OR DO I HAVE TO PAY FOR ANYTHING?

No payment will be given for participating in the study. You will be reimbursed for expenses associated with parking at the University of Calgary Health Science Center.

WILL MY RECORDS BE KEPT PRIVATE?

Participant confidentiality will be maintained by referring to the participants as individual MRI study numbers only. The reference list to correlate participant names and MRI study numbers will be maintained confidentially by Dr. Janet Ronsky. The MRI study data will be transferred directly to digital tape, and a copy will be retained on the MR Centre servers. Access to data will be limited to authorized individuals only (Dr. Ronsky, E. Bishop) for assessment purposes.

Upon completion of the study, all data files related to the study will be removed from the workstations and saved to tape. These data and the MR image data stored on the main and backup digital tapes will be maintained by Dr. Janet Ronsky for a period of seven years, after which time it will be destroyed. The Seaman MR Centre will keep copies of the MR image files on password protected research PACS. These images will not have any personnel identifiers.

IF I SUFFER A RESEARCH-RELATED INJURY, WILL I BE COMPENSATED?

In the event that you suffer injury as a result of participating in this research, no compensation will be provided to you by the University of Calgary, the Alberta Health Services, the Researchers, Alberta Innovates Technology Futures, or the Natural Sciences and Engineering Research Council of Canada. You still have all your legal rights. Nothing said in this consent form alters your right to seek damages.

SIGNATURES

Your signature on this form indicates that you have understood to your satisfaction the information regarding your participation in the research project and agree to participate as a subject. In no way does this waive your legal rights nor release the investigators or involved institutions from their legal and professional responsibilities. You are free to withdraw from the study at any time without jeopardizing your health care. If you have further questions concerning matters related to this research, please contact:

Dr. Janet Ronsky [redacted]

If you have any questions concerning your rights as a possible participant in this research, please contact The Chair of the Conjoint Health Research Ethics Board, University of Calgary, at 403-220-7990.

Participant's Name	Signature and Date
Investigator/Delegate's Name	Signature and Date
Witness' Name	Signature and Date

The University of Calgary Conjoint Health Research Ethics Board has approved this research study. A signed copy of this consent form has been given to you to keep for your records and reference.

APPENDIX B: SHAPIRO WILKS TEST RESULTS

Table B-1: Shapiro Wilks statistic for FHA measures in the healthy group (Squat-Swing Differences)

	Dom		Con	
Measure	**Flex**	**Ext**	**Flex**	**Ext**
loc x	.071	.399	.392	.995
loc y	.871	.713	.060	.049
trans	.532	.615	.994	.713
orient	.999	.338	.015	.010
disp	.005	.623	.084	.337
path	.525	.006	.205	.140
APex	.120	.045	.801	.503
PDex	.008	.836	.533	.652
Total # significant	4		3	
Total # measures	16		16	
Percent significant (%)	25		19	
TA	.001	.004	.000	.000
LG	.023	.443	.010	.039
VM	.001	.021	.299	.020
VL	.009	.504	.021	.026
BF	.056	.001	.000	.000
SEM	.165	.021	.020	.003
ratio	.460	.028	.004	.162
Total # significant	9		12	
Total # measures	14		14	
Percent significant (%)	64		86	

Table B-2: Shapiro Wilks statistic for FHA and ATT measures in the healthy and ACLD group at 6 and 12 weeks post-injury

			Healthy			ACLD 6 weeks			ACLD 12 weeks			ACLD over time	
Task	**Phase**	**Measure**	**Dom**	**Con**	**Side to side**	**Inj**	**Con**	**Side to side**	**Inj**	**Con**	**Side to side**	**Inj**	**Con**
Swing	**Flex**	**loc x**	.547	.487	.621	.516	.219	.573	.152	.508	.067	.691	.568
		loc y	.770	.981	.288	.428	.641	.098	.577	.528	.603	.770	.007
		trans	.724	.034	.295	.110	.835	.269	.188	.404	.344	.030	.125
		orient	.829	.602	.924	.210	.437	.414	.861	.800	.809	.407	.283
		disp	.000	.029	.004	.255	.269	.930	.821	.335	.106	.741	.603
		path	.996	.361	.131	.002	.024	.807	.093	.018	.645	.685	.066
		APex	.370	.259	.227	.872	.247	.017	.063	.149	.542	.675	.446
		PDex	.196	.932	.974	.053	.356	.711	.088	.015	.833	.277	.297
	Ext	**loc x**	.743	.717	.366	.621	.026	.522	.434	.286	.271	.228	.352
		loc y	.953	.946	.311	.245	.728	.052	.701	.411	.281	.546	.030
		trans	.595	.208	.755	.505	.303	.552	.145	.890	.243	.018	.766
		orient	.412	.531	.835	.369	.384	.159	.689	.858	.894	.694	.493
		disp	.001	.039	.998	.118	.265	.431	.098	.285	.708	.572	.564
		path	.002	.012	.008	.000	.005	.816	.765	.513	.454	.013	.951
		APex	.343	.243	.902	.962	.002	.283	.172	.224	.214	.866	.430
		PDex	.002	.228	.025	.061	.896	.261	.270	.001	.995	.467	.831
Squat	**Flex**	**loc x**	.114	.053	.173	.624	.721	.117	.742	.255	.901	.452	.979
		loc y	.593	.693	.575	.268	.023	.030	.294	.845	.332	.027	.948
		trans	.572	.272	.283	.258	.048	.875	.745	.421	.537	.563	.463
		orient	.949	.126	.008	.967	.421	.348	.672	.651	.918	.058	.688
		disp	.463	.029	.727	.312	.726	.209	.502	.828	.334	.446	.911
		path	.620	.680	.140	.929	.737	.789	.049	.863	.011	.510	.803

		APex	.657	.533	.852	.853	.818	.178	.631	.895	.887	.304	.998
		PDex	.015	.818	.665	.014	.718	.637	.112	.001	.526	.131	.774
	Ext	**loc x**	.052	.043	.392	.515	.508	.387	.880	.279	.480	.652	.598
		loc y	.596	.274	.456	.157	.033	.039	.274	.942	.722	.046	.936
		trans	.103	.171	.573	.062	.672	.592	.933	.693	1.000	.334	.614
		orient	.264	.028	.028	.917	.098	.616	.746	.882	.034	.990	.865
		disp	.962	.368	.227	.097	.302	.072	.073	.453	.450	.166	.221
		path	.093	.042	.232	.402	.168	.021	.176	.488	.250	.012	.626
		APex	.015	.193	.858	.364	.694	.678	.379	.153	.589	.488	.697
		PDex	.175	.009	.596	.125	.334	.706	.358	.900	.220	.079	.428
ATT			.105	.160	.494	.227	.346	.522	.147	.383	.325	.153	.878
Total # significant			6	9	5	3	7	4	1	4	2	6	2
Total # FHA measures			32	32	32	32	32	32	32	32	32	32	32
Percent significant (%)			**19**	**28**	**16**	**9**	**22**	**13**	**3**	**13**	**6**	**19**	**6**

Table B-3: Shapiro Wilks statistic for muscle power for the healthy and ACLD group at 6 and 12 weeks post-injury

Task	Measure	Healthy			ACLD 6 weeks			ACLD 12 weeks			ACLD over time	
		Dom	Con	Side to side	Inj	Con	Side to side	Inj	Con	Side to side	Inj	Con
Swing	TA	.000	.251	.000	.011	.488	.890	.009	.161	.008	.015	.940
	LG	.000	.178	.000	.350	.077	.152	.007	.052	.320	.384	.639
	VM	.030	.660	.001	.106	.191	.029	.485	.960	.758	.423	.137
	VL	.138	.494	.790	.089	.893	.242	.104	.987	.489	.018	.348
	BF	.794	.003	.016	.000	.517	.000	.030	.245	.278	.006	.428
	SEM	.000	.000	.024	.010	.323	.813	.505	.892	.672	.335	.679
Squat	TA	.003	.001	.006	.083	.116	.186	.390	.794	.428	.776	.434
	LG	.279	.028	.582	.702	.384	.420	.416	.006	.425	.204	.277
	VM	.208	.000	.003	.142	.859	.292	.001	.244	.291	.563	.961
	VL	.121	.010	.003	.020	.005	.002	.001	.466	.018	.614	.125
	BF	.021	.001	.001	.000	.028	.000	.096	.118	.356	.007	.762
	SEM	.013	.002	.155	.965	.049	.544	.041	.867	.515	.070	.973
Total # significant		7	9	9	5	3	4	6	1	2	4	0
Total # measures		12	12	12	12	12	12	12	12	12	12	12
Percent significant (%)		**58**	**75**	**75**	**42**	**25**	**33**	**50**	**8**	**17**	**33**	**0**

Table B-4: Shapiro Wilks statistic for muscle volume for the ACLD group at 6 and 12 weeks post-injury

	ACLD							
	6 weeks			12 weeks			Day to Day	
Measure	**Inj**	**Con**	**Side to Side**	**Inj**	**Con**	**Side to Side**	**Inj**	**Con**
VM	0.304	0.957	0.76	0.394	0.707	0.539	.514	.332
VL	0.022	0.300	0.985	0.242	0.552	0.517	.282	.978
BF	0.546	0.522	0.361	0.942	0.462	0.091	.991	.776
SEM	0.022	0.500	0.019	0.343	0.782	0.810	.313	.408
Total # significant	2	0	1	0	0	1	0	0
Total # measures	4	4	4	4	4	4	4	4
Percent significant (%)	50	0	25	0	0	25	0	0

Table B-5: Shapiro Wilks statistic for IKDC and Lysholm scores for the Healthy and ACLD group at 6 (ACLD 6) and 12 (ACLD 12) weeks post injury

Measure	**Healthy**	**ACLD 6**	**ACLD 12**	**ACLD b/w day diff**
IKDC	<0.001	0.340	0.404	0.718
Lysholm	0.002	0.992	0.473	0.961

APPENDIX C: ASME PERMISSION TO REPRINT FIGURE

Gmail by Google

Emily Bishop [redacted]

Request for permission to re-print figure

Beth Darchi [redacted] Wed, Dec 3, 2014 at 9:00 AM
To: Janet Lenore Ronsky [redacted]
Cc: Emily Bishop [redacted]

Dear Ms. Ronsky,

It is our pleasure to grant you permission to publish the ASME **Figures 3,4** from "The Knee Loading Apparatus: Axial, Anterior, and Compressive Loading With Magnetic Resonance Imaging," by Jessica C. Küpper, Ion Robu, Richard Frayne and Janet L. Ronsky, J. Mech. Des. Volume 135(2), 2013, as cited in your letter for inclusion in a PhD thesis entitled Quantifying Temporal Changes in Knee Joint Laxity and Dynamic Knee Stability for Healthy and Acute ACL Injured Individuals to be published by University of Calgary & National Library of Canada.

Permission is granted for the specific use as stated herein and does not permit further use of the materials without proper authorization. Proper attribution must be made to the author(s) of the materials. As is customary, we request that you ensure proper acknowledgment of the exact sources of this material, the authors, and ASME as original publisher. Acknowledgment must be retained on all pages printed and distributed.

Royalty fees have been waived for the ASME author.

Many thanks for your interest in ASME publications.

Sincerely,

ASME SETTING THE STANDARD

Beth Darchi
Publishing Administrator
ASME
[redacted]

Figure C-1: Permission from ASME to re-print Figures 3 and 4 from Kupper et al. (2013)

APPENDIX D: BIOMECHANICAL ASSESSMENT REPORT

McCaig Institute

Clinical Movement Assessment Laboratory
Biomechanical Assessment Report

UNIVERSITY OF CALGARY

Patient [redacted]
Injury: Left ACL rupture

Date of Injury: November 10, 2013
Date of testing: December 16, 2013

Knee Laxity

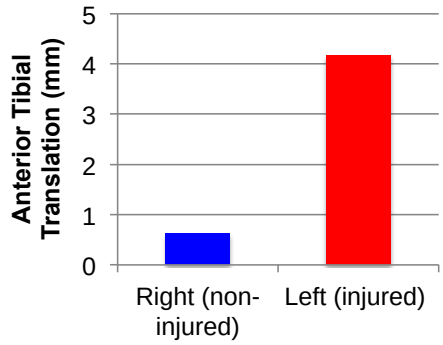

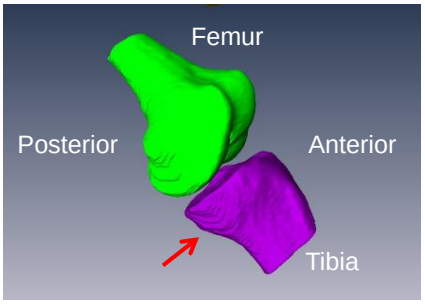

Description: An anterior force of 89N was applied to the tibia using a custom knee loading device while an MRI scan of the knee joint was obtained. Anterior translation of the tibia for the right limb (red) and left limb (blue) are presented. There is a lot of variability in this measure across people, therefore the best comparison for an individual is between legs.
Results: The left limb exhibits 3.5 mm greater anterior tibial translation compared to the right limb.
Significance: The results are consistent with the diagnosis of ACL rupture of the left limb.

Single-leg Squat

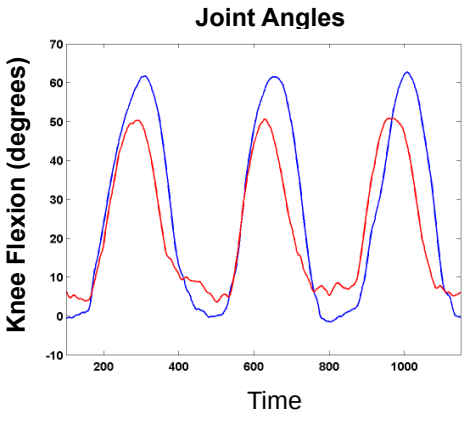

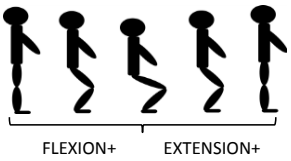

Left Limb (Injured)

Right Limb (Non-injured)

Description: Bilateral joint angle data for the knee joint during a single-leg squat. Left limb (red) and right limb (blue) are presented.
Results: The left limb consistently exhibits a lower peak flexion angle during the squat task.
Significance: The injured limb goes through less range of motion. This could be due to pain, weakness, range of motion, confidence. This is consistent with a functional deficit following injury.

Single-leg Squat

Muscle Activity Patterns

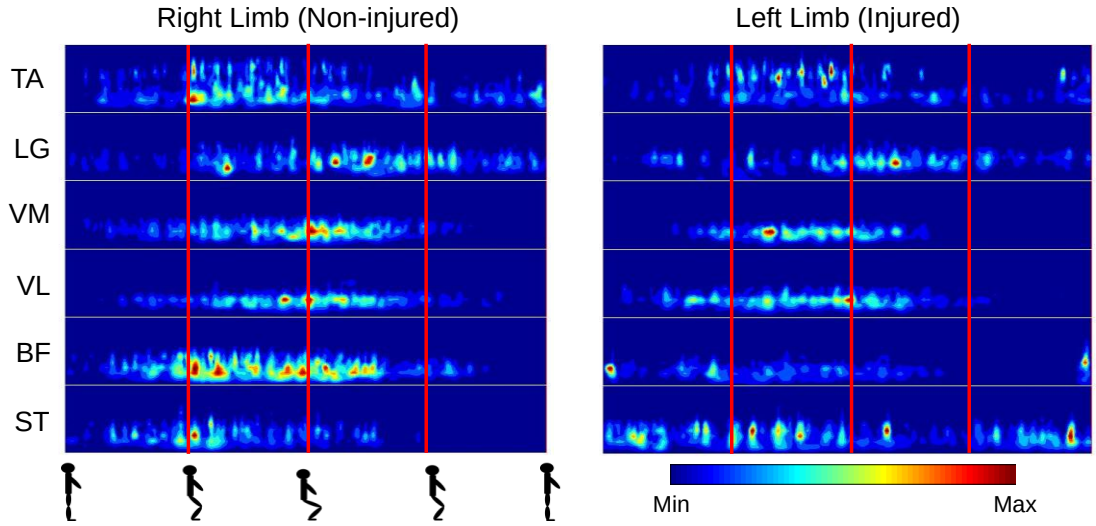

Description: Activity patterns for tibialis anterior (TA), gastrocnemius lateralis (LG), vastus medialis (VM), vastus lateralis (VL), biceps femoris (BF) and semitendinosus (ST) of the right and left limb. Intensity patterns are presented on a scale ranging from no activity (blue) to maximal activity (red) with frequency in the vertical and time in the horizontal axis. Red lines correspond to mid squat lowering, deep squat, land mid squat rising.
Results: There is less muscle activity in the left limb, especially in the hamstrings (BF, ST).
Significance: This is consistent with a pattern of decreased muscle activity, where the lower limb muscles are being under recruited following injury.

Muscle Volume/Size

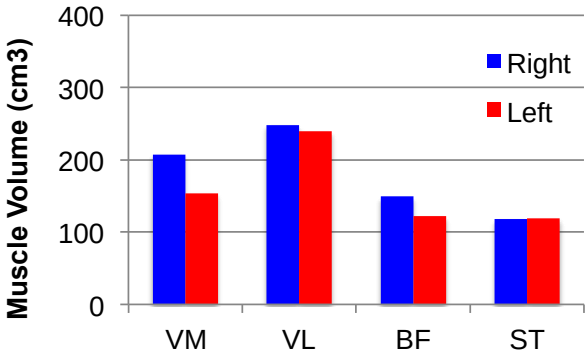

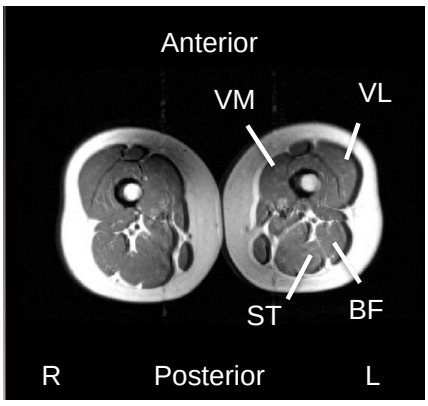

Description: Volume for vastus medialis (VM), vastus lateralis (VL), biceps femoris (BF) and semitendinosus (ST) of the right and left limb. Volumes were computed from MRI scans of the thigh muscles.
Results: Muscle volume slightly reduced in the injured limb compared to the non-injured limb.
Significance: Muscle atrophy (shrinkage) in the left limb may be due to persisting inflammation and/or decreased use and will likely result in a decrease in strength.

Summary:

Greater tibial laxity (movement) was observed in the left limb compared to the right under an 89N anterior force, which is consistent with the diagnosis of a complete ACL rupture. During the single leg squat peak knee flexion angle was reduced and full extension was not achieved in the left limb, suggesting reduced range of motion on the injured side. A pattern of reduced muscle activity was observed in the left limb, suggesting that the thigh muscles are being under recruited during dynamic tasks following injury. A decrease in muscle volume (size) was observed in the left limb compared to the right. This is likely related to reduced muscle activity in the injured limb and will likely result in a decrease in strength.

It is recommended that the client follow up with a qualified physiotherapist to restore range of motion, work toward a pattern of healthy muscle recruitment strategy throughout the full range of motion during loaded, dynamic tasks, and perform resistance training. It is recommended that range of motion and strength be optimized prior to reconstructive surgery.

Emily Bishop, PhD Candidate
Biomedical Engineering
McCaig Institute for Bone and Joint Health
University of Calgary

[redacted]